

**VLC 4630 - Impacts of volcanic ash on road transportation:
Considerations for resilience in Central Auckland (EQC
funded project 13/U646)**

Daniel Blake (supervised by Tom Wilson), University of
Canterbury - December 2017

Project No 13/U646 – Impacts of volcanic hazards on ground transportation: Considerations for evacuation and urban recovery in Auckland – Daniel Blake (supervised by Tom Wilson) UC

- Publications/Presentations/Papers in prep and review

2013:

DEVORA CDEM Poster	<i>Volcanic ash impacts on ground transportation in Auckland</i>
VISG Slides	<i>Volcanic ash impacts on ground transportation in Auckland</i>

2014:

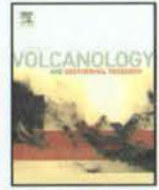
DEVORA CDEM Poster	<i>Volcanic ash impacts on ground transportation in Auckland</i>
Cities On Volcanoes 8 Indonesia	<i>Quantifying the impacts of volcanic hazards on surface transportation: an Auckland, New Zealand perspective</i>
DEVORA Forum	<i>Modelling an emergency evacuation in Auckland Impacts of volcanic hazards on surface transportation</i>
DEVORA Mini Workshop	<i>Impacts of volcanic hazards on surface transportation</i>
Disastrous Doctorates	<i>Impacts of volcanic hazards on surface transportation: considerations for evacuation and urban recovery in Auckland</i>
HAZM476 Course	<i>Quantifying the impacts of volcanic hazards on surface transportation: an Auckland, New Zealand perspective</i>
S Korea VDPRC Visit	<i>Impacts of volcanic hazards on ground transportation: considerations for evacuation and urban recovery in Auckland</i>
VISG Seminar Kelud	<i>Kelud volcano impact assessment trip – Eruption: Feb 2014, Impact Trip – Sept 2014</i>

2015

EQC Workshop Scenario Confidential	<i>Extended Exercise Ruaumoko scenario: Estimated physical impacts to the population and built environment (Workshop package prepared for EQC by UC and GNS) Extended Exercise Ruaumoko scenario: Critical infrastructure impacts summary</i>
GNS Kelud Report (published)	<i>The 2014 eruption of Kelud volcano, Indonesia: Impacts on infrastructure, utilities, agriculture and health</i>
ERI AVF Report (published)	<i>Economics of resilient infrastructure Auckland volcanic field scenario</i>
DEVORA Forum_ ERI Scenario	<i>Potential consequences of a volcanic eruption in an urban environment – Mt Ruaumoko scenario, Auckland, New Zealand</i>
DEVORA Forum	<i>Volcanic ash testing lab update: surface transport</i>
Disastrous Doctorates	<i>Impacts of volcanic ash on surface transportation in Auckland</i>
ERI AVF Meeting – Roads	<i>Roads in Auckland</i>
GSNZ Conference	<i>Impacts of an Auckland volcanic field eruption on critical infrastructure</i>
LAVA News Newsletter (published)	<i>Ash impacts on roads: Lessons from Kagoshima, Japan</i>
VISG Newsletter (published)	<i>Ash impacts on roads: Lessons from Kagoshima, Japan</i>
Riskscape Meeting	<i>Volcanic vulnerability function development for surface transport</i>
VISG Seminar	<i>Kelud volcano impact assessment trip-Eruption 2014 Transportation – what's the problem</i>
Volcano Short Course	<i>Impacts of volcanic ash on surface transport</i>
Volcano 2015 Conference Poster	<i>Volcanic ash impacts on road transport: New lab testing procedures</i>

2016

JVGR Kelud Special Issue - Abstract	<i>Evacuations to clean-up: transportation impacts from the 2014 eruption of Kelud volcano</i>
Paper – in prep (being edited by Tom Wilson)	<i>Visibility in airborne volcanic ash: considerations for surface transport using a laboratory-based method</i>
Journal of Environmental Earth Sciences – manuscript in review	<i>Road marking coverage by volcanic ash: an experimental approach</i>
Journal of Transportation Research Part D: Transport & Environment – in review	<i>Impact of volcanic ash on road and airfield surface skid resistance</i>
Journal of Applied Volcanology – in prep	<i>Developing volcanic ash fragility functions through laboratory studies: a case for surface transport</i>
Journal of Applied Volcanology – in review	<i>Framework for developing volcanic fragility and vulnerability functions for critical infrastructure</i>
IPENZ Transportation Group Conference, Auckland – 7-9 March 2016 (published)	<i>Impacts of volcanic ash on road transportation: Considerations for resilience in central Auckland</i>
NZTA STAG (January 2016) (research summary document published)	<i>Impacts of volcanic ash on road asphalt skid resistance</i>
VISG Newsletter ERI Article (March 2016) (published)	<i>"Mt Ruamoko": Exploring consequences of an Auckland volcanic field eruption</i>



Investigating the consequences of urban volcanism using a scenario approach II: Insights into transportation network damage and functionality



Daniel M. Blake^{a,*}, Natalia I. Deligne^b, Thomas M. Wilson^a, Jan M. Lindsay^c, Richard Woods^b

^a Department of Geological Sciences, University of Canterbury, Private Bag 4800, Christchurch, New Zealand

^b GNS Science, PO Box 30-368, Lower Hutt 5040, New Zealand

^c School of Environment, The University of Auckland, Private Bag 92019, Auckland, New Zealand

ARTICLE INFO

Article history:

Received 19 October 2016

Received in revised form 29 March 2017

Accepted 6 April 2017

Available online 9 April 2017

Keywords:

Tephra

Volcano

Hazard

Evacuation

Service

Road

ABSTRACT

Transportation networks are critical infrastructure in urban environments. Before, during and following volcanic activity, these networks can incur direct and indirect impacts, which subsequently reduces the Level-of-Service available to transportation end-users. Additionally, reductions in service can arise from management strategies including evacuation zoning, causing additional complications for transportation end-users and operators. Here, we develop metrics that incorporate Level-of-Service for transportation end-users as the key measure of vulnerability for multi-hazard volcanic impact and risk assessments.

A hypothetical eruption scenario recently developed for the Auckland Volcanic Field, New Zealand, is applied to describe potential impacts of a small basaltic eruption on different transportation modes, namely road, rail, and activities at airports and ports. We demonstrate how the new metrics can be applied at specific locations worldwide by considering the geophysical hazard sequence and evacuation zones in this scenario, a process that was strongly informed by consultation with transportation infrastructure providers and emergency management officials. We also discuss the potential implications of modified hazard sequences (e.g. different wind profiles during the scenario, and unrest with no resulting eruption) on transportation vulnerability and population displacement.

The vent area of the eruption scenario used in our study is located north of the Māngere Bridge suburb of Auckland. The volcanic activity in the scenario progresses from seismic unrest, through phreatomagmatic explosions generating pyroclastic surges to a magmatic phase generating a scoria cone and lava flows. We find that most physical damage to transportation networks occurs from pyroclastic surges during the initial stages of the eruption. However, the most extensive service reduction across all networks occurs ~6 days prior to the eruption onset, largely attributed to the implementation of evacuation zones; these disrupt crucial north-south links through the south eastern Auckland isthmus, and at times cause up to ~435,000 residents and many businesses to be displaced. Ash deposition on road and rail following tephra-producing eruptive phases causes widespread Level-of-Service reduction, and some disruption continues for >1 month following the end of the eruption until clean-up and re-entry to most evacuated zones is completed. Different tephra dispersal and deposition patterns can result in substantial variations to Level-of-Service and consequences for transportation management. Additional complexities may also arise during times of unrest with no eruption, particularly as residents are potentially displaced for longer periods of time due to extended uncertainties on potential vent location. The Level-of-Service metrics developed here effectively highlight the importance of considering transportation end-users when developing volcanic impact and risk assessments. We suggest that the metrics are universally applicable in other urban environments.

© 2017 The Authors. Published by Elsevier B.V. This is an open access article under the CC BY license (<http://creativecommons.org/licenses/by/4.0/>).

Abbreviations: AVF, Auckland Volcanic Field; CAA, Civil Aviation Authority; CDEM, Civil Defence and Emergency Management; FL, Flight Level; LoS, Level-of-Service; MCDEM, Ministry of Civil Defence and Emergency Management; NIWA, National Institute of Water and Atmospheric Research; NOTAM, Notice to Airmen; NZTA, New Zealand Transport Agency; PEZ, Primary Evacuation Zone; RNZAF, Royal New Zealand Air Force; SEZ, Secondary Evacuation Zone; SH, State Highway; VAL, Volcanic Alert Level; VHZ, Volcanic Hazard Zone.

* Corresponding author.

E-mail addresses: daniel.blake@pg.canterbury.ac.nz (D.M. Blake), n.deligne@gns.cri.nz (N.I. Deligne), thomas.wilson@canterbury.ac.nz (T.M. Wilson), j.lindsay@auckland.ac.nz (J.M. Lindsay), r.woods@gns.cri.nz (R. Woods).

1. Introduction

Efficient transportation networks are a prerequisite for future growth of top performing economies (NEC, 2014), and vital for societies worldwide. However, volcanic activity can cause substantial cumulative disruption to transportation, causing a reduction in the ability of networks to convey goods and people. This is particularly relevant in urban areas with complex transportation systems, high demand and/

or little network redundancy. Even before eruptions commence, proactive strategies to reduce exposure such as evacuation zoning can cause transportation disruption through access restrictions (Jenkins et al., 2014a). Potentially widespread cascading consequences caused by changes in demand across the network may also result (Woo, 2008; Wolshon, 2009). If a volcanic eruption ensues, further complexities for transportation end-users may be introduced by damage or disruption resulting from proximal volcanic hazards such as pyroclastic density currents and lava flows, and distal hazards such as tephra fall, which can affect areas up to hundreds of kilometers from the vent itself (Wilson et al., 2012a; Wilson et al., 2014). Table 1 illustrates the multitude of damage and disruption that has occurred on transportation networks due to proximal and distal volcanic hazards.

Roads are particularly important for the movement of people and freight in urban areas due to many interdependencies with other critical infrastructure types and often-widespread public use (Daly and Johnston, 2015). However, rail, aviation and maritime transportation may also have crucial roles during volcanic activity in some locations, with all modes potentially affected by volcanic hazards. For example, ash from the 2010 eruption of Eyjafjallajökull volcano in Iceland caused serious disruption to aviation across the North Atlantic and Europe, with global economic losses of around US\$5 billion (Ragona et al., 2011; Loughlin et al., 2015). Once direct volcanic threats have subsided and any exclusion zones are lifted, transportation plays a crucial role in both immediate and long-term recovery, including the provision of access for clean-up operations and facilitating the restoration of other critical infrastructure and businesses in affected areas (Cova and Conger, 2003; Hayes et al., 2015; Hayes et al., 2017).

Vulnerability assessments can be used as part of volcanic risk assessments to describe the likelihood that assets will incur loss for a range of hazard intensities (Rossetto et al., 2013). In the past, the majority of volcanic vulnerability assessments have focused on direct physical damage to infrastructure, especially concerning the structural components of buildings, and associated loss of life (e.g. Spence et al., 1999; Magill and Blong, 2005; Zuccaro et al., 2008; Jenkins et al., 2013; Hampton et al., 2015). However, disruption through the loss of critical infrastructure functionality from volcanic hazards may be equally, if not more, important to consider than direct damage in many situations (Wilson et al., 2014; Blake et al., in review c). Loss of functionality can cause widespread and cumulative effects on society (Jenkins et al., 2015) and subsequent complexities for governments and local authorities (Mei et al., 2013). For example, if a pyroclastic surge crosses (or is forecast to cross) a section of road, authorities may quickly decide that the affected section should be closed due to life-safety considerations. However, deciding whether to close the same road section if it is affected by light volcanic ash fall instead may be riddled with complexities; it may be that it remains open, albeit with reduced functionality. Importantly, the functional loss of transportation networks during volcanic activity, results in the end-users of the system experiencing a degree of disruption to service (Deligne et al., 2017), such as reduced speeds, temporary traffic management systems, congestion, or increased accident rates (Blake et al., in review c). Such disruption can be described by the overall usability of the network section or facility of interest, which we term Level-of-Service (LoS). Transportation authorities are increasingly focusing on LoS measures, with a general shift from maintaining networks primarily through technical solutions to maintenance approaches which address end-user needs. An example of this is the 'One Network Road Classification' performance measures implemented by the New Zealand Transport Agency, which "places the customer at the heart of every investment decision" (NZTA, 2013, p.3). LoS can be expressed descriptively as a series of general qualitative metrics, and/or as quantitative metric values, that consider site-specific details (e.g. Robinson et al., 2015). However, studies focusing on detailed assessments of transportation LoS are rare, especially during and after volcanic activity, despite the numerous multi-hazard impacts that can occur (e.g. Table 1).

The aim of this paper is to design and develop a universally-applicable but location-adaptable impact assessment model that incorporates LoS as a key measure of transportation vulnerability. We develop LoS metrics by considering the consequences of damage from geophysical hazards and evacuations during volcanic activity for the end-users of key transportation modes (road, rail, aviation and infrastructure at ports). This contributes to the volcanic risk assessment discipline by considering the impact of volcanic hazards on transportation end-users, whether it be from disruption caused by the effects of management strategies that act to reduce population and infrastructure exposure (such as evacuation zoning or volcanic deposit clean-up), or that from physical damage caused by volcanic hazards directly impacting transportation networks.

We adopt the "Māngere Bridge" scenario of the Auckland Volcanic Field (AVF), New Zealand, described by Deligne et al. (2017), as a basis to demonstrate the application of LoS metrics. LoS metrics are evaluated at key times during the course of the hypothetical eruption and its aftermath. In our application, the conceptual approach for impact assessment model development is guided by official emergency management policies, the latest data for transportation impacts from post-eruption and laboratory studies, and direct consultation with officials from transportation and emergency management authorities. We also consider two geophysical adaptations to the established Māngere Bridge scenario – a sequence of volcanic unrest, similar to that in the original scenario but with no resultant eruption, and a sequence of events the same as the original scenario but with a predominant south-westerly wind direction (the dominant wind direction for Auckland; Chappell, 2014). This allows us to explore the effects that potential alterations in the geophysical hazard sequence may have on evacuations, displaced populations, transportation damage and, importantly, LoS. Interdependencies with other critical infrastructure are briefly discussed but not analysed in detail.

2. Transportation in Auckland

In Auckland, New Zealand's largest and most populous city (population ~ 1.6 million; Statistics New Zealand, 2015), functional transportation networks are important for the regional and national economy (AELP-1, 1999). However, Auckland's geography poses some major challenges as it generally acts to constrain transportation networks on the ground; the Waitemata and Manukau Harbours act as major obstacles (Fig. 1), constricting routes through narrow stretches of land. There are two main isthmuses, which lie around 10 km from Auckland City; one to the south east (~2.3 km wide), and one to the south west (~5.2 km wide) (Tomsen, 2010). Additionally, Auckland City is built directly on top of the 360 km² basaltic AVF (Deligne et al., 2015a), and as transportation routes service highly populated areas, the consequences of disruption caused by volcanic activity could be substantial and widespread. There are four key transportation modes in Auckland, all of which are vulnerable to future volcanic activity in the field:

2.1. Road

Auckland has an extensive road network, with multiple highways, arterial (Fig. 1) and local routes, spanning over 8000 km across the region (NZTA, 2008). The majority of trips are made by car (Auckland Council, 2013a) and the bus network provides the bulk of public transport (ARTA, 2009; Tomsen, 2010). Walking mostly takes place within a transport system that must work for a range of road users (NZTA, 2009). As Auckland's geography acts to constrain the road transportation network (Fig. 1), generally one of four highway bridges must be crossed in order to enter or leave the city area by highway.

2.2. Rail

Most rail in the central and suburban areas is electrified (Fig. 1), with the electric system supplied by two connections to the national grid, at

Table 1

Examples of damage and disruption to transportation from volcanic hazards associated with infamous worldwide eruptions; x = road, o = rail, Δ = maritime, ◇ = airport. (Adapted from Blake et al., 2016 and Blake et al., in review a, b, c).

Note that impacts to aircraft in flight are excluded from this summary – we refer the reader to Guffanti et al. (2010) for this.

(Information from: Hurlbut and Verbeek, 1887; Corwin and Foster, 1959; Tazieff, 1977; Sarkinen and Witala, 1981; Tyler and Reynertson, 1981; Warrick, 1981; Labadie, 1983; Blong, 1984; Hirano et al., 1992; Yanagi et al., 1992; Bitschene and Fernández, 1995; Blong and McKee, 1995; Johnston and Daly, 1997; Casadevall et al., 1999; Nakada, 1999; Stammers, 2000; Arana-Barradas, 2001; Becker et al., 2001; Durand et al., 2001; Nairn, 2002; Oppenheimer, 2003; Barnard, 2004; Cole and Blumenthal, 2004; Cole et al., 2005; Kagoshima City Office, 2015, pers. comm; Leonard et al., 2006; Wilson et al., 2007; Guffanti et al., 2009; Barnard, 2009; USGS, 2009; Wilson, 2008; Wilson, 2009; Wilson et al., 2009a; Wilson et al., 2009b; Barsotti et al., 2010; Jamaludin, 2010; Sword-Daniels et al., 2011; Surono et al., 2012; Wardman et al., 2012; Wilson et al., 2012b; GVP, 2013; Jenkins et al., 2013; Magill et al., 2013; USGS, 2013; Wilson et al., 2013; Folch et al., 2014; Volcano Discovery, 2014; AccuWeather, 2015; Blake et al., 2015; Blake et al., 2016; Craig et al., 2016; Cubellis et al., 2016; Blake et al., in review a, b, c).

Volcano and country	Year	Physical damage from proximal hazards					Disruption from volcanic ash					
		Pyroclastic density current	Lava flow	Lahar	Tsunami	Deformation or degassing	Reduced skid resistance	Visibility issues	Marking coverage	Closure or obstruction	Vehicle or engine issues	Derailment (tram)
Komagatake, Japan	1640				Δ							
Garachico, Spain	1706		Δ									
Oshima, Japan	1741				Δ							
Sakurajima, Japan	1779											
Tambora, Indonesia	1815				Δ							
Cotopaxi, Ecuador	1877			x								
Vulcan, Papua New Guinea	1878											
Krakatau, Indonesia	1883				xoΔ			Δ			Δ	
Sagir, Indonesia	1891										Δ	
La Soufrière, St. Vincent and the Grenadines	1902											o
Matavanu, Samoa	1905–07		x		x							
Vesuvius, Italy	1906		o	o								
Matavanu, Samoa	1907				Δ							
Novaruputa, U.S.A.	1912									Δ		Δ
Sakurajima, Japan	1914		xΔ									
San Salvador, El Salvador	1917		o									Δ
Deception Island, (Antarctic Treaty administration)	1921											Δ
Kilauea, U.S.A.	1924					o						
Etna, Italy	1928		o									
Deception Island, (Antarctic Treaty administration)	1930									Δ		Δ
Tavurvur, Papua New Guinea	1937			x	Δ					Δ		Δ
Vesuvius, Italy	1944		o									Δ
Usu, Japan	1944					xo						
Ruapehu, New Zealand	1945			o				x				x
Lamington, Papua New Guinea	1951			x								Δ
Bayonnaise Rocks (submarine), Japan	1952											Δ
Iwo-jima, Japan	1957					◇						
South Sandwich Islands, U.K. (overseas territory)	1960s									Δ		Δ
Calbuco, Chile	1961			x								
Agung, Indonesia	1963			x								
Irazu, Japan	1964			x								
Kilauea, U.S.A.	1968					x						
Mayon, Philippines	1968			o								
Villarrica, Chile	1971			x								
Heimaey, Iceland	1973		Δ									
Ruapehu, New Zealand	1975			x								
Piton de la Fournaise, France (overseas territory)	1977		x									
Nyiragongo, Democratic Republic of Congo	1977		x									
Etna, Italy	1979		x									x
Lamington, Papua New Guinea	1979	x										
Mount St Helens, U.S.A.	1980	x			xo		x	xo	x	xoΔ◇		xo
Galunggung, Indonesia	1982									◇		
Miyakejima, Japan	1983									◇		
(Unknown, South China Sea)	1986									Δ		
Redoubt, U.S.A.	1989–90									◇		
Hudson, Chile	1991						x	x	x	xΔ◇		x
Pinatubo, Philippines	1991			x						◇		◇
Spurr, U.S.A.	1992							x				x
Unzen, Japan	1991–92	x		xo				x				x

Table 1 (continued)

Volcano and country	Year	Physical damage from proximal hazards					Disruption from volcanic ash					
		Pyroclastic density current	Lava flow	Lahar	Tsunami	Deformation or degassing	Reduced skid resistance	Visibility issues	Marking coverage	Closure or obstruction	Vehicle or engine issues	Derailment (tram)
Tavurvur and Vulcan, Papua New Guinea	1994	x		x			x			x Δ◇	x	
Sakurajima, Japan	1995						x			x		
Ruapehu, New Zealand	1995–96			x			x	x	x	x◇		
Popocatepetl, Mexico	1997									◇		
Soufrière Hills, U.K. (overseas territory)	1997	◇					x					
Reventador, Ecuador	1999									◇		
Pichincha, Ecuador	1999									◇		
Miyakejima, Japan	2000–08					◇						
Etna, Italy	2002–03		x				x	x		x◇		
Reventador, Ecuador	2002						x		x	x◇	x	
Nyiragongo, Democratic Republic of Congo	2002		◇									
Popocatepetl, Mexico	2003									◇		
Anatahan, Mariana Islands	2003–05									◇		
Merapi, Indonesia	2006	x										
Home Reef, Tonga (submarine)	2006									Δ		Δ
Etna, Italy	2006									◇		
Chaitén, Chile	2008			x			x○	x		xΔ◇		xΔ
Okmok, U.S.A.	2008											Δ
Redoubt, U.S.A.	2009											x
Merapi, Indonesia	2010			x			x					
Pacaya, Guatemala	2010						x	x	◇	◇		x
Tungurahua, Ecuador	2010									◇		
Cordón Caulle, Chile	2011			x			x	x		Δ◇		x
Sakurajima, Japan	2011						x		x	○◇		x
Shinmoedake, Japan	2011						x	x		○		x○
Etna, Italy	2013								x	◇		x
San Cristóbal, Nicaragua	2013							x				
Kelud, Indonesia	2014			x			◇	x◇		◇		◇
Sakurajima, Japan	2014								x			
Sinabung, Indonesia	2014						x					
Tungurahua, Ecuador	2014									◇		
Calbuco, Chile	2015							x				
Villarrica, Chile	2015			x								

Southdown and Penrose substations (Deligne et al., 2017). At the time of writing, a diesel shuttle service runs between Papakura and Pukekohe on the Southern Line (Fig. 1). Diesel freight services also operate on the rail network through Auckland (Auckland Transport, 2013a). In many instances rail routes consist of two or three tracks, but their close proximity means that if one is damaged the others are likely to be too (AELP-2, 2014).

2.3. Aviation

The main aviation hub (passenger and cargo) is Auckland Airport (Fig. 1), the largest and busiest passenger airport in New Zealand. It is one of only two civilian airports in New Zealand capable of handling the largest of passenger aircraft. In the Auckland region there is also an aerodrome at Ardmore and Royal New Zealand Air Force (RNZAF) base at Whenuapai, both of which have active airfields (Beca Planning, 2003).

2.4. Maritime

There are three key port sites in Auckland (Fig. 1), referred to in this paper as: the Port of Auckland (the main seaport located in the Waitemata Harbour with cargo and cruise services), the Port of Onehunga (in the Manukau Harbour with a limited cargo service), and the Wiri Intermodal Freight Hub (in Wiri, South Auckland). Many ferry terminals, marinas and boat ramps also serve the region.

3. Methodology and application

The approach used to assess transportation LoS and produce time series maps is shown in Fig. 2. In our methodology, we first consider the geophysical hazards (section 3.1), using hazards in the Māngere Bridge scenario (Deligne et al., 2017) as a basis, to consider the effect on direct damage to the transportation network (section 3.2). This is required to inform the core vulnerability component of our model: LoS metric development for transportation (section 3.3). We then consider the latest emergency and transportation management policies for Auckland to demonstrate how LoS metrics can be applied in a particular location (section 3.4).

3.1. Geophysical hazards

The Māngere Bridge scenario includes an unrest sequence with earthquakes, gas emission and ground deformation, followed by an eruption sequence which includes the six volcanic hazards of edifice formation, pyroclastic surges, tephra, ballistics, lava flows, and tsunami – all are described in Deligne et al. (2017). Potential secondary hazards such as fire and flooding are beyond the scope of this study due to uncertainties in their location and extent. We build upon the extent and severity of hazards in the original scenario by also considering the implications on transportation of different (south-westerly) wind profiles on tephra deposition (section 3.1.1) and a sequence of activity involving unrest with no eruption (section 3.1.2). These additions to the original

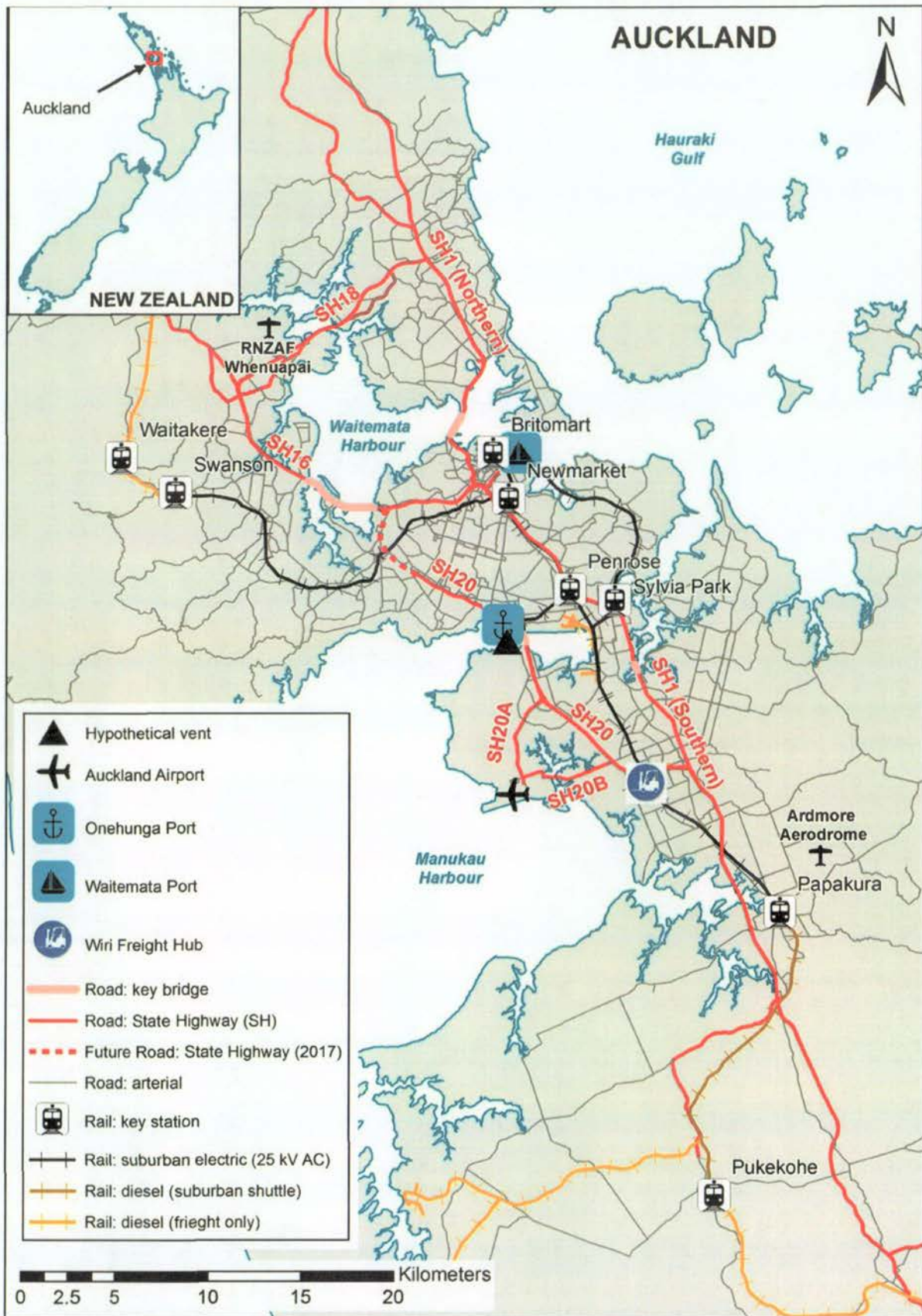


Fig. 1. Major transportation routes and facilities in the Auckland City area. Inset shows location of Auckland City study area within New Zealand.

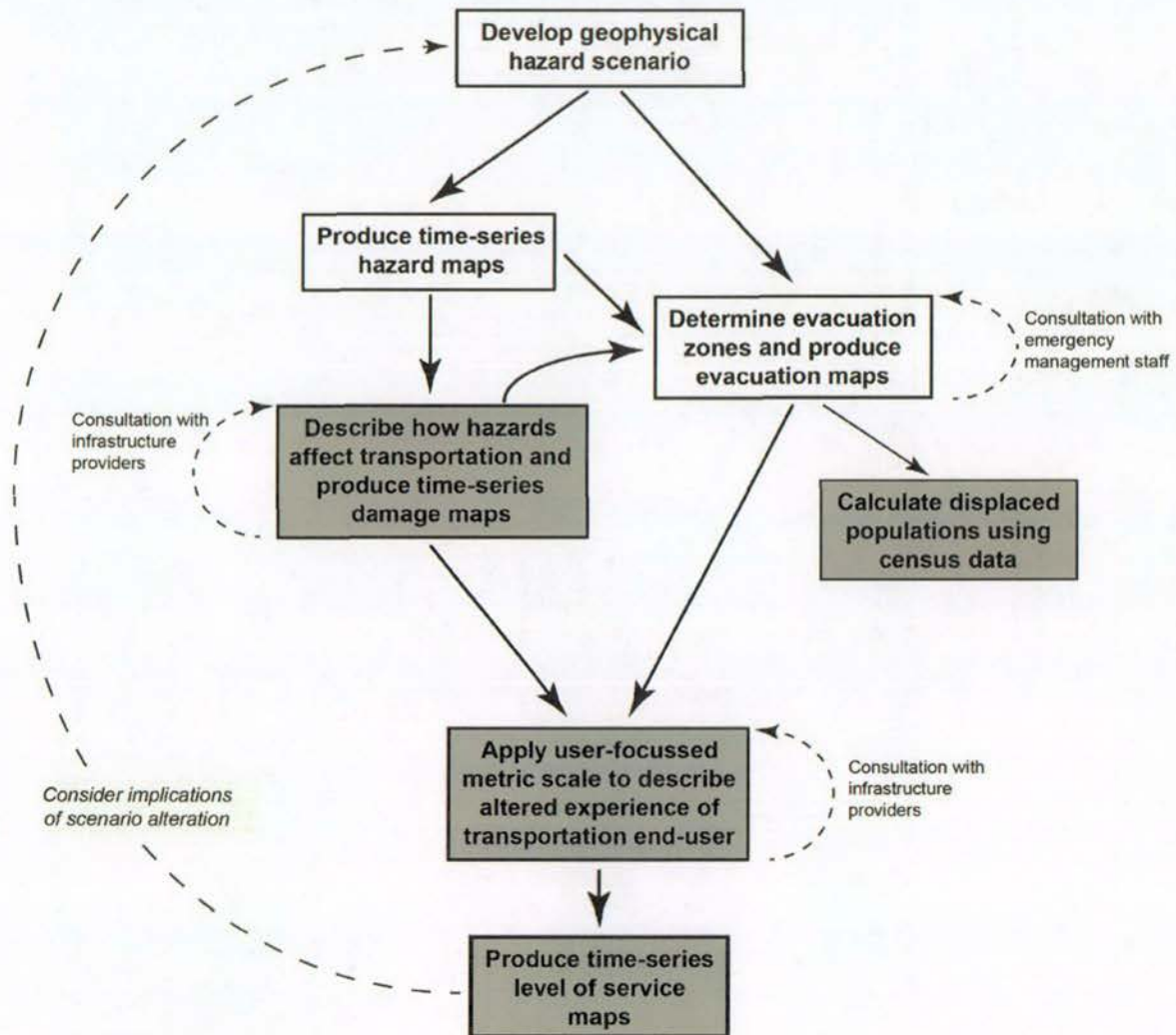


Fig. 2. Summary of methodological approach and processes used to assess transportation Level-of-Service. White-filled boxes indicate work outlined in Deligne et al. (2017). Grey-filled boxes indicate work explored in this paper.

scenario are later used to demonstrate how LoS metrics can be applied in different situations.

3.1.1. Predominant south-westerly wind

As discussed in Deligne et al. (2017), in the Māngere Bridge scenario the tephra dispersal event with the largest hazard footprint has an unusual wind direction for Auckland; the scenario adopted wind profiles for specific dates in March 2014 which may be seasonally constrained and atypical for the city. Therefore, we consider an additional option to the original Māngere Bridge scenario – new wind profiles which represent the predominant wind direction in Auckland, south-westerly winds. We perform additional modelling using the TEPHRA2 program (Bonadonna et al., 2005; Connor et al., 2011) to model ash deposition from the existing eruptive sequence with south-westerly winds prevalent throughout to make comparisons with the previously modelled ash deposition (Deligne et al., 2017) and discuss potential consequences for transportation.

The first south-westerly wind profile was chosen from the New Zealand National Climate Database (NIWA CliFlo) from a random selection of 6-hourly profiles at Auckland Airport within a 10 year period between 01 January 1975 and 31 December 1984 – a similar method to that used by Magill et al. (2006). The date and time of the wind profile selected was 24 January 1976 at 12:00 (Supplementary Material 1).

This wind profile was adopted for TEPHRA2 modelling for the first tephra plume of the scenario (i.e. 14 March PM), with subsequent tephra plumes modelled using corresponding dates between the scenario timeframe and days following the first wind profile; a random time was selected from the 4 NIWA CliFlo wind profile options on each day (Supplementary Material 1). Minor adjustments were made to other TEPHRA2 input parameters to those used in the original Māngere Bridge scenario modelling to most appropriately reflect current knowledge of volcanic ash characteristics that could occur in the AVF using analogue worldwide eruptions. The new suite of tephra parameters (Supplementary Material 2) was adopted for modelling our south-westerly wind addition. The input mass for each eruptive phase was kept consistent with the original scenario and all thicknesses below 0.1 mm were converted to 0 mm as before.

3.1.2. Unrest with no eruption

For the purpose of exploring the consequences of volcanic unrest with no eruption, we adopt the same unrest sequence that occurred during the original Māngere Bridge scenario from 19 February (when small swarms of high frequency non-volcanic earthquakes are detected), through to early on 14 March (where tremor earthquakes and acceleration of deformation occurs). Although this is accompanied by visual observation of cracking near Māngere and an increase in volcanic

gases, no phreatic eruption follows the sequence. From there onwards, we adopt the general sequence of events described in Pallister et al. (2010) for the series of earthquakes that occurred in the Harrat lava province of Saudi Arabia (April–June 2009), attributed to a magmatic dyke intrusion. There is currently no evidence for shallow dyke intrusions or surface ruptures without subsequent eruptions in the AVF. However, we cannot rule out the possibility of this occurring in the future and thus such a scenario is important to consider for emergency planning purposes.

For the unrest scenario, we consider policy outlined in the AVF Contingency Plan (Auckland Council, 2015) and Auckland Evacuation Plan (Auckland Council, 2014) regarding the establishment of Primary Evacuation Zones (PEZs) and Secondary Evacuation Zones (SEZs).

3.2. Physical damage to transportation

We consider the six volcanic hazards in the hypothetical Māngere Bridge eruption and earthquakes associated with prior unrest activity by producing time-series maps that display the physical damage to transportation through the scenario. Each transportation mode is considered separately, as is damage from proximal volcanic hazards and volcanic ash. Deligne et al. (2017) adopted the ‘worst-case’ and ‘average-case’ scenarios for pyroclastic surges. These were originally proposed by Brand et al. (2014), who provide guidance on the physical impact to buildings through the consideration of previous studies, but are used for transportation infrastructure in this paper. We apply expert judgment to consider transportation buildings (e.g. rail stations, port facilities) and linear components of the network (e.g. rail lines, roads) separately, particularly through the application of existing knowledge of transportation impacts by volcanic hazards from field and laboratory observations. We classify the physical damage from pyroclastic surges using radial distance thresholds (established from dynamic pressures) using expert judgment from transportation infrastructure managers.

For earthquakes, we assume minimal direct damage to infrastructure given the relatively modest magnitudes (up to $M_t 4.8$) for the Māngere Bridge scenario, and considering that the New Zealand building code is deemed adequate at a worldwide scale (Daniell et al., 2014). However, some minor blockages from landslides and other debris, and damage to specific components, may occur on the ground transportation network during earthquakes which are shallow and with epicenters nearby. As such, we take a conservative approach and apply the same damage category (“minor damage and blockage possible”) to all roads and rail lines that fall within an area ~5 km from earthquake zone boundaries in the scenario, also including all of the central Auckland area between the two isthmuses.

In areas beyond the zones affected by the edifice, pyroclastic surges and earthquakes, we apply findings from Blake et al. (2016) and Blake et al. (in review a, b) and Wilson et al. (2014) to evaluate physical damage from tephra fall. We designate the same ‘possible damage’ category (section 5.1) adopted for the outer extent of surges (i.e. radial extents with relatively low dynamic pressures) to electric rail lines in these areas. We do not anticipate any direct physical damage to road networks in this area. However, we allocate a distinct category termed ‘no damage (but minor deposit accumulation)’ to road sections affected by this tephra layer, to highlight areas where potential knock-on consequences may exist (for example, subsequent indirect impacts caused by accidents or blockage of stormwater networks). In scenarios elsewhere, where tephra accumulation is more extensive in distal areas, additional physical damage categories should be considered for tephra fall based on laboratory and observational data. For further information on quantifying physical vulnerability to critical infrastructure, including transportation networks, we refer the reader to Jenkins et al. (2014b), Blake et al. (in review c), and Wilson et al. (in review).

Following an eruption, clean-up of the transportation network is required for it to return to full functionality, and also for key site access to maintain or restore other critical infrastructure. In this study, we adopt

the volcanic tephra clean-up model and timeframe examined in Hayes et al. (2015) and Hayes et al. (2017).

3.3. Level-of-Service metric development for transportation

To develop the metric series, we consider the expected disruption resulting from physical damage caused by hazards (section 3.2) and operational activities such as evacuation zoning and area exclusions outlined in the Māngere Bridge scenario. Expert knowledge from transportation infrastructure managers informed the development of metrics. Specifically, LoS metrics for road and rail include the consideration of:

- Destruction of the network by geophysical hazards
- Deposits on the network from geophysical hazards
- Inspection and maintenance requirements (e.g. due to ground shaking)
- Access (e.g. due to evacuation zones or blockage)
- Use of infrastructure for alternative purposes (e.g. rail stations used as shelters).

For road transportation, a single suite of LoS metrics is developed to consider the linear part of the network (i.e. components such as bridges and traffic signals are not considered separately). For the purpose of this study we assume that all road surfaces are sealed, although we recognise that a small proportion may be unsealed with potential variations in impact and clean-up characteristics (Nairn, 2002). LoS metrics are developed around similar principles for the rail line network (i.e. rail tracks and overhead lines which are both equally important to end-users and considered as one in this study). However, rail stations are also critical components, as stations and lines may be impacted and restored differently, and ultimately could affect end-users of rail transportation in different ways; we thus develop separate LoS metrics for rail stations.

We developed LoS metrics for aviation in consultation with the Auckland Airport Compliance and Quality Assurance Manager. The aim was to best describe possible partial or complete closure scenarios for an international airport. We assumed that the location of the arrival/destination city (e.g. whether it is a domestic or international flight) is correlated with the type of aircraft used and scheduling complexities, and that the quantity of flights departing/arriving relative to a benchmark is an appropriate proxy for how well the aviation sector is delivering service. In other words, the metric had to reflect that different operations at an airport have different response capabilities (e.g. international flights will often require more time to change schedules than domestic flights), and that different aircraft types have different airfield requirements.

3.4. Level-of-Service metric application

We illustrate how the LoS metrics can be applied using the Māngere Bridge scenario by considering the spatial and temporal extents of evacuation zones, damage from geophysical hazards, operational priorities, and clean-up that has occurred on sections of the network. LoS metrics in each area are informed by expert judgment, with guidance from local infrastructure managers and emergency management officials taking priority as they often have the best knowledge of the system. Sometimes, overlaying the spatial extent of particular evacuation zones and/or physical damage layer is sufficient to designate a specific LoS metric to sections of the network. However, sometimes a more manual approach is required – for example, where particular routes and facilities are prioritised for reopening to restore vital connections.

We use the Māngere Bridge scenario to display the LoS for end-users of the Auckland transportation network at key stages throughout the hypothetical eruption and its aftermath. We also suggest metric values

for Auckland Airport as the percentage proportion of 'typical capacity' can be estimated.

3.4.1. Road and rail

Due to the relatively large spatial distribution of road and rail networks, we display maps of LoS for these modes of transportation. Road sections are defined as the segments between intersections or highway on/off ramps, and therefore differ in length. Where hazard or evacuation zone boundaries cross road boundaries, the same LoS calculated within the boundary is often extended outside of the zone to the nearest intersection. A similar method is used for rail lines, where the same LoS from within zones is extended out to the nearest station. In comparison, LoS for Auckland Airport, the Port of Auckland and Port of Onehunga, which are single point sources, are only described in text and tables. Following consultation with transportation and emergency management officials in Auckland we make the following assumptions when applying LoS metrics and developing maps:

- Highways and critical arterial roads are prioritised for reopening, especially when restoring a north-south link through the south eastern isthmus is required.
- Only volcanic hazards are responsible for the destruction, damage or functional loss of transportation networks. In reality, particularly for rapid-onset eruptions, substantial human-induced modification may also occur (e.g. the intentional blockage or destruction of some state highway on/off ramps to facilitate contraflow).
- All roads and rail networks may be used for the purposes of evacuating residents when an evacuation zone is first implemented (rail services would only collect passengers and not allow disembarkation at stations within the evacuation zones).
- In some cases, critical road routes may be opened to allow travel through an evacuation zone (with no stopping or exit allowed from the critical routes within the evacuation zone itself).
- The spatial extent of areas affected by direct tephra fall and pyroclastic surge deposits is not extended due to the re-suspension and secondary deposition of deposits (although this is discussed in places).
- Congestion and accidents do not cause any impact on subsequent LoS designations.
- There are no major cascading effects resulting from other critical infrastructure failure or disruption.

3.4.2. Aviation

To determine aviation LoS metrics, we applied New Zealand Civil Aviation Authority (CAA) policy for airspace management during a volcanic crisis (Lechner, 2015) to determine airspace restrictions over the course of the Māngere Bridge scenario (Fig. 3). We then assigned LoS metrics in consultation with the Auckland Airport Compliance and Quality Assurance Manager, making the following assumptions:

- There is progressive closure of Auckland Airport during the unrest sequence.
- Airports are closed when within evacuated zones on the ground (although prioritised reinstatement may occur when they lie close to boundaries of these zones).
- There is minimal aircraft operation within Volcanic Hazard Zones (VHZs), which are established in response to VALs of 1 or greater, and corresponding Notices to Airmen (NOTAMs).¹
- Airfields at RNZAF Whenuapai base and Ardmore Aerodrome can accommodate limited domestic, trans-Tasman and Pacific island traffic, primarily cargo.

¹ Although aircraft are permitted to operate within VHZs during daylight hours and in visual meteorological conditions, this only occurs at the specific request of pilots. Otherwise, air traffic control will not clear an aircraft to operate on any route or procedure that infringes VHZs, and aircraft under radar control will be vectored clear of VHZ boundaries (AIP NZ, 2016).

Our results were then vetted by an Air New Zealand Senior Business Continuity Management Advisor to check that they were realistic. We stress that our work should not be taken as policy endorsement or an indication of how individual airlines would respond in a similar situation.

3.4.3. Maritime

Although we consider the impacts to both port infrastructure and the navigation of ships in harbour areas for the development of LoS metrics, the operation of ports themselves is the main focus for the Māngere Bridge scenario. This was undertaken using best judgment taking into account post-eruption impacts observed elsewhere. Marinas and boat ramps are not considered in this paper. Similar to our approach for applying LoS metrics for Auckland Airport, we only describe LoS for the Port of Auckland and Port of Onehunga in text and tables (rather than on maps) as they are point sources.

3.4.4. Evacuation and displaced populations

As transportation LoS is strongly influenced by the establishment and alteration of evacuation zones, we consider the consequences of the evacuations summarised in Deligne et al. (2017) with regard to the number of residents impacted and considerations for transportation demand. Consultation with emergency management staff in Auckland confirmed that throughout eruptions such as in our scenario, the national emergency management body in New Zealand (Ministry of Civil Defence and Emergency Management; MCDEM) and Auckland CDEM would work alongside infrastructure providers to assess when cordoned areas can be entered for clean-up, repair and maintenance (Auckland Council, 2015). CDEM, through the provisions of the CDEM Act (2002), can grant concessions for staff to access evacuation areas to expedite reinstatement of critical services. Thus, while evacuated areas are off limits to residents and businesses, infrastructure providers such as transportation management authorities will sometimes be able to temporarily enter during lulls in volcanic activity, especially since activity in the AVF could continue for months to years (Sherburn et al., 2007). Consultation with transportation infrastructure providers in Auckland highlighted that the Southern Motorway (SH1) would remain open whenever possible, albeit at limited capacity with access restrictions, even when it is within officially evacuated zones.

The number of residents displaced by evacuation and exclusion zones is calculated using night-time resident population data. For the Māngere Bridge scenario, we use data collected in the 2013 New Zealand Census (Statistics New Zealand, 2013). Rather than an estimate of those who reside within the exact extent of the evacuation zones, we adopt census meshblock² values using all meshblocks that fall within and intersect the zone boundaries and round values to the nearest hundred (Fig. 4). This is deemed to be a more accurate representation as the true extent of any evacuation zone will likely reach beyond the initially designated extent in places due to features on the ground such as roads, potentially isolated neighbourhoods, and large property boundaries. Accounting for the number of businesses displaced by evacuation zones is beyond the scope of this study.

4. Level-of-Service metrics

The suites of LoS metrics developed for road, rail stations, rail lines and ports are shown in Tables 2–5 respectively.

Consultation with transportation infrastructure managers suggested that lower speed restrictions may be imposed for LoS metric codes II and III for roads, with temporary traffic management measures such as additional signage, cones and/or barriers. Road metric codes IV and V would

² A meshblock is the smallest geographic unit for which statistical data is collected and processed by Statistics New Zealand. Meshblocks in Auckland have a median land area of 0.039 km².

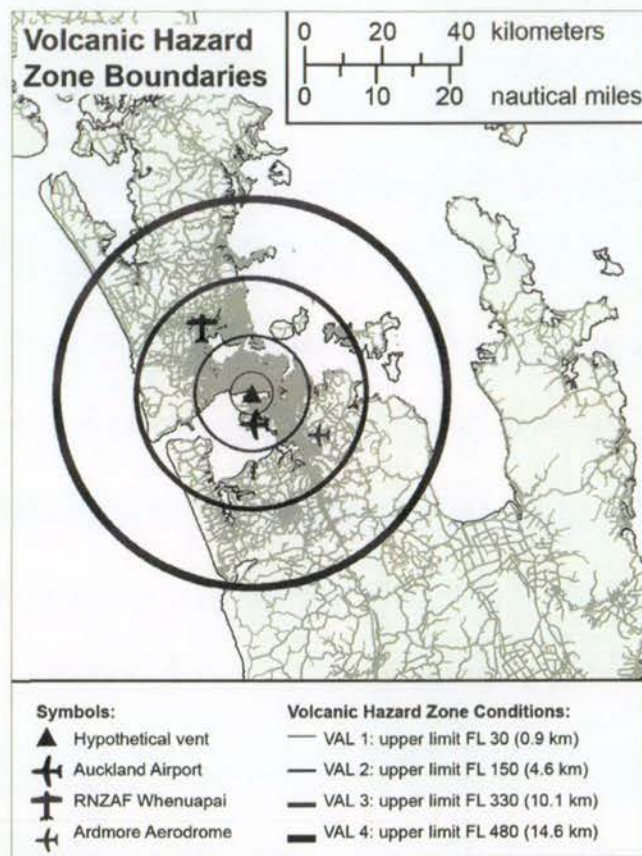


Fig. 3. Hypothetical Volcanic Hazard Zone boundaries for the original Māngere Bridge scenario based on VALs (using zone radii of 3, 8, 16, and 27 nautical miles for VAL 0 and 1, 2, 3, and 4 respectively; Lechner, 2015). The legend indicates the Flight Level (FL) below which pilots require specific permission to enter VHZs. For example, at VAL 0 or 1, pilots require permission to enter areas below FL 30 within 3 nautical miles of the volcanic vent.

require major traffic management with signed diversions and potential presence of officials, such as Police or Military personnel, and/or physical measures, to ensure compliance. We note that there might be occasional overlaps between metrics. For example, as indicated by the italic text for metric IIIa (Table 2), critical routes may be restored through evacuation zones with access restricted (due to operational purposes rather than any deposits) onto and off these routes through the zones themselves. However, deposits may also reduce the LoS somewhat in such areas (e.g. tephra may remain from previous falls or accumulate through secondary deposition from remobilised material – i.e. metric code IIb). Where such overlaps occur, we suggest that the routes of interest be allocated the metric with the largest overall LoS reduction.

Different suites of metrics are presented for rail stations and lines as the separate components of the rail system could affect end-users in different ways. As with roads, there may be slight overlaps between LoS metrics. For example, evacuation services may also be non-stopping when travelling through much of the evacuation zone. Again, best judgment should be used to determine the largest impact on service and most appropriate LoS metric.

For aviation, the LoS is described slightly differently. We consider domestic and international destinations separately. As we focus our studies in New Zealand, we also consider 'trans-Tasman and Pacific island routes' which refers to flights between New Zealand and eastern Australia and some South Pacific island nations. For each market, the LoS is the percent capacity of flights relative to normal airport operations for the time of year. Thus, a LoS metric for aviation could be 50% capacity in the domestic market – this means that half of domestic

flights that are normally scheduled to land and depart from the airport are able to do so.

The effects of congestion, accidents and breakdowns on traffic flow are not directly considered for the LoS metrics provided in this study. Although we recognise that such impacts could be substantial at times, further work is required to more accurately understand travel behavior during ashfall to make estimations of traffic demand and flow. Various other constraints will be required to make such estimations including the time of day or day of the week (Tomsen et al., 2014), and considerations of new transportation projects in the area of interest.

5. Results and discussion – Māngere Bridge scenario

5.1. Physical damage

The physical damage to road and rail networks from volcanic hazards which occur in the original Māngere Bridge scenario is summarised in Table 6, with maps to illustrate the damage in Fig. 5 (roads) and Fig. 6 (rail).

Most physical damage to road and rail transportation results from the initial pyroclastic surge on 14 March in the scenario, which was derived from the following radial damage thresholds:

- Destroyed: <0.5 km (average-case), <2.5 km (worst-case)
- Severe damage/complete blockage: 0.5–2 km (average-case), 2.5–4 km (worst-case)
- Some damage/minor blockages: 2–4 km (average-case), 4–6 km (worst-case).

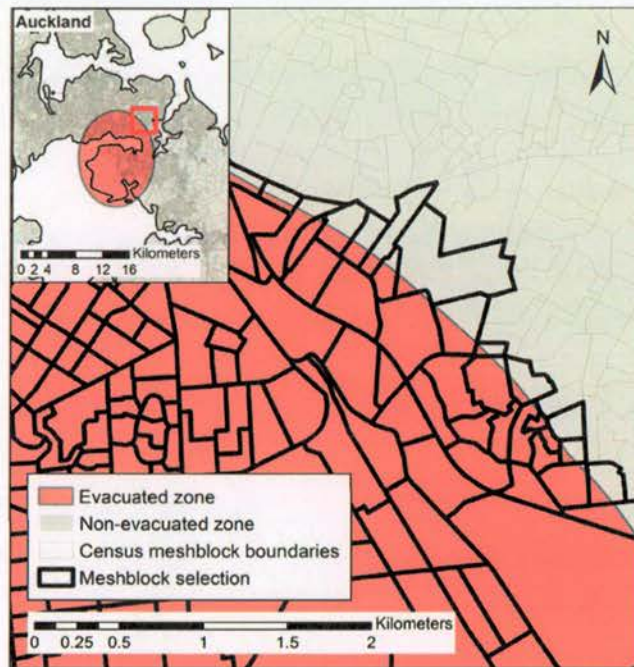


Fig. 4. Example calculation of displaced populations using census meshblocks (using the Primary Evacuation Zone on 21–30 April for the scenario involving unrest but no eruption). In this case, the thick boundaries indicate the census meshblocks which would be used to calculate the population displaced by the evacuation zone (i.e. night-time resident populations in the meshblocks either completely inside the evacuation zone or which intersect the evacuation zone boundary).

We note that surges in other locations may require the modification of radial distance thresholds, considering the dynamic pressures expected from different eruption styles, and specific infrastructure types.

Other damage and potential blockage of networks in our scenario results from ground shaking due to earthquakes and tephra fall. These effects are generally more temporary with road-cleaning and inspections occurring soon after each hazard where possible to restore functionality. The general priority is to repair and maintain critical north–south links through the south eastern isthmus. However, the effects of ash remobilisation on transportation could be substantial and extend the

Table 2
Road network Level-of-Service metrics. Metrics are descriptive, and the codes are simply used as references and do not necessarily indicate incremental differences in network availability.

Metric code	Road Level-of-Service	Example situations that could lead to LoS
I	Full service – road fully open	
IIa	Reduced service with no direct deposits (no access restrictions)	<ul style="list-style-type: none"> • Inspection requirements following ground shaking • Preparatory road maintenance or traffic control measure.
IIb	Reduced service due to direct deposits (no access restrictions)	<ul style="list-style-type: none"> • Minor tephra accumulation (0.1–5.0 mm)
IIIa	Access restrictions with no direct deposits	<ul style="list-style-type: none"> • New evacuation zone being implemented (e.g. one-way travel to outside of zone) • Critical routes through evacuation zones (with hazard thresholds for immediate re-closure)
IIIb	Access restrictions due to direct deposits	<ul style="list-style-type: none"> • Moderate to severe tephra accumulation (>5.0 mm) • Pyroclastic surge, lava flow and lahars
IV	Critical infrastructure and maintenance staff access only	<ul style="list-style-type: none"> • Lull in volcanic activity before or during an eruption (within evacuation zone)
V	No service – road closed to all	<ul style="list-style-type: none"> • Road infrastructure destroyed or severely damaged beyond repair • Road closed due to being in evacuated area

temporal and spatial extent of impacts. Detailed ash resuspension modelling, such as that conducted by Reckziegel et al. (2016), would be required to investigate these impacts more fully.

Auckland Airport does not encounter any direct physical damage from any volcanic hazards over the course of the scenario. However, it is indirectly impacted by restricted access (due to evacuation zoning, and volcanic hazards affecting nearby roads), airspace restrictions, and physical damage to other critical infrastructure such as the wastewater system (Stewart et al., in press).

Only one of the ports in Auckland, the Port of Onehunga, the smallest and arguably least important of the facilities, is directly impacted by geophysical hazards in the original Māngere Bridge scenario. However, the facilities at the port are closed due to the effects of evacuation zoning (on 08 March) before being destroyed by pyroclastic surges (on 14 March), which results in permanent closure. The eruption changes the landscape where the Port of Onehunga used to be and also devastates the local built environment. A rebuild would not be practical at the same site because the area becomes landlocked. However, it is possible that another port elsewhere in the Manukau Harbour, or indeed somewhere else in the Auckland region, would be built.

Table 3
Rail station Level-of-Service metrics.

Metric code	Rail station Level-of-Service	Example situations that could lead to LoS
I	Full service - station fully open	
II	Partial service	<ul style="list-style-type: none"> • Evacuation - no exit from stopping trains, i.e. entry-only • Limited station facilities due to volcanic hazard damage (e.g. shelter, ticketing, retail)
III	Only used for different purpose	<ul style="list-style-type: none"> • Line damage renders station inoperable for rail network (other purposes may include shelter from tephra fall, evacuation welfare facility, and temporary bus stop)
IV	No service - station closed	<ul style="list-style-type: none"> • Station destroyed or severely damaged beyond repair • Station closed due to being in evacuated area

Table 4
Rail line Level-of-Service metrics.

Metric code	Rail line Level-of-Service	Example situations that could lead to LoS
I	Full service – line fully open	
II	Restricted service	<ul style="list-style-type: none"> • New timetabling with fewer services • Speed restrictions due to minor airborne ash
III	Rolling/temporary outage	<ul style="list-style-type: none"> • Temporary damage to components due to ground shaking or deposits • Inspection requirements • Re-distribution of fleet
IV	No stopping service	<ul style="list-style-type: none"> • Evacuations require transportation of people through evacuated areas • Severe damage to stations and surrounding infrastructure but line operable
V	Evacuation service only	<ul style="list-style-type: none"> • Evacuations require special service to transport residents from newly established evacuation zone
VI	No service – line closed	<ul style="list-style-type: none"> • Line destroyed or severely damaged beyond repair • Line closed due to being in evacuated area

The Port of Auckland at Waitemata Harbour is not directly impacted in the original Māngere Bridge scenario; no major damage or substantial LoS reduction is expected from earthquakes, and tephra accumulation over much of The Port of Auckland on 21 March is <1 mm thick, which is not deemed substantial enough to close port operations (although indirect impacts such as access restrictions may have cascading implications for port operations). However, different wind directional profiles may have consequences for tephra thicknesses at the port and subsequent LoS (section 5.4.1).

5.2. Level-of-Service

Table 7 details the considerations for assigning LoS metrics to the road and rail (station and line) network, and to Auckland Airport over the course of the scenario. This is followed by a selection of associated time-series maps for road (Fig. 7) and rail (Fig. 8) to illustrate LoS metrics at key stages in the scenario, in addition to a table to show specific LoS metric values (based on capacity and guided by policy) for Auckland Airport (Table 8).

Importantly, the LoS for all transportation modes is affected by evacuation zoning before the modes are impacted by geophysical hazards and experience any physical damage. LoS reductions occur from 08 March onwards for all modes, the scenario date when the first PEZ is implemented. This includes the closure of a major highway (SH20), which is expected to lead to increased traffic on alternative arterial and highway routes. In the Māngere Bridge scenario road and rail encounter the greatest overall LoS loss on 13 and 14 March, and all north-south ground transportation links across the south eastern isthmus are blocked at this time. Some service is restored on 16 March, although subsequent tephra fall and threat of surges on 21 March causes secondary temporary disruption. The strength and direction of wind on 22

Table 5
Port Level-of-Service metrics.

Value	Port Level-of-Service	Example situations that could lead to LoS
I	Full service – port fully open	
II	Partial service	<ul style="list-style-type: none"> • Volcanic deposits affect operations at the port or navigation of vessels • Evacuation zone affects some navigation routes • Staff unable to access port facilities
III	No service – port closed	<ul style="list-style-type: none"> • Port destroyed or severely damaged beyond repair • Severe sedimentation in shipping channels means vessels cannot operate • Port closed due to being in evacuated area

March in the Māngere Bridge scenario mean that the impact of tephra fall then is minimal, and restoration is possible again from this date forward. However, full restoration takes several weeks for most road and rail transportation networks in the area extending 4 km radially from the vent, even following the end of effusive activity. Some infrastructure within 2 km of the vent is permanently destroyed.

LoS reduction also starts on 08 March at Auckland Airport. From 08 March to 01 May, VALs determine the volume of airspace affected by volcanic ash, described by NOTAMs that invoke VHZs. During this time, air traffic control will not clear aircraft to operate on routes that infringe a VHZ, unless specifically requested by the pilot during daylight hours only (AIP NZ, 2016). Auckland Airport is only within evacuated areas on the ground from 11 to 15 March. Ardmore and Whenuapai airfields are outside evacuated areas for the duration of the scenario and are within VHZs for shorter periods than Auckland Airport; they may be used for some aircraft diversions from Auckland Airport at times. As the Auckland Airport runway is roughly oriented east-west and the Māngere Bridge scenario vent location is to the north, the flight approach shouldn't be substantially compromised by the VHZ implemented at VAL 1. However, airport officials indicated that it would take a few days for international airlines to start flying into Auckland again once they are allowed to land, in part due to the time it would take to reorganise schedules and redistribute aircraft.

Onehunga Port closes on 08 March when it falls within evacuation zones, and all vessels are diverted elsewhere (i.e. LoS metric code III). No LoS is restored in the same location as the port is subsequently destroyed by pyroclastic surges from 14 March onwards.

We do not apply metric code III ("only used for a different purpose") for rail stations for any of the timesteps in the scenario. This is because stations that are inoperable for rail operations often fall within evacuated areas and would thus not be suitable for any other purpose. Additionally, the detailed information required to allocate this metric is beyond the scope of this paper. Similarly, metric code II for rail lines ("restricted service") has only been allocated where speed restrictions are expected due to minor airborne deposits; consultation with rail network managers suggested that speeds of 40 km h⁻¹ would be typical in such situations on Auckland's network. Restrictions are likely on other sections of the network during this scenario. However, often the more severe LoS reduction of "rolling outages" (i.e. metric code III) occurs at the same time and we adopted this metric where the two exist simultaneously. Timetabling restrictions may occur at times across other parts of the suburban network. However, as we do not consider knock-on consequences in detail in this study and as rail demand is unknown, the potential for new timetabling is simply noted in Table 7 and the associated LoS metric (i.e. metric code IV for rail lines) is not displayed on Fig. 8. In future scenarios involving a predominantly diesel fleet, which is impacted by minor tephra fall, metric code II should be considered over code III in some situations due to the potentially higher resilience of diesel locomotives (over electric alternatives) in such conditions. However, observational data of such impacts is limited and we suggest a conservative approach be taken (adopting the more severe of the two LoS metrics) in situations where epistemic uncertainty is high.

Specific LoS metric values are not calculated for road or rail networks for the Māngere Bridge scenario. Although we do make calculations for the expected numbers of displaced residents due to evacuation zones with potential implications for transportation (section 5.3), further work is required to more accurately understand the impacts on traffic demand and flow and thus allow estimations of proportional network availability from what is typical in Auckland. Furthermore, new transportation projects in the city (e.g. Waterview Connection (NZTA, 2016a); City Rail Link (Auckland Transport, 2016); East West Link (NZTA, 2016b)) may have substantial impacts on network capacity with knock-on implications for traffic demand and flow. Nonetheless, the allocation of LoS metric descriptors using a scenario approach as demonstrated in this study is an important contribution in representing the disruption encountered by transportation end-users.

Table 6

Physical damage to road and rail networks from geophysical hazards examined in Deligne et al. (2017). A more detailed version of the table, showing network specifics to Auckland can be found in Supplementary Material 3.

Scenario date	Event specifics	Road physical damage	Rail physical damage
22 February	VAL increases from 0 to 1	None	None
08 March	08 March Primary Evacuation Zone (PEZ)		
11 March	11 March PEZ		
12 March	12 March Secondary Evacuation Zone (SEZ)		
13 March	Volcanic gases detected Shallow earthquakes (up to $M_L4.5$)	<ul style="list-style-type: none"> Potential minor damage and blockages possible (inspections may be required) Length of road in impacted area ~2900 km 	Rail stations: <ul style="list-style-type: none"> None Rail lines: <ul style="list-style-type: none"> Potential damage and blockage on suburban electric network (inspections required) Southern part more susceptible to ground-shaking due to peat and ash geology
14 March AM	Pyroclastic surge causes complete destruction 0–4 km from vent and some damage 4–6 km from vent. Shallow earthquakes (up to $M_L4.5$)	<ul style="list-style-type: none"> Road infrastructure destroyed or severely damaged 0–4 km from vent Some road infrastructure damaged with major blockages 4–6 km from vent Additional damage/blockage the same as 13 March 115 km destroyed 202 km severely damaged with complete blockage. 457 km some damage and major blockages	Rail stations: <ul style="list-style-type: none"> Two stations close to vent destroyed or severely damaged beyond repair Possible damage to stations 4–6 km from vent Rail lines: <ul style="list-style-type: none"> Lines up to 4 km from vent destroyed or severely damaged Possible damage to lines 4–6 km from vent Potential damage and blockage on suburban electric network (inspections required)
14 March PM	Tephra fallout to west Shallow earthquakes (up to $M_L4.8$)	(Also see Fig. 5a) <ul style="list-style-type: none"> Tephra deposition on some minor roads to west of vent Additional damage/blockage the same as 13 March 163 km outside of the initial surge area experiences direct tephra deposition	Rail stations: (same as 14 March AM) Rail lines: (same as 14 March AM) Tephra fall to west does not directly fall on the rail network. Remobilised ash may reach some lines but no impacts are anticipated.
16 March	11 March PEZ and 12 March SEZ lifted 16 March PEZ and 16 March SEZ implemented	Remobilised ash may extend to roads beyond the area mentioned but no substantial impacts are anticipated. <ul style="list-style-type: none"> Minor accumulation of deposits remains on cleaned sections including critical routes through SEZ. Other sections within initial surge area remain destroyed, damaged or blocked. Tephra deposition is cleaned-up or removed by rainfall beyond the SEZ extent. Any minor damage from previous earthquakes has been repaired with no further impacts to the road network at this stage. (Also see Fig. 5b)	Rail stations: (same as 14 March AM) Rail lines: <ul style="list-style-type: none"> Damage within 6 km from vent remains same as 14 March AM Any damage to components from previous earthquakes is repaired with no impact to the rail network beyond 6 km from the vent at this stage. (Also see Fig. 6b) Rail stations: (same as 14 March AM)
21 March	Tephra fallout to north west Pyroclastic surge	<ul style="list-style-type: none"> Some further accumulation of surge and tephra deposits up to 6 km from vent Tephra deposition on roads to north west of SEZ 984 km road beyond the initial surge area experiences tephra accumulation. Thus, a total of 1758 km of road is impacted at this stage (the largest extent throughout the scenario).	Rail lines: <ul style="list-style-type: none"> Damage within 6 km from vent remains same as 14 March AM Possible damage to rail components on lines affected by tephra fall to north west of SEZ Initial damage from ash accumulation beyond the SEZ is fixed by late on 22 March. However, some failures may continue due to ash remobilisation on the network.
30 March	Tephra fallout to south east	<ul style="list-style-type: none"> Only minor accumulation of deposits on cleaned critical routes All other roads within initial surge area remain destroyed, damaged or blocked to some degree. (Also see Fig. 5c)	Rail stations: (same as 14 March AM) Rail lines: (same as 16 March, before tephra fall) (Also see Fig. 6c) Rail stations:
05 April	Lava flows 16 March SEZ lifted	<ul style="list-style-type: none"> Continued clean-up of remobilised tephra, means only minor accumulation of deposits remains on many critical routes. All other roads within initial surge area remain destroyed, damaged or blocked to some degree, although are widely accessible from this date for clean-up following the lifting of the SEZ.	Rail stations: (same as 16 March, before tephra fall) Rail lines: (same as 16 March, before tephra fall) <ul style="list-style-type: none"> Two stations closest to vent remain destroyed by initial surge. Previous damage to other stations within 6 km of vent is repaired.

(continued on next page)

Table 6 (continued)

Scenario date	Event specifics	Road physical damage	Rail physical damage
01 May	16 March PEZ lifted Permanent exclusion zone implemented	<ul style="list-style-type: none"> Restoration has occurred beyond the extent of the severe damage/complete blockage zone caused by the initial surge (0–4 km from the vent) <p>The road length in this area at the start of the scenario was 305 km</p>	<p>Possible damage from tephra continues 4–6 km from vent until clean-up prevents further remobilisation and infiltration.</p> <p>Rail stations: (same as 05 April) Rail lines:</p> <ul style="list-style-type: none"> Lines remain destroyed up to 4 km from vent <p>Demand to reconstruct the infrastructure required to reopen the above section of the line is expected to be low. The stations and line may be decommissioned or relocated based on rebuild activities</p>

5.3. Displaced populations and consequences for transportation

Displaced population numbers during the Māngere Bridge scenario resulting from the evacuation zones of Deligne et al. (2017) are shown in Table 9. We expect some residents beyond official evacuation zone boundaries will also evacuate, causing a shadow evacuation effect. The concept of shadow evacuation in Auckland aligns with discussions

in Tomsen et al. (2014) and with findings from a recent risk perception survey conducted in the city (Coomer et al., 2015). As indicated in Deligne et al. (2017), there may also be self-evacuations before official evacuation zones are established and different evacuation conditions for some patients in major hospitals. However, the numbers of self-evacuees and relevant patients is unknown and not shown in Table 9.

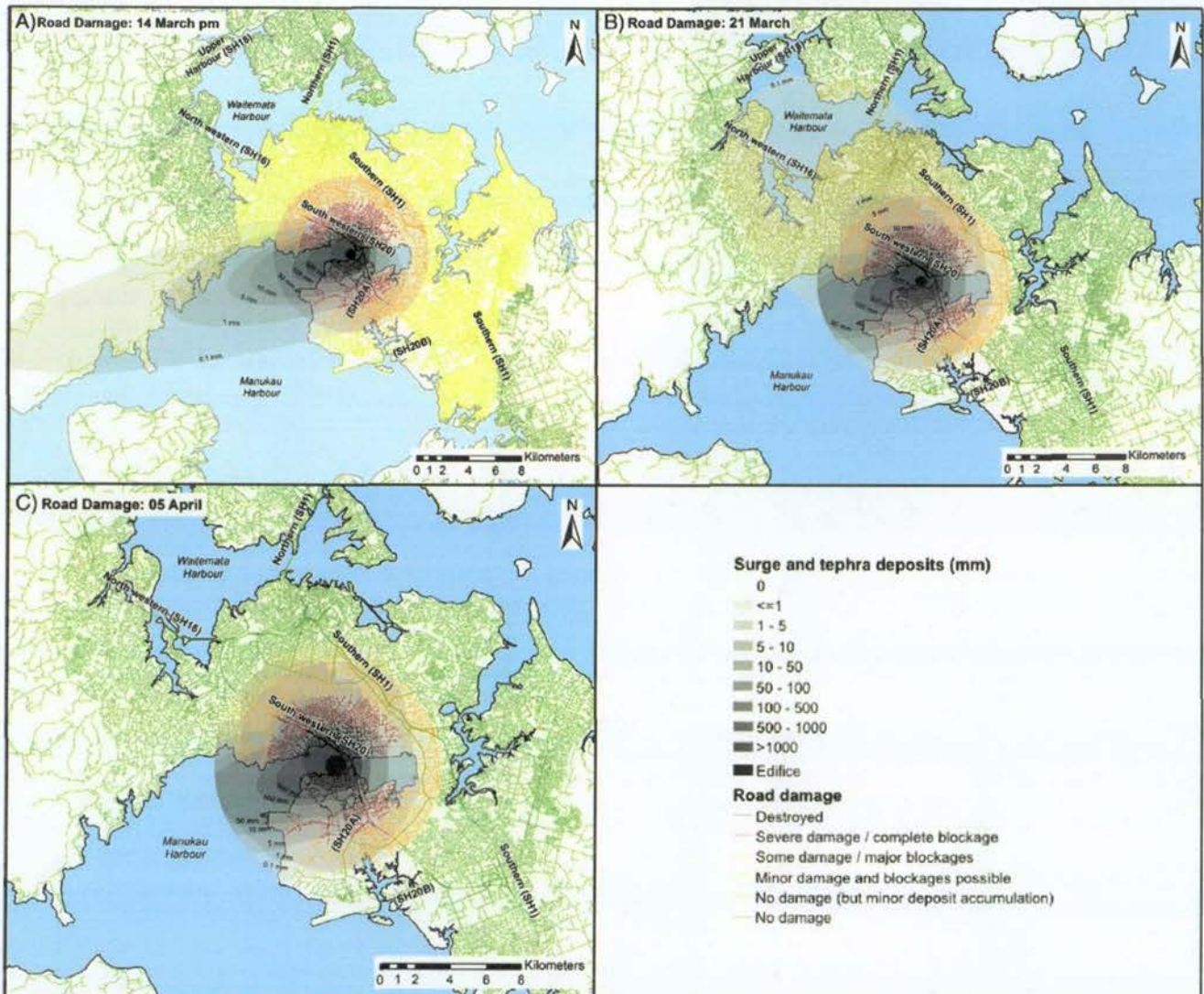


Fig. 5. Physical damage to the road network at a selection of key times during the scenario. Note that the full series of physical damage road maps can be seen in Supplementary Material 4.

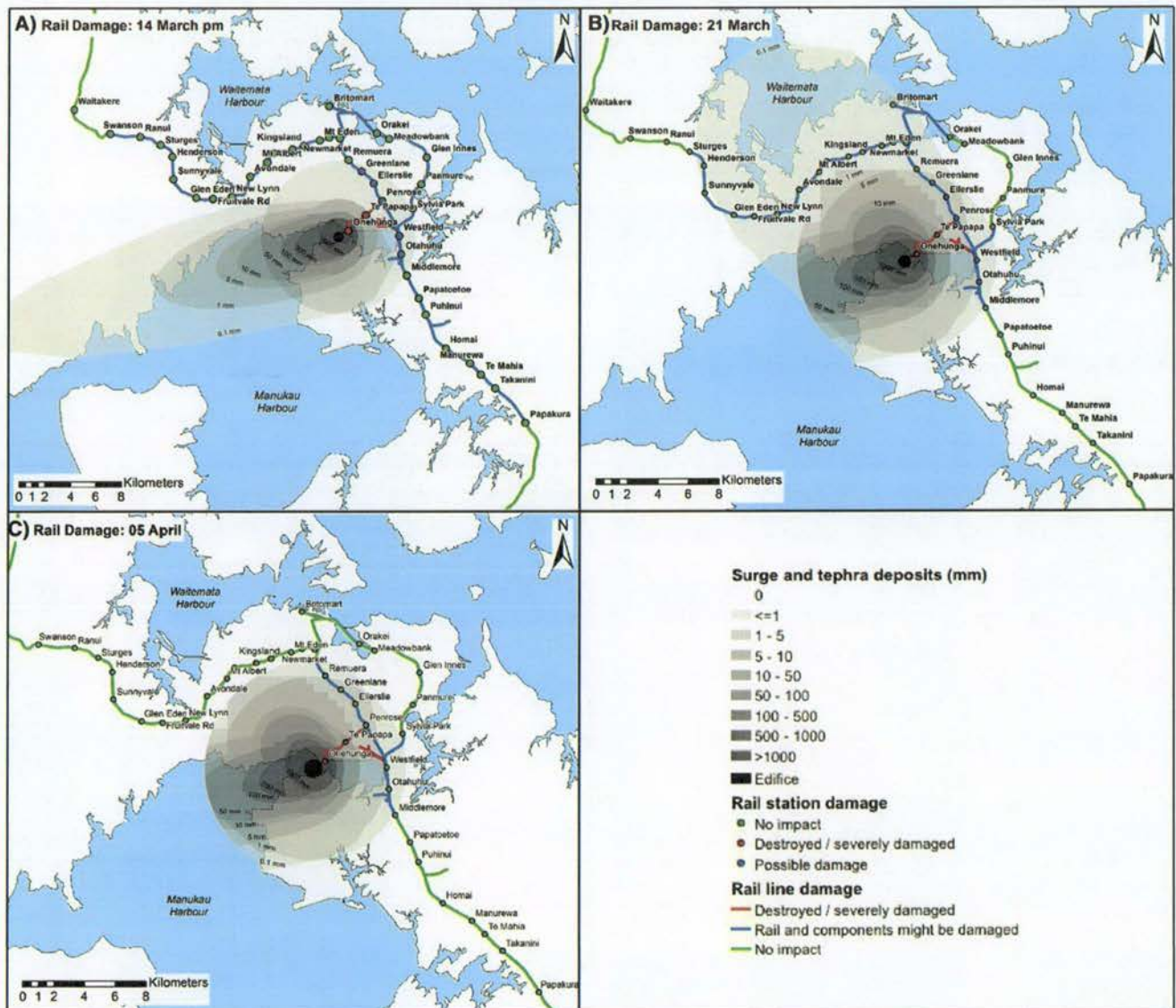


Fig. 6. Physical damage to the rail network at a selection of key times during the scenario. Note that the full series of physical damage rail maps can be seen in Supplementary Material 5.

During volcanic activity in the Māngere Bridge scenario, large populations are evacuated, with the highest displacement totals on 12–15 March. Emergency management officials may try to encourage evacuations in a progressive manner in some eruptive situations, particularly to minimise traffic disruption. Auckland road network operators indicated that during evacuations from city areas in Auckland, on-ramp signals to highways will likely be set to operate on typical peak weekday evening settings with the aim of assisting traffic flow along highways but potentially causing additional congestion along arterial routes that lead to highways. Evacuation zone boundaries would usually be managed so that residents are prevented access to their homes. Business owners and workers would also be prevented from accessing their properties, which can have cascading impacts on other businesses due to disruptions in the supply chain. Transportation may be impacted in such situations through having to relocate headquarters or operation centres, and from disruption to the supply of materials or components required for transportation maintenance or repair. Additionally, businesses can suffer when staff members are displaced or have uncertainty in their living situation, an important consideration for all

transportation operators and highlighted several times through consultation. For example, further transportation disruption would result if there are shortages of pilots, train drivers, rail maintenance crew or officials that control traffic flow and manage accidents.

5.4. Alternative scenario considerations

We applied our methods for determining damage and LoS to assess the consequences of modifications to the geophysical hazard sequence in the original Māngere Bridge scenario, specifically different wind directions and unrest with no eruption. This allows us to assess differences in societal outcomes, particularly related to transportation.

5.4.1. Predominant south westerly wind

Tephra deposits from the same individual eruptions as in the original Māngere Bridge scenario (Deligne et al., 2017), but modelled in TEPHRA2 using the south westerly wind profiles (Supplementary Material 1), are shown in Fig. 9. No change to impact or LoS at Auckland Airport is expected from the different tephra deposition, with most

Table 7

Level-of-Service descriptions for Auckland's road, rail and airport transportation networks over the course of the Māngere Bridge scenario. A more detailed version of the table, showing network specifics to Auckland can be found in Supplementary Material 6.

Scenario date	Event specifics	Road Level-of-Service	Rail Level-of-Service	Airport Level-of-Service
22 February	VAL increases from 0 to 1	Full service Note. Some self-evacuation and preparation for evacuation may lead to increase in traffic congestion.	Full service Some self-evacuation may lead to increase in passengers and delays at stations.	Auckland Airport starts making plans for a potential closure.
08 March	08 March PEZ implemented VAL increases from 1 to 2	<ul style="list-style-type: none"> • Evacuations occur from the PEZ. Access becomes restricted for most entering the zone. Some critical lifelines staff can still enter. • All road transport between north and south Auckland is disrupted. All other infrastructure remains fully operational, although some measures may be implemented to control evacuation flow. 784 km road affected by 08 March PEZ	Rail stations: <ul style="list-style-type: none"> • Partial service within PEZ Rail lines: <ul style="list-style-type: none"> • Evacuation service only on lines within and intersecting PEZ (with speed restrictions) Restricted service may occur on the remaining suburban electric rail network from now onwards due to timetable changes and redistribution of fleet.	Auckland Airport issues NOTAM indicating airport closure. Minor domestic traffic at other airfields in Auckland. Most domestic traffic possibly diverted outside of region.
11 March	11 March PEZ implemented	<ul style="list-style-type: none"> • No access to roads affected by the initial PEZ on 08 March except critical lifelines staff • Evacuations occur from a new PEZ section in the Māngere area. Access is restricted for most. 1019 km road is now affected by the new wider (11 March) PEZ.	Rail stations: <ul style="list-style-type: none"> • Stations within 08 March PEZ now closed • Partial service within newly established PEZ area Rail lines: <ul style="list-style-type: none"> • Lines affected by 08 March PEZ now closed • Evacuation service only on lines affected by new PEZ area Diesel freight through-traffic ceases	Auckland Airport issues NOTAM indicating that the airport is within evacuation zone
12 March	12 March SEZ implemented	<ul style="list-style-type: none"> • No service (roads closed) in area covered by 11 March PEZ • Evacuations occur from SEZ with restricted access for most. • Some measures may be implemented elsewhere to control evacuation flow 1415 km road is now affected by evacuation zones (11 March PEZ and 12 March SEZ).	Rail stations: <ul style="list-style-type: none"> • Stations affected by 08 and 11 March PEZ now closed • Partial service within newly established SEZ Rail lines: <ul style="list-style-type: none"> • Lines affected by 08 and 11 March PEZ now closed. • Evacuation service only on lines affected by new SEZ Rail stations: <ul style="list-style-type: none"> • Stations within evacuation zones closed Rail lines: <ul style="list-style-type: none"> • Lines directly affected by evacuation zones closed • Rolling outages on remainder of suburban network 	
13 March	Volcanic gases detected Shallow earthquakes (up to $M_L 4.5$)	<ul style="list-style-type: none"> • No service (roads closed) in area covered by 11 March PEZ and 12 March SEZ • Reduced service possible on roads impacted by ground shaking from earthquakes 	Rail stations: <ul style="list-style-type: none"> • Stations within evacuation zones closed Rail lines: <ul style="list-style-type: none"> • Lines directly affected by evacuation zones closed • Rolling outages on remainder of suburban network 	
14 March AM	Pyroclastic surge causes complete destruction 0–4 km from vent and some damage 4–6 km from vent. Shallow earthquakes (up to $M_L 4.8$) VAL increases from 2 to 3	<ul style="list-style-type: none"> • LoS in morning remains the same as 13 March Impact on electricity transmission and distribution may affect road LoS for the entire Auckland region.	<ul style="list-style-type: none"> • LoS remains the same as 13 March. 	No air traffic in or out of Auckland Airport
14 March PM	Tephra fallout to west VAL increases from 3 to 4. Clean-up outside of SEZ begins (for ~ 1 day) Some critical routes also cleaned through SEZ	<ul style="list-style-type: none"> • Tephra in afternoon causes reduced LoS on some arterial and minor roads to west of vent. 		
16 March	11 March PEZ and 12 March SEZ lifted 16 March PEZ and 16 March SEZ implemented VAL 2 (after reducing to 3 on 15 March)	<ul style="list-style-type: none"> • Road service restored on roads beyond new 16 March PEZ and SEZ extents • Partial road service on some critical routes through evacuation zones during daytime • No service on all other roads within PEZ and SEZ 	Rail stations: <ul style="list-style-type: none"> • Station within new evacuation zones closed Rail lines: <ul style="list-style-type: none"> • No service on all other roads within PEZ and SEZ 	Auckland Airport issues NOTAM indicating it is no longer in evacuation zone but that airport remains closed

Table 7 (continued)

Scenario date	Event specifics	Road Level-of-Service	Rail Level-of-Service	Airport Level-of-Service
21 March	Tephra fallout to north west Pyroclastic surge. VAL 4 (after increasing to 3 on 18 March)	<ul style="list-style-type: none"> No service (roads closed again) through PEZ and SEZ due to threat from surge and tephra fall Tephra deposition causes reduced service on many roads to north west of SEZ. 	<ul style="list-style-type: none"> Lines within or intersecting new PEZ closed No stopping (with speed restrictions) occurs through new SEZ <p>Some diesel freight services restored with restrictions due to operational infrastructure damage.</p> <p>New timetabling may be implemented on remainder of suburban rail network.</p> <p>Rail stations:</p> <ul style="list-style-type: none"> (same as 16 March) <p>Rail lines:</p>	Volcanic eruption resumes. No air traffic in or out of Auckland Airport
22 March	Tephra VAL reduces to 3 Clean-up outside of PEZ and SEZ begins (for ~ 1 week). Some critical routes also cleaned through PEZ and SEZ	<ul style="list-style-type: none"> LoS remains the same on roads to north west affected by 21 March tephra. Partial service restored on major critical routes through SEZ from north to south Some critical lifelines staff can enter SEZ No service elsewhere within PEZ and SEZ 	<ul style="list-style-type: none"> Same as 16 March except for rolling outages and speed restrictions on lines affected by new tephra Rolling outages are expected to be short-lived (until late on 22 March). However, further outages are possible due to ash remobilisation. 	
30 March	Tephra fallout to south east	<ul style="list-style-type: none"> Full service restored to roads beyond SEZ affected by 21 March tephra fall Service within PEZ and SEZ remains same as 22 March except some further critical routes which are reopened during daytime. 	<p>Rail stations:</p> <ul style="list-style-type: none"> (same as 16 March) <p>Rail lines:</p> <ul style="list-style-type: none"> Same as 21 March except restoration of service when recent tephra fall occurred outside SEZ 	
05 April	Lava flows 16 March SEZ lifted Major clean-up operation within lifted SEZ begins (for ~ 1 month)	<ul style="list-style-type: none"> Further critical routes through the now lifted SEZ are re-established with partial service. Only reduced service due to tephra deposits remain on some roads beyond the outer initial surge. Very limited access occurs on roads affected by the initial surge deposit up to the extent of the previous PEZ. No service (roads closed) within PEZ. 	<p>Rail stations:</p> <ul style="list-style-type: none"> Only stations within PEZ remain closed <p>Rail lines:</p> <ul style="list-style-type: none"> Lines within or intersecting PEZ remain closed Speed restrictions on lines affected by previous SEZ <p>All diesel freight services restored.</p>	<p>Auckland Airport issues a NOTAM indicating it remains outside of the evacuation zone with new evacuation orders in place</p> <p>Airport is re-opened with minimal service.</p>
08 April				Auckland Airport resumes full operations.
16 April	VAL reduces to 2			Auckland Airport issues a NOTAM that VAL has decreased.
01 May	16 March PEZ lifted Permanent exclusion zone implemented VAL reduces to 1. Major clean-up operation within lifted PEZ begins (for ~ 1 month)	<ul style="list-style-type: none"> Full service restored to all roads beyond 4 km from the vent Very limited access 2–4 km from the vent No service (remaining roads closed indefinitely) 0–2 km from the vent 	<p>Rail stations:</p> <ul style="list-style-type: none"> Stations closed on 05 April remain closed for coming months <p>Rail lines:</p> <ul style="list-style-type: none"> Some lines closed on 05 April remain closed for coming months 	Auckland Airport partially re-opened
01 June	VAL reduces to 0			Auckland Airport re-opens

disruption still resulting from evacuation zoning, VAL changes and VHZ areas (which would remain the same). However, the disruption to road and rail networks, as well as operations at ports is expected to be more severe, especially because of greater tephra accumulation on Auckland City and critical routes. Expected consequences from the revised tephra deposits include:

- Greater physical damage and LoS reduction on 14 March; tephra covers most of the central city area rather than being deposited towards the west. This coincides with the timing and spatial extent

of the largest evacuation zone and area potentially affected by earthquakes.

- Complications managing evacuations and inspecting road and rail networks for physical damage from the earthquakes are expected due to the additional tephra hazard (up to 50 mm in places outside of the PEZ).
- A decision may be made to extend the extent and/or duration of evacuation zones established on 12 March to reflect increased LoS reduction on transportation networks.

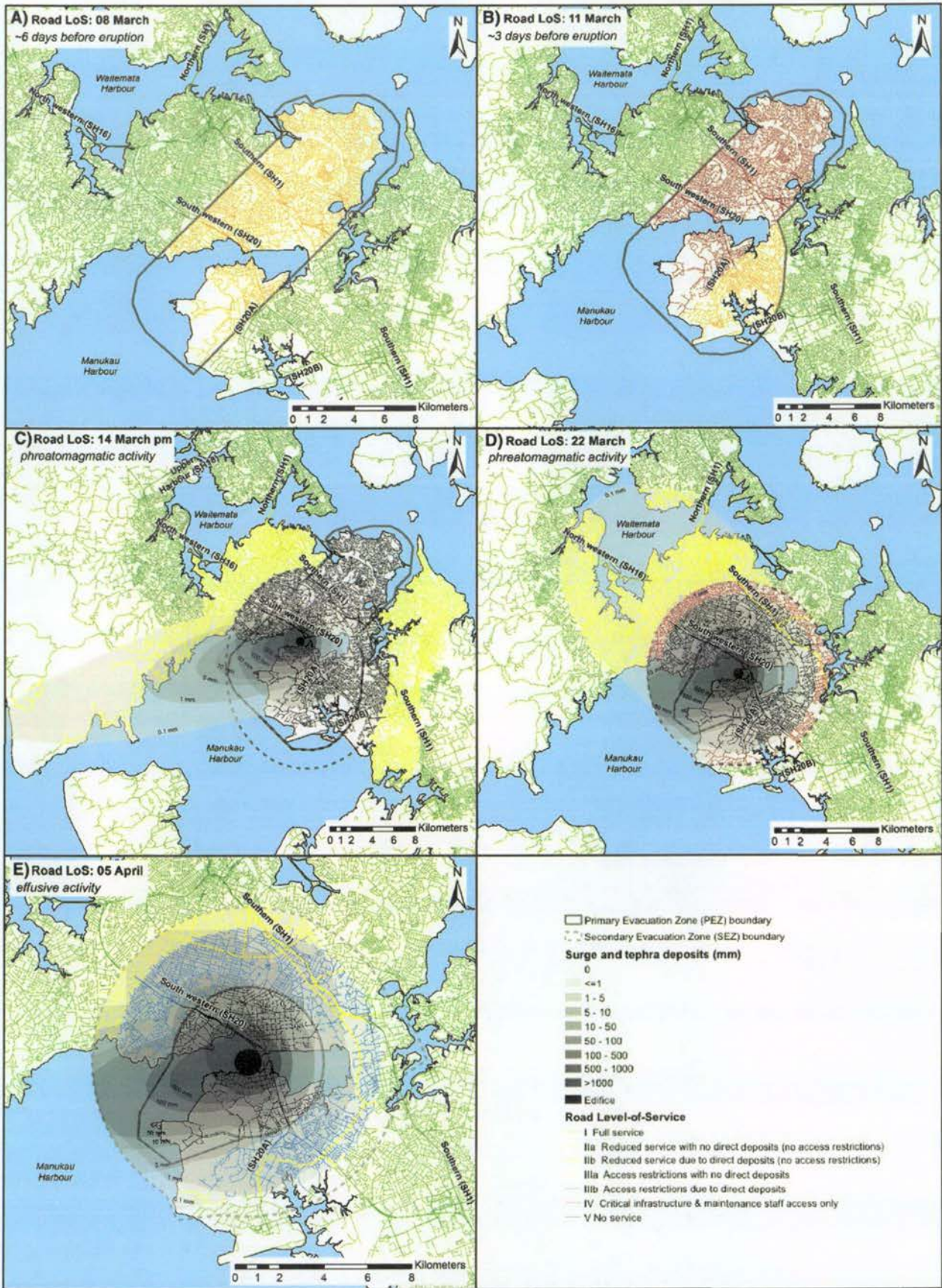


Fig. 7. Level-of-Service metrics for the road network at a selection of key times during the scenario. Note that the full series of Level-of-Service road maps can be seen in Supplementary Material 7.

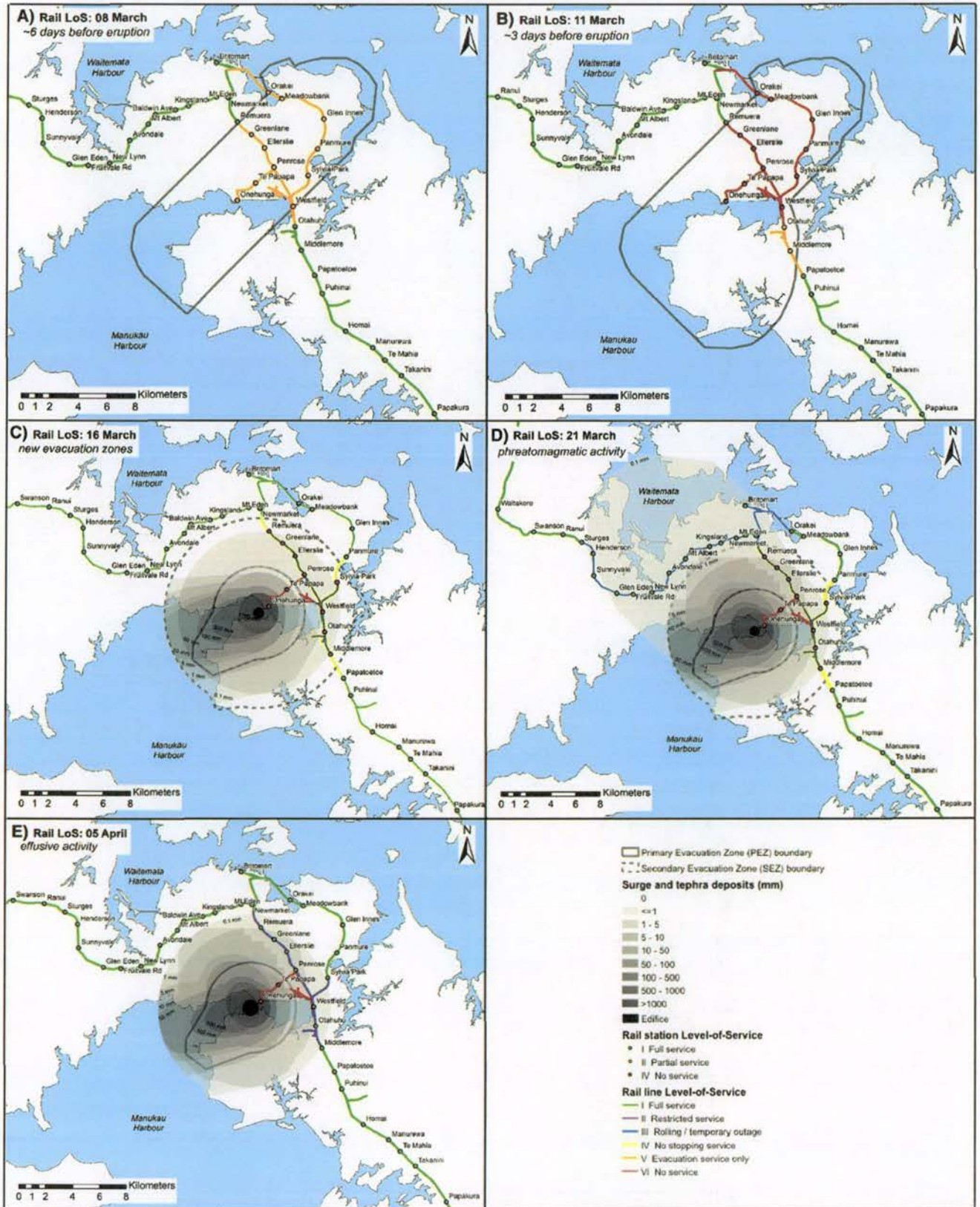


Fig. 8. Level-of-Service metrics for the rail network at a selection of key times during the scenario. Note that the full series of Level-of-Service rail maps can be seen in Supplementary Material 8.

Table 8

Changes in Level-of-Service metric percentage values for Auckland Airport for the Māngere Bridge scenario. Percentage values indicate the capacity with 100% = 'typical' operating capacity and 0% = no capacity.

Scenario Date	Domestic	Trans-Tasman and Pacific Islands	Long-Haul International
22 February	100	100	100
08 March	80	50	50
11 March	5	0	0
14 March	0	0	0
16 March	5	0	0
21 March	0	0	0
05 April	10	0	0
08 April	80	25	10
16 April	80	30	10
01 May	80	50	10
01 June	80	80	25
15 June	100	100	100

- o Critical north-south links through the south eastern isthmus would likely take longer to restore.
- o Substantially more resources will be required for clean-up of tephra in this urban area once access to the PEZ is permitted.
- o Unlike the original Māngere Bridge scenario, the Port of Auckland at Waitemata Harbour may be affected (by up to 5 mm of tephra). Both the port itself and maritime navigation in the Waitemata Harbour may encounter reduced LoS due to tephra fall and associated visibility impairment (Blake et al., in review b).
- With tephra being dispersed further east on 21 March, the central city area is less affected by this event than in the original scenario. However, disruption to road and rail is expected to be as, if not more, severe due to critical north-south links receiving greater accumulation of tephra. The restoration of any links through the evacuation zones would be unlikely before new tephra deposition on 22 March.
- The new wind profiles on 22 and 29–30 March cause substantially different tephra deposition patterns to the original scenario with much more widespread effects.
 - o As on 14 March, LoS reduction would occur on transportation routes through the city area, again including the Port of Auckland, which may receive up to 5 mm ash on 22 March.
 - o Further tephra accumulation on north-south links through the south eastern isthmus also occurs.
 - o The spatial extent and duration of evacuation zones may be increased and clean-up activities would take longer than in the original scenario.

During this scenario modification, it is expected that north-south ground transportation routes will be completely blocked (or only partially accessible at best) for a total period of ~2 weeks. There may also be a higher number of displaced residents due to the more persistent nature of tephra fall over highly populated areas and different

Table 9

Displaced populations during the Māngere Bridge scenario.

Note that shadow evacuees are calculated as the total number of residents within 1 km from the outer evacuation zone boundaries to align with the findings in Coomer et al. (2015) where relevant.

Scenario Date	Total Evacuees
21 February	0
22 February–07 March	(Potential for self-evacuation – number unknown)
08–10 March	199,200
11 March	253,700
12–15 March	434,300 (incl. 72,300 shadow evacuees)
16 March–04 April	275,900
05–30 April	57,300
01 May onwards	8700

evacuation zones. Therefore, in addition to expected disruption on maritime and aviation transportation, the provision of sufficient accommodation, food and other resources in Auckland City should be carefully considered.

5.4.2. Unrest with no eruption

The geophysical hazard sequence for the alternative to the Māngere Bridge scenario involving an unrest sequence with no eruption is shown in Table 10.

Damage from the geophysical hazard sequence would thus be very different to that in the original scenario, the majority of which would occur due to ground shaking and surface rupture. As with the evacuations in the original Māngere Bridge scenario (Deligne et al., 2017), we develop evacuation zones for the alternative sequence through information derived from the AVF Contingency Plan (Auckland Council, 2015) and Auckland Evacuation Plan (Auckland Council, 2014):

- The same evacuation zones are used up until and including 15 March.
- On 16 March, evacuation zones are revised due to continued unrest focused on the Māngere area and overall decrease in seismicity, deformation and gas levels.
 - o The PEZ consists of a 3 km buffer from the extent of the probable vent location area determined on 12 March.
 - o Unlike the original scenario, the SEZ now remains the same as on 12 March (5 km from the probable vent location area) (Fig. 10d).
- On 21 April, one week after the decrease in seismicity to around background levels, the SEZ is removed (Fig. 10e).
- Following seismic inactivity, the size of the PEZ is reduced on 01 May so that previously included 1 km buffer is removed (the PEZ now covers the same area as the 12 March probable vent location) (Fig. 10f).
- One month later on 01 June, the PEZ is removed, allowing the return of residents to all areas and use of all transportation routes and facilities.

We note that some areas where PEZs and SEZs are removed may temporarily transition to *restricted recovery zones* or similar due to the potential effects of previous volcanic activity on re-habitation such as inspection and service restoration requirements. These are not displayed on Fig. 10 but may occur on 16 March–20 April (in the area to the north east of the vent) and on 21–30 April (in the area where the SEZ is removed).

Fig. 11 shows the expected population displaced by the original Māngere Bridge scenario compared to the modified scenario. We suggest that up to 434,300 residents would seek alternative accommodation at times during the eruptive sequence of the original Māngere Bridge scenario (accounting for the shadow evacuation effect). However, business activities would also be affected and forced to relocate (e.g. Seville et al., 2014). An estimated 8700 residents are permanently displaced by the eruption. In the alternative scenario involving unrest but no eruption, the maximum number of displaced residents is the same as for the original scenario (both on 12 March). However, from 16 March until 01 June, there is a higher number of displaced people overall despite fewer geophysical hazards and less damage.

The large number of evacuees during the revised sequence highlights the substantial influence that evacuation zoning may have on society during volcanic unrest, even if there was no substantial damage from surficial volcanic hazards. In Auckland, the longer duration of larger evacuation zones would have substantial implications for transportation, particularly as more of the Southern Motorway (SH1) and north-south rail line are covered by evacuation zones for longer. Furthermore, the greater number and magnitude of earthquakes may lead to structural damage of some critical infrastructure. Inspections of key transportation routes, components and facilities will be required in areas that experienced the greatest shaking, and closures may be necessary due to inspections, physical damage and/or blockage. If possible, a decision to open some critical transportation routes that lie within the

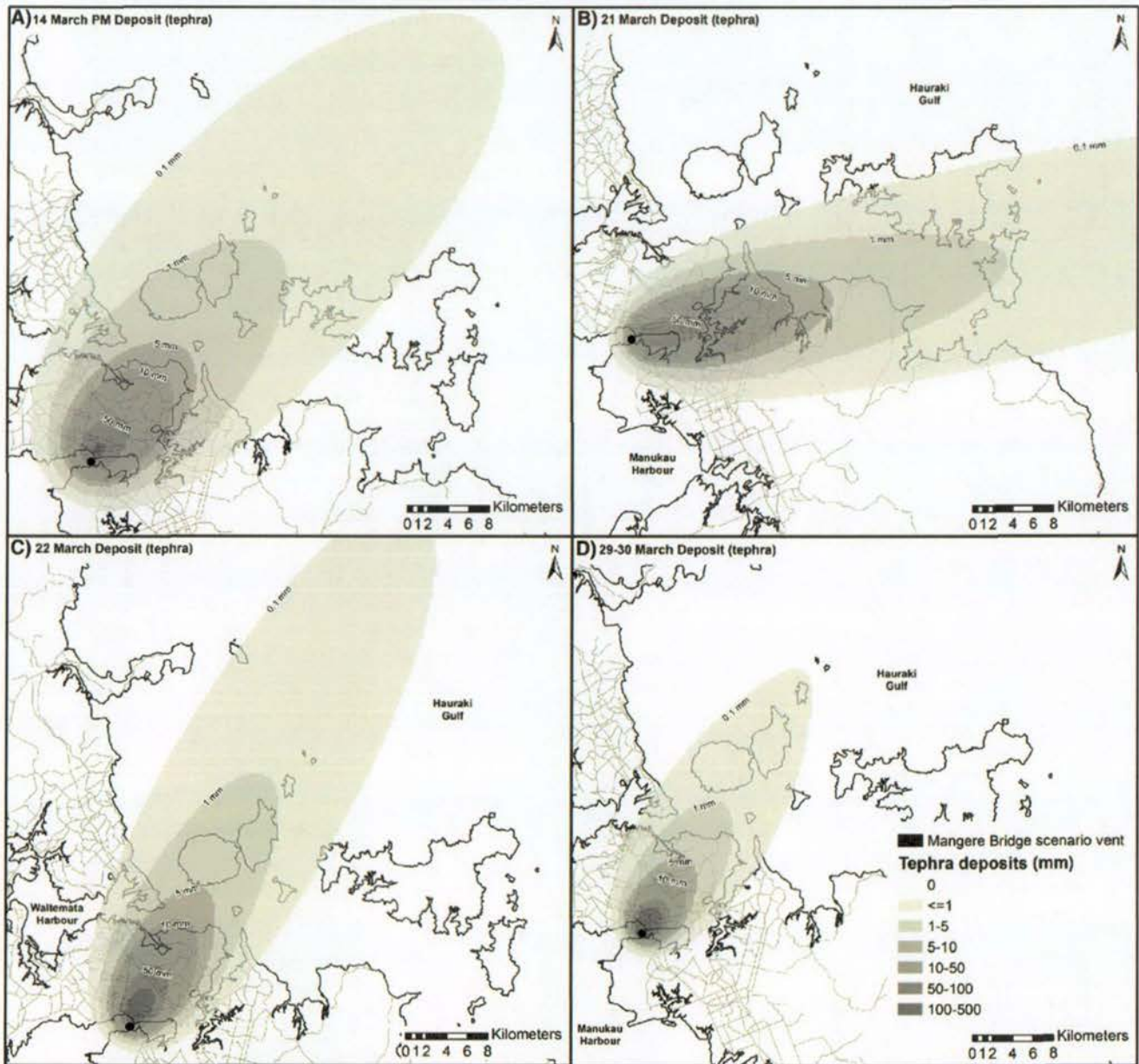


Fig. 9. Tephra deposits for the four tephra plume-producing eruptions during the Māngere Bridge scenario, modelled using south westerly wind profiles.

evacuation zones close to the boundaries would be likely, especially to maintain crucial north-south links through Auckland (albeit with restricted entry/exit points and hazard thresholds for immediate re-closure). Most critical routes through Auckland are accessible from 01 May for the alternative scenario. However, part of the South western Motorway (SH20) remains firmly within the PEZ (since 08 March), which will likely cause greater than usual congestion across the Auckland road network, especially with the return of previously displaced residents.

During the scenario involving unrest with no eruption, according to existing policy (section 3.4.2) Auckland Airport falls within the PEZ for ~6 weeks, in contrast to 5 days in the original Māngere Bridge scenario. However, due to the major LoS implications that would result from such a closure, we speculate that social, political and economic pressure may result in amendments to the PEZ boundary. This would mean that

Auckland Airport and some access routes lie outside of the boundary allowing services to be partially reinstated, albeit with established hazard thresholds for immediate re-closure.

5.5. Transportation network interdependencies

Failure or disruption of electricity supply is arguably one of the most important infrastructure interdependencies for ground transportation. For roads, traffic signal and variable message sign failure may occur (Hughes and Healy, 2014), with police support required at major intersections and traffic congestion expected as a result. In Auckland, electricity is also crucial for the suburban rail network, although there is a limited diesel fleet that could be distributed across the network (although not sufficient to maintain typical capacity). Effective business continuity measures where electricity is crucial could include the use

Table 10

Geophysical hazard sequence for the unrest sequence with no eruption. Italicised text indicates where the geophysical hazard and monitoring sequence remains consistent with the original Māngere Bridge scenario (i.e. Deligne et al., 2017).

Scenario Day	Geophysical hazards and monitoring "Observations"
19 February	Small swarms of high-frequency (non-volcanic) earthquakes
22 February	Swarm of low frequency earthquakes at 39–45 km depth (M_L 1.8–2.2)
01–05 March	125 mostly low frequency earthquakes at 34–45 km depth (M_L 1.8–2.2)
07–10 March	Some high frequency earthquakes, increasing in magnitude and shallowing. Swarms with up to 300 quakes per day. Ground deformation detected
11 March	Seismic activity becomes focussed in the Māngere area
12–13 March	Volcanic gases detected. Some high frequency earthquakes, increasing in magnitude and shallowing. Swarms with up to 300 quakes per day
14 March (early)	Tremor earthquakes, acceleration of deformation. Visual observation of cracking near Māngere. Volcanic gases increase.
14 March (late)–19 March	Number and magnitude of earthquakes decreases. Deformation and gas level reduction
20–31 March	Swarm of ~3000 earthquakes at 5–10 km depth. Most are M_L < 3.5, but during peak of activity on 29 March, 8 earthquakes of M_L 4.0 or greater occur, including a M_L 5.3 event (some structural damage from the larger earthquakes). ENE-trending 8 km long surface rupture accompanies largest earthquakes (with the direction determined from the direction of the inferred Manukau fault in the area (Kenny et al., 2012)). Gas levels increase slightly.
01 April	Number and magnitude of earthquakes decreases dramatically.
02–13 April	Seismicity remains at relatively constant low level, except for a few increases in event rate, which last < 6 h. No gas emissions detected
14 April	Seismicity diminishes to typical background levels.

of emergency generators and stockpiles of diesel fuel, as occurs at Auckland Airport. Conversely, the electricity sector also depends on functional transportation for access to sites damaged or in need of maintenance and for material delivery. In the Māngere Bridge scenario, transmission towers will need to be installed when new transmission lines are required (Deligne et al., 2017), and the restoration of electricity may be required before evacuation zones are lifted (Auckland Council, 2014).

Fuel supply is also recognised as a particularly important interdependency for transportation, and disruption to critical routes such as in the Māngere Bridge scenario will affect supply to fuel stations by tanker, even within non-evacuated areas. We also note that the Refinery Auckland Pipeline would be directly impacted by deformation and other hazards in the Māngere Bridge scenario, with severe impacts on aviation and road fuel supply likely for weeks (Auckland Council, 2013b; Deligne et al., 2015b). Large changes in demand may occur, whether it be due to evacuations or the relocation of residents and businesses from impacted areas. Operationally, the aviation sector and ports are reliant on fuel. In Auckland, the ports and associated operations account for nearly a quarter of diesel fuel used daily by critical consumers in the region (Auckland Council, 2013b). Tephra clean-up operations will require the mobilisation of a large number of trucks, sweepers, bulldozers, and graders (Hayes et al., 2015; Hayes et al., 2017), all of which require fuel. Fuel supply restrictions could increase the time it takes to clean up, which could have cascading impacts on health, infrastructure and economic activities. Additionally, increased demand for water for clean-up and potential water restrictions due to eruption impacts (Stewart et al., in press) may affect the ability to clean ground transportation networks. Without water for firefighting capabilities and sewerage, airports may be effectively shut (Stewart et al., in press).

Changes in road demand may result from impacts on other transportation infrastructure. For example, when rail services cease to

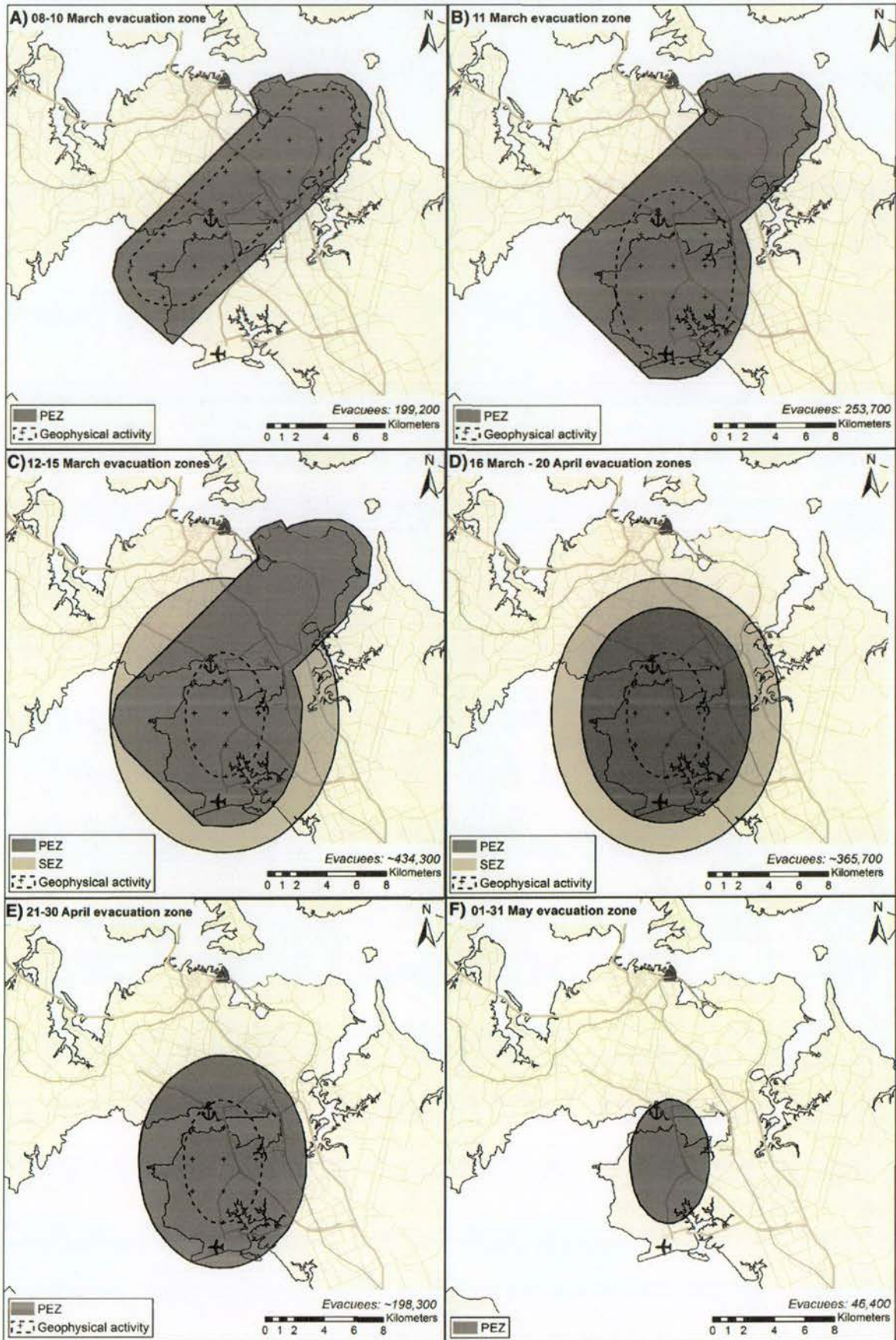
operate, some passengers may revert to road transport and the diversion of flights will likely increase demand and traffic on roads elsewhere. Similarly, rail, aviation and maritime transportation may be affected by impacts to roads as they all require staff to operate. Maintaining a roster of additional staff that can be called in when required and having alternative sites with suitable capabilities (e.g. immigration facilities for international flights diverted to alternative airports) will aid business continuity and improve transportation end-user LoS. In some situations following volcanic activity, it may be that certain features of all transportation modes are adjusted or react in such a way, that overall transportation LoS incurs only minimal reduction, or even improves. However, detailed modelling of interdependency relationships is required to more accurately explore impacts on overall LoS.

6. Summary and conclusions

The LoS metrics developed in this paper account for the various disruptive events through considering damage from geophysical hazards and operational activities such as evacuation and exclusion zoning. The LoS metric development process was heavily informed by consultation with transportation infrastructure providers and emergency management officials who generally have expert knowledge of particular transportation systems and their operation. Although the LoS metrics were formed using an eruption scenario in the AVF as a basis, many of the considerations in their compilation are universal and we thus suggest that the metrics can be applied in other locations affected by volcanic activity worldwide. We believe them to be particularly relevant in urban areas containing relatively advanced transportation networks and established emergency and transportation management policies.

We have demonstrated how small-scale explosive and effusive basaltic volcanic activity within an urban area can result in substantial disruption to transportation networks. Even in the absence of surficial volcanic hazards, the implementation of evacuation zones can have severe consequences on LoS for transportation end-users. Indeed, activity involving unrest episodes but with no, or few, surficial volcanic hazards may lead to equally, if not more, disruption for transportation end-users than activity with surficial hazards. This is largely due to uncertainties associated with potential vent areas and possibly large evacuation zones which could remain for longer durations. Critical routes and transportation hubs may be closed as a result with possible cascading consequences on other critical infrastructure which rely on transportation, whether it be through staff unable to access key sites or the breakdown of supply chains affecting the delivery of resources for maintenance and repair. Additionally, there may be large societal implications with normally resident and working populations displaced by evacuation zones and forced to find accommodation elsewhere and relocate business activities. Such potentially large consequences for LoS based on operational decisions such as evacuation boundary delineation highlight the importance of robust policy and guidance that can be applied during events.

We considered multiple volcanic hazards for impact assessment and LoS analysis. Although physical damage to transportation networks from proximal volcanic hazards such as pyroclastic density currents can be severe, other damage and potential blockage of transportation networks may also occur from volcanic hazards that extend further from the vent; this includes earthquakes accompanying volcanic activity and tephra accumulation which could be substantial in places, especially during highly explosive eruptions and/or with consistent wind direction. The impact of tephra fall is generally considered more temporary and easily remedied through clean-up operations. However, evacuation zones and ash remobilisation may complicate clean-up and repair, and extend the duration and spatial extent of LoS reduction. Importantly, even if there is minimal physical damage from hazards such as tephra and



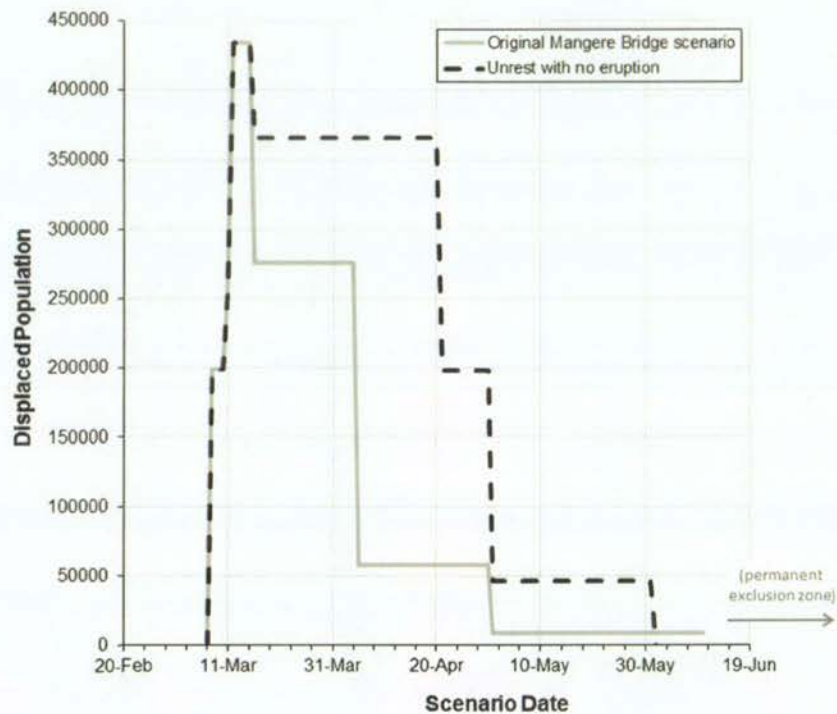


Fig. 11. Displaced populations during the original Māngere Bridge scenario (grey line) and alternative (unrest with no eruption) option to the scenario (black-dashed line).

earthquakes, widespread disruption to end-users can occur due to required inspections of networks and components.

Specifically for the Māngere Bridge scenario, all modes of transportation encounter disruption and a reduced LoS before being impacted by geophysical hazards. No service exists on some critical north-south road and rail routes across the south eastern Auckland isthmus at times due to the restrictions from evacuation zones, and Auckland Airport and the Port of Onehunga experience closure. Most LoS reduction for transportation networks starts ~6 days before the eruption due to the first PEZ being implemented, although some earlier self-evacuations may occur. Overall, LoS experiences fluctuations throughout the scenario due to different eruptive episodes and revisions to the extent of evacuation zones. Up to 435,000 residents, as well as many businesses are displaced at times. A degree of LoS reduction continues for several weeks after the eruption itself due to clean-up and repair requirements, and 8700 residents are permanently displaced due to the final exclusion zone.

For the modified Māngere Bridge scenario involving unrest but no eruption, the estimated maximum displaced population is the same as for the original scenario but residents and businesses are generally displaced for longer. Auckland Airport and critical transportation links are severely affected in this version of the scenario due to the large spatial extent and duration of evacuation zones. Relatively minor alterations to the geophysical hazard sequence such as different wind profiles can also have major consequences for LoS. Different wind profiles for the Māngere Bridge scenario demonstrate potential changes to:

- Evacuation zone management and network restoration due to different tephra accumulation patterns.
- Spatial and temporal extents of evacuation zones and networks impacted by geophysical hazards.
- The quantity of resources required to manage clean-up and recovery.

Our findings demonstrate the importance of considering transportation end-users when assessing the vulnerability of transportation

networks to volcanic activity. LoS metrics account for all disruption that may be encountered by transportation end-users and ultimately aid the development of robust impact and risk assessments for transportation networks.

Supplementary data to this article can be found online at <http://dx.doi.org/10.1016/j.jvolgeores.2017.04.010>.

Funding

We acknowledge support from the Economics of Resilient Infrastructure (ERI) and Determining Volcanic Risk in Auckland (DEVORA) research programmes; ERI is funded by the New Zealand Ministry of Business, Innovation, and Employment (MBIE) and DEVORA is funded by the New Zealand Earthquake Commission (EQC) and Auckland Council. The authors were also supported through Natural Hazards Research Management Platform (NHRP) funding (contract C05X0804), University of Canterbury Mason Trust grants (DMB), additional EQC and DEVORA funds (DMB), and the GNS Science Core Research Programme (NID).

Acknowledgements

We are grateful for the support provided by Emily Grace (GNS Science) in organising and attending most of the meetings with transportation authority officials in Auckland and her involvement with initial LoS metric development. We also express our sincere thanks to all of the officials from transportation authorities in New Zealand that were involved in the consultation process, and heavily informed the findings of this study. In particular, we thank Roy Robertson (Auckland Airport), Peter Halliwell (Air New Zealand), Peter Lechner (CAA, New Zealand), Murray Parker (NZTA), Peter Scott and Paul Jenkinson (Auckland Transport), David Murphy (Auckland Transport Operations Centre; ATOC), and Peter Ramsay and Mark Goodman (KiwiRail).

Although this paper focuses on transportation impacts, other critical infrastructure impacts have been assessed to some extent, and our

paper has benefitted from this work, especially through the brief consideration of interdependencies. We would thus like to thank Josh Hayes and Alistair Davies (University of Canterbury, New Zealand), Grant Wilson (State Emergency Management Committee Secretariat, WA, Australia), and Carol Stewart (Massey University, New Zealand). DMB would also like to thank his co-supervisor, Jim Cole, for his guidance and editing of the paper.

References

- AccuWeather, 2015. First Calbuco Eruption in 42 Years Suspends Flights in Buenos Aires. AccuWeather.com <http://www.accuweather.com/en/weather-news/more-than-4000-evacuated-after/46042985> (Accessed 23 November 2015).
- AELP-1, 1999. Final Report: Stage 1. Auckland Engineering Lifelines Project Technical Publication No. 112, November 1999. Auckland Regional Council, Auckland, New Zealand.
- AELP-2, 2014. Auckland Engineering Lifelines Project Stage 2: Assessing Auckland's Infrastructure Vulnerability to Natural and Man-made Hazards and Developing Measures to Reduce Our Region's Vulnerability. Auckland Engineering Lifelines Group Report Version 1.1. <http://www.aelg.org.nz/document-library/critical-infrastructure-reports/> Accessed 01 August 2016.
- AIP NZ, 2016. ENR 5.3, Aeronautical Information Publication New Zealand: Other Hazardous Airspace, Civil Aviation Authority of New Zealand. http://www.aip.net.nz/pdf/ENR_5.3.pdf Accessed 20 September 2016.
- Arana-Barradas, A., 2001. Out of the ashes after Mount Pinatubo. *Airman* (November 2001).
- ARTA, 2009. Auckland Report Narrative 2009/10: What We do. Auckland Regional Transport Authority, New Zealand <https://at.govt.nz/media/imported/4468/AT-ARTA-Report-AnnualReportNarrative2009-2010.pdf> Accessed 24 August 2015.
- Auckland Council, 2013a. The Auckland Plan: Chapter 13. Auckland Council <http://theplan.theaucklandplan.govt.nz/auckland-transport/> Accessed 20 August 2015.
- Auckland Council, 2013b. Auckland CDEM Fuel Contingency Plan, Version 3.1. <http://www.aucklandcouncil.govt.nz/media/30013/Final%20Auckland%20Fuel%20Plan%20V3.1%20October%202013.pdf> Accessed 20 August 2015.
- Auckland Council, 2014. Auckland Evacuation Plan. Civil Defence and Emergency Management <http://www.aucklandcouncil.govt.nz/about-us/document-library/supporting-plans/> Accessed 09 September 2015.
- Auckland Council, 2015. Auckland Volcanic Field Contingency Plan. Civil Defence and Emergency Management <http://www.aucklandcouncil.govt.nz/about-us/document-library/supporting-plans/> Accessed 09 September 2015.
- Auckland Transport, 2013. Electric Trains. Auckland Transport <https://at.govt.nz/projects-roadworks/auckland-rail-upgrade/electric-trains/> Accessed 09 September 2015.
- Auckland Transport, 2016. City Rail Link: Project Overview. Auckland Transport <https://at.govt.nz/projects-roadworks/city-rail-link/> Accessed 01 August 2016.
- Barnard, S., 2004. Results of a reconnaissance trip to Mt. Etna, Italy: the effects of the 2002 eruption of Etna on the province of Catania. *Bull. N. Z. Soc. Earthq. Eng.* 37 (2), 47–61.
- Barnard, S., 2009. The Vulnerability of New Zealand Lifelines Infrastructure to Ashfall. PhD Thesis. Hazard and Disaster Management. University of Canterbury, Christchurch, New Zealand.
- Barsotti, S., Andronico, D., Neri, A., Del Carlo, P., Baxter, P.J., Aspinall, W.P., Hincks, T., 2010. Quantitative assessment of volcanic ash hazards for health and infrastructure at Mt. Etna (Italy) by numerical simulation. *J. Volcanol. Geotherm. Res.* 192, 85–96.
- Beca Planning, 2003. Whenuapai Air Base: Planning Issues and Constraints. New Zealand Defence Force <http://www.nzdf.mil.nz/downloads/pdf/whenuapai/whenuapai-airbase.pdf> Accessed 10 September 2015.
- Becker, J., Smith, R., Johnston, D., Munro, A., 2001. Effects of the 1995–1996 Ruapehu eruptions on communities in central North Island, New Zealand, and people's perceptions of volcanic hazards after the event. *The Australasian Journal of Disaster and Trauma Studies* 2001, 1.
- Bitschene, P.R., Fernández, M.J., 1995. Volcanology and petrology of fallout ashes from the August 1991 eruption of Volcán Hudson (Patagonian Andes). In: Bitschene, P.R., Mendia, J. (Eds.), *The August 1991 Eruption of Volcán Hudson (Patagonian Andes): A Thousand Days After*. Cuvillier, Göttingen, pp. 27–54.
- Blake, D.M., Deligne, N.L., Wilson, T.M., Wilson, G., 2017c. Improving volcanic ash fragility functions through laboratory studies: example of surface transportation networks. *J. Appl. Volcanol.* (in review).
- Blake, D.M., Wilson, G., Stewart, C., Craig, H.M., Hayes, J.L., Jenkins, S.F., Wilson, T.M., Horwell, C.J., Andreastuti, S., Daniswara, R., Ferdiwijaya, D., Leonard, G.S., Hendrasto, M., Cronin, S., 2015. The 2014 Eruption of Kelud Volcano, Indonesia: Impacts on Infrastructure, Utilities, Agriculture and Health. GNS Science Report 2015/15, p. 139.
- Blake, D.M., Wilson, T.M., Cole, J.W., Deligne, N.L., Lindsay, J.M., 2017a. Impact of volcanic ash on road and airfield surface skid resistance. *Transp. Res. Part D: Transp. Environ.* (in review).
- Blake, D.M., Wilson, T.M., Stewart, C., 2017b. Visibility in airborne volcanic ash: considerations for surface transport using a laboratory-based method. *Nat. Hazards* (in review).
- Blake, D.M., Wilson, T.W., Gomez, C., 2016. Road marking coverage by volcanic ash: an experimental approach. *Environ. Earth Sci.* 75 (20), 1–12.
- Blong, R.J., 1984. *Volcanic Hazards: A Sourcebook on the Effects of Eruptions* (New South Wales, Australia).
- Blong, R.J., McKee, C., 1995. The Rabaul Eruption 1994: Destruction of a Town. Natural Hazards Research Centre, Macquarie University, Australia, p. 52.
- Bonadonna, C., Connor, C.B., Houghton, B.F., Connor, L., Byrne, M., Laing, A., Hincks, T.K., 2005. Probabilistic modeling of tephra dispersal: hazard assessment of a multiphase rhyolitic eruption at Tarawera, New Zealand. *J. Geophys. Res.* 110.
- Brand, B.D., Gravley, D., Clarke, A., Lindsay, J., Boomberg, S.H., Agustin-Flores, J., Németh, K., 2014. Combined field and numerical approach to understanding dilute pyroclastic density current dynamics and hazard potential: Auckland volcanic field, New Zealand. *J. Volcanol. Geotherm. Res.* 276, 215–232.
- Casadevall, T.J., Reyes, P.J.D., Schneider, D.J., 1999. The 1991 Pinatubo Eruptions and Their Effects on Aircraft Operations. <http://pubs.usgs.gov/pinatubo/casa/> Accessed 03 June 2014.
- Chappell, P.R., 2014. *The Climate and Weather of Auckland*, second ed. NIWA Science and Technology Series Number 60 NIWA Taihoro Nukurangi, New Zealand.
- Cole, J.W., Blumenthal, E., 2004. Evacuate! What an Evacuation Order Given Because of a Pending Volcanic Eruption Could Mean to Residents of the Bay of Plenty. Natural Hazards Research Centre, University of Canterbury, New Zealand.
- Cole, J.W., Sabel, C.E., Blumenthal, E., Finnis, K., Dantas, A., Barnard, B., Johnston, D.M., 2005. GIS-based emergency and evacuation planning for volcanic hazards in New Zealand. *Bull. N. Z. Soc. Earthq. Eng.* 38 (2), 149–164.
- Connor, L., Connor, C., Courtland, L., Saballos, A., 2011. *Tephra2 Users Manual*, Spring 2011. University of South Florida, Tampa https://vhub.org/resources/756/download/Tephra2_Users_Manual.pdf Accessed 01 August 2016.
- Coomer, M.A., Lambie, E.S., Wilson, T., Potter, S.H., Leonard, G.S., Maxwell, K., Bates, A., Keith, H., 2015. DEVORA Volcanic Survey: People's Panel. GNS Science Report 2015/39, p. 60.
- Corwin, G., Foster, H.L., 1959. The 1957 explosive eruption on Iwo Jima. *Volcano Islands. American Journal of Science* 257, 161–171.
- Cova, T.J., Conger, S., 2003. Transportation hazards. In: Kutz, M. (Ed.), *Handbook of Transportation Engineering*. McGraw-Hill Handbook.
- Craig, H., Wilson, T., Stewart, C., Outes, V., Villarosa, G., Baxter, P., 2016. Impacts to agriculture and critical infrastructure in Argentina after ashfall from the 2011 eruption of the Cordón Caulle volcanic complex: an assessment of published damage and function thresholds. *J. Appl. Volcanol.* 5 (7), 31.
- Cubellis, E., Marturano, A., Pappalardo, L., 2016. The last Vesuvius eruption in March 1944: reconstruction of the eruptive dynamic and its impact on the environment and people through witness reports and volcanological evidence. *Nat. Hazards* 82 (1), 95–121.
- Daly, M., Johnston, D., 2015. The genesis of volcanic risk assessment for the Auckland engineering lifelines project: 1996–2000. *J. Appl. Volcanol.* 4, 7.
- Daniell, J.E., Wenzel, F., Khazai, B., Santiago, J.G., Schaefer, A., 2014. A Worldwide Seismic Code Index, Country-by-Country Global Building Practice Factor and Socioeconomic Vulnerability Indices for Use in Earthquake Loss Estimation. Second European Conference on Earthquake Engineering and Seismology, Istanbul, August 25–29. http://www.eaee.org/Media/Default/2ECCES/2ecces_eaee/1400.pdf Accessed 09 September 2016.
- Deligne, N.L., Blake, D.M., Davies, A.J., Fitzgerald, R., Hayes, J.L., Kennedy, B., Stewart, C., Wilson, G., Wilson, T.M., Carneiro, R., Muspratt, S., Woods, R., 2017. Investigating the consequences of urban volcanism using a scenario approach I: development and application of a hypothetical eruption in the Auckland volcanic field, New Zealand. *J. Volcanol. Geotherm. Res.* 336, 192–208.
- Deligne, N.L., Blake, D.M., Davies, A.J., Grace, E.S., Hayes, J., Potter, S., Stewart, C., Wilson, G., Wilson, T.M., 2015b. Economics of Resilient Infrastructure Auckland Volcanic Field Scenario. ERI Research Report 2015/03, p. 151.
- Deligne, N.L., Lindsay, J.M., Smid, E., 2015a. An integrated approach to determining volcanic risk in Auckland, New Zealand: the multi-disciplinary DEVORA project. In: Loughlin, S.C., Sparks, R.S.J., Brown, S.K., Jenkins, S.F., Vye-Brown, C. (Eds.), *Global Volcanic Hazards and Risk*. Cambridge University Press, United Kingdom.
- Durand, M., Gordon, K., Johnston, D., Lorden, R., Poirot, T., Scott, J., Shephard, B., 2001. Impacts and Responses to Ashfall in Kagoshima From Sakurajima Volcano – Lessons for New Zealand. GNS Science Report 2001/30, p. 53.
- Folch, A., Mingari, L., Osoreo, M.S., Collini, E., 2014. Modeling volcanic ash resuspension – application to the 14–18 October 2011 outbreak episode in central Patagonia, Argentina. *Nat. Hazards Earth Syst. Sci.* 14, 119–133.
- Guffanti, M., Casadevall, T.J., Budding, K., 2010. Encounters of Aircraft with Volcanic Ash Clouds: A Compilation of Known Incidents, 1953–2009. USGS Report. <https://pubs.er.usgs.gov/publication/ds545> Accessed 27 March 2017.
- Guffanti, M., Mayberry, G.C., Casadevall, T.J., Wanderman, R., 2009. Volcanic hazards to airports. *Nat. Hazards* 51, 287–302.
- GVP, 2013. Report on San Cristobal (Nicaragua): January 2013. Global Volcanism Program. <http://volcano.si.edu/showreport.cfm?doi=10.5479/si.GVP.BGVN201301-344020> Accessed 23 November 2015.
- Hampton, S.J., Cole, J.W., Wilson, G., Wilson, T.M., Broom, S., 2015. Volcanic ashfall accumulation and loading on gutters and pitched roofs from laboratory empirical experiments: implications for risk assessment. *J. Volcanol. Geotherm. Res.* 304, 237–252.
- Hayes, J.L., Wilson, T.M., Deligne, N.L., Cole, J., Hughes, M., 2017. A model to assess tephra clean-up requirements in urban environments. *J. Appl. Volcanol.* 6 (1), 1–23.
- Hayes, J.L., Wilson, T.M., Magill, C., 2015. Tephra fall clean-up in urban environments. *J. Volcanol. Geotherm. Res.* 304, 359–377.
- Hirano, M., Hashimoto, H., Moriyama, T., 1992. Debris flows in Mt. Fugen. In: Yanagi, T., Okada, H., Ohta, K. (Eds.), *Unzen Volcano: the 1990–1992 Eruption*. Nishinippon Co., Ltd., Fukuoka, Japan, pp. 67–73.
- Hughes, J.F., Healy, K., 2014. Measuring the Resilience of Transport Infrastructure. New Zealand Transport Agency Research Report 546. New Zealand Transport Agency, Wellington, New Zealand.
- Hurlbut, G.C., Verbeek, R.D., 1887. Krakatau. *J. Am. Geogr. Soc. N. Y.* 19, 233–253.
- Jamaludin, D., 2010. BORDA Respond to Merapi Disaster. Bremen Overseas Research and Development Association, Indonesia <http://www.borda-sea.org/news/borda-sea-news/article/borda-respond-to-merapi-disaster.html> Accessed 23 November 2015.
- Jenkins, S., Komorowski, J.-C., Baxter, P.J., Spence, R., Picquout, A., Lavigne, F., 2013. The Merapi 2010 eruption: an interdisciplinary impact assessment methodology for studying pyroclastic density current dynamics. *J. Volcanol. Geotherm. Res.* 261, 316–329.
- Jenkins, S., Wilson, T.M., Magill, C.R., Miller, V., Stewart, C., 2014a. Volcanic Ash Fall Hazard and Risk: Technical Background Paper for the UN-ISDR Global Assessment Report on

- Disaster Risk Reduction 2015. Global Volcano Model and IAVCEI www.preventionweb.net/english/hyogo/gar Accessed 09 August 2016.
- Jenkins, S.F., Spence, R.J.S., Fonseca, J.F.B.D., Solidum, R.U., Wilson, T.M., 2014b. Volcanic risk assessment: quantifying physical vulnerability in the built environment. *J. Volcanol. Geotherm. Res.* 276, 105–120.
- Jenkins, S.F., Wilson, T., Magill, C., Miller, V., Stewart, C., Blong, R., Marzocchi, W., Boulton, M., Bonadonna, C., Costa, A., 2015. Volcanic ash fall hazard and risk. In: Loughlin, S.C., Sparks, R.S.J., Brown, S.K., Jenkins, S.F., Vye-Brown, C. (Eds.), *Global Volcanic Hazards and Risk*. Cambridge University Press, United Kingdom.
- Johnston, D.M., Daly, M., 1997. Auckland erupts! *New Zealand. Sci. Mon.* 8 (10), 6–7.
- Kagoshima City Office, 2015. Discussion With Staff at the Kagoshima City Office, Kagoshima, Japan. Personal Communication (08 June 2015).
- Kenny, J.A., Lindsay, J.M., Howe, T.M., 2012. Post-Miocene faults in Auckland: insights from borehole and topographic analysis. *N. Z. J. Geol. Geophys.* 55 (4), 323–343.
- Labadie, J.R., 1983. Volcanic Ash Effects and Mitigation. Air Force Office of Scientific Research and the Defence Advanced Research Projects Agency, U.S., p. 17.
- Lechner, P., 2015. Living With Volcanic Ash Episodes in Civil Aviation: The New Zealand Volcanic Ash Advisory System (VAAS) and The International Airways Volcano Watch (IAVW), Version 13, November 2015. Civil Aviation Authority of New Zealand https://www.caa.govt.nz/Meteorology/Living_with_Volcanic_Ash.pdf Accessed 20 September 2016.
- Leonard, G.S., Johnston, D.M., Williams, S., Cole, J.W., Finnis, K., Barnard, S., 2006. Impacts and Management of Recent Volcanic Eruptions in Ecuador: Lessons for New Zealand. *GNS Science Report 2005/20*, p. 52.
- Loughlin, S.C., Vye-Brown, C., Sparks, R.S.J., Brown, S.K., Barclay, J., Calder, E., Cottrell, E., Jolly, G., Komorowski, J.-C., Mandeville, C., Newhall, C., Palma, J., Potter, S., Valentine, G., 2015. An introduction to global volcanic hazard and risk. In: Loughlin, S.C., Sparks, R.S.J., Brown, S.K., Jenkins, S.F., Vye-Brown, C. (Eds.), *Global Volcanic Hazards and Risk*. Cambridge University Press, United Kingdom.
- Magill, C., Wilson, T., Okada, T., 2013. Observations of tephra fall impacts from the 2011 Shinmoedake eruption, Japan. *Earth Planets and Space* 65, 677–698.
- Magill, C.R., Blong, R.J., 2005. Volcanic risk ranking for Auckland, New Zealand. II. Hazard consequences and risk calculation. *Bull. Volcanol.* 67, 340–349.
- Magill, C.R., Hurst, A.W., Hunter, L.J., Blong, R.J., 2006. Probabilistic tephra fall simulation for the Auckland Region, New Zealand. *J. Volcanol. Geotherm. Res.* 153, 370–386.
- Mei, E.T.W., Lavigne, F., Picquout, A., de Béilzal, E., Brunstein, D., Grancher, D., Sartohadi, J., Cholikh, N., Vidal, C., 2013. Lessons learned from the 2010 evacuations at Merapi volcano. *J. Volcanol. Geotherm. Res.* 261, 348–365.
- Nairn, I.A., 2002. The Effects of Volcanic Ash Fall (tephra) on Road and Airport Surfaces. Institute of Geological and Nuclear Sciences Science Report 2002/13, p. 32.
- Nakada, S., 1999. Overview of the 1990–1995 eruption at Unzen Volcano. *J. Volcanol. Geotherm. Res.* 89, 1–22.
- NEC, 2014. An Economic Analysis of Transportation Infrastructure Investment. National Economic Council and the President's Council of Economic Advisors, The White House, Washington https://www.whitehouse.gov/sites/default/files/docs/economic_analysis_of_transportation_investments.pdf Accessed 08 August 2016.
- NIWA CliFlo. National Climate Database on the Web. <http://cliflo.niwa.co.nz>, National Institute of Water and Atmospheric Research, Accessed 1 August 2015.
- NZTA, 2008. Regional Summary: Auckland, New Zealand Transport Agency, December 2008. <http://www.nzta.govt.nz/assets/resources/regional-summaries/auckland/docs/auckland-regional-summary.pdf> Accessed 25 July 2016.
- NZTA, 2009. Pedestrian Planning and Design Guide. New Zealand Transport Agency, October 2009, Wellington, New Zealand <https://www.nzta.govt.nz/resources/pedestrian-planning-guide/> Accessed 24 August 2015.
- NZTA, 2013. One Network Road Classification. Road Efficiency Group, New Zealand Transport Agency, New Zealand <https://www.nzta.govt.nz/roads-and-rail/road-efficiency-group/onrc/> Accessed 24 August 2016.
- NZTA, 2016a. Waterview Connection: Project Overview. New Zealand Transport Agency <http://www.nzta.govt.nz/projects/the-western-ring-route/waterview-connection/> Accessed 01 August 2016.
- NZTA, 2016b. East West Link: Project Overview. New Zealand Transport Agency <http://www.nzta.govt.nz/projects/east-west-link/> Accessed 01 August 2016.
- Oppenheimer, C., 2003. Climatic, environmental and human consequences of the largest known historic eruption: Tambora volcano (Indonesia) 1815. *Prog. Phys. Geogr.* 27 (2), 230–259.
- Pallister, J.S., McCausland, W.A., Jónsson, S., Lu, Z., Zahran, H.M., Hadidy, S.E., Aburukbah, A., Stewart, I.C.F., Lundgren, P.R., White, R.A., Moufti, M.R.H., 2010. Broad accommodation of rift-related extension recorded by dyke intrusion in Saudi Arabia. *Nat. Geosci.* 3 (10), 705–712.
- Ragona, M., Hannstein, F., Mazzocchi, M., 2011. The impact of volcanic ash crisis on the European airline industry. In: Alemanno, A. (Ed.), *Governing Disasters: The Challenges of Emergency Risk Regulations*. Edward Elgar Publishing.
- Reckziegel, F., Bustos, E., Mingari, L., Báez, W., Villarosa, G., Folch, A., Collini, E., Viramonte, J., Romero, J., Osoreo, S., 2016. Forecasting volcanic ash dispersal and coeval re-suspension during the April–May 2015 Calbuco eruption. *J. Volcanol. Geotherm. Res.* 321, 44–57.
- Robinson, T.R., Buxton, R., Wilson, T.M., Cousins, W.J., Christophersen, A.M., 2015. Multiple Infrastructure Failures and Restoration Estimates From an Alpine Fault Earthquake: Capturing Modelling Information for MERIT. *ERI Research Report 2015/04*, p. 80.
- Rossetto, T., Ioannou, I., Grant, D.N., 2013. Existing Empirical Vulnerability and Fragility Functions: Compendium and Guide for Selection. GEM Technical Report 2013-X. GEM Foundation, Pavia, Italy.
- Sarkinen, C.F., Wiitala, J.T., 1981. Investigation of volcanic ash on transmission facilities in the Pacific Northwest. *IEEE Transactions on Power Apparatus and Systems PAS-100* (5), 2278–2286.
- Seville, E., Stevenson, J., Brown, C., Giovinazzi, S., Vargo, J., 2014. Disruption and Resilience: How Organisations Coped With the Canterbury Earthquakes. *ERI Research Report 2014/002*, p. 45.
- Sherburn, S., Scott, B.J., Olsen, J., Miller, C., 2007. Monitoring seismic precursors to an eruption from the Auckland volcanic field, New Zealand. *N. Z. J. Geol. Geophys.* 50, 1–11.
- Spence, R.J.S., Pomonis, A., Baxter, P.J., Coburn, A.W., White, M., Dayrit, M., 1999. Building Damage Caused by the Mount Pinatubo Eruption of June 15, 1991. <http://pubs.usgs.gov/pinatubo/spence/> Accessed 08 August 2016.
- Stammers, S.A.A., 2000. The Effects of Major Eruptions of Mt Pinatubo, Philippines and Rabaul Caldera, Papua New Guinea, and the Subsequent Social Disruption and Urban Recovery: Lessons for the Future. University of Canterbury, New Zealand.
- Statistics New Zealand, 2013. 2013 Census Meshblock Dataset. <http://www.stats.govt.nz/Census/2013-census/data-tables/meshblock-dataset.aspx> Accessed 15 July 2015.
- Statistics New Zealand, 2015. Subnational Population Estimates. <http://nzdotstat.stats.govt.nz/wbos/Index.aspx?DataSetCode=TABLECODE7502> Accessed 31 August 2016.
- Stewart, C.S., Deligne, N.I., Davies, A., Grace, E., Wilson, T.M., 2017. Investigating the consequences of urban volcanism using a scenario approach III: contrasting implications for water supply, wastewater, and stormwater networks. *J. Volcanol. Geotherm. Res.* (in press).
- Surono, Jousset, P., Pallister, J., Boichu, M., Buongiorno, M.F., Budi-Santoso, A., Costa, F., Andreastutti, S., Prata, F., Schneider, D., Lieven, C., Humaida, H., Sumarti, S., Bignami, C., Griswold, J., Carn, S., Oppenheimer, C., Lavigne, F., 2012. The 2010 explosive eruption of Java's Merapi volcano – a '100-year' event. *J. Volcanol. Geotherm. Res.* 241–242, 121–135.
- Sword-Daniels, V., Stewart, C., Johnston, D., Wardman, J., Wilson, T., Rossetto, T., 2011. Infrastructure Impacts, Management and Adaptations to Eruptions at Volcán Tungurahua, Ecuador, 1999–2010. *GNS Science Report 2011/24*, p. 73.
- Tazieff, H., 1977. An exceptional eruption: Mt. Niragongo, Jan. 10th, 1977. *Bull. Volcanol.* 40 (3), 189–200.
- Tomsen, E., 2010. GIS-Based Mass Evacuation Planning for the Auckland Volcanic Field. Master's Thesis. School of Environment, University of Auckland, Auckland, New Zealand.
- Tomsen, E., Lindsay, J., Gahegan, M., Wilson, T., Blake, D.M., 2014. Auckland volcanic field evacuation planning: a spatio-temporal approach for emergency management and transportation network decisions. *J. Appl. Volcanol.* 3, 6.
- Tyler, J.L., Reynertson, K.D., 1981. A pain in the ash: the effort of the men and women of Fairchild AFB overcame the neighborhood nuisance, Mt. St. Helens. *Engineering and Services Quarterly* 16–19.
- USGS, 2009. Small Explosion Produces Light Ash Fall at Soufriere Hills Volcano, Montserrat. United States Geological Survey <https://volcanoes.usgs.gov/ash/ashfall.html#eyewitness> Accessed 20 October 2015.
- USGS, 2013. Volcanic ash: Effects and Mitigation Strategies. United States Geological Survey <http://volcanoes.usgs.gov/ash/trans/> Accessed 21 September 2015.
- Volcano Discovery, 2014. Sinabung Eruption Update: 13 January 2014. *Volcano Discovery* <http://www.volcanodiscovery.com/sinabung-eruptions.html> Accessed 16 January 2014.
- Wardman, J., Sword-Daniels, V., Stewart, C., Wilson, T., 2012. Impact Assessment of the May 2010 Eruption of Pacaya Volcano, Guatemala. *GNS Science report 2012/09*, p. 90.
- Warrick, R.A., 1981. Four Communities Under Ash After Mount St. Helens. Institute of Behavioral Science, Boulder, Colorado, U.S.
- Wilson, G., Wilson, T.M., Deligne, N.I., Blake, D.M., Cole, J.W., 2017. Framework for developing volcanic fragility and vulnerability functions for critical infrastructure. *J. Appl. Volcanol.* (in review).
- Wilson, G., Wilson, T.M., Deligne, N.I., Cole, J.W., 2014. Volcanic hazard impacts to critical infrastructure: a review. *J. Volcanol. Geotherm. Res.* 286, 148–182.
- Wilson, T., Daly, M., Johnston, D., 2009a. Review of Impacts of Volcanic Ash on Electricity Distribution Systems, Broadcasting and Communication Networks. Auckland Regional Council Technical Publication No. 051. Auckland Engineering Lifelines Group, Auckland, New Zealand.
- Wilson, T., Kaye, G., Stewart, C., Cole, J., 2007. Impacts of the 2006 Eruption of Merapi Volcano, Indonesia, on Agriculture and Infrastructure. *GNS Science Report 2007/07*, p. 69.
- Wilson, T., Outes, V., Stewart, C., Villarosa, G., Bickerton, H., Rovere, E., Baxter, P., 2013. Impacts of the June 2011 Puyehue-Cordón Caulle Volcanic Complex Eruption on Urban Infrastructure, Agriculture and Public Health. *GNS Science report 2012/20*, p. 88.
- Wilson, T.M., 2008. Unpublished Field Notes From the Chaiten Eruption Field Visit. University of Canterbury, Christchurch, New Zealand.
- Wilson, T.M., 2009. Unpublished Field Notes From the Hudson Eruption Field Visit. University of Canterbury, Christchurch, New Zealand.
- Wilson, T.M., Cole, J., Johnston, D., Cronin, S., Stewart, C., Dantas, A., 2012b. Short- and long-term evacuation of people and livestock during a volcanic crisis: lessons from the 1991 eruption of Volcán Hudson, Chile. *J. Appl. Volcanol.* 1 (1), 1–11.
- Wilson, T.M., Stewart, C., Cole, J.W., Dewar, D.J., Johnston, D.M., Cronin, S.J., 2009b. The 1991 Eruption of Volcán Hudson, Chile: Impacts on Agriculture and Rural Communities and Long-term Recovery. *GNS Science Report 2009/66*, p. 99.
- Wilson, T.M., Stewart, C., Sword-Daniels, V., Leonard, G.S., Johnston, D.M., Cole, J.W., Wardman, J., Wilson, G., Barnard, S., 2012a. Volcanic ash impacts on critical infrastructure. *Phys. Chem. Earth* 45–46, 5–23.
- Wolshon, B., 2009. Transportation's Role in Emergency Evacuation and Reentry: A Synthesis of Highway Practice. National Cooperative Highway Research Program, Synthesis 392. Transportation Research Board, Washington D.C.
- Woo, G., 2008. Probabilistic criteria for volcano evacuation decisions. *Nat. Hazards* 45, 87–97.
- Yanagi, T., Okada, H., Ohta, K., 1992. Unzen Volcano, the 1990–1992 Eruption. The Nishinippon and Kyushu University Press, Fukuoka, p. 137.
- Zuccaro, G., Cacace, F., Spence, R.J.S., Baxter, P.J., 2008. Impact of explosive eruption scenarios at Vesuvius. *J. Volcanol. Geotherm. Res.* 178 (3), 416–453.

Visibility in airborne volcanic ash: considerations for surface transportation using a laboratory-based method

Daniel M. Blake¹ · Thomas M. Wilson¹ · Carol Stewart²

Received: 22 June 2016 / Accepted: 1 February 2018 / Published online: 12 February 2018
© The Author(s) 2018. This article is an open access publication

Abstract All modes of surface transportation can be disrupted by visibility degradation caused by airborne volcanic ash. Despite much qualitative evidence of low visibility on roads following historical eruptions worldwide, there have been few detailed studies that have attempted to quantify relationships between visibility conditions and observed impacts on network functionality and safety. In the absence of detailed field observations, such gaps in knowledge can be filled by developing empirical datasets through laboratory investigations. Here, we use historical eruption data to estimate a plausible range of ash-settling rates and ash particle characteristics for Auckland city, New Zealand. We propose and implement a new experimental set-up in controlled laboratory conditions, which incorporates a dual-pass transmissometer and solid aerosol generator, to reproduce these ash-settling rates and calculate visual ranges through the associated airborne volcanic ash. Our findings demonstrate that visibility is most impaired for high ash-settling rates (i.e. $> 500 \text{ g m}^{-2} \text{ h}^{-1}$) and particle size is deemed the most influential ash characteristic for visual range. For the samples tested (all $< 320 \mu\text{m}$ particle diameter), visibility was restricted to $\sim 1\text{--}2 \text{ m}$ when ash settling was replicated for very high rates (i.e. $\sim 4000 \text{ g m}^{-2} \text{ h}^{-1}$) and was especially low when ash particles were fine-grained, more irregular in shape and lighter in colour. Finally, we consider potential implications for disruption to surface transportation in Auckland through comparisons with existing research which investigates the consequences of visual range reduction for other atmospheric hazards such as fog. This includes discussing how our approach might be utilised in emergency and transport management planning. Finally, we summarise strategies available

Electronic supplementary material The online version of this article (<https://doi.org/10.1007/s11069-018-3205-3>) contains supplementary material, which is available to authorized users.

✉ Daniel M. Blake
daniel.blake@canterbury.ac.nz

¹ Department of Geological Sciences, University of Canterbury, Private Bag 4800, Christchurch 8140, New Zealand

² Joint Centre for Disaster Research, Massey University/GNS Science, PO Box 756, Massey University Wellington Campus, Wellington 6140, New Zealand

for the mitigation of visibility degradation in environments contaminated with volcanic ash.

Keywords Vehicle · Road · Visual range · Experimental · Opacity · Transmissometer

1 Introduction

Reduced visibility may occur during primary volcanic ashfall or through the remobilisation and resuspension of existing fall deposits (Sparks et al. 1997; Baxter and Horwell 1999; USGS 2013; Folch et al. 2014) into the atmosphere by wind, vehicle movement, cleaning processes or other human activities. Both primary and remobilised ash may produce potential issues for transportation (Barsotti et al. 2010; Folch 2012; Wilson et al. 2014; Blake et al. 2016a, b, 2017a, b). There have been many cases where reduced visibility following volcanic eruptions has impacted surface transportation¹ function, particularly road (Table 1), but also rail, maritime and at airports, sometimes to near-total darkness (Blong 1982; Guffanti et al. 2009). For example, following the Mount St Helens eruption in 1980, “zero visibility” caused traffic to come to a standstill in several places including on Interstate 90 near Ellensburg in Washington, with visibility so poor that the authorities used flares to guide motorists to nearby schools and churches (Warrick 1981, p.19). Once the initial ashfall was over, it became imperative to control traffic movement through speed restrictions, spacing vehicles on roads and road closures to avoid vehicles creating “great clouds of ash” and again reducing visibility on the roads (Warrick 1981, p.20). Hundreds of accidents in the affected areas were attributed to the billowing of ash behind vehicles and associated loss in visibility (Blong 1984). More recently, following the eruption of Cordón Caulle, Chile, in 2011, visibility in neighbouring Argentina, where ash fell, was so low that several main roads including Route 40 (linking Bariloche city and the Neuquén province) were subsequently closed. This affected the transportation of people and freight at a national level (Folch et al. 2014). Vehicle headlights and brake lights are often reported to be ineffective in such conditions and barely visible to other drivers (Cole and Blumenthal 2004; Wilson et al. 2012a; USGS 2013). Disruption to rail and maritime transportation caused by poor visibility during ashfall and resulting in safety and navigational issues has also been documented (Johnston 1997; Wilson et al. 2012a). For example, rail operations were shutdown during the initial Mount St Helens 1980 ashfall due to reduced visibility (as well as health concerns), with substantial speed restrictions and inspections necessary in the following days (Warrick 1981; Blong 1984).

Despite the many impacts to surface transportation that have been documented (Table 1), there has been little quantitative analysis into the effects of airborne volcanic ash on reducing visibility and the subsequent consequences for network functionality and safety. Contemporary critical infrastructure management increasingly aims to optimise network performance during natural hazards, especially for non-damaging events, such as minor ashfalls (Wilson et al. 2014). Ash thickness has usually been the key measure of hazard intensity adopted in the past (Table 1), but is likely to be of little relevance when assessing visibility impacts. Airborne ash concentration and ash-settling rates are more important for such impacts. The lack of an evidence base implies that surface transportation operators typically can only make crude management decisions of either taking a

¹ The term *surface transportation* is used in this paper to refer to common modes of transportation on land and at sea (i.e. road, rail, airport and maritime). It excludes airborne aircraft.

Table 1 Historical records of visibility impacts on road following volcanic eruptions. Other occurrences described as general impacts to transportation, where impacts on visibility may have occurred but are not specified in the literature, are not shown

Volcano (Year)	Ash thickness (mm)	Initial ashfall visibility observations	Resuspended ash visibility observations	Mitigation measures	References
Ruapehu (1945)	“Few mm”	Reduced visibility on roads was common Ash made streetlights hazy	Bus headlamps blacked out by thick ash Recently deposited ash easily lifted by passing vehicles Resuspended ash similar to dust produced on unsealed roads	Road closures Drivers reduced speeds (to as low as $\sim 25 \text{ km h}^{-1}$) Ash removal Rain improved visibility	Johnston (1997)
St Helens (1980)	< 50	Traffic reduced to a virtual standstill because of zero visibility Gravel and sealed roads had similar visibility problems Flares had to be used to guide people	Ash billowing up behind fast-moving vehicles reduced visibility and likely caused hundreds of accidents Bus services shutdown and then limited services	Road closures Stricter speed limits Convoys Restrictions on vehicle type and numbers Advice not to drive except in emergencies Speed bumps constructed from ash Ash removal with some dampening first	Sarkinen and Wiitala (1981), Warrick (1981), Blong (1984); Johnston (1997)
Hudson (1991)	20–50		$\sim 1 \text{ m}$ visual range a week after eruption (“transport virtually closed down”) Poor visibility on main coastal highway for up to a month	Road closures Rainfall contributed to ash hazards diminishing People avoided going outside Cleaning of streets prioritised	Wilson et al. (2009), Wilson (2009) (unpublished field notes)
	200–300	People could not drive partly due to visibility Ashfall blocked sun and visibility was as low as 1 m in daytime			

Table 1 continued

Volcano (Year)	Ash thickness (mm)	Initial ashfall visibility observations	Resuspended ash visibility observations	Mitigation measures	References
Spurr (1992)	3	Ash limited visibility on roads	Bus services shutdown and then limited service	City trimmed bus schedules and sent 40% of workforce home Rain alleviated issues	Johnston (1997), Barnard (2009)
Unzen (1992)		Visibility reduced on roads by suspended ash			Yanagi et al. (1992), Barnard (2009)
Ruapehu (1995–1996)	“Thin”	Reduced visibility	Visibility on roads commonly reduced after ashfalls	Nearby state highway closed three times Diversions Ash removal	Johnston (1997), Barnard (2009)
Etna (2002)	< 2		Ash remobilisation by traffic and wind caused reduced visibility		Barnard (2009)
Chaitén (2008)		Reduced visibility “to nil” meant that maintenance crews were unable to traverse the access road to a hydroelectric dam	Visibility issues from vehicles travelling too fast (~ 50 m visual range in places)	Roads restricted by army to emergency vehicle use only Some roads made one-way to reduce accidents Permanent crew at dam for 1 month (rather than shifts) to reduce remobilisation Drivers reduced speeds Headlights used Rain alleviated issues	Wilson et al. (2012b), Wilson (2008) (unpublished field notes)
Pacaya (2011)	~ 300 20–30	10–15 m visibility Difficult to drive due to impaired visibility		Ash removal Rain helped consolidate tephra	Wardman et al. (2012)

Table 1 continued

Volcano (Year)	Ash thickness (mm)	Initial ashfall visibility observations	Resuspended ash visibility observations	Mitigation measures	References
Cordón Caulle (2011)			Low visibility led to difficult driving conditions for 2 weeks and accidents Visibility reduction meant no urban clean-up for a week in places	Road closures Lower speed enforcement and recommendations (some 20 km h ⁻¹) Ash dampened with water Ash removal	Wilson et al. (2013), Folch et al. (2014), Craig et al. (2016)
Shinmoedake (2011)	> 100	“No visibility”—decreased visibility Reduced visibility	Visibility problems lasted for some time	Roads closed Rapid clean-up operation	Magill et al. (2013)
San Cristóbal (2013)		Visibility greatly reduced ~ 15 km from vent		Headlights used	GVP (2013)
Kelud (2014)		Reduced visibility	Accident rates increased up to 220 km from vent Bus services shutdown and then limited service	Advice to not drive if possible Headlights used Drivers reduced speeds Ash removal Rain improved visibility	Blake et al. (2015)
Calbuco (2015)	~ 50	Visibility reduced to 500 m ~ 100 km from vent	500 m visual range recorded ~ 500 km from vent 3 days after last eruptive pulse		AccuWeather (2015), Reckziegel et al. (2016)

precautionary approach of shutting systems down in the presence of ash (or in the event of forecasted ash), or a reactive approach if airborne ash causes problems for a surface transportation system. However, several contemporary ash dispersion and fallout forecasting models, which are outlined in detail by Scollo et al. (2008) and Folch (2012), can provide outputs that include atmospheric concentrations and settling rates (e.g. FLEX-PART—Stohl et al. 1998, 2005; VOL-CALPUFF—Barsotti et al. 2008; FALL3D—Costa et al. 2006; Folch et al. 2009). Therefore, the capacity now exists for surface transportation vulnerability assessments to adopt these metrics. Furthermore, settling rate and airborne concentration are important metrics to consider for other impacts to transportation. For example, it has been determined that concentrations as low as $1 \times 10^{-4} \text{ g m}^{-3}$ can cause substantial damage to aircraft (Witham et al. 2007; Folch and Sulpizio 2010).

In this paper, we next present a background section which summarises the interdisciplinary literature including the physical properties of volcanic ash, visibility degradation and surface transportation impacts. The background section also includes a summary of our Auckland case study site, which gives context to the work through the application of experimental processes and replication of ash types/colours, particle sizes and settling rates expected in the city from various volcanic sources. We then outline the methods used to simulate volcanic ashfall in a laboratory setting to investigate the effect of ash characteristics and settling rate on visibility degradation. Precise and consistent ash-generation rates (g h^{-1}) are produced in a purpose-built container using a Solid Aerosol Generator (*Topas SAG 410*). We also use a dual-pass transmissometer (*Dynoptics DSL-460 MkII*) for the measurement of opacity as a proxy for particulate emissions. We use datasets containing ash characteristic and geospatial information from the literature available following worldwide historical eruptions to test our methodology, specifically focusing on the Auckland case study. Results from the experimental tests are presented before a discussion of the findings related to visibility in airborne ash and forecasts for Auckland. Finally, we discuss key limitations of the experimental approach, provide suggestions for future work and suggest evidence-based, semi-quantitative transportation mitigation strategies that could be implemented in operational environments.

2 Background

2.1 Ash deposit thickness and visibility relationship

Ash deposit thickness is the most frequently (and often only) reported hazard intensity metric following volcanic eruptions (Pyle 1989; Wilson et al. 2012a, 2014, 2017; Blake et al. 2017a, b). There is generally a decreasing trend in ash thickness with distance from eruptive vents, although other spatial variations are possible due to ash aggregation and/or an unusually large proportion of mid-sized particles, which can lead to secondary maxima on a thickness versus distance plot (see Carey and Sigurdsson 1982; Pyle 1989; Sparks et al. 1992; Scasso et al. 1994; Bonadonna et al. 1998; Bonadonna and Phillips 2003; Bonadonna and Houghton 2005; Costa et al. 2009; Parfitt and Wilson 2009; Bonasia et al. 2012; Folch et al. 2010; Macedonio et al. 2016). Ash deposit thickness is clearly an important parameter for certain transportation impact types at quite low levels. For example, line marking coverage and loss of skid resistance on roads can occur with 0.1–1.0-mm-thick ash in some situations (Blake et al. 2016a, b, 2017a, b). However, ash thickness is generally a poor indicator for estimating likely effects on visibility. Some

studies indicate that thickness plays a minimal role in controlling airborne ash concentration, initial levels of visibility degradation and associated impact to transportation (e.g. Warrick 1981; Blong 1982). For example, reporting on the Mount St Helens 1980 eruption, Warrick (1981) states that “ash depth had little influence on the initial level of impact on the transportation systems”. Conversely, other studies suggest that thickness can be used to inform visibility impacts to a degree (e.g. Thorarinsson 1971; Johnston 1997; Searl et al. 2002). While there is potential for uncompacted fine ash to become airborne by disturbance of the deposit, and thicker deposits can prolong the duration of such remobilisation and subsequent recovery time (Searl et al. 2002; Hincks et al. 2006; Wilson et al. 2011), we propose that *ash-settling rate*² (especially for direct ashfall) and airborne particle concentration³ (for both direct and resuspended ash) are more appropriate metrics to adopt when assessing visibility impairment in environments containing volcanic ash. Therefore, the thicknesses outlined in Table 1 have little direct link to the visibility observations and should only be used as a loose proxy for airborne ash concentration and duration of exposure.

2.2 Volcanic ash-settling rate

Two fundamental processes affect ash-settling rate, which are depicted in Fig. 1:

- 1) Primary ashfall from the eruptive vent, which is the result of explosive volcanic eruptions causing the disintegration of magma or vent material and production of rock fragments (Jenkins et al. 2014). The *terminal fall velocity*⁴ of sedimenting particles affects ash-settling rate and is mainly dependent on their diameter, densities and, to some extent, their shape (see: Bonadonna et al. 1998; Riley et al. 2003; Parfitt and Wilson 2009; Pardini et al. 2016).
- 2) The remobilisation and resuspension of existing ash into the atmosphere from entrainment by meteorological winds, small-scale atmospheric turbulence caused by vehicle movement, cleaning processes and/or other human activities. The quantity of volcanic ash which becomes resuspended is dependent on the particle size, density, water content, shape, roughness of the ground material on which it has settled, and the degree of binding and compaction (Fowler and Lopushinsky 1986; Sivakumar 2005; Wilson et al. 2011)

We suggest that different ash-settling rates can be established under laboratory conditions. However, compared to other hazard intensity metrics such as ash thickness and

² Settling rate is defined here as the mass of particles falling onto a surface over time ($\text{g m}^{-2} \text{h}^{-1}$). However, we note that settling rate may also be referred to as *ash-deposition rate* or *ash accumulation rate* in other literature.

³ Many countries have well-established networks to monitor airborne particle concentrations in relation to legal standards on ambient air quality. Historically, the main parameter measured was total suspended particulates (TSP), which includes all airborne particles (typically 0–40 μm). More recently, regulatory standards are based on PM_{10} (the concentration in $\mu\text{g m}^{-3}$ of particles with a diameter of 10 μm or less), and $\text{PM}_{2.5}$, with the latter being considered of greater relevance to public health (WHO 2013). Air quality monitoring networks have been used to track volcanic ash plumes (Elliot et al. 2010; Leonard et al. 2014).

⁴ Ash particles released from an umbrella cloud accelerate downward until the air drag retarding them is balanced by their gravitational weight, at which point they reach a steady final speed, or *terminal fall velocity* (Parfitt and Wilson 2009; Rose and Durant 2009).

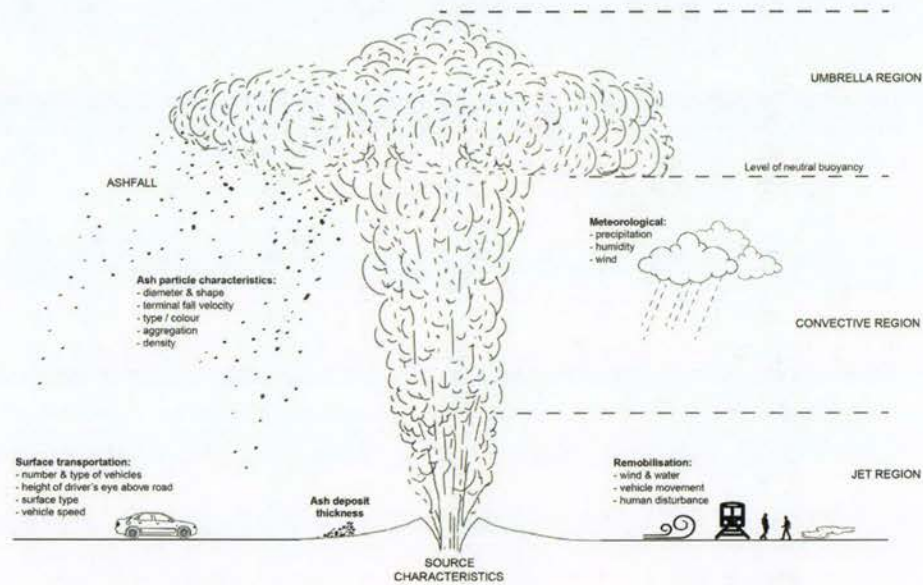


Fig. 1 Eruption and environmental characteristics that influence volcanic ash-settling rates and airborne concentrations (eruption column characteristics modified from Sparks 1986; Carey and Bursik 2015)

particle size, there are somewhat limited primary empirical data available for volcanic ash-settling rates obtained from field measurements or indeed from records of ashfall duration associated with ash thickness or loading in the field. Mean settling rates can be estimated based on the total ashfall duration (e.g. see: Hill 2014), although it is possible that pulses of ashfall with periods of quiescence occur during that time (Scasso et al. 1994). Furthermore, complications from plume and atmospheric turbulence, particle–particle interaction and atmospheric conditions (Bonadonna et al. 2011) mean that accurate correlations between total ash thicknesses and settling rates are difficult to produce.

2.3 Particle size

Unlike airborne mineral dust, which often has a homogeneous internal structure consisting of similar-sized particles, volcanic ash is generally inhomogeneous; the size of erupted material may vary by several orders of magnitude (Weinzierl et al. 2012). However, the most important volcanic ash particle size range in terms of impact to infrastructure including transportation is generally fine-grained ash (e.g. Wilson et al. 2012a; Blake et al. 2016b) (i.e. often < 100 μm diameter, and particularly < 64 μm diameter; Carey and Sigurdsson 1982). Fine ash can disperse for up to hundreds of kilometres from the vent before settling due to gravity and therefore generally settles over extensive areas. The proportions of ash in these fine fractions increase with increasing eruption explosivity (Moen 1981; Horwell 2007; Durant et al. 2009; White et al. 2011), and fine ash is more susceptible to remobilisation by the processes described in point 2 above (Wilson et al. 2011). Particle size distributions of volcanic deposits are poorly constrained due to sparse data, variations in wind conditions and dimensions of eruption columns, and inconsistencies in the methods of measurement. Many particle size analyses carried out for ash deposits are incomplete, lacking data below 63 μm (Bonadonna and Houghton 2005).

2.4 Particle shape

The less spherical a particle shape of the same weight, the lower its settling rate (Komar and Reimers 1978; Wilson and Huang 1979). Volcanic ash particles are often more elongated in shape than other particulates such as mineral dust. Wilson and Huang (1979) found that for volcanic particles of 30–500 μm diameter, glass and feldspar fragments have a very high proportion of flattened particles, whereas pumice consists of a greater variety of shapes (Fagents et al. 2013). More recently, Weinzierl et al. (2012) compared the physical properties of volcanic ash and mineral dust by using samples from Eyjafjallajökull Volcano, Iceland, and the Sahara Desert. The median aspect ratio (i.e. ratio of the width to the height) of Eyjafjallajökull ash was 2.0, compared to a median aspect ratio of 1.6 for the mineral dust. Therefore, because of the general absence of sphericity, settling rates of volcanic ash may be slower than expected on the basis of particle size and weight.

2.5 Measurement of visibility

Visibility involves human perception of the environment, and thus, no instrument truly measures visibility (Malm 1979). Aerosols in the atmosphere, including volcanic ash, interact with light waves leading to absorption and scattering. The amount of light energy redirected from its original path is referred to as the extinction coefficient (b_{ext}) and is equal to the sum of four interactions (Robinson 1968; Hyslop 2009):

$$b_{\text{ext}} = b_{\text{scat,p}} + b_{\text{scat,g}} + b_{\text{abs,p}} + b_{\text{abs,g}} \quad (1)$$

where $b_{\text{scat,p}}$ is the light scattering by particles, $b_{\text{scat,g}}$ is that by gases, $b_{\text{abs,p}}$ is the light absorption by particles, and $b_{\text{abs,g}}$ is that by gases.

The extinction coefficient is thus the optical parameter which is the best proxy for visibility assessment. Once the extinction coefficient is calculated, the corresponding visual range (VR) in metres can be estimated, defined as the longest distance that a large, black object can be seen against the sky at the horizon with the unaided eye (Binkowski et al. 2002; Seinfeld and Pandis 2006; Hyslop 2009; Blake et al. 2016a):

$$\text{VR} = 3.912/(b_{\text{ext}}) \quad (2)$$

where the value at the numerator is constant.

Further information on the extinction coefficient and visual range can be found in Online Resource 1.

Particles smaller than the wavelength of visible light (particle diameter $< 0.05 \mu\text{m}$ in white light) have little effect on visual range. Larger particles (particle diameter $> 2 \mu\text{m}$ in white light), however, have a much greater effect with characteristics such as size, shape and composition being much more influential (Conner 1974; EPA 2000). Although some studies assess the optical properties of volcanic ash at high altitude using remote sensing techniques for the purposes of flying aircraft operability (e.g. Weinzierl et al. 2012), to the best of our knowledge, there have been no detailed quantitative studies of visual range during ashfall near ground level. However, if visibility characteristics associated with volcanic ash can be quantified near the ground, then comparisons with other, more studied atmospheric hazards such as fog and dust storms can be made, and impacts on surface transportation and vehicle mobility estimated. We suggest that where visibility in volcanic ash has not been quantified, precise comparisons to visibility during other atmospheric

hazards cannot be made as the characteristics of certain particles and subsequent effect on light attenuation may be different.

2.6 Effects of visibility degradation on surface transportation networks

Through the common effect of visibility degradation, many atmospheric hazards produce similar consequences for surface transportation. Specifically, previous studies document that the presence of thick fog, smoke or dust influences roads by: (1) reducing the volume of traffic; and (2) increasing the risk of accidents despite lower traffic volumes and an overall reduction in speed—particularly accidents that involve multiple vehicles and cause a higher percentage of severe injuries (OECD 1986; Musk 1991; Ashley et al. 2015; Hardy 2015; Ibrahim 2015).

There have been many studies into the impacts of fog and mineral dust on visibility (e.g. Codling 1971; Moore and Cooper 1972; Hagen and Skidmore 1977; Summer et al. 1977; Perry 1981; Musk 1991; Taylor and Moogan 2010; Abdel-Aty et al. 2011; Weinzierl et al. 2012; USDOT 2013; Ashley et al. 2015). High concentrations of fog droplets and/or mineral dust particulates are required to cause low visibilities and disrupt transportation networks. For example, Hagen and Skidmore (1977) highlight that mineral dust concentrations exceeding 50 to 100 mg m⁻³ seriously reduce visibility during daylight, with lower concentrations hazardous at night. Other atmospheric hazards including smoke from wildfires and airborne volcanic ash, routinely disrupt road networks and inhibit operations at airports, and accidents have been attributed to volcanic ashfall (e.g. Bartney 1980; Folch et al. 2014; Blake et al. 2015). However, they remain relatively under-researched hazards in transportation studies (Cova and Conger 2003, Abdel-Aty et al. 2011).

A recent study by Brooks et al. (2011) used a driver-simulation method to determine how drivers react when driving in varying levels of fog and to assess whether drivers are willing to drive at speeds where their lane-keeping performance is degraded due to the reduced visibility. Observed speed reductions were as follows:

- For visual ranges of 496–31 m, average speeds decreased from 91.3 to 89.1 km h⁻¹
- For 18 m visual range, speeds decreased further to 82.9 km h⁻¹
- In the foggiest condition tested (6 m visual range) speeds decreased to 71.7 km h⁻¹, representing a decrease of ~ 20 km h⁻¹ from clear conditions.

Despite the speed reductions for the most reduced visibility however, it was calculated that drivers would likely be incapable of stopping to avoid obstacles in the roadway (Brooks et al. 2011; Blake et al. 2016a), a situation that corresponds to what has been recorded on actual roads in inclement weather (Edwards 1999). Additionally, lane-keeping ability was reduced when fog resulted in visibility distances < 30 m (Brooks et al. 2011). Mueller and Trick (2012) also used a driver-simulation method to investigate average speeds in fog (with 600 m visual range) and found that all drivers reduced their speed in fog compared to clear conditions, with an average speed reduction of 6.4 km h⁻¹.

Mitigation measures available for managing reduced visibility due to airborne volcanic ash include reducing vehicle speeds (including the implementation of lower-than-usual speed limits); restricting the number and/or type of vehicles on the network; increasing the space between moving vehicles; dampening surfaces with water to minimise the resuspension of ash, and closing roads in especially contaminated areas (Table 1). The only complete solution is the total removal of ash deposits, but this may not be possible or cost-effective.

2.7 Auckland case study

We use Auckland as a case study location to apply our methodology due to the relatively large population (~ 1.6 million people, Statistics New Zealand 2015), extensive transport networks and exposure to multiple sources and types of volcanic ash (Fig. 2).

Basaltic ash may originate from new eruptions in the Auckland Volcanic Field (AVF), on which the city is built, or potentially from Whangarei and Bay of Island volcanic fields to the north (Smith and Allen 1993). Andesite can be deposited from eruptions within the Tongariro Volcanic Centre, located in the Taupo Volcanic Zone (TVZ) and from Taranaki Volcano. Rhyolite may be deposited in Auckland from eruptions within the Taupo and Okataina Volcanic Centres of the TVZ with rhyolitic ash from Mayor Island also possible. Recent work by Zawalna-Geer (2016) suggests that Auckland has been inundated by tephra at least once every 424 years on average. However, any recurrence rates must be considered with caution due to different climatic regimes and because not all eruptions will be preserved in the geologic ash record, and certainly not all eruptions will be represented by ash at specific coring sites (Lindsay and Peace 2005). Auckland is exposed to ashfall with a relatively wide range of airborne concentrations, settling rates, as well as particle sizes, densities and shapes (Smith and Allen 1993). As such, many of the methods and results in this paper are internationally applicable.

Visual range for excellent conditions is typically taken to be > 70 km (MFE 2001). Indeed, the mean visual range taken over a three year period (from 2001 to 2003) from readings over Auckland City (Dr Gerda Kuschel, Auckland Council, pers comm, 21 June 2016) is similar, calculated at 66.5 km with 95% CI [65.1, 67.8]; the shorter visual range is unsurprising given the city environment with likely higher background particulate concentrations than “typical excellent” conditions.

3 Methodology

Our methodology outlines the novel technique used to simulate ashfall and to simultaneously measure ash-settling rates and extinction coefficients (subsequently used to calculate visual ranges using Eq. 2) in a laboratory environment. Visual ranges through ashfalls of different particle sizes and types and settling rates, representing those considered possible in Auckland, may thus be determined.

3.1 Experimental set-up

The key equipment used for our experimental set-up is a transmissometer to calculate visual range, and solid aerosol generator to disperse ash, both selected specifically for the purpose and incorporated into a custom-made experimental set-up.

3.1.1 Transmissometer

We use a dual-pass transmissometer (DynOptic DSL-460 MkII) for our experiments. The transmissometer is adopted to measure the optical characteristics over a preset path length of 1.4 m. It measures a specific amount of green light transmitted from the source/transceiver securely mounted to the side of a container, to a reflector mounted opposite and back to the same transceiver (Fig. 3). This allows the direct and continuous (1 s interval)

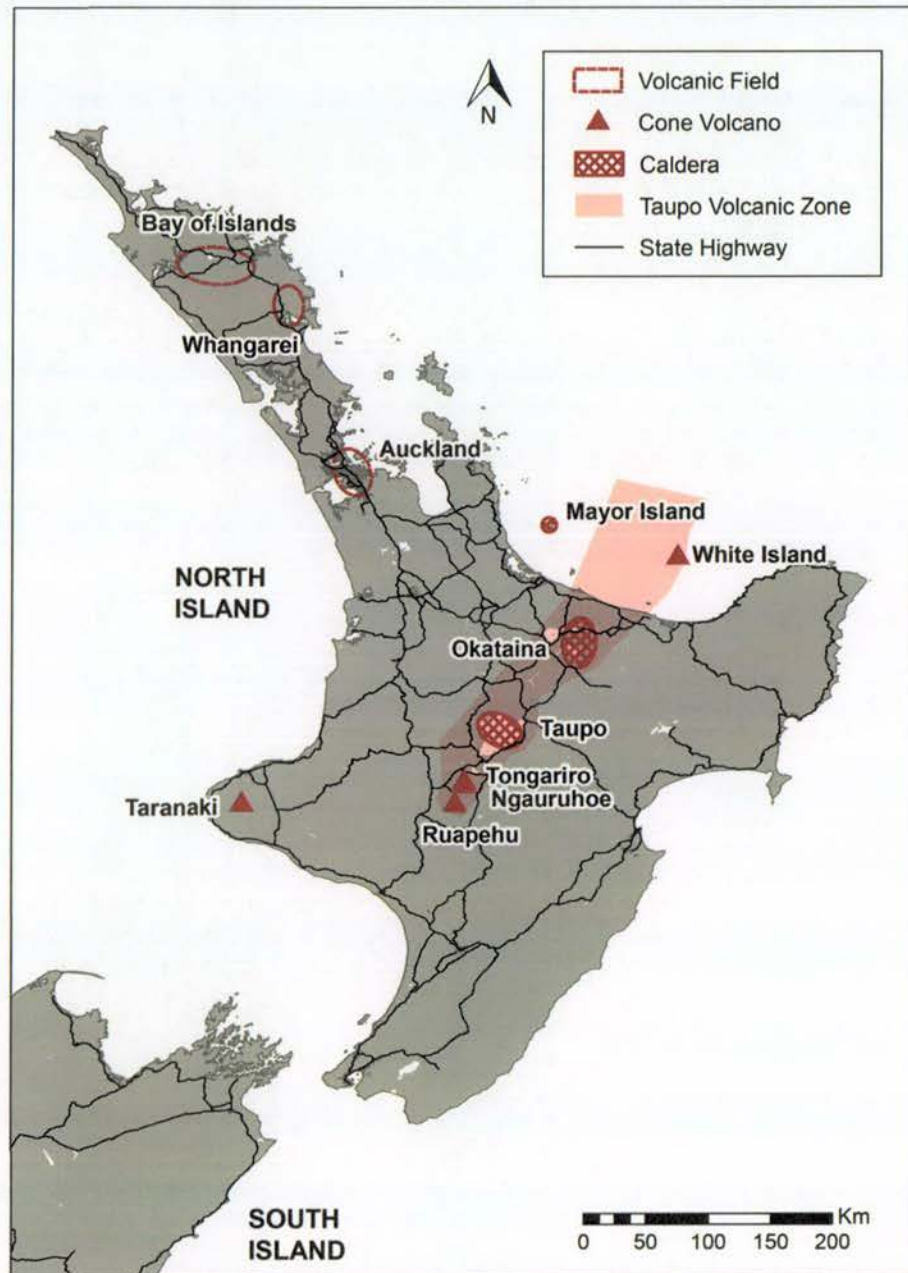


Fig. 2 Potential sources of volcanic ash in New Zealand that could affect Auckland

calculation of the extinction coefficient of the air along the path length for light with a wavelength at which the human eye observes. A small amount of ash accumulates on the optics of the transmissometer during each test. However, following trial tests, this was substantially limited by extracting purge air (which the instrument uses to clean the optics

during operation) through ducting from an adjacent clean room. Following the extraction of purge air from a clean source, the accumulation of ash on the optics accounted for only $\sim 1.0 \times 10^{-6}\%$ of the maximum values recorded which is deemed insufficient to substantially affect findings. The transceiver and reflector are simply cleaned with

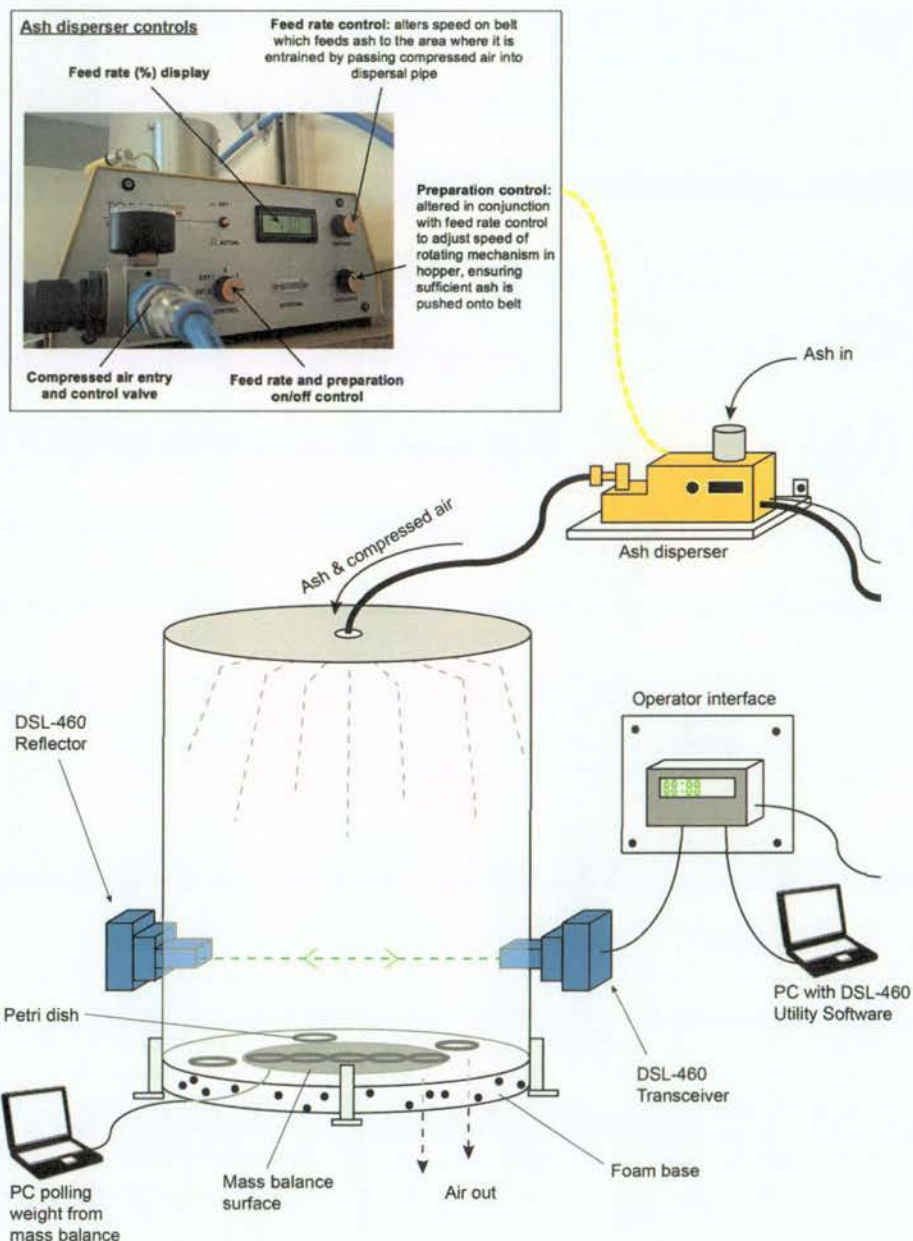


Fig. 3 Experimental set-up developed and implemented for visibility testing (adapted from Blake et al. 2016a)

compressed air between each experiment and results corrected so as to always start with zero values for the extinction coefficient and avoid drift. We refer the reader to Online Resource 2 for further information on transmissometers, and to the DynOptic DSL-460 MkII operation manual (DynOptic 2014) for detailed information on the calibration and operation procedures for this particular transmissometer.

3.1.2 Ash disperser

Precise and consistent ash-generation rates (g h^{-1}) are produced using a solid aerosol generator (Topas SAG 410) (named *ash disperser* from herein) into the top and centre of a purpose-built stainless-steel cylindrical container (Fig. 3), shaped as such to encourage evenly distributed flow because trial tests suggested that cylinders were preferential to cuboids where ash-settling rate varied in corners.

Two simultaneous methods for calibration of the ash disperser for each ash type of particular particle diameter size distribution were used to determine the machine settings required for different generation rates and estimated ash-settling rates in the container; a gain-in-weight technique where ash dispersed from the instrument is collected in filter bags and weighed, and a loss-in-weight technique where the whole instrument weight is recorded before and after ash dispersal.

3.1.3 Ash-settling rate measurement

When the ash enters the container, a purpose-built nozzle on the end of the tube causes the ash to be dispersed in all directions before settling under gravity. The height of the container (1.3 m total, with a 1 m fall distance to the light beam of the transmissometer) was chosen by considering formulas derived from Bonadonna et al. (1998), which suggest that the majority of ash particles dispersed reach terminal velocity before passing through the measurement level. However, the set-up was also constrained by workspace limitations and accessibility requirements to the hopper of the ash disperser, which had to be positioned above. Beneath the measurement level of the transmissometer, the ash settles at the base of the container (0.75 m^2 in area). Half of the area (i.e. 0.375 m^2) at the centre of the base is dedicated to a circular board on top of an automated mass balance set to poll and record the weight of ash every 10 s. The other half around the edge consists of foam, which allows the air to evenly escape from the base of the container and the vast majority of ash to remain static when out of suspension. Trial tests suggested that the solid board at the centre had little influence on ash flow currents towards the base of the container and that there was minimal remobilisation of ash that would affect results.

Some radial differences in ash-settling rates were identified for samples, both for individual experiments and between experiments. However, the consistent airflow within the container, along with the light beam traversing the entire diameter, means that there is negligible effect on the transmissometer readings and that the entire horizontal transect would appropriately represent a steady ashfall. To account for the radial differences in settled ash at the base (i.e. because the board does not cover the whole area), a series of ten petri dishes are equally positioned (five on the central board and five on the foam edge). These are weighed after each experiment to analyse the distribution profile for the settling ash in our experiments. The results from the petri dishes, in conjunction with the centred mass balance weights, are used to calculate and record mean “actual” (rather than estimated) ash-settling rates ($\text{g m}^{-2} \text{ h}^{-1}$) at the base (Sect. 4.1).

Preliminary test runs revealed that equilibriums between ash generation into the container and ash settling at the base occurred within 15 min for all ash types. Therefore, every experiment for each ash type at a specific generation rate and distribution for particle diameter size is run for a total of 1 h where possible (some high generation rates caused ash supply to be exhausted within 45 min). This allows at least 30 min of continuous measurement at equilibrium conditions, which is sufficient time for a mean value of the extinction coefficient and visual range for each sample and ash-generation rate to be calculated. The transmissometer is then left operating for at least a further 15 min after the disperser is switched off to allow continued monitoring, whilst all the ash settles out. Ash is cleaned from the board, foam and container edges between each experiment and a thorough clean of all equipment is conducted. The ash disperser tube is disposed of and replaced at the end of testing with each ash sample.

3.2 Application to Auckland

Methods used to replicate ash types, particle sizes and settling rates that can be expected in the city given a future volcanic eruption in the AVF or from the larger volcanoes of the central North Island of New Zealand are described in Sects. 3.2.1–3.2.3, respectively.

3.2.1 Ash type

Basaltic, andesitic and rhyolitic ashfall is possible in Auckland, and we conduct experiments with all three types; a dark-coloured basalt which is sourced from a deposit of Pupuke Volcano in the AVF, a mid-coloured andesite derived from a deposit from the Poutu eruption of Tongariro Volcano, and a light-coloured rhyolite from the Kaharoa eruption of Tarawera Volcano, in New Zealand (Table 2). The raw samples were largely selected from sources outside of the AVF, as many of those within the AVF have been weathered, contaminated by organic material and/or disturbed or removed by human activity (e.g. Alloway et al. 2004; Cassidy and Locke 2004; Howe et al. 2011; Adams 2013). Our samples were modified through pulverisation to achieve a range of particle diameter size distributions possible in Auckland and thus likely contain a higher than natural proportion of particles that are blocky in nature with a high degree of angularity due to the milling process (Broom 2010). Therefore, an additional fine-grained sample (sourced from the 2008 eruption of Chaitén in Chile—Table 2) is also tested to investigate the effects of particle shape on visual range. This sample was not altered through pulverisation and only sieved to remove the larger particles that can cause clogging of the ash disperser. All samples were dried at 65 °C for > 48 h prior to testing.

3.2.2 Particle size

Following a detailed literature review, we further developed work by Hill (2014) to estimate ash particle sizes that can be expected in Auckland from volcanic sources in New Zealand (Fig. 4). Unlike Hill (2014) however, who focussed solely on median data, we incorporate all available data for particle size, including individual data or median size recorded at specific locations from a vent (shown as points in Fig. 4), modes (bold points or bold ranges), full distributions (vertical “error bars”) and distributions in spatial extent (horizontal “error bars”). Triangles in Fig. 4 denote maximum clast sizes of blocks, and black data points show particle sizes and distances from vents determined from recent

Table 2 Characteristics of the four ash types used for experimentation

	Pupuke, Auckland Volcanic Field, New Zealand	Poutu, Tongariro, New Zealand	Kaharoa, Tarawera, New Zealand	Chaitén, Chile
Year of eruption	~ 200,000 BP (Leonard et al. 2017)	~ 11,000–12,000 BP (Hitchcock and Cole 2007)	1314 (Sahetapy-Engel et al. 2014)	2008 (Lara 2009)
Ash type	Basalt	Andesite	Rhyolite	Rhyolite
Colour (determined from Munsell Rock Colour Chart)	N4: medium dark grey	5Y 6/1: light olive grey	5YR 5/2: pale brown	5Y 8/1: yellowish grey
SiO ₂ content (determined by Philips PW2400 XRF analysis)	44% (mafic)	52% (intermediate)	75% (felsic)	75% (felsic)
Dominant minerals (determined by Philips XRD analysis)	Diopside, Forsterite, Anorthite	Albite, Augite	Albite, Quartz	Albite
<u>Particle size group</u>	<u>a</u> <u>b</u> <u>c</u>	<u>b</u>	<u>b</u>	<u>b</u>
Mode particle size (µm) (see Fig. 5)	12 45 105	22	30	21
Dry bulk density (g cm ⁻³)	0.92 1.12 1.28	0.89	0.87	0.83

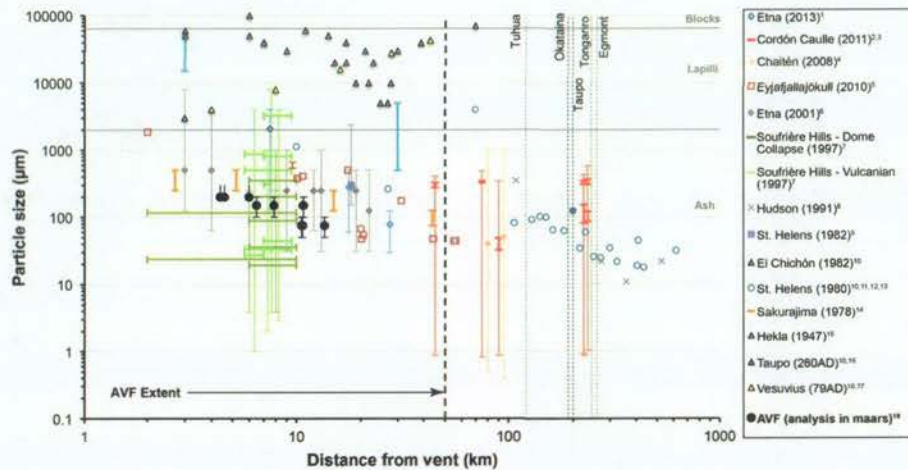


Fig. 4 Particle sizes of ash deposits and their associated distances from 15 worldwide eruptive vents and analysis from maars in the AVF. The distances from central Auckland (depicted as 0 km) to New Zealand volcanic ash sources are identified by a series of dashed vertical lines, and approximate maximum axial extent of the AVF by a bold dashed vertical line. Solid horizontal grey lines denote the boundaries between ash and lapilli (2 mm) and lapilli and block (64 mm) particle diameters. Data from: ¹Andò et al. (2014), ²Wilson et al. (2013), ³Heather Craig, University of Canterbury, pers comm, 17 July 2014, ⁴Watt et al. (2009), ⁵Bonadonna et al. (2011), ⁶Scollo et al. (2007), ⁷Bonadonna et al. (2002), ⁸Scasso et al. (1994), ⁹Harris and Rose (1983), ¹⁰Carey and Sigurdsson (1986), ¹¹Scheidegger and Federman (1982), ¹²Sarna-Wojcicki et al. (1981), ¹³Carey and Sigurdsson (1982), ¹⁴Eto (2001), ¹⁵Wilcox (1959), ¹⁶Walker (1981), ¹⁷Sigurdsson et al. (1985), ¹⁸Jenni Hopkins, Victoria University of Wellington, pers comm, 19 July 2014

analysis of deposits in six Auckland maars from historical AVF eruptions of One Tree Hill, Three Kings and Mt Eden Volcanoes (Jenni Hopkins, Victoria University of Wellington, pers comm, 19 July 2014).

Due to the maximum particle size constraints of the ash disperser and likely clogging when particle diameters exceed $\sim 300 \mu\text{m}$, our experiments focus on samples defined as *fine ash* by Carey and Sigurdsson (1982) and Folch et al. (2009), in that mode particle diameters for most samples are $< 64 \mu\text{m}$. All mode particle diameters are $< 110 \mu\text{m}$ (Fig. 5). However, we subdivide our samples into three categories of mode particle diameter size for ease of interpretation; a. $< 20 \mu\text{m}$, b. $20\text{--}50 \mu\text{m}$ and c. $> 50 \mu\text{m}$ (Table 2). For the basalt sample, we test ash for all three categories to investigate the effect of particle diameter size on visual range. For the andesite and rhyolite samples however, we only test for the category b range due to ash sample availability. Specific ash particle sizes were achieved using a rock pulveriser with different disc separation distance and sieves with different mesh aperture sizes, followed by laser sizing to determine the particle diameter size distributions. Total particle diameters for all samples used are $\sim 1\text{--}320 \mu\text{m}$ (Fig. 5) which corresponds with the mid- to lower-grain sizes of ash particles that can be expected in Auckland given a future eruption in New Zealand (Fig. 4).

3.2.3 Estimated ash-settling rates

As the generation rate of each ash type and particle size is determined as part of the instrument calibration, estimations of settling rate can be made given the known volume of the container where the ash is dispersed and replicated under controlled conditions. As with

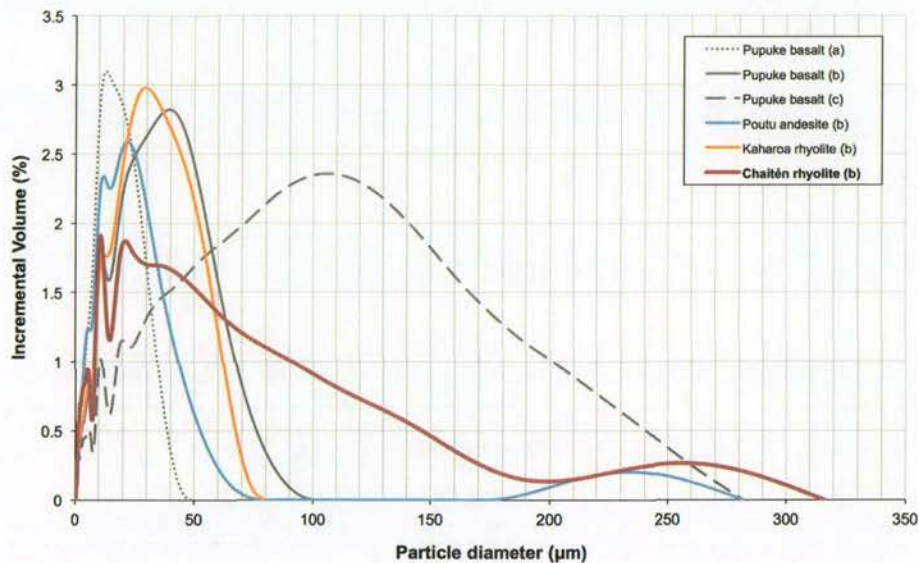


Fig. 5 Particle diameter size distribution plots for the ash used in experimentation, derived from three tests per sample using a Micromeritics Saturn DigiSizer II laser sizer instrument. **a–c** refer to the mode size categories shown in Table 2. All ash samples used generally have a normal distribution for particle sizes, with the exception of the rhyolite sample from Chaitén, where particle sizes have a distinctive positive skew

particle sizes, all available worldwide ash-settling rate data were plotted, which showed a generally decreasing settling rate with distance from vent (Fig. 6).

Based on the settling rates in Fig. 6, and the particle sizes adopted for experimentation (Table 2), which represent ashfall in Auckland from distal eruptions or mid- to lower-particle sizes expected from an AVF eruption, we attempt to replicate ash-settling rates between 50 and $1000 \text{ g m}^{-2} \text{ h}^{-1}$ (four specific ash-settling rates within this range per sample) for all six of the samples. However, we also attempt to replicate settling rates towards the upper limit of what can be expected in Auckland (i.e. around 2000 and $10,000 \text{ g m}^{-2} \text{ h}^{-1}$) for the Pupuke basalt and Chaitén rhyolite (category b) samples, where more material was available, to determine expected absolute minimum visual ranges from direct ashfall in the AVF. Thus, in addition to multiple trial tests, a total of 28 experiments are conducted as part of this study.

We highlight that the ash-settling rates determined at this stage are those forecast using the ash disperser calibration results. Actual ash-settling rates at the base of the container are lower; particularly for high ash-generation conditions, due to:

- Adherence of some ash to the container side and top reducing the airborne concentration and settling rate.
- An increase in pressure within the container acting against more ash entering as compressed air continues to enter at the top of the container, but the foam at the base becomes clogged.
- Leakage of some ash from the container altogether, either through the foam or small gaps, especially when the air pressure inside is very high.

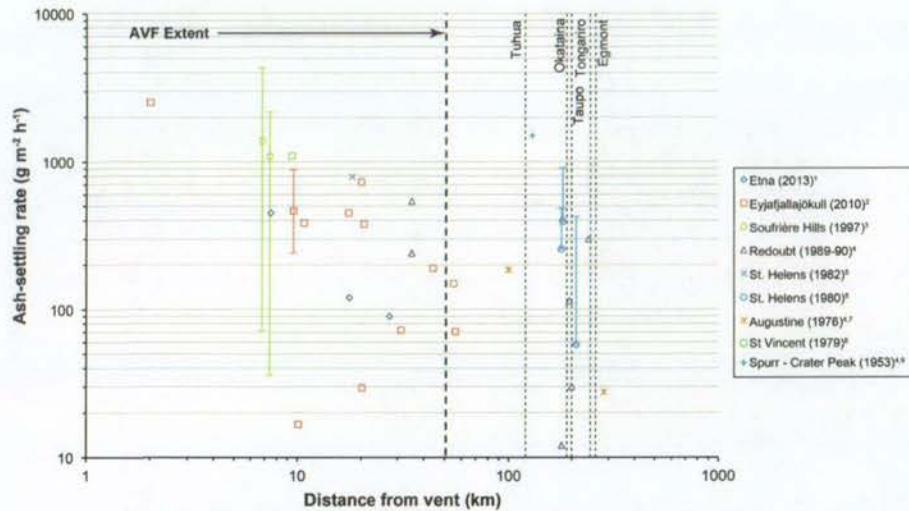


Fig. 6 Ash-settling rates and their associated distances from nine worldwide eruptive vents. The distances from central Auckland (depicted as 0 km) to New Zealand volcanic ash sources are identified by a series of dashed vertical lines, and approximate maximum axial extent of the AVF by a bold dashed vertical line. Data from: ¹Andò et al. (2014), ²Bonadonna et al. (2011), ³Bonadonna et al. (2002), ⁴Scott and McGimsey (1994), ⁵Harris and Rose (1983), ⁶Scheidegger and Federman (1982), ⁷Kienle and Swanson (1985), ⁸Brazier et al. (1982), ⁹Wilcox (1959). A value of $1100 \text{ g m}^{-2} \text{ s}^{-1}$ was also identified in Self et al. (1974), but the duration of this rate is unclear and it involved scoria material with a predominant particle size of $\sim 6 \text{ mm}$. Therefore, we decided not to extrapolate it to 1 h for the purpose of this chart

Actual ash-settling rates are determined from the centred mass balance and petri dish procedure outlined in Sect. 3.1.3.

4 Results

4.1 Ash concentrations and settling rates

Measurements of airborne ash concentration taken directly from the transmissometer were $\sim 40\text{--}1600 \text{ mg m}^{-3}$ for all experiments, with higher values corresponding to the highest ash-settling rates and lowest visual ranges (Online Resource 3–4). There were no distinct differences between airborne particle concentration reductions for the different ash samples or ash-generation rates we used in experimentation. It took 11 min (± 2 min) for airborne concentrations to return to original levels. However, given the exponential decay in airborne particle concentration following the cessation of new ash entering the container, values decreased to $< 10\%$ of their maximum values in less than 5 min.

For the relatively coarse-grained ash samples (particularly size category c, and to some extent b), a greater weight of ash and more ash of larger particle size fell towards the centre of the container base, with ash becoming more fine-grained towards the edge. Fine-grained ash adhered to the edge and top of the container (Fig. 7). Adherence was prevalent for the ash samples with the finest particle sizes (i.e. category a, and to some extent b), and especially so for the Chaitén rhyolite sample, causing sometimes large decreases in ash-settling rates towards the extreme edge of the base.

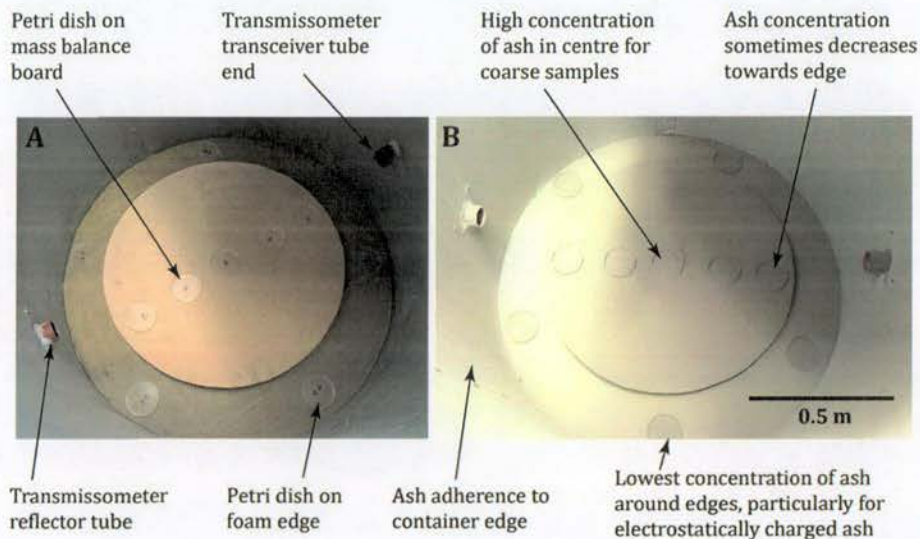


Fig. 7 Annotated plan-view photographs taken looking down into the container showing **a** petri dishes on the central mass balance board and foam edge, and **b** describing general ash accumulation patterns across the container base, determined from the mass of ash on the centred board and in petri dishes, and through visual observations after each experiment

Due to the inconsistencies across the container base, results displayed for ash-settling rates are in the form of three values, corrected for a 1-h period over 1 m^2 :

1. A minimum value calculated from the weight recorded on the centred mass balance board at the container base multiplied by a correction factor determined by the weight difference between ash in the petri dishes on the board and on the foam edges for that particular sample.
2. A maximum value calculated by doubling the weight recorded on the central mass balance board at the container base for that sample to assume the same weight falls on the foam edge.
3. The midpoint between points 1 and 2 above, which is deemed the value most likely to represent the true ash-settling rate.

Based on these values, although ash-settling rates forecast from the ash disperser calibration were $\sim 50\text{--}10,000 \text{ g m}^{-2} \text{ h}^{-1}$ (Sect. 3.2.3), the actual ash-settling rates for our results are calculated at $28\text{--}4800 \text{ g m}^{-2} \text{ h}^{-1}$.

4.2 Visual ranges

Figure 8 shows an example of the direct visual range reading from the transmissometer for one experimental run. In our results, the maximum and minimum values recorded by the transmissometer have greater deviation from the mean for the lowest airborne concentrations and ash-settling rates.

For the Pupuke basalt, which had the highest bulk density of the four ash types used, testing was conducted using three distinct particle diameter size distributions, the results of which are summarised in Fig. 9 with data values in Online Resource 3. It is evident that for a given ash-settling rate, visual range is less for ash predominantly containing finer

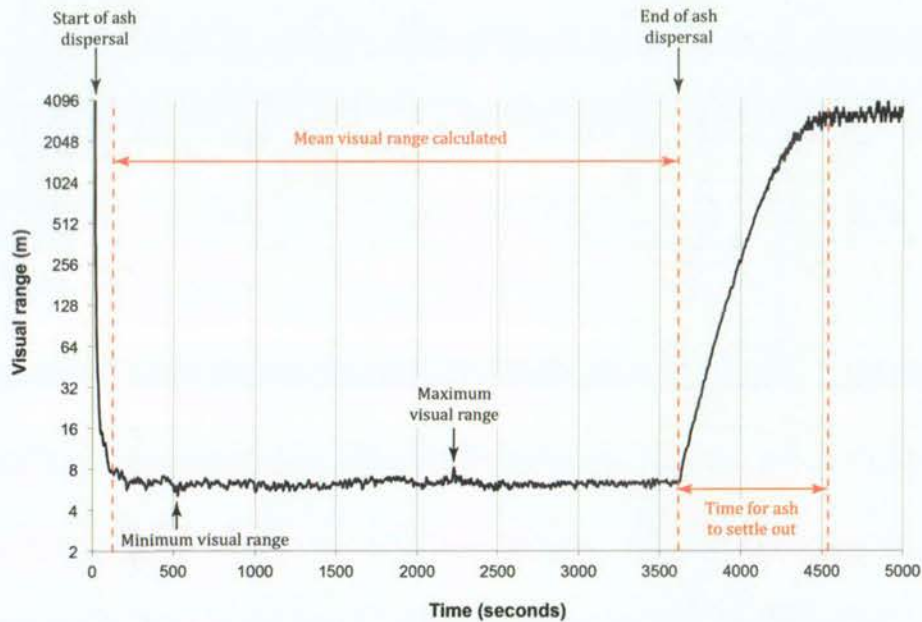


Fig. 8 Unprocessed transmissometer results for the Kaharoa rhyolite sample when ash was dispersed at the highest generation rate tested. Annotations show how the mean, maximum and minimum visual ranges were determined, as well as time taken for all ash to settle out and airborne concentration and visual range to return to original conditions

particles. Lines of best fit follow inverse power relationships (Fig. 9). Similarly, relationships between visual range and ash-settling rates are best described by inverse power law relationships for the rhyolitic and andesitic ash types (Fig. 10 and Online Resource 4 for data values). The Chaitén sample produced results with greater visual ranges than all other types in the same particle size category, despite being the lightest-coloured ash we tested.

5 Discussion

This section includes a discussion of our experimental approach and considerations for visibility in airborne volcanic ash in both a general sense and specifically forecast conditions for Auckland. We then outline key limitations of the approach adopted and recommendations for future adaptations and additions to the methodology. Finally, we consider implications of reduced visibility for transportation operation and provide examples of mitigation strategies that transportation and emergency management officials could implement based on findings from this study and other recent work.

5.1 Visibility in airborne volcanic ash

Our results demonstrate that the new methodology and experimental set-up developed is suitable to produce sufficiently consistent ash-settling rates to analyse visual range through airborne volcanic ash in laboratories. Compared to most other airborne particulate matter,

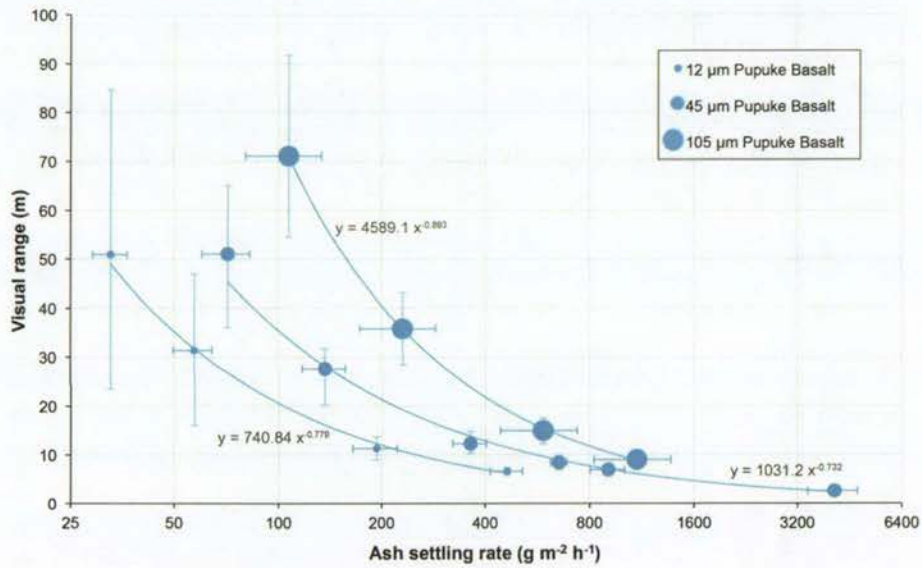


Fig. 9 Visual ranges for the three Pupuke basalt particle diameter size distributions. Each point is for the mean visual range when ash flow into the container was at equilibrium with ash-settling rate at the base for each experiment. Horizontal minimum and maximum error bar values and the point values correspond to bullet points 1–3 in Sect. 4.1, respectively. Vertical error bars show the maximum and minimum values recorded by the transmissometer during the periods of equilibrium (Fig. 8)

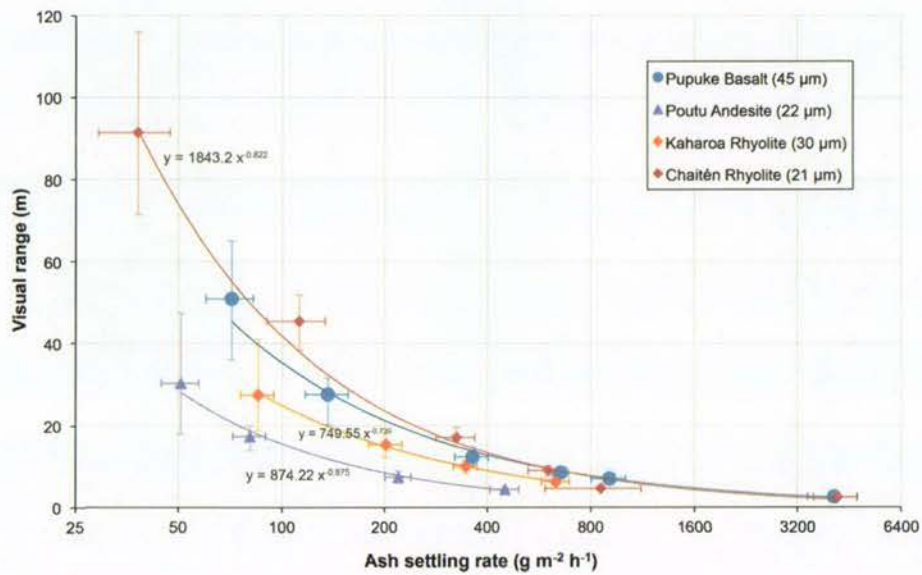


Fig. 10 Visual ranges for the four ash samples in particle diameter size distribution category b (i.e. 20–50 μm mode diameters). Each point is for the mean visual range when ash flow into the container was at equilibrium with ash-settling rate at the base for each experiment. Horizontal minimum and maximum error bar values and the point values correspond to bullet points 1–3 in Sect. 4.1, respectively. Vertical error bars show the maximum and minimum values recorded by the transmissometer during the periods of equilibrium (Fig. 8)

ash particles are relatively large in size. However, their occurrence in large concentrations, like fog droplets, can cause substantial reductions in visibility, although they generally fall to the ground and out of suspension more quickly.

The time taken for the airborne ash concentration to reduce to zero upon cessation of dispersal at the top of the container is of particular interest. It provides an indication of how long remobilised ash would take to settle from a 1 m height above the ground given no ongoing disturbances such as wind or traffic and in the absence of rainfall. This type of information can be used to inform transportation management strategies such as the spacing of rail or road vehicles to allow sufficient time for ash to settle and reduce visual impairment to drivers (Sect. 5.3). Adherence of ash to the container is likely explained by the electrostatic charging of ash particles (Bonadonna and Phillips 2003; Folch 2012). However, as the light beam of the transmissometer passes the width of the container (1.4 m path length) and because inconsistencies occur in a radial pattern, this allowed the accurate calculation of mean ash-settling rates.

Visual range fluctuates between readings (Fig. 8), depending on the quantity and characteristics of particles within the light beam of the transmissometer at the precise time of measurement. However, as values are recorded at one-second intervals and because we calculate each mean visual range result from at least 30 min of experimentation, i.e. > 1800 data points, we consider our results reliable.

The result that visual range is lower for ash containing finer particles corresponds to the findings by Conner (1974), in that the mass scattering efficiency of light decreases as particle size increases. Comparing the Pupuke basalt and Kaharoa rhyolite, which were pulverised and sieved with the same dimension controls, results suggest that the light-coloured rhyolite causes lower visual ranges than the dark-coloured basalt. This makes intuitive sense, as there is more reflection from light-coloured surfaces. Low visual ranges for the andesite sample are perhaps explained by augite being one of the dominant minerals (constituting ~ 20% of the sample). With two prominent cleavages, meeting at angles near 90 degrees for augite, light scattering may be relatively high. Furthermore, the particle sizes for the andesitic ash are low compared to the basalt and Kaharoa rhyolite, and fallout of the andesite may be slowed by relatively irregular particle shapes (Riley et al. 2003; Pardini et al. 2016).

The most likely explanation for the unexpected visual range results obtained for the Chaitén sample is due to the larger positive particle size distribution from the mode than the other samples (Fig. 5), and thus higher proportion of relatively large diameter particles. Additionally, the comparatively low processing undertaken when producing this sample led to particles that are relatively spherical in shape (Fig. 11). As such, they reflect less light than the irregular-shaped particles of the other samples we tested. In fact, the Chaitén ash is more representative of fresh volcanic ash samples and our results for the other samples, which were all mechanically pulverised, thus provide a worst-case situation for visual range reduction during initial ashfall in this regard.

5.1.1 Consequences of ashfall events in Auckland for visibility

Our results sufficiently cover the range of settling rates that can be expected in Auckland given a future eruption in New Zealand based on correlation with the limited dataset available from worldwide eruptions (Fig. 6). Ash-settling rates of ~ 1000 g m⁻² h⁻¹, possibly up to ~ 4000 g m⁻² h⁻¹, may occur in Auckland from any of these eruption locations (Fig. 6), and extrapolation of the line of best fit for the finest grained ash we

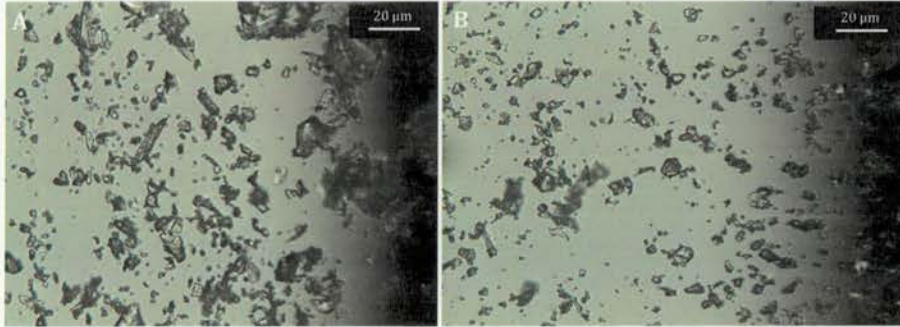


Fig. 11 Microscope images for **a** Kaharoa rhyolite sample, **b** Chaitén rhyolite sample, both in particle size group b. The individual particles of the Chaitén sample are generally more spherical in shape. A Leica DM2500P microscope (with $\times 40$ zoom) and Leica DFC295 camera attachment was used to capture the images

tested ($12\ \mu\text{m}$ mode particle diameter) to these settling rates suggest that visual ranges as low as $\sim 1\text{--}2\ \text{m}$ can occur under such conditions.

Ash-settling rates are likely to be higher (resulting in shorter visual ranges) nearer to the vent and for explosive eruptions, which generally produce a relatively large proportion of fine-grained ash (White et al. 2011). For Auckland, small ash particle diameter sizes are possible from eruptions in both the AVF and TVZ of New Zealand (given appropriate wind directions). However, even the smallest estimated ash-settling rates in Auckland ($\sim 10\ \text{g m}^{-2}\ \text{h}^{-1}$) during an eruption would cause a visibility reduction of over two hundred times from typical baseline visual range (i.e. $< 300\ \text{m}$ rather than $70\ \text{km}$ visual ranges) for ash with characteristics in the range we tested.

5.2 Key limitations and suggestions for future work

- Accurate source data for ash-settling rates (and particle concentrations) following past eruptions are somewhat limited, and forecasts remain constrained by the small dataset. We anticipate that the recent development of automated ash sampling instrumentation (e.g. Shimano et al. 2013; Weber et al. 2013, Andò et al. 2014; Tajima et al. 2015) and their deployment during and following future eruptions will improve understanding of settling rates and reduce uncertainty.
- All of our experiments incorporated only fine-grained ash (all particle diameters $< 320\ \mu\text{m}$ with mode sizes $< 110\ \mu\text{m}$) due to limitations of the ash dispersal equipment which was prone to clogging by coarse particles. However, the particle size distributions of our ash samples are generally polydisperse and appropriately replicate fine-grained ashfall that could occur in Auckland from diverse sources.
- All ash samples were oven-dried to obtain consistent dryness prior to investigating particle characteristics. Therefore, we have not accounted for relative humidity affecting the ash over time, although the ash was exposed to relatively stable humidity in the laboratory when conducting the experiments. Visibility in mineral dust storms is known to decrease if the relative humidity is high, particularly if more than 70% (Hagen and Skidmore 1977). We speculate that if volcanic ash encounters higher relative humidity, there will likely be greater light scattering and lower visual range due

to the hygroscopic properties that the particles exhibit (Malm et al. 2003; Barsotti et al. 2010). Therefore, Eq. 2 may underestimate visibility reduction.

- Although the transmissometer records regular measurements of airborne particle concentration, we view these data with caution in this study, as precise values would require the density correction factor (set as 1.00 for our tests) to be adjusted between each sample. In the absence of complex isokinetic sampling of the airborne ash in the container, this cannot be achieved (DynOptic 2014), and we recommend this addition for future work. However, we adopted ash-settling rate as an alternative unit of measurement, which avoided the need for isokinetic sampling processes in our study.
- It was evident that the Chaitén sample became highly electrostatically charged with many discharges occurring when touching the container both during experimentation and subsequent cleaning. More specifically, we suggest that the process of triboelectrification, described in relation to volcanic ash by Aplin et al. (2014) and Aplin et al. (2015), occurred frequently for the Chaitén sample. Triboelectrification is the type of contact electrification that occurs when two materials make contact with each other; Some electrical charge transfers from one material to the other with one gaining and the other losing electrons (Electrostatic Solutions Ltd. 2000). This process can occur readily in volcanic ash with a polydisperse particle size distribution dominated by very fine particle sizes (Aplin et al. 2014), such as our Chaitén sample (Fig. 5). If charged particles are physically separated, charges dissipate to earth, generating sudden electrostatic discharges. Additional testing using further samples is required to confirm this hypothesis and appropriately account for these electrostatic properties.
- Given that ash deposits are often characterised across transects or accessible lines rather than across grids (Folch 2012), and given the number and complexity of variables associated with the remobilisation and resuspension of ash (e.g. meteorological conditions, ash wetness, particle characteristics, road surface specifics and vehicle type), we do not investigate the conditions for resuspended ash in detail. Rather, our calculations of visibility impairment largely represent conditions that can be expected during initial ashfall when ash accumulation on the ground is minimal. Current developments in resuspension modelling (e.g. Folch et al. 2014; Reckziegel et al. 2016; Miwa et al. 2018) will aid the future understanding of interactions between ash remobilisation and visibility effects. Our results are presently most reliable for road transportation where ground surfaces are wet and for maritime transportation, as atmospheric remobilisation will be minimal under these conditions. For ongoing eruptions however, our results should be treated as highly conservative for most land-based transportation types where cleaning has not occurred.

5.3 Considerations for transportation

From recent studies that examine impacts on road transportation from visibility degradation caused by fog (Sect. 2.6), we make comparisons to our experimental findings for airborne ash. It is evident that even the lowest ash-settling rates expected in Auckland and the largest particle diameter sizes ($< 110 \mu\text{m}$ mode) used in our research would cause disruption to road transportation from speed reduction due to visibility degradation ($< 600 \text{ m}$ visual ranges). Speed reduction in volcanic ashfall may be even greater than for fog due to additional transportation impacts such as road marking coverage by ash and reduced skid resistance (Wilson et al. 2012a; Wilson et al. 2014; Blake et al. 2016b, 2017a). In the absence of key research on driver behaviour in volcanic ashfall and

assuming no speed restrictions, based on data available for other atmospheric hazards we estimate an average free-flow speed of 30 km h^{-1} for a visual range of 5 m, with an increased chance of accidents due to lack of lane-keeping ability and obstructions hidden from view. With 20 m visual range, 50 km h^{-1} may be possible, but for the lowest expected visual ranges in Auckland ($\sim 1\text{--}2 \text{ m}$), driving is likely to become highly impractical and dangerous.

In an operational environment, transportation and emergency management officials may use knowledge of anticipated driver behaviour, along with results from our study and information on previous mitigation measures following historical eruptions (Table 1), to appropriately deal with reduced visibility (in addition to other impact types) from volcanic ash. For example, in dry conditions or during prolonged eruptions with recurring ashfalls, a 5-min spacing of road and rail vehicles may be appropriate as this allows $\sim 90\%$ of ash to settle (assuming no wind or other atmospheric disturbances). Additionally or alternatively, lower speed limits may be appropriate to minimise the resuspension of ash behind vehicles and reduce accident rates. Such mitigation measures align well with what was implemented on major routes following the 1980 Mount St Helens eruption; as Warrick (1981) states, “although the highways were officially closed, [vehicles] were allowed to proceed westward on I-90 and northward on US 97 at a rate of one vehicle every 5 min and a maximum speed of 25 mph” (p.21).

Transportation management policies and local regulations are likely to have a large influence on the level of disruption from volcanic ashfall in many locations. For example, in Auckland a “restricted visibility routine” for maritime area/s affected may come into effect when visibility of less than 1 nautical mile from a vessel’s bridge is encountered (AC 2014). This would have implications for the numbers and types of vessels permitted in certain areas, and their speeds (AC 2014; MNZ 2015). For airport operations at Auckland Airport, assuming no preceding closure due to other factors such as potential damage to aircraft engines, the visual ranges expected from most initial ashfalls mean that low visibility procedures would be initiated (triggered by $< 1500 \text{ m}$ visual range) (CAA 2008). Only essential ground support traffic directly involved with the arrival or departure of an aircraft will be allowed to operate in the manoeuvring area during such conditions. As the runway at Auckland Airport is equipped with a Category III B Instrument Landing System, aircraft and pilots with the appropriate ratings can land if the visual range is $> 50 \text{ m}$ (Auckland Airport 2008), with a maximum of six aircraft take-off and landing movements per hour (CAA 2008). With lower visual ranges, operations at the airport would cease, although closure would likely be necessary due to other factors by this stage.

6 Conclusions

We have developed an experimental approach to allow the calculation of visual range from given ash-settling rates for a range of different volcanic ash samples with different particle size and compositional characteristics. We have also tested this approach using a selection of volcanic ash samples that represent a range of characteristics that can be expected in Auckland, New Zealand, from multiple sources.

Our results demonstrate that visibility decreases with increasing ash-settling rate. Ash particle size has the greatest effect on visual range. For a given settling rate, fine-grained ash causes a shorter visual range than coarse-grained ash, a finding that aligns with existing research involving other particulate types. The influence of ash type, colour and shape on

visual range reduction is not as clear-cut as for particle size. We conclude that samples with a higher proportion of irregular-shaped particles cause a greater reduction in visual range than those with more spherical shapes. Light-coloured ash such as rhyolite appears to result in lower visual ranges than dark-coloured ash such as basalt; a trend that may be explained on the basis of increased reflection off light-coloured surfaces. However, further laboratory or field-based studies are required to confirm the true extent that particle colouration and shape impacts visual range.

We emphasise that our results are for initial volcanic ashfall only and that any remobilised and resuspended ash from fall deposits could cause lower visual ranges for extended periods of time post-eruption, exacerbating impacts to transportation. Our study highlights the need for rapid syn-eruptive and reliable measurements or calculations of airborne metrics including particle concentration, ash-settling rate and visual range. It also demonstrates the importance of considering different ash properties besides ash thickness in volcanic eruptions, including particle size distribution, shape and colour.

Contemporary ash dispersion and fallout models, which provide outputs of airborne ash concentration and/or ash-settling rate given particular eruptions, can be used to produce scenarios of transportation disruption from reduced visibility, as well as other assessments including for human and animal health hazards. In conjunction with scenarios for other impact types (e.g. reduced skid resistance and line marking coverage by ash), the findings enable the improvement of transportation management strategies during and following future volcanic ashfall.

Acknowledgements We acknowledge the support of the University of Canterbury Department of Geological Sciences, for (a) capex funding for the *TOPAS SAG-410 solid aerosol generator* (ash disperser) and *DynOptic DSL-460 MkII transmissometer* for experimentation; and (b) technical laboratory work support from Peter Jones, Rob Spiers, Chris Grimshaw, Matt Cockcroft, Sacha Baldwin-Cunningham, Cathy Higgins, Sarah Pope, Connor Jones and Stephen Brown, who we gratefully thank. Additionally, we thank the Chartered Institute of Logistics and Transport (CILT) for their financial contribution towards equipment costs. Funding support for the authors from the New Zealand Earthquake Commission (EQC), Determining Volcanic Risk in Auckland (DEVORA) project, Natural Hazards Research Platform (NHRP) and University of Canterbury Mason Trust is also greatly appreciated. We also acknowledge and appreciate the technical support provided by Stephan Große of TOPAS GmbH as well as Jozua Taljaard and Andrew Blair of Ecotech NZ Environmental for the operation and adaptations of the ash disperser and transmissometer, respectively. Daniel Blake would also like to thank his other PhD supervisors, Natalia Deligne (GNS Science), Jan Lindsay (The University of Auckland) and Jim Cole (University of Canterbury), for their edits, guidance and advice throughout the project. Additionally, we thank the two anonymous reviewers for critical review of this paper, which guided subsequent improvements.

Open Access This article is distributed under the terms of the Creative Commons Attribution 4.0 International License (<http://creativecommons.org/licenses/by/4.0/>), which permits unrestricted use, distribution, and reproduction in any medium, provided you give appropriate credit to the original author(s) and the source, provide a link to the Creative Commons license, and indicate if changes were made.

References

- Abdel-Aty M, Akram A, Huang H, Choi K (2011) A study on crashes related to visibility obstruction due to fog and smoke. *Accid Anal Prev* 43(5):1730–1737
- AC (2014) Harbourmaster's Office operation of vessels during periods of restricted visibility: navigation safety operating requirements. Auckland Council, Auckland
- AccuWeather (2015) First Calbuco eruption in 42 years suspends flights in Buenos Aires. *AccuWeather.com*. <http://www.accuweather.com/en/weather-news/more-than-4000-evacuated-after/46042985>. Accessed 23 Nov 2015

- Adams C (2013) Identification of tuff rings in the Auckland Volcanic Field using LiDAR and ground penetrating radar. *New Zealand Journal of Geology and Geophysics*. <http://frontiersabroad.com/wp-content/uploads/2014/03/Cameron-Adams.pdf>. Accessed 08 June 2016
- Alloway B, Westgate J, Pillans B, Pearce N, Newnham R, Byrami M, Aarburg S (2004) Stratigraphy, age and correlation of middle Pleistocene silicic tephra in the Auckland region, New Zealand: a prolific distal record of Taupo Volcanic Zone volcanism. *NZ J Geol Geophys* 47:447–479
- Andò B, Baglio S, Marletta V (2014) Selective measurement of volcanic ash flow-rate. *IEEE Transact Instrum Measurement* 63(5):1356–1363
- Aplin K, Houghton I, Nicoll K, Humphries M, Tong A (2014) Electrical charging of volcanic ash. In: Proceedings of the ESA annual meeting on electrostatics. http://www.electrostatics.org/images/ESA_2014_G_Aplin_et_al.pdf. Accessed 10 Mar 2016
- Aplin K, Nicoll K, Houghton I (2015) Electrical charging of volcanic ash from Eyjafjallajökull. In: Geophysical research abstracts, 17, EGU General assembly 2015
- APTI (2000) OS 411: Computational atmospheric sciences. Air Pollution Training Institute, Shodor Education Foundation Inc., US EPA. <https://www.shodor.org/os411/index.html>. Accessed 27 Feb 2016
- Ashley WS, Strader S, Dziubla DC, Haberlie A (2015) Driving blind: weather-related vision hazards and fatal motor vehicle crashes. *American Meteorology Society, Northern Illinois University*. <http://journals.ametsoc.org/doi/pdf/10.1175/BAMS-D-14-00026.1>. Accessed 07 Apr 2016
- Auckland Airport (2008) Newsroom: fog at Auckland Airport and Category IIIB, 19 November 2008, Auckland Airport. http://www.aucklandairport.co.nz/~media/3FF843AAFCBB4C23B941EAA7406EAB7B.ashx?sc_database=web. Accessed 19 Mar 2016
- Barnard S (2009) The vulnerability of New Zealand lifelines infrastructure to ashfall. PhD Thesis, Hazard and Disaster Management, University of Canterbury, Christchurch, New Zealand
- Barsotti S, Neri A, Scire JS (2008) The VOL-CALPUFF model for atmospheric ash dispersal: 1. approach and physical formation. *J Geophys Res* 113:12p
- Barsotti S, Andronico D, Neri A, Del Carlo P, Baxter PJ, Aspinall WP, Hincks T (2010) Quantitative assessment of volcanic ash hazards for health and infrastructure at Mt. Etna (Italy) by numerical simulation. *J Volcanol Geoth Res* 192:85–96
- Bartney B (1980) Showers of muddy ash fall from fresh eruption. *The Lawrence Daily: Journal—World, Kansas*, 26 May 1980, vol 122, p 20
- Baxter P, Horwell CJ (1999) Impacts of eruptions on human health. In: Sigurdson H (ed) *Encyclopedia of Volcanoes*, 2nd edn. Academic Press, New York
- Binkowski FS, Roselle SJ, Mebest MR, Eder BK (2002) Modeling atmospheric particulate matter in an air quality modelling system using a modal method. In: Chock DP, Carmichael GR (eds) *Atmospheric modelling. The IMA Volumes in Mathematics and its Applications*, vol 130. Springer
- Blake DM, Wilson G, Stewart C, Craig HM, Hayes JL, Jenkins SF, Wilson TM, Horwell CJ, Andreastuti S, Daniswara R, Ferdiwijaya D, Leonard GS, Hendrasto M, Cronin S (2015) The 2014 eruption of Kelud volcano, Indonesia: impacts on infrastructure, utilities, agriculture and health. *GNS Sci Rep* 2015(15):139p
- Blake DM, Wilson TM, Deligne NI, Lindsay JL, Cole JW (2016a) Impacts of volcanic ash on road transportation: considerations for resilience in central Auckland. In: Proceedings paper for the Institute of Professional Engineers New Zealand (IPENZ) transportation group conference (March 2016), Auckland, New Zealand
- Blake DM, Wilson TW, Gomez C (2016b) Road marking coverage by volcanic ash: an experimental approach. *Environ Earth Sci* 75:1348
- Blake DM, Wilson TM, Cole JW, Deligne NI, Lindsay JM (2017a) Impact of volcanic ash on road and airfield surface skid resistance. *Sustainability* 9:1389
- Blake DM, Deligne NI, Wilson TM, Wilson G (2017b) Improving volcanic ash fragility functions through laboratory studies: example of surface transportation networks. *Journal of Applied Volcanology* 6:16
- Blong RJ (1982) *The time of darkness: local legends and volcanic reality in Papua New Guinea*. Australian National University Press, Canberra
- Blong RJ (1984) *Volcanic hazards: a sourcebook on the effects of eruptions*. Academic Press, Sydney
- Bonadonna C, Houghton B (2005) Total grain-size distribution and volume of tephra-fall deposits. *Bull Volc* 67:441–456
- Bonadonna C, Phillips J (2003) Sedimentation from strong volcanic plumes. *J Geophys Res Solid Earth* 108:B7
- Bonadonna C, Ernst GGJ, Sparks RSJ (1998) Thickness variations and volume estimates of tephra fall deposits: the importance of particle Reynolds number. *J Volcanol Geoth Res* 81:173–187
- Bonadonna C, Mayberry GC, Calder ES, Sparks RSJ, Choux C, Jackson P, Lejeune AM, Loughlin SC, Norton GE, Rose WI, Ryan G, Young SR (2002) Tephra fallout in the eruption of Soufrière Hills

- Volcano, Montserrat. In: Druitt TH, Kokelaar BP (eds) *The eruption of Soufrière Hills Volcano, Montserrat, from 1995 to 1999*, vol 21. Geological Society, London, pp 483–516
- Bonadonna C, Genco R, Gouhier M, Pistolesi M, Cioni R, Alfano F, Hoskuldsson A, Ripepe M (2011) Tephra sedimentation during the 2010 Eyjafjallajökull eruption (Iceland) from deposit, radar, and satellite observations. *J Geophys Res* 116:B12202
- Bonasia R, Costa A, Folch A, Capra L, Macedonio G (2012) Numerical simulation of tephra transport and deposition of the 1982 El Chichon eruption and implications for hazard assessment. *J Volcanol Geoth Res* 231–232:39–49
- Brazier S, Davis AN, Sigurdsson H, Sparks RSJ (1982) Fall-out and deposition of volcanic ash during the 1979 explosive eruption of the Soufriere of St. Vincent. *J Volcanol Geoth Res* 14:335–359
- Brooks JO, Crisler MC, Klein N, Goodenough R, Beeco RW, Guirl C, Tyler PJ, Hilpert A, Miller Y, Grygier J, Burroughs B, Martin A, Ray R, Palmer C, Beck C (2011) Speed choice and driving performance in simulated foggy conditions. *Accid Anal Prev* 43(3):698–705
- Broom SJ (2010) Characterisation of “pseudo-ash” for quantitative testing of critical infrastructure components with a focus on roofing fragility. BSc (Hons) Thesis, Hazard and Disaster Management, University of Canterbury, Christchurch, New Zealand
- CAA (2008) Low visibility operations at Auckland Airport. Vector: pointing to safer aviation, Issue 4, Civil Aviation Authority of New Zealand. https://www.caa.govt.nz/Publications/.../Vector_2007_Issue4_JulAug.pdf. Accessed 19 Mar 2016
- Carey S, Bursik M (2015) Volcanic plumes. In: Sigurdsson H (ed) *Encyclopedia of Volcanoes*. Academic Press, New York, pp 571–585
- Carey S, Sigurdsson H (1982) Influence of particle aggregation on deposition of distal tephra from the May 18, 1980 eruption of Mount St. Helens Volcano. *J Geophys Res* 87(B8):7061–7072
- Carey S, Sigurdsson H (1986) The 1982 eruptions of El Chichon volcano, Mexico (2): observations and numerical modelling of tephra-fall distribution. *Bull Volc* 48:127–141
- Cassidy J, Locke C (2004) Temporally linked volcanic centres in the Auckland Volcanic Field. *NZ J Geol Geophys* 47:287–290
- Codling JP (1971) Thick fog and its effect on traffic flow and accidents. In: *Transport and road research laboratory TRRL report LR 397*, TRRL, Crowthorne
- Cole J, Blumenthal E (2004) Evacuate!: what an evacuation order given because of a pending volcanic eruption could mean to residents of the Bay of Plenty. *Tephra*, June 2004. Natural Hazards Research Centre, University of Canterbury, Christchurch
- Conner WD (1974) Measurement of opacity and mass concentration of particulate emissions by transmissometry, EPA 650/2-74-128. United States Environmental Protection Agency, Washington, D.C
- Conner WD, Knapp KT, Nader JS (1979) Applicability of transmissometers to opacity measurement of emissions—oil-fired power plants and Portland cement plants, EPA 600/2-79-188. United States Environmental Protection Agency, Washington, D.C
- Costa A, Macedonio G, Folch A (2006) A three-dimensional Eulerian model for transport and deposition of volcanic ashes. *Earth Planet Sci Lett* 241(3–4):634–647
- Costa A, Dell’Erba F, Di Vito MA, Isaia R, Macedonio G, Orsi G, Pfeiffer T (2009) Tephra fallout hazard assessment at the Campi Flegrei caldera (Italy). *Bull Volc* 71(3):259–273
- Cova TJ, Conger S (2003) Transportation hazards. In: Kutz M (ed) *Handbook of transportation engineering*. McGraw-Hill Handbook, New York City
- Craig H, Wilson T, Stewart C, Outes V, Villarosa G, Baxter P (2016) Impacts to agriculture and critical infrastructure in Argentina after ashfall from the 2011 eruption of the Cordón Caulle volcanic complex: an assessment of published damage and function thresholds. *J Appl Volcanol* 5(7):31p
- Durant AJ, Rose WI, Sarna-Wojcicki AM, Carey S, Volentik AC (2009) Hydrometeor-enhanced tephra sedimentation from the 18 May 1980 Mount St. Helens (USA) volcanic cloud. *J Geophys Res* 114:B03204
- DynOptic (ed) (2014) DSL-460 double pass opacity/dust monitor: operators manual v1.4. DynOptic Systems Ltd, Brackley
- Edwards JB (1999) Speed adjustment of motorway commuter traffic to inclement weather. *Transp Res Part F* 2:1–14
- Electrostatic Solutions Ltd. (2000) Electrostatic solutions technical brief No. 6: triboelectrification—how materials charge by contact. Hampshire, UK. <http://www.electrostatics.net/pdf/TB6-triboelectrification.pdf>. Accessed 15 May 2016
- Elliot AJ, Singh N, Loveridge P, Harcourt S, Smith S, Pnaiser R, Kavanagh K, Robertson C, Ramsay CN, McMenamin J, Kibble A, Murray V, Ibbotson S, Catchpole M, McCloskey B, Smith GE (2010) Syndromic surveillance to assess the potential public health impact of the Icelandic volcanic ash plume across the United Kingdom, April 2010. *Eurosurveillance* 15(23)

- EPA (2000) Current knowledge of particulate matter (PM) continuous emission monitoring: final report. United States Environmental Protection Agency. <https://www3.epa.gov/ttnemc01/cem/pmccmsknowfinalrep.pdf>. Accessed 14 Mar 2016
- EPA (2001) Protecting visibility: an EPA report to congress, chapter 3. United States Environmental Protection Agency. <http://www.epa.gov/nscep>. Accessed 06 Mar 2016
- Eto T (2001) Estimation of amount and dispersal volcanic ash-fall deposits ejected by vulcanian type eruption. *Rep Fac Sci Kagoshima Univ* 34:35–46
- Fagents SA, Gregg TKP, Lopes RMC (2013) Modelling volcanic processes: the physics and mathematics of volcanism. Cambridge University Press, Cambridge
- Folch A (2012) A review of tephra transport and dispersal models: evolution, current status, and future perspectives. *J Volcanol Geoth Res* 235–236:96–115
- Folch A, Sulpizio R (2010) Evaluating long-range volcanic ash hazard using supercomputing facilities: application to Somma-Vesuvius (Italy), and consequences for civil aviation over the Central Mediterranean area. *Bull Volc* 72:1039–1059
- Folch A, Costa A, Macedonia G (2009) FALL3D: a computational model for transport and deposition of volcanic ash. *Comput Geosci* 35:1334–1342
- Folch A, Costa A, Durant A, Macedonio G (2010) A model for wet aggregation of ash particles in volcanic plumes and clouds: 2. Model application. *J Geophys Res Chem Phys Miner Rocks Volcanol* 115:B9
- Folch A, Mingari L, Osorio MS, Collini E (2014) Modeling volcanic ash resuspension—application to the 14–18 October 2011 outbreak episode in central Patagonia, Argentina. *Nat Hazards Earth Syst Sci* 14:119–133
- Fowler WB, Lopushinsky W (1986) Wind-blown volcanic ash in forest and agricultural locations as related to meteorological conditions. *Atmos Environ* 20(3):421–425
- Jenkins S, Wilson T, Magill C, Miller V, Stewart C, Warner M, Boulton M (2014) Volcanic ash fall hazard and risk. UN-ISDR 2015 Global Assessment Report on Disaster Risk Reduction Technical Background Paper, United Nations Office for Disaster Risk Reduction. <https://www.unisdr.org/we/inform/publications/49769>. Accessed 09 Feb 2018
- Guffanti M, Mayberry GC, Casadevall TJ, Wanderman R (2009) Volcanic hazards to airports. *Nat Hazards* 51:287–302
- GVP (2013) Report on San Cristobal (Nicaragua): January 2013. Global Volcanism Program. <http://volcano.si.edu/showreport.cfm?doi=10.5479/si.GVP.BGVN201301-344020>. Accessed 23 Nov 2015
- Hagen LJ, Skidmore EL (1977) Wind erosion and visibility problems. *Trans Am Soc Agric Eng* 20(5):898–903
- Hardy SEJ (2015) Major incident in Kent: a case report. *Scand J Trauma Resusc Emerg Med* 23(71)
- Harris DM, Rose WI (1983) Estimating particle sizes, concentrations, and total mass of ash in volcanic clouds using weather radar. *J Geophys Res* 88(C15):10969–10983
- Hill DJ (2014) Filtering out the ash: mitigating volcanic ash ingestion for generator sets. Masters Thesis, Hazard and Disaster Management, University of Canterbury, Christchurch, New Zealand
- Hincks TK, Aspinall WP, Baxter PJ, Searl A, Sparks RSJ, Woo G (2006) Long term exposure to respirable volcanic ash on Montserrat: a time series simulation. *Bull Volc* 68:266–284
- Hitchcock DW, Cole JW (2007) Potential impacts of a widespread subplinian andesitic eruption from Tongariro volcano, based on a study of the Poutu Lapilli. Department of Geological Sciences, University of Canterbury, Christchurch
- Horwell CJ (2007) Grain-size analysis of volcanic ash for the rapid assessment of respiratory health hazards. *J Environ Monit* 9:1107–1115
- Howe T, Lindsay JM, Mortimer N, Leonard G (2011) DEVORA borehole database: status update and manual, IESE Report 1-2011.03. Institute of Earth Science and Engineering, Auckland, New Zealand
- Hyslop N (2009) Impaired visibility: the air pollution people see. *Atmos Environ* 43(1):182–195
- Ibrahim D (2015) Massive dust storm triggers deadly pileup in Colorado. The Weather Network. <http://www.theweathernetwork.com/us/news/articles/massive-dust-storm-triggers-deadly-pileup-in-colorado/52592/>. Accessed 18 Jan 2016
- Johnston DM (1997) Physical and social impacts of past and future volcanic eruptions in New Zealand. PhD Thesis, Earth Science, Massey University, Palmerston North, New Zealand
- Kienle J, Swanson SE (1985) Volcanic hazards from future eruptions of Augustine Volcano. University of Alaska Geophysical Institute, Alaska
- Komer PD, Reimers CE (1978) Grain shape effects on settling rates. *J Geol* 86:193–209
- Koschmieder H (1925) Theorie de horizontalen Sichtweite, Keim and Nemnich
- Lara LE (2009) The 2008 eruption of the Chaitén Volcano, Chile: a preliminary report. *Andean Geol* 36(1):125–129

- Leonard GS, Stewart C, Wilson TM, Proctor JN, Scott BJ, Keys HJ, Jolly GE, Wardman JB, Cronin SJ, McBride SK (2014) Integrating multidisciplinary science, modelling and impact data into evolving, syn-event volcanic hazard mapping and communication: a case study from the 2012 Tongariro eruption crisis, New Zealand. *J Volcanol Geoth Res* 286:208–232
- Leonard GS, Calvert AT, Hopkins J, Wilson CJL, Smid ER, Lindsay JM, Champion DE (2017) High-precision $^{40}\text{Ar}/^{39}\text{Ar}$ dating of Quaternary basalts from Auckland Volcanic Field, New Zealand, with implications for eruption rates and paleomagnetic correlations. *J Volcanol Geoth Res* 343:60–74
- Lindsay JM, Peace C (2005) Project AELG-7: health and safety issues in a volcanic ash environment. In: Auckland Regional Council Technical Publication 290, Auckland Engineering Lifelines Group
- Macedonio G, Costa A, Scollo S, Neri A (2016) Effects of eruption source parameter variation and meteorological dataset on tephra fallout hazard assessment: example from Vesuvius (Italy). *J Appl Volcanol* 5:5
- Magill C, Wilson T, Okada T (2013) Observations of tephra fall impacts from the 2011 Shinmoedake eruption, Japan. *Earths Planets Space* 65:677–698
- Malm W (1979) Visibility: a physical perspective. In: Fox D, Loomis RJ, Greene TC (eds). In: Proceedings of the workshop in visibility values. U.S. Department of Agriculture, Fort Collins, Colorado 56–68
- Malm CW, Day DE, Kreidenweis SM, Collett JL, Lee T (2003) Humidity-dependent optical properties of fine particles during the Big Bend Regional Aerosol and Visibility Observational Study. *J Geophys Res* 108:D9
- MFE (2001) Good practice guide for monitoring and management of visibility in New Zealand. Ministry for the Environment Report, Wellington
- Miwa T, Nagai M, Kawaguchi R (2018) Resuspension of ash after the 2014 phreatic eruption at Ontake volcano Japan. *J Volcanol Geoth Res* 351:105–114
- MNZ (2015) Maritime Rules Part 22: collision prevention. Maritime New Zealand, Wellington, New Zealand. <https://www.maritimenz.govt.nz/Rules/Rule-documents/Part22-maritime-rule.pdf>. Accessed 19 Mar 2016
- Moen WS (1981) Physical and chemical properties of ash from the May 18, 1980, eruption of Mount St. Helens. In: Moen WS, McLucas GB (eds) Mount St. Helens Ash—properties and possible Uses, report of investigations 24, Washington Department of Natural Resources, Division of Geology and Earth Resources
- Moore RL, Cooper L (1972) Fog and road traffic. Transport and Road Research Laboratory. In: TRRL Report LR 446, TRRL, Crowthorne
- Mueller AS, Trick LM (2012) Driving in fog: the effects of driving experience and visibility on speed compensation and hazard avoidance. *Accid Anal Prev* 48:472–479
- Musk L (1991) Climate as a factor in the planning and design of new roads and motorways. In: Perry AH, Symons LJ (eds) Highway Meteorology. E. & F.N. Spon, London
- OECD (1986) Road Safety Research 1986. OECD, Paris
- Pardini F, Spanu A, Vitturi MM, Salvetti MV, Neri A (2016) Grain size distribution uncertainty quantification in volcanic ash dispersal and deposition from weak plumes. *J Geophys Res Solid Earth* 121(2):538–557
- Parfitt L, Wilson L (2009) Fundamentals of Physical Volcanology. In: Sigurdsson H (ed) Encyclopedia of Volcanoes. Academic Press, Cambridge
- Perry AH (1981) Environmental hazards in the British Isles. George Allen and Unwin, London
- Pyle DM (1989) The thickness, volume and grain size of tephra fall deposits. *Bull Volc* 51:1–15
- Reckziegel F, Bustos E, Mingari L, Báez W, Villarosa G, Folch A, Collini E, Viramonte J, Romero J, Osoreo S (2016) Forecasting volcanic ash dispersal and coeval resuspension during the April–May 2015 Calbuco eruption. *J Volcanol Geoth Res* 321:44–57
- Riley CM, Rose WI, Bluth GJS (2003) Quantitative shape measurements of distal volcanic ash. *J Geophys Res* 108:B10
- Robinson E (1968) Effect on the physical properties of the atmosphere. In: Stern AC (ed) Air Pollution, 1:2. Academic Press, New York, pp 349–400
- Rose WI, Durant AJ (2009) Fine ash content of explosive eruptions. *J Volcanol Geoth Res* 186:32–39
- Sahetapy-Engel S, Self S, Carey RJ, Nairn IA (2014) Deposition and generation of multiple widespread fall units from the c. AD 1314 Kaharoa rhyolitic eruption, Tarawera, New Zealand. *Bull Volc* 76:836
- Sarkinen CF, Wiitala JT (1981) Investigation of volcanic ash on transmission facilities in the Pacific Northwest. *IEEE Trans Power Appar Syst* 5:2278–2286
- Sarna-Wojcicki AM, Shipley S, Waitt RB, Dzurisin D, Wood SH (1981) Areal distribution, thickness, mass, volume, and grain size of air-fall ash from six major eruptions of 1980. In: Lipman PW, Mullineaux DR (eds) The 1980 eruptions of Mount St. Helens, Washington, USGS Professional Paper 1250, pp 577–600

- Scasso RA, Corbella H, Tiberi P (1994) Sedimentological analysis of the tephra from the 12–15 August 1991 eruption of Hudson volcano. *Bull Volcanol* 56:121–132
- Scheidegger KF, Federman AN (1982) Compositional heterogeneity of tephra from the 1980 eruptions of Mount St. Helens. *J Geophys Res* 87(B13):10861–10881
- Scollo S, Del Carlo P, Coltelli M (2007) Tephra fallout of 2001 Etna flank eruption: analysis of the deposit and plume dispersion. *J Volcanol Geoth Res* 160:147–164
- Scollo S, Folch A, Costa A (2008) A parametric and comparative study of different tephra fallout models. *J Volcanol Geoth Res* 176(2):199–211
- Scott WE, McGimsey RG (1994) Character, mass, distribution, and origin of tephra-fall deposits of the 1989–1990 eruption of Redoubt Volcano, south-central Alaska. *J Volcanol Geoth Res* 62:251–272
- Searl A, Nicholl A, Baxter PJ (2002) Assessment of the exposure of islanders to ash from the Soufriere Hills volcano, Montserrat, British West Indies. *Occup Environ Med* 59:523–531
- Seinfeld JH, Pandis SN (2006) Atmospheric chemistry and physics: from air pollution to climate change. Wiley, Hoboken
- Self S, Sparks RSJ, Booth B, Walker GPL (1974) The 1973 Heimaey Strombolian scoria deposit, Iceland. *Geol Mag* 111(6):539–548
- Shimano T, Nishimura T, Nobuyuki C, Shibasaki Y, Iguchi M, Miki D, Yokoo A (2013) Development of an automatic volcanic ash sampling apparatus for active volcanoes. *Bull Volcanol* 75:773
- Sigurdsson H, Carey S, Cornell W, Pescatore T (1985) The eruption of Vesuvius in AD 79. *Natl Geogr Res* 1:332–387
- Sivakumar MVK (2005) Impacts of sand storms/dust storms on agriculture. In: Sivakumar MVK, Motha RP, Das HP (eds) Natural disasters and extreme events in agriculture. Springer, Berlin, pp 159–177
- Smith IEM, Allen SR (1993) Volcanic hazards: Auckland Volcanic Field. Department of Geology, University of Auckland, Auckland
- Sparks R (1986) The dimensions and dynamics of volcanic eruption columns. *Bull Volc* 48:3–15
- Sparks RSJ, Bursik MI, Ablay GJ, Thomas RME, Carey SN (1992) Sedimentation of tephra by volcanic plumes. Part 2: controls on thickness and grain-size variations of tephra fall deposits. *Bull Volc* 54:685–695
- Sparks RSJ, Bursik MI, Carey SN, Gilbert JS, Glaze LS, Sigurdsson H, Woods AW (1997) Volcanic plumes. Wiley, Hoboken
- Statistics New Zealand (2015) Subnational population estimates. <http://nzdotstat.stats.govt.nz/wbos/Index.aspx?DataSetCode=TABLECODE7502>. Accessed 31 Aug 2016
- Stohl A, Hittenberger M, Wotawa G (1998) Validation of the Lagrangian particle dispersion model FLEXPART against large scale tracer experiments. *Atmos Environ* 32:4245–4264
- Stohl A, Forster C, Frank A, Siebert P, Wotawa G (2005) Technical note: the Lagrangian particle dispersion model FLEXPART version 6.2. *Atmos Chem Phys* 5:2461–2474
- Summer R, Baguley C, Burton J (1977) Driving in fog on the M4. In: Transport and road research laboratory TRRL report LR 281, TRRL, Crowthorne
- Tajima Y, Ohara D, Fukuda K, Shimomura S (2015) Development of automatic tephrometer for monitoring of volcano. https://www.n-koei.co.jp/business/technology/library/thesis/pdf/forum23_005.pdf. Accessed 17 June 2016
- Tang IN (1996) Chemical and size effects of hygroscopic aerosols on light scattering coefficients. *J Geophys Res* 101:19245–19250
- Taylor JR, Moogan JC (2010) Determination of visual range during fog and mist using digital camera images. In: IOP conference series: earth and environmental science, 11. 17th national conference of the Australian meteorological and oceanographic society
- Thorarinsson S (1971) Damage caused by tephra fall in some big Icelandic eruptions and its relation to the thickness of tephra layers. In: Acta of the first international science congress on the Volcano of Thera, Greece, vol 1969, pp 15–23
- USDOT (2013) How do weather events impact roads? Weather Management Program. www.ops.fhwa.dot.gov/weather/q1_roadimpact.htm. Accessed 07 Apr 2016
- USGS (2013) Volcanic ash: effects and mitigation strategies. United States Geological Survey. <http://volcanoes.usgs.gov/ash/trans/>. Accessed 21 Sep 2015
- Uthe EE (1980) Evaluation of an infrared transmissometer for monitoring particulate mass concentrations of emissions from stationary sources. *J Air Pollut Control As* 30:382–386
- van de Hulst HC (1957) Light scattering by small particles. Wiley, New York
- Walker GPL (1981) The Waimihia and Hatepe plinian deposits from the rhyolitic Taupo Volcanic Centre. *NZ J Geol Geophys* 24(3):305–324
- Wardman J, Sword-Daniels V, Stewart C, Wilson T (2012) Impact assessment of the May 2010 eruption of Pacaya volcano, Guatemala. GNS Science Report 2012/09

- Warrick RA (1981) Four communities under ash. University of Colorado, Boulder, U.S. Institute of Behavioural Science
- Watt SFL, Pyle DM, Mather TA, Martin RS, Matthews NE (2009) Fallout and distribution of volcanic ash over Argentina following the May 2008 explosive eruption of Chaitén, Chile. *J Geophys Res* 114:B04207
- Weber K, Fischer C, Vogel A, Pohl T, Böhlke C (2013) First results of an airborne release of volcanic ash for testing of volcanic ash plume measurement instruments. In: *Proceedings of Energy and Environment*, pp 169–172
- Weinzierl B, Sauer D, Minikin A, Reitebuch O, Dahlkötter F, Mayer B, Emde C, Tegen I, Gasteiger J, Petzold A, Veira A, Kueppers U, Schumann U (2012) On the visibility of airborne volcanic ash and mineral dust from the pilot's perspective in flight. *Phys Chem Earth* 45–46:87–102
- White WH (1990) The components of atmospheric light extinction: a survey of ground-level budgets. *Atmos Environ* 24A:2673–2679
- White J, Stewart C, Wareham D, Wilson T (2011) Treatment of volcanic ash-contaminated surface waters through the optimisation of physical and chemical processes. *GNS Science Report* 2011/35
- WHO (2013) Review of evidence on health aspects of air pollution—REVIHAAP project: final technical report. World Health Organisation European Centre for Environment and Health, Bonn
- Wilcox RE (1959) Some effects of recent Volcanic Ash falls with especial reference to Alaska. *Geol Sur Bull* 1028-N. <https://pubs.usgs.gov/bul/1028n/report.pdf>. Accessed 09 Feb 2018
- Wilson TM (2008) Unpublished field notes from the Chaitén eruption field visit. University of Canterbury, Christchurch
- Wilson TM (2009) Unpublished field notes from the Hudson eruption field visit. University of Canterbury, Christchurch
- Wilson L, Huang TC (1979) The influence of shape on the atmospheric settling velocity of volcanic ash particles. *Earth Planet Sci Lett* 44:311–324
- Wilson TM, Stewart C, Cole JW, Dewar DJ, Johnston DM, Cronin SJ (2009) The 1991 eruption of Volcan Hudson, Chile: impacts on agriculture and rural communities and long-term recovery. *GNS Science Report* 2009/66
- Wilson TM, Cole JW, Stewart C, Cronin SJ, Johnston DM (2011) Ash storms: impacts of wind-remobilised volcanic ash on rural communities and agriculture following the 1991 Hudson eruption, southern Patagonia, Chile. *Bull Volc* 73:223–239
- Wilson TM, Stewart C, Sword-Daniels V, Leonard GS, Johnston DM, Cole JW, Wardman J, Wilson G, Barnard ST (2012a) Volcanic ash impacts on critical infrastructure. *Phys Chem Earth* 45–46:5–23
- Wilson T, Cole J, Johnston D, Cronin S, Stewart C, Dantas A (2012b) Short- and long-term evacuation of people and livestock during a volcanic crisis: lessons from the 1991 eruption of Volcan Hudson, Chile. *J Appl Volcanol* 1:2
- Wilson T, Stewart C, Bickerton H, Baxter P, Outes V, Villarosa G, Rovere E (2013) Impacts of the June 2011 Puyehue-Cordon Caulle volcanic complex eruption on urban infrastructure, agriculture and public health. *GNS Science Report* 2012/20
- Wilson G, Wilson TM, Deligne NI, Cole JW (2014) Volcanic hazard to critical infrastructure: a review. *J Volcanol Geoth Res* 286:148–182
- Wilson G, Wilson TM, Deligne NI, Blake DM, Cole JW (2017) Framework for developing volcanic fragility functions for critical infrastructure. *J Appl Volcanol* 6:14
- Witham C, Hort M, Potts R, Servranckx R, Husson P, Bonnardot F (2007) Comparison of VAAC atmospheric dispersion models using the 1 November 2004 Grimsvotn eruption. *Meteorol Appl* 14:27–38
- Yanagi T, Okada H, Ohta K (1992) Unzen volcano, the 1990–1992 eruption. The Nishinippon and Kyushu University Press, Fukuoka
- Zawalna-Geer A (2016) Towards a tephra framework for the Auckland maar lake sediments and the potential of applying cryptotephra techniques. PhD Thesis, Geology, The University of Auckland, Auckland, New Zealand

RESEARCH

Open Access



Improving volcanic ash fragility functions through laboratory studies: example of surface transportation networks

Daniel Mark Blake^{1*}, Natalia Irma Deligne², Thomas McDonald Wilson¹ and Grant Wilson^{1,3}

Abstract

Surface transportation networks are critical infrastructure that are frequently affected by volcanic ash fall. Disruption to surface transportation from volcanic ash is often complex with the severity of impacts influenced by a vast array of parameters including, among others, ash properties such as particle size and deposit thickness, meteorological conditions, pavement characteristics, and mitigation actions. Fragility functions are used in volcanic risk assessments to express the conditional probability that an impact or loss state will be reached or exceeded for a given hazard intensity. Most existing fragility functions for volcanic ash adopt ash thickness as the sole hazard intensity metric that determines thresholds for functional loss. However, the selection of appropriate hazard intensity metrics has been highlighted as a crucial factor for fragility function development and recent empirical evidence suggests that ash thickness is not always the most appropriate metric. We review thresholds of functional loss for existing published surface transportation (i.e. road rail, maritime and airport) fragility functions that use ash thickness. We then refine these existing functions through the application of results from a series of recent laboratory experiments, which investigate the impacts of volcanic ash on surface transportation. We also establish new fragility thresholds and functions, which applies ash-settling rate as a hazard intensity metric. The relative importance of alternative hazard intensity metrics to surface transportation disruption is assessed with a suggested approach to account for these in existing fragility functions. Our work demonstrates the importance of considering ash-settling rate, in addition to ash thickness, as critical hazard intensity metrics for surface transportation, but highlights that other metrics, especially particle size, are also important for transportation. Empirical datasets, obtained from both post-eruption field studies and additional laboratory experimentation, will provide future opportunities to refine fragility functions. Our findings also justify the need for rapid and active monitoring and modelling of various ash characteristics (i.e. not ash thickness alone) during volcanic eruptions, particularly as potential disruption to surface transportation can occur with only ~0.1 mm of ash accumulation.

Keywords: Tephra, Volcano, Road, Rail, Maritime, Airport, Risk, Hazard, Intensity, Critical infrastructure

Introduction

Surface transportation including road, rail and maritime networks (see Table 1 for terminology) are critical for many social and economic functions. Disruption to surface transportation can affect commuter travel, access for emergency services, distribution and provision of goods and services, other infrastructure (e.g. electricity systems, water and fuel) and the economy. Damage and

loss of function to surface transportation networks from historical volcanic eruptions worldwide has been qualitatively and semi-quantitatively recorded for roads and airports (e.g. Blong 1984, Nairn 2002, Barnard 2009, Guffanti et al. 2009, Wilson et al. 2014). Quantitative data sourced from historical eruptions or controlled laboratory experimentation has been lacking, meaning that there have been limited empirical or hybrid datasets to develop robust relationships between hazard intensity and network impact (damage and disruption) (Wilson et al. 2017).

* Correspondence: daniel.blake@pg.canterbury.ac.nz

¹Department of Geological Sciences, University of Canterbury, Private Bag, Christchurch 4800, New Zealand

Full list of author information is available at the end of the article

Table 1 Definitions and context of key terminology used within this paper

Term	Definition	Paper specifics	References
Airport	Surface transportation site consisting of airfield and facilities used to service aircraft.	Surface and near-surface (< 10 m above ground) environmental conditions at airfields are considered when referring to airports.	
Exposure	People, property, systems, or other elements present in hazard zones that are thereby subject to potential losses.		UNISDR 2009, Craig et al. 2016b
Fragility function	Probabilistic vulnerability models that describe the probability that a damage or functional state will be reached or exceeded for a given hazard intensity.	Only fragility functions for volcanic ash are discussed in detail.	Singhal and Kiremidjian 1996, Choi et al. 2004, Rossetto et al. 2013, Tarbotton et al. 2015
Hazard	A phenomenon that may cause loss of life, injury or other health impacts, property damage, loss of livelihoods and services, social and economic disruption, or environmental damage.	Hazard is referred to in the context of a dangerous phenomenon from volcanoes (i.e. volcanic tephra, pyroclastic density currents, lava flows, lahars).	UNISDR 2009
Hazard Intensity Metric (HIM)	A measure used to describe the intensity of a volcanic hazard at a particular site, which is the independent variable of vulnerability and fragility functions.	Ash thickness is often used as the HIM for volcanic ash fragility functions. Alternative HIMs are explored here including ash-settling rate and particle size.	Wilson 2015, Wilson et al. 2017
Impact	The effect a hazardous event has on an exposed system. Defined as a function of the hazard, and the vulnerability and exposure of a system ($I = H*V*E$).	Multiple impact types are inferred when discussing impact.	Jenkins et al. 2014b, Craig et al. 2016b
Impact State (IS)	States of damage or disruption defined by qualitative impact descriptions.	These are numbered numerically with 0 being "no damage or disruption", and increasing numbers referring to an increasing level of damage or disruption.	Blong 2003, Wilson et al. 2017
Impact type	An individual feature of an infrastructure system that can be affected by the function of hazard, vulnerability and exposure.	Surface transportation impact types include skid resistance reduction, visibility impairment, road marking coverage and engine air inlet filter blockage.	
Maritime	Surface transportation connected with the sea.	Covers trade shipping, recreational boating and ferry services.	
Mitigation	The lessening or limitation of the adverse impacts of hazards and related disasters.		UNISDR 2009
Rail	Surface transportation on wheeled vehicles running on rails.	Covers electric and diesel modes on conventional tracks.	
Risk	The combination of the probability of an event and its negative consequences.	A volcanic hazard is implied to be the "event".	UNISDR 2009
Road	Surface transportation on dedicated sealed or unsealed routes.	We generally refer to paved surfaces, particularly asphalt concrete.	
Skid resistance	The force developed when a tyre that is prevented from rotating slides along pavement surface.	(Often referred to as traction in post-eruption literature.)	Highway research board 1972, Blake et al. 2017a
Surface transportation	Transportation types on land or water used to convey passengers and/or goods.	Road, rail and maritime transport are covered, as well as transport that occurs on the ground at airports.	
Visual range	The longest distance that a large, black object can be seen against the sky at the horizon with the unaided eye.	Used as a measure of visibility.	Hyslop 2009, Binkowski et al. 2002, Blake 2016
Vulnerability	The characteristics and circumstances of a community, system or asset that make it susceptible to the damaging effects of a hazard.	Largely transportation systems or assets are referred to.	UNISDR 2009
Vulnerability function	A correlation of hazard intensity to a component's damage or function loss as a value relative to total impact or as an economic cost.	We generally refer to fragility functions instead, which incorporate probability.	Wilson 2015

Figure 1 summarises recorded impacts for road, rail and airports, caused by various volcanic hazards with a focus on tephra, following historical eruptions since 1980. Impacts to transportation networks can be complex, particularly when exposed to multiple volcanic hazards during eruptions causing a range of impact states.

Volcanic hazards such as pyroclastic density currents (PDCs) and lava flows (shown in the top sections of the charts in Fig. 1) are geographically well constrained. Volcanic ash (i.e. the component of tephra with particle size < 2 mm) however, is often widespread (Blong 1984) and generally has far-reaching and complex interactions with

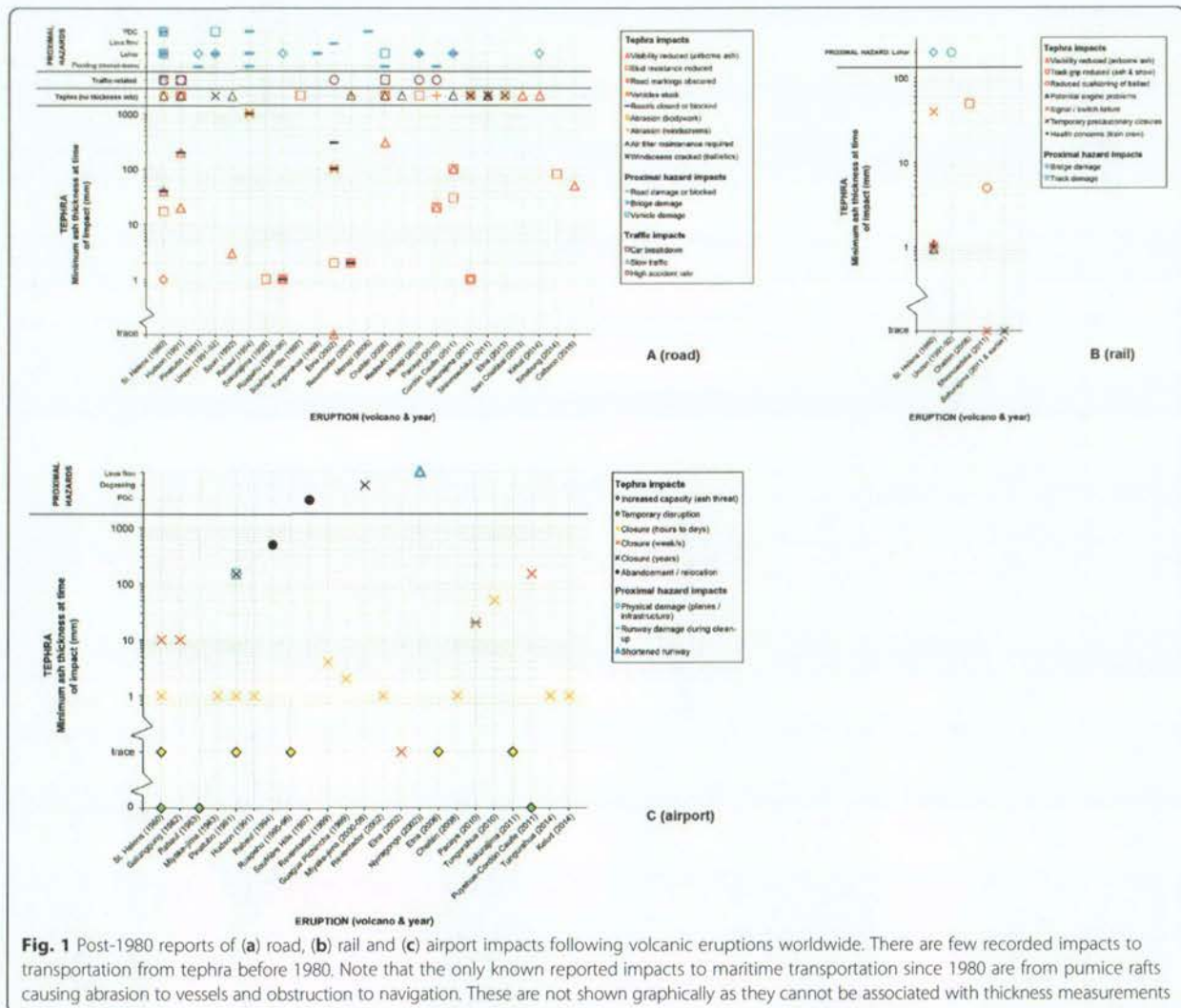


Fig. 1 Post-1980 reports of (a) road, (b) rail and (c) airport impacts following volcanic eruptions worldwide. There are few recorded impacts to transportation from tephra before 1980. Note that the only known reported impacts to maritime transportation since 1980 are from pumice rafts causing abrasion to vessels and obstruction to navigation. These are not shown graphically as they cannot be associated with thickness measurements

surface transportation. Studies since the 1980 Mount St Helens eruption (e.g. Blong 1984, Johnston 1997, Guffanti et al. 2009, Horwell et al. 2010, Wilson et al. 2011, Dunn 2012, Wardman et al. 2012, Wilson et al. 2012, Stewart et al. 2013, Wilson et al. 2014, Blake et al. 2016, 2017a) demonstrate that volcanic ash frequently reduces skid resistance and covers markings on paved surfaces. Reduced visibility caused by airborne ash and the abrasion or cracking of vehicle windscreens are also common, and engine failure may result if vehicle air intake filters are not adequately maintained. All of these impacts can affect transportation functionality, whether it is by reduced vehicle volumes and speed, an increase in accident rates and congestion, or network closures. As such, we focus on the impacts associated with volcanic ash in this paper.

Globally there is limited quantitative data for the impact of ash on surface transportation networks.

Similarly, experimental data is sparse due to the complexities of replicating infrastructural components and volcanic ash properties in laboratories (Jenkins et al. 2014a, Wilson et al. 2014). Where quantitative data exist, impacts on transportation, as well as other critical infrastructure, have generally been related to the thicknesses of ash on the ground. For example, Wilson et al. 2017 use the ash thickness variable (defined as a *Hazard Intensity Metric* (HIM); Table 1) to produce a series of volcanic ash fragility functions for different infrastructure types. Although adopting ash thickness as a HIM has distinct advantages, particularly in that it is a frequently modelled and often relatively readily measured variable following eruptions, it is not always appropriate to consider this metric alone. Characteristics such as ash particle size, ash type, the quantity of soluble components, wetness and airborne concentration or ash-settling rate may have large effects on overall impact

intensity and subsequent loss of functionality in some cases. Recent work by Blake (2016), Blake et al. (2016 and 2017a) has focused on targeted experiments investigating common surface transportation impact types for volcanic ash under controlled laboratory conditions through a series of targeted experiments. New quantitative data available from these studies enables analysis of HIM importance and appropriateness, the refinement of thresholds for functional loss (termed *Impact State (IS)*), and opportunities to improve fragility and vulnerability functions. Such approaches, whereby the vulnerability of infrastructure is assessed using laboratory studies to supplement field-based empirical observations, has been proven in other disciplines including earthquake engineering and for structural loading in tsunami (e.g. Rossetto et al. 2013, Nanayakkara and Dias 2016).

In this paper, we summarise existing IS thresholds for surface transportation from previous, largely qualitative, post-eruption literature, and using ash thickness on the ground as the HIM. Next we adopt the empirical results from Blake (2016), and Blake et al.'s (2016 and 2017a) (see Additional file 1 for key findings summary) suite of targeted laboratory experiments to refine these established thresholds for ash thickness, and to develop new IS options for visibility impairment based on ash-settling rate as the HIM. The importance of additional HIMs (such as ash particle size and colour) as measures of functional loss for specific impact types is investigated through relative comparisons to one another. This allows us to propose a credible strategy to enhance fragility functions for surface transportation networks, by means of incorporating related uncertainty. We only consider discrete and direct ash fall events and not effects that may occur from remobilised ash. Our focus is on road disruption as most garnered data is directly related to road infrastructure. However, disruption to airports and rail and maritime transportation are also discussed, particularly as recent empirical studies of visibility reduction apply to all surface transportation modes.

Background: Quantitative volcanic impact assessments

Risk assessments may incorporate vulnerability functions to describe the likelihood that an asset will sustain varying degrees of loss over a range of hazard intensities (Rossetto et al. 2013). The 'loss' may be expressed as economic cost, damage (e.g. physical damage of a sealed road surface from ballistics) and/or functionality (e.g. reduced speeds on roads from volcanic ash). However, vulnerability functions are less common in volcanic risk assessments than they are in risk assessments for many other disciplines such as seismic engineering due to the variety of volcanic hazards and associated complexities (Jenkins et al. 2014a).

Qualitative data obtained following eruptions is often considered sufficient to establish and communicate information relating to expected impacts during future events. For example, exclusion zones may be implemented in the immediate vicinity of the vent due to qualitative knowledge gained from past eruptions about the high likelihood of severe damage from proximal hazards such as pyroclastic density currents (PDCs) and lahars, and advice can be issued to avoid travel in relatively short-lived and localised ashfall events until ash has been cleared. Residents often heed such advice due to health concerns (Stewart et al. 2013) and to avoid potential damage to their vehicles (e.g. Blake et al. 2015). However, the volcanic ash hazard can have complex impacts on infrastructure networks causing widespread disruption (Johnston and Daly 1997), potentially affecting thousands of kilometres of surface transportation routes. Loss of functionality can also be prolonged due to ongoing volcanic activity and the remobilisation, re-suspension and secondary deposition of ash (sometimes for months to years after an eruption has ceased) by wind, fluvial processes, and/or anthropogenic disturbance. As such, it is beneficial to establish thresholds from semi-quantitative and/or quantitative data (e.g. ash thickness measurements) to indicate when specific impact types (e.g. road marking coverage or visibility impairment), and of what severity, occur. These impact thresholds can in turn inform damage ratios, which express the economic cost required to restore infrastructure (i.e. absolute damage) by indicating the damaged proportion of the infrastructure (i.e. relative loss) (Reese and Ramsay 2010, Tarbotton et al. 2015). Impact thresholds and damage ratios can be adopted by emergency management officials and in transportation maintenance guidelines such as for informing when to commence road sweeping or implement road closures following volcanic ashfall (Hayes et al. 2015). Sometimes however, a more gradational approach to assess the vulnerability of infrastructure to volcanic ash is required and fragility functions can be used in such situations.

Fragility functions are probabilistic vulnerability models that describe the probability that a damage or functional state will be reached or exceeded for a given hazard intensity (Singhal and Kiremidjian 1996, Choi et al. 2004, Rossetto et al. 2013, Tarbotton et al. 2015). They allow the quantification of risk and provide a basis for cost-benefit analysis of mitigation strategies (Jenkins et al. 2014a, Wilson et al. 2014). Data used to create fragility functions can be derived from a variety of sources and is generally classified into four types: 1) empirical data from field and/or laboratory observations, 2) analytical data from numerical modelling, 3) data from expert opinions / judgement, 4) hybrid data from a combination of these approaches (Porter et al. 2012, Wilson et

al. 2017). Variables can take on either discrete values or a continuous range of values, and as such fragility functions can comprise a number of forms (Porter et al. 2007, Wilson et al. 2017). The reader is referred to Wilson et al. (2017) for more detailed discussion on impact data types and fitting of volcanic fragility functions. To date, most volcanic fragility functions have focused on damage, particularly the physical damage to buildings and roofs. However, loss of infrastructure functionality may be as, if not more, important than damage in some cases. The loss of infrastructure functionality can have potentially large implications for governments and local authorities (e.g. deciding whether to shut down parts of a network) and cause substantial, sometimes unexpected, effects on end-users of critical infrastructure such as drivers and residents through a reduced 'level of service'. It is important to note that there are often many impact types, along with factors such as infrastructure characteristics and decision-making by authorities, which influence whether networks remain open. For example, in New Zealand a main state highway was closed following < 3 mm of ash accumulation from the 2012 Tongariro eruption (Jolly et al. 2014, Leonard et al. 2014), but in Argentina after the 2011 Cordón Caulle eruption, many key roads remained open despite receiving up to 50 mm of ash (Craig et al. 2016a). Such differences are likely due to duration of disruption, threat of future ashfall, criticality of the road, previous experiences with volcanic ash and different tolerance levels in different regions (Craig et al. 2016a).

It is difficult to incorporate all factors which contribute to surface transportation closure (Table 2) into volcanic fragility functions. However, these variations in damage and disruption can be accounted for by introducing estimates of uncertainty within fragility functions. Uncertainties include aleatory uncertainties such as natural variations between volcanic eruption hazard severity and resulting infrastructure response, and epistemic uncertainties such as those associated with limited data or choosing appropriate HIMs and ISs (Rossetto et al. 2014, Wilson et al. 2017). These uncertainties are outlined more fully by Wilson et al. (2017). Sometimes, HIMs cannot be measured in the field in real time (Jenkins et al. 2013, Wilson et al. 2017); for example, it may be dangerous to measure ash characteristics due to the ash or other volcanic hazards potentially impacting health. Laboratory experimentation can be used to reduce epistemic uncertainty through the provision of larger impact data sets. Additionally, the controlled nature of laboratory experimentation means that particular conditions can be assessed, and uncertainty can often be reduced in this respect as well. However, the introduction of new data that differs from previous data may reflect either aleatory or epistemic uncertainty. As was conducted by

Wilson et al. (2017), where possible, we account for uncertainties by calculating the probability that the surface transportation mode could be in each IS at each HIM value. Binning the HIM values and adopting the median HIMs on each chart accounts for the variation in values (Wilson et al. 2017). It is important that uncertainties are subsequently transferred across to plans and strategies that utilise fragility functions, ideally using probabilistic techniques to ensure that different outcomes are considered (Jenkins et al. 2014a). However, as new qualitative field data and quantitative data from further laboratory experiments becomes available, existing datasets can be reviewed and fragility functions adjusted accordingly, thus reducing overall uncertainty.

Selection of appropriate HIMs and establishment of representative IS thresholds are crucial to produce robust fragility functions (Rossetto et al. 2013). Wilson et al. (2014) and Wilson et al. (2017) highlight that fragility functions in volcanology are poorly developed compared to those from other natural hazard disciplines. They also outline that the range of intrinsic volcanic hazard properties, such as the particle size of ash, can cause different impacts, leading to difficulties in deriving functions. Additionally, much of the data that has informed volcanic fragility functions is qualitative or semi-quantitative with limited quantitative empirical, analytical or theoretical data from field studies or laboratory experiments.

To date, the most common HIM for volcanic ash fragility functions to assess surface transportation disruption is the thickness of ash on the ground (Wilson et al. 2014). This is largely due to its extensive use in existing impact datasets and applicability to hazard model outputs at the time. Previous IS thresholds that have been defined using thickness as the HIM (Wilson et al. 2017) are shown in our results (section 4.1) for comparative purposes. Of particular note is that IS₁ (reduced visibility, loss of traction, covering of road markings and/or road closures) was previously identified as occurring with thicknesses of ~1 mm or more, due to reduced traction (technically known as *skid resistance*) and impaired visibility disrupting most transportation types. Impacts to maritime transportation have not been considered in detail in relation to thickness, as most ash types (with the exception on pumiceous material, which can form pumice rafts) do not accumulate, or are readily dispersed, on water and are thus difficult to monitor. The majority of data used to inform previous ISs was from qualitative post-eruption impact assessments and media reports. Observations from Barnard (2009), who conducted a number of semi-quantitative field experiments on Mt. Etna, Italy, also informed ISs for road transportation where thicknesses exceed 50 mm.

Blake (2016), and Blake et al. (2016 and 2017a) conducted targeted experiments under controlled laboratory

Table 2 Factors that can contribute to surface transportation closure during ashfall. This excludes interdependencies from impacts to other infrastructure, as it is difficult to consider all factors when producing fragility functions

			Details for surface transportation mode				
			Road	Rail	Airport	Maritime	
Factors that contribute to closure	Hazard	Ash characteristics	Thickness, density on ground, settling rate / airborne concentration, particle size, shape / irregularity, colour, wetness, soluble components, hardness, friability.				
		Meteorological conditions	Precipitation (rain, snow, hail, sleet), humidity, temperature, fog, ice, wind speed and direction.				
	Asset	Static infrastructure type and condition	Priority of infrastructure, requirement for emergency operations (e.g. evacuation, transport of goods), users, capacity, critical infrastructure interdependencies.	Sealed or unsealed surfaces and properties, slope of road, road marking properties, drainage.	Track and ballast properties, overhead line and pylon properties (if electric), gradient, station facilities, track-locomotive communications, collision avoidance systems.	Sealed or unsealed surfaces and properties, length of runway/s, terminal facilities, landing system technology.	Port facilities and technology.
		Mobile infrastructure type and condition	Fuel supply, extent of autonomous operation, requirement for emergency operations (e.g. evacuation, transport of goods).	Petroleum or electric, drive of vehicles (e.g. four-wheel drive, rear wheel drive), tyres, weight, power and torque, ground clearance, differential, traction control, transmission.	Electric or diesel locomotives and interchangeability, locomotive-track communications, collision avoidance systems.	Aircraft type (e.g. turboprop, turbine engine, helicopter), on-board technology (e.g. volcanic ash avoidance systems).	Vessel type and method of mobility (e.g. cargo ship, ferry, yacht), size and weight, on-board technology (e.g. GPS and automatic identification systems).
		Impact type	Visibility impairment, signage and lighting covered, air filter blockage, engine failure due to ash ingestion, abrasion (bodywork and windscreens), cracked windscreens, health concerns.	Skid resistance reduction, road marking coverage, vehicles stuck, traffic light and variable message sign failures.	Track grip reduced, ballast contamination (potential for reduced cushioning), signal/switch failure, trains stuck.	Skid resistance reduction, light and airfield marking coverage, airspace closure.	Pumice raft obstruction to navigation, sedimentation in channels, accumulation of tephra on vessels.
	Preparedness / Mitigation	Population attributes	Frequency of ashfall events in area, prior vehicle operation in environments containing ash, knowledge sharing and traditions.				
		Organisational involvement	Infrastructure providers, local authorities, regional government, emergency management, national government, scientific research and monitoring organisations, goods and service logistic companies, other businesses, aid agencies, cleaning and disposal organisations.	Motoring associations, residents.	Rail companies.	Airport operators, Civil Aviation Authority, Volcanic Ash Advisory Centres.	Maritime bodies, harbourmasters.
		Physical measures	Cleaning of static and mobile infrastructure, drainage system changes, air filter maintenance and replacement, light and signage alterations, diversions.	Bridge strengthening, road surface and marking alterations, vehicle alterations, driving advice.	Bridge strengthening, ballast and track alterations, locomotive alterations, locomotive driver training changes.	Airfield surface and marking alterations, terminal facility changes, aircraft adaptations, pilot training changes.	Port facility changes, vessel adaptations, captain / helmsman training changes.

conditions to investigate the most frequent surface transportation impact types identified from post-eruption assessments: skid resistance reduction, visibility impairment and road marking coverage (see Additional file 1 for key findings summary). The studies assessed the effect of key HIMs (Table 3) on functionality and we refer the reader to each of the corresponding papers for detailed information on the methodologies adopted for the experiments including different approaches used to measure HIMs.

The studies by Blake (2016), Blake et al. (2016) and 2017a) suggest that ash thickness and ash-settling rate are the most critical HIMs for the assessment of surface transportation functionality during initial volcanic ashfall events, particularly as they are two of the most readily measured variables in the field. There would rarely be impacts to transportation when there is no ground accumulation of ash and no suspended ash in the atmosphere, which further emphasises the importance of these two HIMs. However, recent laboratory work has also revealed that alternative HIMs to ash thickness and settling rate (Table 3) should not be disregarded.

Methodology

Figure 2 summarises previous and current developments to volcanic ash fragility functions for surface transportation. Most steps in the diagram indicate anticipated improvements to data accuracy. However, as fragility functions are developed, requirements for more impact data are often introduced to test and improve new findings and reduce uncertainty.

Impact state thresholds

Using the key findings of the skid resistance and road marking coverage laboratory studies, we refine the IS thresholds for surface transportation established by Wilson et al. (2017) which adopt ash thickness as the HIM (Fig. 2). New thresholds are applied directly from laboratory study analysis results but some require

rounding to the nearest order of magnitude to account for uncertainties such as those associated with the variation in results between individual tests and lack of extensive datasets in some cases. This is achieved using the authors' expert judgement, particularly through application of existing knowledge of surface transportation impacts by volcanic ash gained from field and laboratory observations. We remove previously suggested correlations between visibility and ash thickness because, as stated by Blake (2016), it is "illogical to associate an atmospheric-related impact to a ground-based measurement", especially as we do not consider effects from remobilised ash in this paper. Laboratory work using ash thickness as the core HIM considered paved surfaces on roads and at airports. Railway tracks were not considered in detail, partly because there has been only one recorded instance of track-wheel adhesion loss following ashfall (Fig. 1b) and the effects were complicated by snowfall at the time. As such, we do not provide any refinements for rail transportation ISs in relation to ash thickness and the previously established thresholds for rail transportation are therefore unchanged by our study. For maritime transportation, a challenge for fragility function development is that due to ash dispersing in water, impact mechanisms from tephra cannot easily be linked to deposition thickness as they can for road, rail and airports. However, as with other forms of transportation, and as occurs in dense fog, it is likely that navigation by sea can be disrupted or even temporarily halted by visibility impairment during ashfall. Therefore, maritime transportation impacts are segregated from the ash thickness HIM and assessed solely in relation to visibility impairment.

As ash deposit thickness has a debatable impact on visibility impairment, and due to recent developments in both field monitoring equipment, and ash dispersion and fallout models which provide settling-rate outputs (Blake 2016), we consider ash-settling rate as an alternative HIM (Fig. 2) and propose new IS thresholds. Our

Table 3 Summary of hazard intensity metrics considered during experimental work

Hazard intensity metric	Skid resistance reduction ^a	Road marking coverage ^b	Visibility impairment ^c
Thickness (mm) – related to area density / loading (kg/m ²) in some cases	✓	✓	
Ash-settling rate (g m ⁻² h ⁻¹)			✓
Particle size (µm)	✓	✓	✓
Colour		✓	✓
Wetness	✓		
Soluble content	✓		
Hardness (proxy: ash type)	✓	✓	✓
Shape (proxy: ash generation method)	✓	✓	✓

^a Blake et al. (2017a), ^b Blake et al. (2016), ^c Blake (2016)

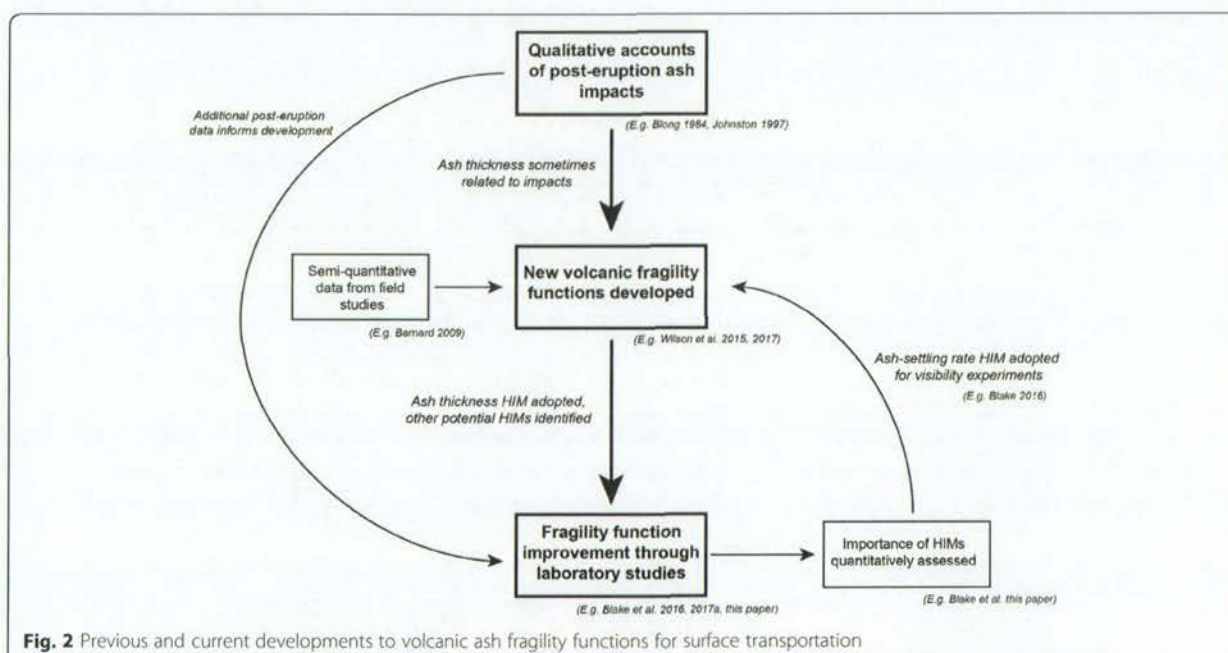


Fig. 2 Previous and current developments to volcanic ash fragility functions for surface transportation

settling rate IS thresholds are developed using a hybrid approach. They are informed by (a) direct empirical laboratory results, adjusted using expert judgement and rounding, (b) literature for shipping in Auckland’s Waitemata Harbour (e.g. Harbourmaster and Maritime New Zealand information for maritime impacts (Auckland Council 2014, MNZ 2015)) and Auckland Airport and CAA guidelines for airport impacts (Auckland Airport 2008, CAA 2008), and (c) expert consultation with critical infrastructure managers (Deligne et al. 2015, Blake et al. 2017b, Deligne et al. 2017). We establish IS thresholds for all modes of surface transportation related to visibility impairment. This is achieved by means of comparison with operational guideline information and impact states expected for corresponding visual ranges in foggy conditions, the data sources of which are discussed in Blake (2016):

- IS thresholds for roads are largely based on comparisons with empirical studies involving driver simulations in fog.
- Comparisons with operational procedures for fog in Auckland are used to establish thresholds for airports and maritime transportation, and thus these thresholds should be treated as more area-dependent than for road.
- IS thresholds for rail are the most subjective of the four transportation modes: we implement higher threshold values than for road due to the often automated controls for the spacing of locomotives along the network and additional

technological safety systems which visibility impairment does not affect.

Hazard intensity metric analysis

We conduct a comparative analysis of HIMs other than ash thickness by assessing their relative importance to surface transportation disruption. Without extensive datasets for all HIMs, this is achieved by applying simple rank values to each HIM for the core HIMs of ash settling rate and at different ash thicknesses. HIMs are ordered by relative importance to one another and given a rank value of between 1 and 6. Although somewhat subjective, the lower the rank value applied, the greater the influence of that HIM on surface transportation disruption. HIMs of similar importance are given the same rank value.

Fragility function development

We use procedures described by Wilson et al. (2017) for volcanic fragility function development, the basic methodological principles of which are summarised as follows:

- Assign each data point a HIM value and IS value;
- Order data set by increasing HIM value;
- Group into HIM bins, such that each bin has approximately the same number of data points;
- Calculate probability of being greater than, or equal to, each IS of interest;
- Obtain discrete HIM values by taking the median of each HIM bin.

- Apply functions as linear segments defined by the available data points after the HIM binning process (as described by Wilson et al. 2017).

New road and airport fragility functions for ash thickness are established through modification of those proposed by Wilson et al. (2017). All points representing median thickness within the HIM bins obtained from post-eruption data are retained as the number of post-eruption records remains unchanged. New points are added to the chart to appropriately display the new findings from IS threshold adjustment following laboratory work, with a focus on improving functions for relatively thin deposits (the focus of laboratory work). More substantial updates are made to airport fragility functions as we also incorporated the duration of airport closure. However, we stress that some points have been corrected using best judgement in order to fit with guidelines outlined by Wilson et al. (2017).

The IS thresholds for ash-settling rate are used to establish separate fragility functions for road, rail and maritime transportation, and at airports. Without reliable field data it is difficult to follow Wilson et al.'s (2017) methodology for fragility function production, especially to accurately calculate probabilities of ash-settling rate values equalling or exceeding each IS. However, we produce functions using empirical laboratory studies and comparisons to research for fog, to indicate expected impact on visibility and vehicles at near-ground level. This is achieved through adopting the basic principles and rules outlined by Wilson et al. (2017). As we cannot group data into HIM bins and obtain discrete HIM values, specific ash-settling rates are chosen based on key changes in impact states instead. We use best judgement to assign probabilities and these are open to revision in future.

Limitations of methodology

Besides the general limitations outlined by Wilson et al. (2017) for fragility function production, our methodology for fragility function improvement through empirically informed data contains several additional limitations which may also introduce uncertainty:

- The laboratory experiments used to inform fragility functions were based on the assessment of key impact types previously identified from post-eruption observations. However, observations of volcanic ash impacts to transportation are relatively limited (at least compared to impacts from other hazards such as earthquake damage to buildings) with an apparent increase in frequency of events after 1980. We suggest that this increase is due to heightened awareness and land-monitoring of volcanic hazards following

the 1980 Mount St Helens eruption, and recent increases in the number of motor vehicles and general population growth and infrastructure development in volcanically active areas worldwide (TRB 1996).

Additionally, there is a higher frequency of impacts recorded for roads than for other modes of surface transportation, likely due to more road networks in the areas affected by volcanic activity. Therefore, the relevance of further impact types may be underestimated by our study, and future observations and additional laboratory testing will verify the extent of this.

- The empirical datasets we use are constrained by the equipment and set-ups that were adopted in the laboratory studies. For example, the skid resistance testing used a Pendulum Skid Resistance Tester, which was restricted to investigating small (< 10 mm) ash thicknesses (Blake et al. 2017a). Furthermore, it was unfeasible to investigate all possible ash characteristics (e.g. every soluble component option, all moisture regimes) during laboratory testing, so our results are limited to those characteristics that we did investigate.
- Laboratory experiments are generally time and resource intensive. As the experiments by Blake (2016), and Blake et al. (2016 and 2017a) were the first to be developed and conducted to specifically assess ash impacts on individual transportation components, the datasets are currently relatively small. The repetition of laboratory experiments will help to reduce uncertainty in the future but our results are limited to those characteristics investigated to date.

Results and discussion

Ash thickness fragility function improvements

Figure 3 shows IS thresholds for surface transportation, which were defined using ash deposit thickness as the HIM. It includes thresholds for rail that were unmodified from Wilson et al. 2017, and original (grey) and newly revised (red) thresholds for roads and airports; the revised thresholds were informed by key findings from recent laboratory experiments that can be directly related to ash accumulation (i.e. skid resistance reduction and road marking coverage (Blake et al. 2016, 2017a), in addition to new post-eruption data where available. Figure 3 illustrates that some disruption to roads and airports can occur with an ash thickness of ~0.1 mm, an order of magnitude less than previously suggested by most anecdotal data. Figure 3 also suggests that larger thicknesses of ash may not always result in greater disruption. For example, an ash thickness of ~10 mm on roads could potentially lead to less disruption than a thickness of ~5 mm as skid resistance reduction is more likely at 5 mm. Although the

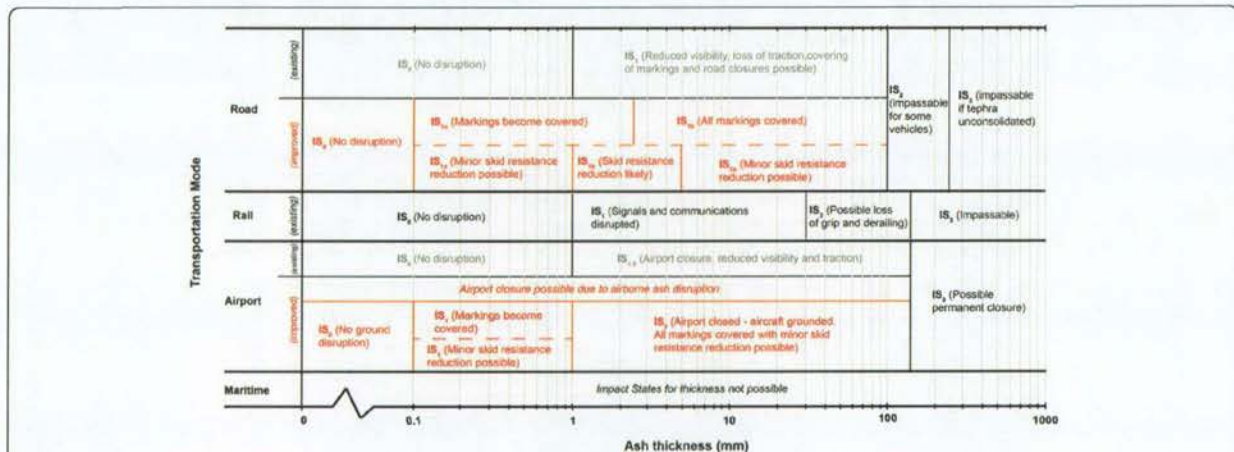


Fig. 3 Impact states for expected ground-related disruption to transportation as a function of ash thickness. The existing impact states (shown in black) were derived from qualitative post-eruption impact assessments and limited semi-quantitative field studies (adapted from Wilson et al. 2017). Impact states that were improved in this study are shown in red

impacts of reduced visibility (accounted for separately) may mask such effects overall, we suggest particularly elevated disruption to road transportation from ash thicknesses between ~2.5 and 5.0 mm. At this range, all road markings are covered and especially reduced skid resistance occurs. Although limited, the post-eruption data available (Blake 2016, Blake et al. 2016 and 2017a) indicate that fewer impacts are identified when ash is ~5–20 mm thick, supporting the hypothesis of elevated disruption regions on the thickness scale. Fluctuating intensities of road transportation disruption with thickness have not been identified in the past, highlighting the

importance of laboratory testing and the complexities that can be involved in determining accurate IS thresholds.

Figure 4 shows corresponding fragility functions for roads, updated from Wilson et al. 2017. Two new points (at 0.1 and 5.0 mm ash thickness) have been added to appropriately account for new findings from laboratory work for IS₁ (i.e. disruption in the form of skid resistance reduction (Blake et al. 2017a) and road marking coverage (Blake et al. 2016)). The decrease in function observed for IS₁ when ash thickness exceeds 5.0 mm is due to the potential increase in skid resistance; it is largely informed by recent laboratory findings (which do

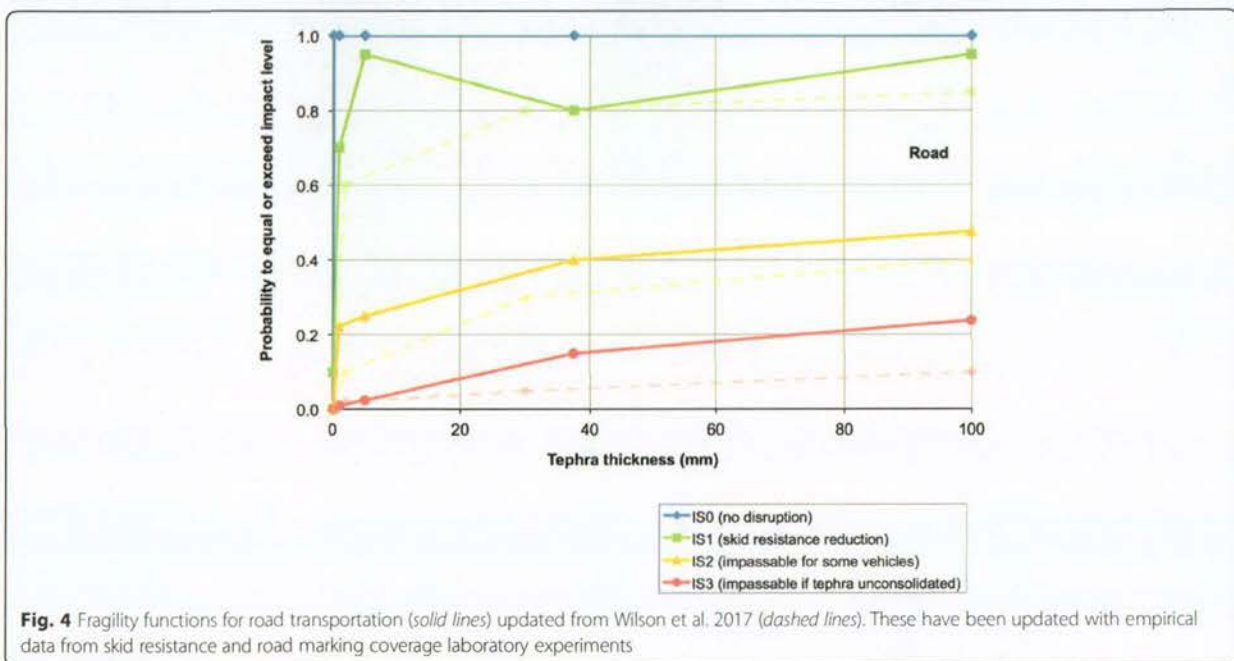


Fig. 4 Fragility functions for road transportation (solid lines) updated from Wilson et al. 2017 (dashed lines). These have been updated with empirical data from skid resistance and road marking coverage laboratory experiments

have limitations – see section 3.4) but is somewhat supported by semi-quantitative field observations. A decreasing fragility function breaks one of the core guidelines established by Wilson et al. 2017, which states that “functions should not decrease as the HIM value increases”. However, this guideline was established for damage rather than functional loss, and for when there is limited data to base vulnerability estimates on (i.e. not accounting for detailed empirical studies).

Airports can be closed due to ash in nearby airspace, without any ground accumulation of ash (Guffanti et al. 2009). Indeed, the International Civil Aviation Organisation (ICAO) advise that “aircraft should avoid volcanic ash encounters” (p.1–1), although “the operator is responsible for the safety of its operations” (p.2–1) and is required to complete a risk assessment as part of its safety management system, and have satisfied the relevant national (or supra-national) CAA before initiating operations into airspace forecast to be, or at airports known to be, contaminated with volcanic ash (ICAO 2012). Aircraft will likely become grounded due to a reduced runway friction coefficient when ash deposits exceed 1 mm (ICAO 2001, Wilson et al. 2017). Furthermore, severe deterioration in local visibility can result when engine exhausts from aircraft taxiing, landing and taking off disturb ash on the runway (ICAO 2001).

We assess functionality loss of airfields by applying the key findings from skid resistance and road marking coverage experiments for airfield concrete surfaces covered by ash (Fig. 3). It is important to consider such impact types, as aircraft operation may be possible when airborne ash concentrations are below aviation authority, and airline and airport guideline values. Although vehicle operation on airfields by ground staff could occur, even when aircraft are grounded, we focus on aircraft operations for the fragility function chart (Fig. 5). These fragility functions estimate the temporal duration of airport function assuming that the surrounding airspace is open and prior to any clean-up. Some functionality loss of the airport surface is possible between 0.1 and 1.0 mm due to markings becoming covered and reduced skid resistance (Blake et al. 2016, 2017a) before the airport is likely closed if ash accumulates to > 1 mm thickness. We display the temporal component for airport closure graphically as separate ISs (Fig. 5) as such information may be beneficial for end-users of fragility functions.

New ash-settling rate fragility functions

Figure 6 shows IS thresholds for visibility with ash-settling rate adopted as the HIM. Forecasts for visibility disruption are particularly useful for areas where there is minimal ash accumulation on the ground (i.e. during initial ashfall events or subsequent events following

thorough clean-up), as well as for maritime transportation and where surfaces are wet due to any re-suspension of ash into the atmosphere being minimised by water. Many of the thresholds established in Fig. 6, and depicted in new fragility function charts in Fig. 7, are particularly influenced by decisions made by local transportation authorities and we stress that our established thresholds are preliminary and open for improvement. Best judgement by the authors is used to determine some thresholds. For example, IS1 starts at $10 \text{ g m}^{-2} \text{ h}^{-1}$ for road, but at $20 \text{ g m}^{-2} \text{ h}^{-1}$ for rail, due to the relative resilience of rail to airborne ash, which results from more automated controls and fixed paths of travel (Blake et al. 2017b). IS thresholds may require adaptation to be compatible in other areas, especially where infrastructure types and associated technology differ. Thresholds are established for visibility only and do not consider other potential disruption caused by airborne volcanic ash such as ingestion into engines or the abrasion of windscreens.

A literature search revealed no quantitative or semi-quantitative data for visual ranges at specified ash-settling rates following previous eruptions worldwide. Figure 7 shows fragility functions for the ash-settling rate HIM, based entirely on empirical laboratory studies and comparisons to research for fog, to indicate expected impact on visibility and vehicles at near-ground level. Further extensive laboratory testing, in addition to syn- and post-eruption field surveys, will help to refine probabilities. Studies of ash remobilisation and re-suspension will likely improve our understanding of potential links between ash thickness and settling rate.

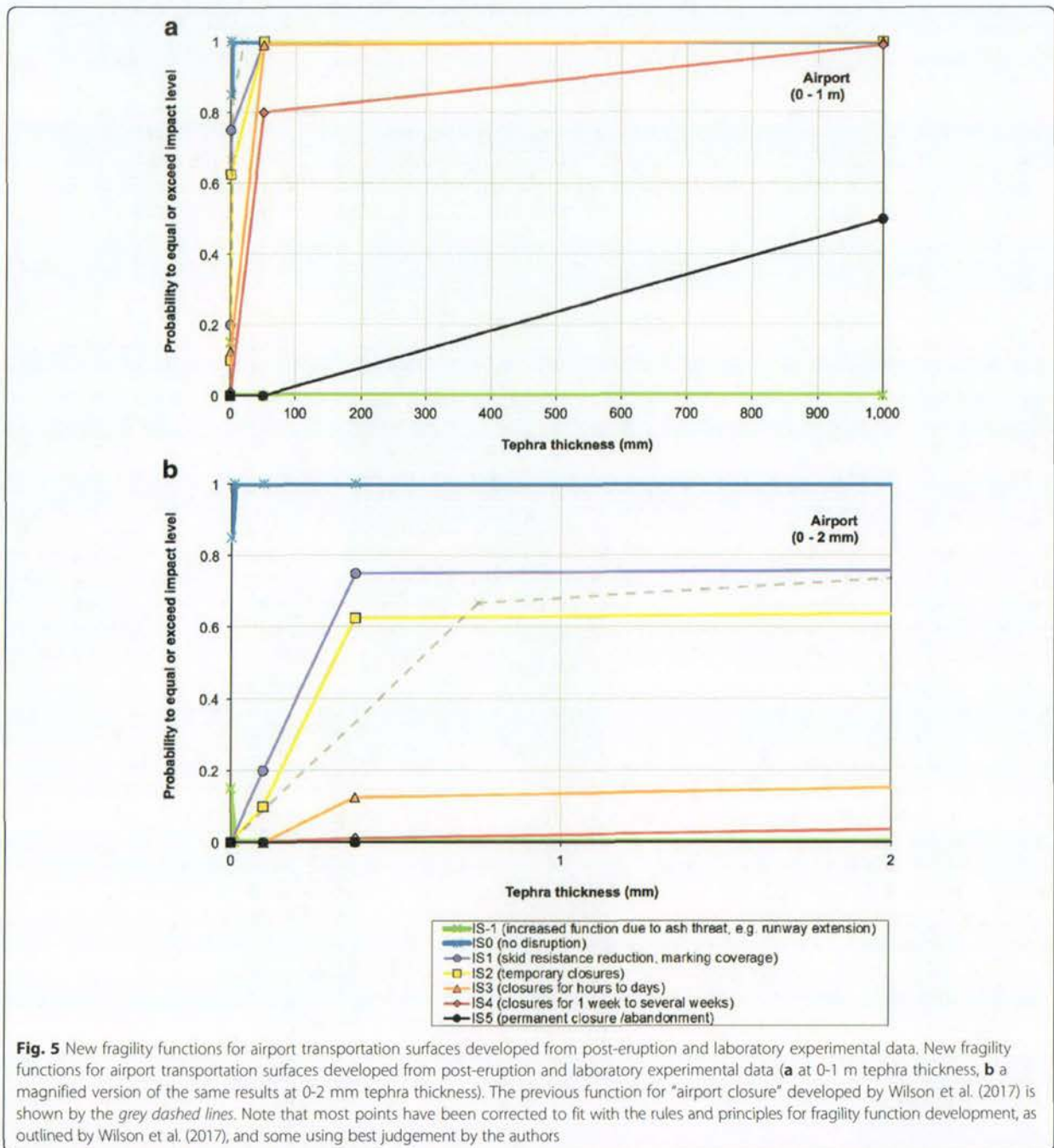
We emphasise that our studies were carried out in the context of transportation infrastructure found in New Zealand (e.g. ash characteristics and pavement properties found in the country) and that fragility functions may vary in different parts of the world. However, we suspect the trends will remain similar.

Multiple hazard intensity metrics

Figure 8 presents the results of comparative analysis of six additional HIMs identified during laboratory experimentation as having effects on surface skid resistance and road marking coverage.

This was achieved by using best judgement considering recent laboratory experiments to apply simple rank values to each HIM. The core HIM of ash thickness was used with the values of alternative HIMs dependent on relative importance to one another.

It is clear from Fig. 8 that as ash increases in thickness on the ground, the effect of different HIMs on surface transportation functionality changes. For example, particle size and colour play an important role below ~1.0 mm thickness due to the effect of fine-grained and



light-coloured ash on road marking coverage, but less of a role when ash thickness exceeds ~1.0 mm. However, the wetness of ash is important compared to other HIMs when ash thicknesses are >10 mm because it influences how readily ash binds together, in turn affecting how easily vehicles can drive through thicker deposits.

Arguably even more relevant for fragility functions is the relative importance of additional HIMs for visibility impairment (Fig. 9). Unlike ash thickness, there is no

evidence to suggest that the importance of different HIMs relative to one another changes as settling rate changes. However, results from Blake (2016) indicate that, as for thickness, the effect of additional HIMs has a lesser effect on functionality loss for greater ash-settling rates. This is likely due to the more dominant effect of there simply being more ash particles in the atmosphere. The HIM characteristics responsible for greater disruption are largely the same as for ash thickness (Fig. 8),

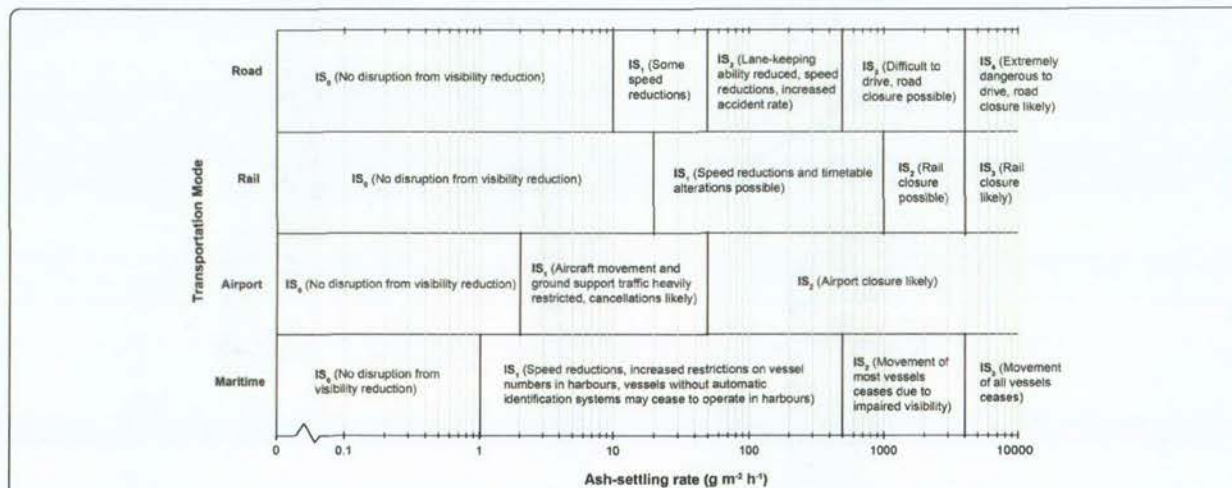


Fig. 6 Impact states for expected visibility-related disruption to surface transportation as a function of ash-settling rate. These are determined from quantitative laboratory experiments by Blake (2016), and comparisons to visual range and driver behaviour in fog. Thresholds have been derived in the context of transportation in New Zealand

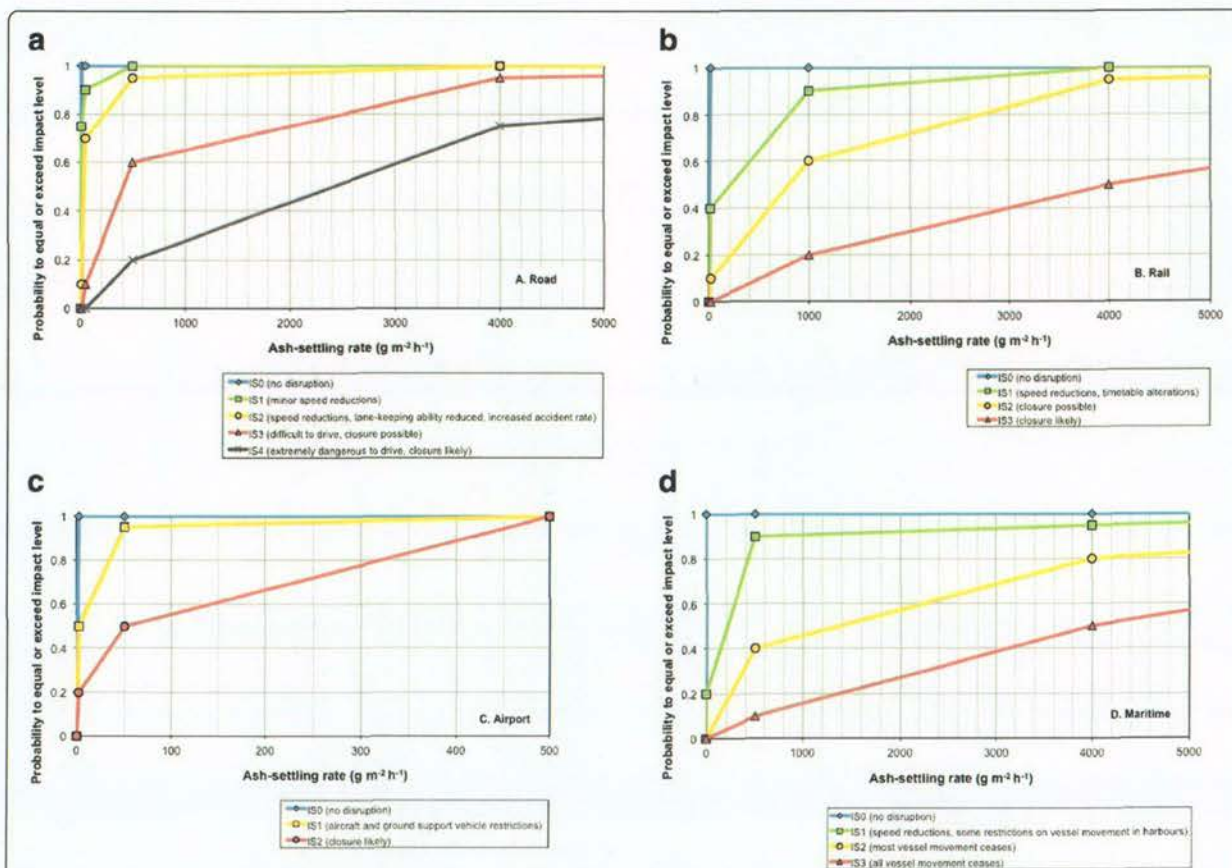
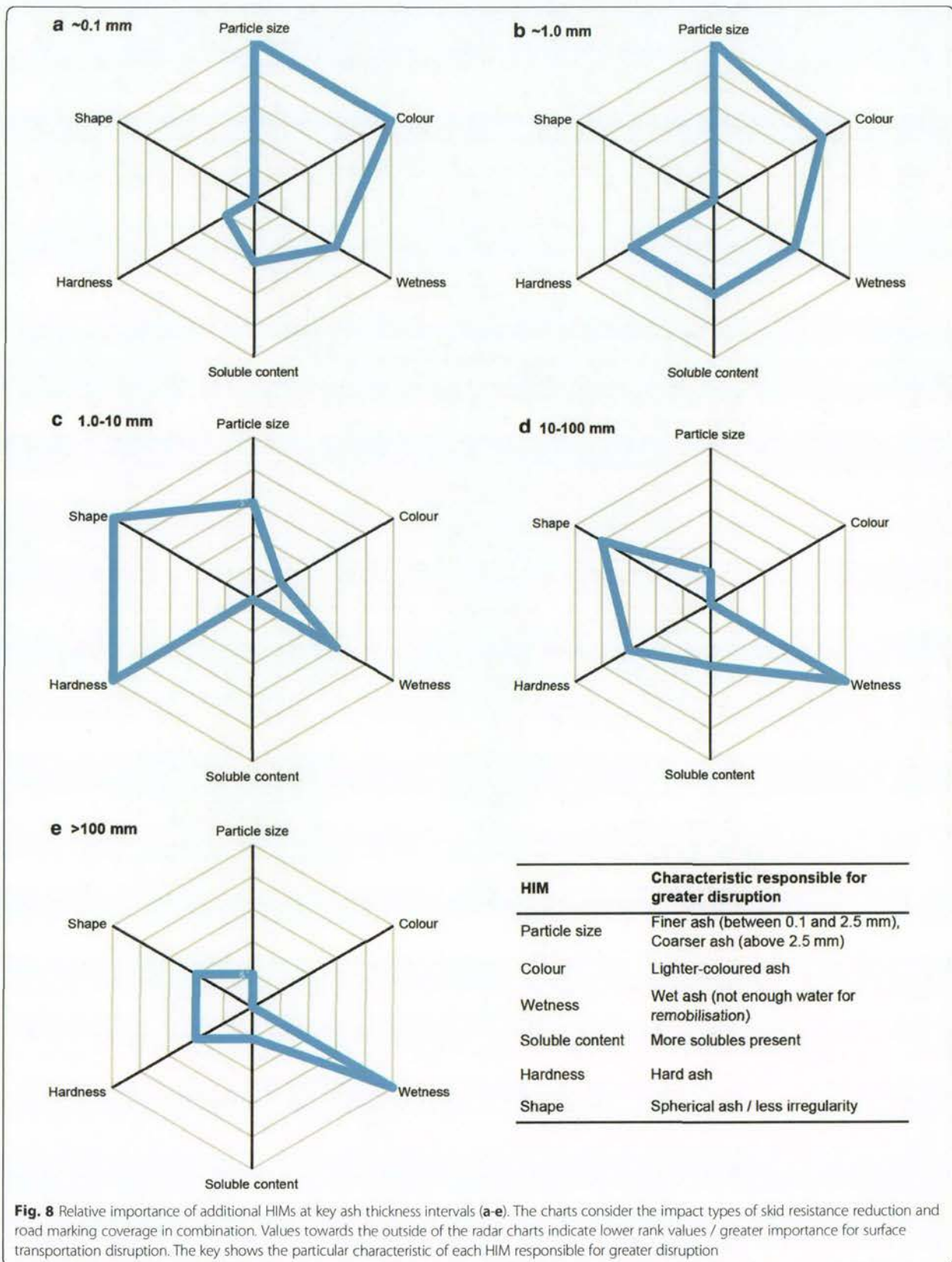
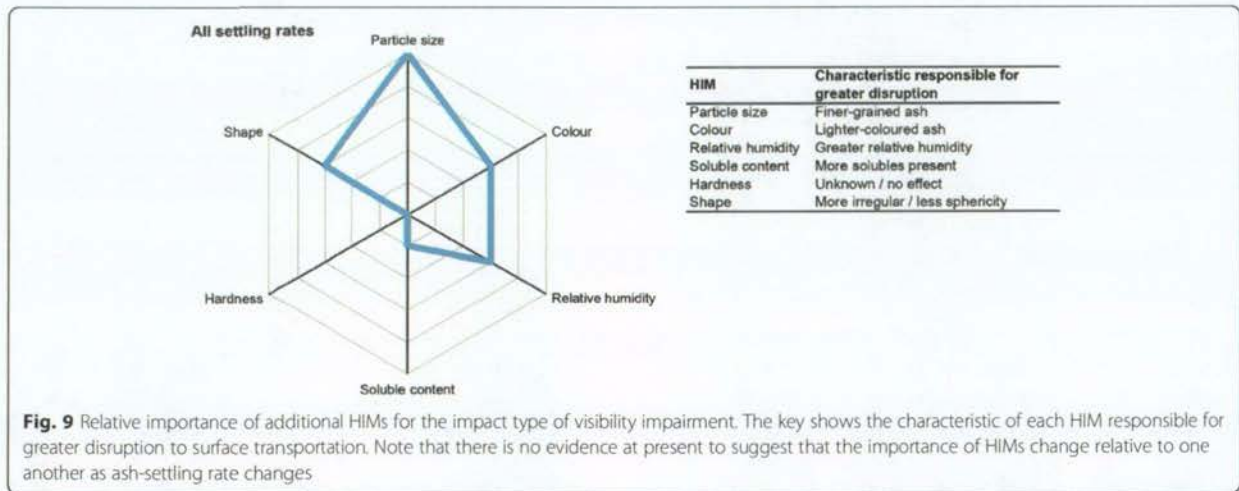


Fig. 7 Fragility function charts for visibility impacts on a road, b rail, c airports, and d maritime transportation, with ash-settling rate as the HIM





with the exception of ash particle shape; irregular-shaped ash particles may lead to greater disruption when airborne due to more light reflectance and subsequently lower visual range, whereas spherical-shaped ash particles can lead to greater disruption when on paved surfaces as a result of lower skid resistance. Particle size is clearly a crucial ash characteristic to consider when assessing surface transportation disruption, especially for < 10 mm thicknesses.

Further repeated laboratory experiments to investigate the effect of each ash characteristic on every surface transportation impact type, along with detailed post-

eruption field sampling and analysis, and subsequent computational probabilistic modelling will assist to fill this gap in knowledge. In the meantime, and in the absence of extensive datasets, it is difficult to evaluate the precise quantitative effect of alternative HIMs (i.e. those other than ash thickness and settling rate) on surface transportation disruption from volcanic ash and perform meaningful statistical analysis. However, we suggest that the importance of multiple HIMs can be accounted for by considering 'error boundaries' that illustrate uncertainty around existing functions for ash thickness and settling rate (Fig. 10) (although other

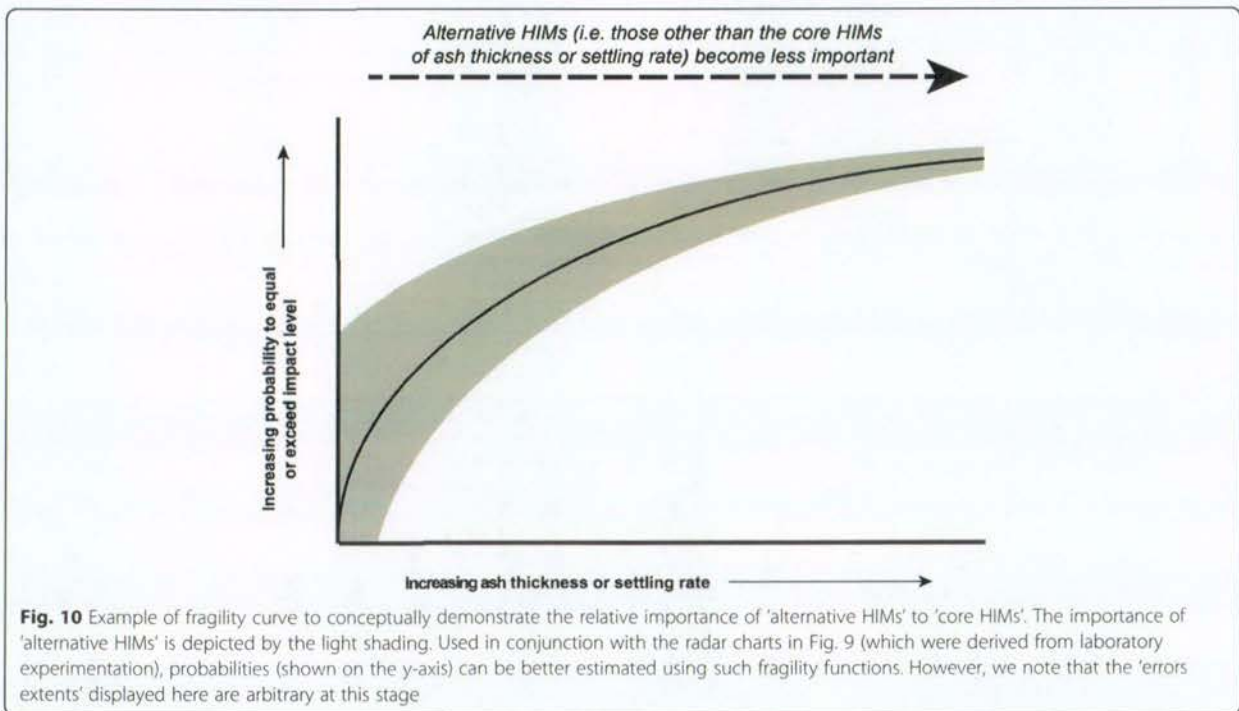


Fig. 10 Example of fragility curve to conceptually demonstrate the relative importance of 'alternative HIMs' to 'core HIMs'. The importance of 'alternative HIMs' is depicted by the light shading. Used in conjunction with the radar charts in Fig. 9 (which were derived from laboratory experimentation), probabilities (shown on the y-axis) can be better estimated using such fragility functions. However, we note that the 'errors extents' displayed here are arbitrary at this stage

uncertainties also exist). The conceptual diagram (Fig. 10) shows that with thicker ash or greater ash-settling rates, alternative HIMs (e.g. particle size, colour, shape) become less important with it being more beneficial to solely consider the core HIMs of ash thickness or ash-settling rate when forecasting impact levels.

Conclusion

We conclude that ash thickness and settling rate are the critical HIMs for the assessment of surface transportation functionality during volcanic ashfall events. However, due to current difficulties in quantifying the impact that ash thickness has on visibility impairment (the key impact type related to ash-settling rate and relevant for all modes of surface transportation), the two HIMs are not directly comparable and should be considered separately. For the ash thickness HIM, we identify the potential for fluctuating intensities of road transportation disruption as thickness increases, a feature that has not been identified in the past from empirical studies and is a product of experimental data obtained from targeted laboratory testing for specific impact types. We highlight that disruption can occur at an order of magnitude less than previously indicated (i.e. for thicknesses of ~0.1 mm rather than 1.0 mm) due to the potential for surface marking coverage; fragility functions for road and airports have been updated accordingly. Although highly subjective, preliminary fragility functions for visibility with ash-settling rate adopted as the HIM have been established using empirical data alone and by making comparisons to impacts previously identified in fog.

Our analysis of alternative HIMs (i.e. other than the critical HIMs of ash thickness and settling rate) and their effect on volcanic ash fragility function development for surface transportation leads to several key findings:

- Although ash thickness and settling rate should be treated as core HIMs for the assessment of surface transportation disruption, alternative HIMs should not be overlooked.
- Ash particle size is identified as the next most important HIM for functionality loss, especially when airborne concentrations and accumulations of ash on the ground are relatively small.
- For different ash thicknesses, the relative importance of alternative HIMs may be different. However, for different ash-settling rates there is no evidence to suggest that alternative HIMs change in their relative importance to one another.
- As ash thickness and ash-settling rates increase, alternative HIMs have less of an influence on surface transportation functionality loss. This confirms that it is indeed appropriate to consider ash thickness

and settling rate as core HIMs for surface transportation impact assessments.

- Without extensive datasets, it is difficult to accurately model the effect of alternative HIMs on disruption. However, we suggest that they could be incorporated into fragility functions by implementing 'error boundaries', alongside descriptors for the specific ash characteristic features responsible for increased probabilities of impact states being reached or exceeded.

Our findings support the need to provide forecasts and actively monitor a range of ash characteristics in areas that may be affected by volcanic ashfall, especially the thickness of deposits on the ground and ash-settling rate, but also other ash properties including particle size distributions, colour, and shape. This should be prioritised where there are abundant exposed surface transportation networks and populations: potential disruption can occur with ~0.1 mm ash thickness on the ground, depending on the ash characteristics present. Additional (particularly quantitative) datasets derived from new eruptions and laboratory tests will assist with the advancement of volcanic ash fragility functions for surface transportation, thus allowing further improvements in risk assessments and contingency planning in volcanically active regions.

Additional file

Additional file 1: Summary of key findings from recent laboratory experiments to investigate impacts of volcanic ash on surface transportation. (DOCX 19 kb)

Abbreviations

CAA: Civil aviation authority; HIM: Hazard intensity metric; ICAO: International civil aviation organisation; IS: Impact state; MNZ: Maritime New Zealand; PDC: Pyroclastic density current; TRB: Transport research board; UNISDR: United nations international strategy for disaster reduction

Acknowledgements

We acknowledge all the technical and financial support received to conduct the extensive laboratory experimentation on surface transportation impacts from volcanic ash. Although the results were not directly covered in this paper (they are covered in separate publications), many of the key findings would not have been possible without these initial studies. Particular thanks are expressed to the New Zealand Earthquake Commission (EQC), Determining Volcanic Risk in Auckland (DEVORA) project, Natural Hazards Research Platform (NHRP), University of Canterbury Mason Trust, and GNS Science Core Programme funding scheme for their recent support to the authors. Also, the financial support from the University of Canterbury Department of Geological Sciences is greatly appreciated, which allowed the purchase of key laboratory equipment. Daniel Blake would like to thank his additional PhD co-supervisors, Jan Lindsay (The University of Auckland) and Jim Cole (University of Canterbury), for their edits, guidance and advice throughout this study. This paper was improved by the comments of two anonymous reviewers.

Authors' contributions

DMB planned, coordinated and led all the laboratory experimental work for volcanic ash surface transportation impacts mentioned in this paper. He also

planned the research and wrote this paper including the development of methodologies and illustrations. NID and TMW assisted with method development and provided suggestions for improvements throughout the process and conducted thorough edits of the manuscript. GW contributed by providing the initial methodologies for fragility function production and a final edit of the manuscript. All authors have read, reviewed and approved the final version.

Competing interests

The authors declare that they have no competing interests.

Publisher's Note

Springer Nature remains neutral with regard to jurisdictional claims in published maps and institutional affiliations.

Author details

¹Department of Geological Sciences, University of Canterbury, Private Bag, Christchurch 4800, New Zealand. ²GNS Science, PO Box 30-368, Lower Hutt 5040, New Zealand. ³Present address: Office of Emergency Management, Havelock Street, West Perth, WA, Australia.

Received: 22 June 2016 Accepted: 30 August 2017

Published online: 03 October 2017

References

- Auckland Airport (2008) Newsroom: Fog at Auckland Airport and Category IIIB. 19 November 2008, Auckland Airport. http://www.aucklandairport.co.nz/~media/3FF843AAF8C23B941EAA7406EAB7B.ashx?sc_database=web. Accessed 19 Mar 2016.
- Auckland Council. Harbourmaster's Office operation of vessels during periods of restricted visibility: navigation safety operating requirements. Auckland, New Zealand: Auckland Council; 2014.
- Barnard S. The vulnerability of New Zealand lifelines infrastructure to ashfall. Christchurch, New Zealand: PhD Thesis, Hazard and Disaster Management, University of Canterbury; 2009.
- Binkowski FS, Roselle SJ, Mebest MR, Eder BK. In: Chock DP, Carmichael GR, editors. Modeling atmospheric particulate matter in an air quality modelling system using a modal method, Atmospheric modelling. The IMA volumes in mathematics and its applications 130; 2002.
- Blake DM, Wilson G, Stewart C, Craig HM, Hayes JL, Jenkins SF, Wilson TM, Horwell CJ, Andreastuti S, Daniswara R, Ferdwijaya D, Leonard GS, Hendrasto M, Cronin S (2015) The 2014 eruption of Kelud volcano, Indonesia: impacts on infrastructure, utilities, agriculture and health. GNS Science Report 2015/15 139p.
- Blake DM. Impacts of volcanic ash on surface transportation networks: considerations for Auckland City, New Zealand. PhD Thesis, Department of Geological Sciences, University of Canterbury, Christchurch, New Zealand. 2016.
- Blake DM, Wilson TW, Gomez C. Road marking coverage by volcanic ash: an experimental approach. *Environ Earth Sci*. 2016;75(20):1–12.
- Blake DM, Wilson TM, Cole JW, Deligne NI, Lindsay JM. Impact of volcanic ash on road and airfield surface skid resistance. *Sustainability*. 2017a;9(8):1389.
- Blake DM, Deligne NI, Wilson TM, Lindsay JM, Woods R. Investigating the consequences of urban volcanism using a scenario approach II: insights into transportation network damage and functionality. *J Volcanology Geotherm Res*. 2017b;340:92–116.
- Blong R. A new damage index. *Nat Hazards*. 2003;30:1–23.
- Blong RJ. Volcanic hazards: a sourcebook on the effects of eruptions. Sydney: Academic Press Inc; 1984.
- Board HR. National Cooperative Highway Research Program Synthesis of highway practice 14: skid resistance. Washington D.C: Highway Research Board, National Academy of Sciences; 1972.
- CAA. Low Visibility Operations at Auckland Airport. Vector: Pointing to Safer Aviation, Issue 4. Civil Aviation Authority of New Zealand. 2007. https://www.caa.govt.nz/Publications/Vector/Vector_2007_Issue4_JulAug.pdf. Accessed 11 Sept 2017.
- Choi E, DesRoches R, Nielson B. Seismic fragility of typical bridges in moderate seismic zones. *Eng Struct*. 2004;26:187–99.
- Craig H, Wilson T, Stewart C, Outes V, Villarosa G, Baxter P. Impacts to agriculture and critical infrastructure in Argentina after ashfall from the 2011 eruption of the Cordón Caulle volcanic complex: an assessment of published damage and function thresholds. *J Appl Volcanol*. 2016a;5(7):31.
- Craig H, Wilson T, Stewart C, Villarosa G, Outes V, Cronin S, Jenkins S. Agricultural impact assessment and management after three widespread tephra falls in Patagonia, South America. *Nat Hazards*. 2016b;82(2):1167–229.
- Deligne NI, Fitzgerald R, Blake DM, Davies AJ, Hayes JL, Stewart C, Wilson G, Wilson TM, Carneiro R, Kennedy B, Muspratt S, Woods R. Investigating the consequences of urban volcanism using a scenario approach I: development and application of a hypothetical eruption in the Auckland Volcanic Field, New Zealand. *J Volcanol Geotherm Res*. 2017;336:192–208.
- Deligne NI, Blake DM, Davies AJ, Grace ES, Hayes J, Potter S, Stewart C, Wilson G, Wilson TM (2015) Economics of Resilient Infrastructure Auckland Volcanic Field scenario. ERI Research Report 2015/03 151p.
- Dunn MG. Operation of gas turbine engines in an environment contaminated with volcanic ash. *J Turbomach*. 2012;134(5):18.
- Guffanti M, Mayberry GC, Casadevall TJ, Wunderman R. Volcanic hazards to airports. *Nat Hazards*. 2009;51:287–302.
- Hayes JL, Wilson TM, Magill C. Tephra fall clean-up in urban environments. *J Volcanol Geotherm Res*. 2015;304:359–77.
- Horwell CJ, Baxter PJ, Hillman SE, Damby DE, Delmelle P, Donaldson K, Dunster C, Calkins JA, Fubini B, Hoskuldsson A, Kelly FJ, Larsen G, Le Blond JS, Livi KJT, Mendis B, Murphy F, Sweeney S, Tetley TD, Thordarson T, Tomatis M. Respiratory health hazard assessment of ash from the 2010 eruption of Eyjafjallajökull volcano, Iceland: a summary of initial findings from a multi-centre laboratory study. Durham, UK: IHHN and Durham University; 2010.
- Hyslop N. Impaired visibility: the air pollution people see. *Atmos Environ*. 2009;43(1):182–95.
- ICAO (2001) Manual on volcanic ash, radioactive material and toxic chemical clouds. http://www3.alpa.org/portals/alpa/volcanicash/12_Doc9691ManualCAOVolAshRadioactiveMaterial.pdf. Accessed 16 Jun 2016.
- ICAO (2012) Flight safety and volcanic ash: risk management of flight operations with known or forecast volcanic ash contamination. International Civil Aviation Organisation. http://www.icao.int/publications/Documents/9974_en.pdf. Accessed 16 Jun 2016.
- Jenkins S, Komorowski J-C, Baxter P, Spence R, Picquout A, Lavigne F. The Merapi 2010 eruption: an interdisciplinary impact assessment methodology for studying pyroclastic density current dynamics. *J Volcanol Geotherm Res*. 2013;261:316–29.
- Jenkins SF, Spence RJS, Fonseca JFBD, Solidum RU, Wilson TM. Volcanic risk assessment: quantifying physical vulnerability in the built environment. *J Volcanol Geotherm Res*. 2014a;276:105–20.
- Jenkins SF, Wilson TM, Magill CR, Miller V, Stewart C (2014b) Volcanic ash fall hazard and risk: technical background paper for the UN-ISDR Global Assessment Report on Disaster Risk Reduction 2015. <http://www.preventionweb.net/english/hyogo/gar/2015/en/home/documents.html>. Accessed 19 Apr 2016.
- Johnston DM. Physical and social impacts of past and future volcanic eruptions in New Zealand. Palmerston North, New Zealand: PhD Thesis, Earth Science, Massey University; 1997.
- Johnston DM, Daly M. Auckland erupts! *New Zealand Sci Monthly*. 1997;8(10):6–7.
- Jolly GE, Keys HJR, Procter JN, Deligne NI. Overview of the co-ordinated risk-based approach to science and management response and recovery for the 2012 eruptions of Tongariro volcano, New Zealand. *J Volcanol Geotherm Res*. 2014;286:184–207.
- Leonard GS, Stewart C, Wilson TM, Procter JN, Scott BJ, Keys HJ, Jolly GE, Wardman JB, Cronin SJ, McBride SK. Integrating multidisciplinary science, modelling and impact data into evolving, syn-event volcanic hazard mapping and communication: a case study from the 2012 Tongariro eruption crisis, New Zealand. *J Volcanol Geotherm Res*. 2014;286:208–32.
- MNZ (2015) Maritime Rules Part 22: Collision Prevention. Maritime New Zealand, Wellington, New Zealand. <http://www.maritimenz.govt.nz/rules/part-22/>. Accessed 19 Mar 2016.
- Nairn IA (2002) The effects of volcanic ash fall (tephra) on road and airport surfaces. GNS Science Report 2002/13 32p.
- Nanayakkara KU, Dias WPS. Fragility curves for structures under tsunami loading. *Nat Hazards*. 2016;80(1):471–86.
- Porter K, Kennedy R, Bachman R. Creating fragility functions for performance-based earthquake engineering. *Earthquake Spectra*. 2007;23(2):471–89.
- Porter KA, Farokhnia K, Cho IH, Rossetto T, Ioannou I, Grant D, Jaiswal K, Wald D, D'Ayala D, Meslem A, So E, Kiremidjian AS, Noh H (2012) Global vulnerability estimation methods for the Global Earthquake Model. Proceedings for the 15th World Conference on Earthquake Engineering, 24–28 September 2012, 4504.

- Reese S, Ramsay D (2010) RiskScape: flood fragility methodology. NIWA Technical Report WLG2010-45 42 p.
- Rossetto T, D'Ayala D, Ioannou I, Meslem A. Evaluation of existing fragility curves. In: Pitilakis K, Crowley H, Kaynia AM (Eds). SYNER-G: typology definition and fragility functions for physical elements at seismic risk. Dordrecht: Springer; 2014.
- Rossetto T, Ioannou I, Grant DN. Existing empirical vulnerability and fragility functions: compendium and guide for selection. GEM technical report 2013-X. Pavia, Italy: GEM Foundation; 2013.
- Singhal A, Kiremidjian AS. Method for probabilistic evaluation of seismic structural damage. *J Struct Eng*. 1996;122:1459–67.
- Stewart C, Horwell C, Plumlee G, Cronin S, Delmelle P, Baxter P, Calkins J, Damby D, Mormon S, Oppenheimer C. Protocol for analysis of volcanic ash samples for assessment of hazards from leachable elements. IAVCEI, IVHHN, Cities on Volcanoes Commission, USGS, GNS Science. 2013. http://www.ivhhn.org/images/pdf/volcanic_ash_leachate_protocols.pdf.
- Tarbotton C, Dall'Osso F, Dominey-Howes D, Goff J. The use of empirical vulnerability functions to assess the response of buildings to tsunami impact: comparative review and summary of best practice. *Earth Sci Rev*. 2015;142:120–34.
- TRB. Transportation options for megacities in the developing world: a working paper, transport research board. In: NRC (1996), editor. Meeting the challenges of megacities in the developing world: a collection of working papers. Washington DC, United States: National Research Council, National Academy Press; 1996.
- UNISDR (2009) UNISDR terminology on disaster risk reduction. United Nations International Strategy for Disaster Reduction, Geneva, Switzerland. http://www.unisdr.org/files/7817_UNISDRTerminologyEnglish.pdf. Accessed 21 Apr 2016.
- Wardman J, Sword-Daniels V, Stewart C, Wilson T (2012) Impact assessment of the May 2010 eruption of Pacaya volcano, Guatemala. *GNS Science Report 2012/09* 90p.
- Wilson G. Vulnerability of critical infrastructure to volcanic hazards. Christchurch, New Zealand: PhD Thesis in Hazards and Disaster Management, Department of Geological Sciences, University of Canterbury; 2015.
- Wilson G, Wilson TM, Deligne NI, Blake DM, Cole JW. Framework for developing volcanic fragility functions for critical infrastructure. *J Applied Volcanol*. 2017.
- Wilson G, Wilson TM, Deligne NI, Cole JW. Volcanic hazard impacts to critical infrastructure: a review. *J Volcanol Geotherm Res*. 2014;286:148–82.
- Wilson TM, Stewart C, Sword-Daniels V, Leonard GS, Johnston DM, Cole JW, Wardman J, Wilson G, Barnard ST. Volcanic ash impacts to critical infrastructure. *Phys Chem Earth*. 2012;45–46:5–23.
- Wilson TW, Stewart C, Cole JW, Dewar DJ, Johnston DM, Cronin SJ (2011) The 1991 eruption of Volcán Hudson, Chile: impacts on agriculture and rural communities and long-term recovery. *GNS Science Report 2009/66* 99 p.

Submit your manuscript to a SpringerOpen® journal and benefit from:

- Convenient online submission
- Rigorous peer review
- Open access: articles freely available online
- High visibility within the field
- Retaining the copyright to your article

Submit your next manuscript at ► springeropen.com

Road marking coverage by volcanic ash: an experimental approach

Environmental Earth Sciences

October 2016, 75:1348 | Cite as

Original Article

First Online: 12 October 2016



Shares Downloads Citations

Abstract

Coverage of road markings by volcanic ash is one of the most commonly reported impacts to surface transportation networks during volcanic ashfall. Even minimal accumulation can obscure markings, leading to driver disorientation, diminished flow capacity and an increase in accidents. Such impacts may recur due to repeated direct ashfall (i.e. during prolonged eruptions) and/or due to the re-suspension of ash by wind, water, traffic or other human activities, and subsequent secondary deposition on the road surface. Cleaning is thus required to restore and maintain road network functionality. Previous studies have not constrained ash accumulation measurements to inform road cleaning initiation or plans for safe road operations in environments containing ash. This study uses a laboratory approach with digital image analysis to quantify the percentage of white road marking coverage by three types of volcanic ash with coarse, medium and fine particle size distributions. We find that very small accumulations of ash are responsible for road marking coverage and suggest that around 8 % visible white paint or less would result in the road markings being hidden. Road markings are more easily covered by fine-grained ash, with ash area densities of $\sim 30 \text{ g m}^{-2}$ (estimated at $< 0.1 \text{ mm}$ surface thickness) potentially causing markings to be obscured. For the coarse ash in our study, road marking coverage occurs at area densities of $\sim 1000\text{--}2200 \text{ g m}^{-2}$ ($\sim 1.0\text{--}2.5 \text{ mm}$ depth) with ash colour and line paint characteristics causing some of the variation. We suggest that risk management measures such as vehicle speed reduction

and the initiation of road cleaning activities should be taken at or before the lower thresholds as our experiments are conducted at a relatively short horizontal distance and the ability to observe road markings when driving will be comparatively reduced.

Keywords

Stone mastic asphalt Visibility Image analysis Road safety
Transportation Hazard Impact

This is a preview of subscription content, [log in to check access](#).

Notes

Acknowledgments

We thank the University of Canterbury Mason Trust scheme, New Zealand Earthquake Commission (EQC) and Determining Volcanic Risk in Auckland (DEVORA) project for their financial support towards the study through the provision of funding for authors Daniel Blake and Thomas Wilson. We also express thanks for the support towards laboratory assistance and equipment provided by several people, whose help was vital to the success of this study. In particular, we wish to thank Janet Jackson and Howard Jamison of Downer Group for coordinating the painting of the asphalt concrete slabs, and Kerry Swanson, Matt Cockcroft, Chris Grimshaw, Stephen Brown, Alec Wild, Connor Jones and Brigitt White for their assistance with sample preparation and conducting experiments at the University of Canterbury's Volcanic Ash Testing Lab. Daniel Blake would also like to thank his PhD co-supervisors, Jim Cole (University of Canterbury), Jan Lindsay (The University of Auckland) and Natalia Deligne (GNS Science) for their edits, guidance and support throughout the project.

References

- ADOT (2011) Dusty roads. Arizona Department of Transportation Blog. <http://www.azdot.gov/media/blog/posts/2011/04/18/dusty-roads> (<http://www.azdot.gov/media/blog/posts/2011/04/18/dusty-roads>). Accessed 13 Oct 2015
- Aljassar AH, Al-Kulaib A, Ghoneim AN, Metwali E-S (2006) A cost effective solution to the problem of sand accumulation on a desert road

Journal of
Environmental Earth Sciences

Road marking coverage by volcanic ash: an experimental approach
--Manuscript Draft--

Manuscript Number:							
Full Title:	Road marking coverage by volcanic ash: an experimental approach						
Article Type:	Original Manuscript						
Corresponding Author:	Daniel Mark Blake University of Canterbury Christchurch, NEW ZEALAND						
Corresponding Author Secondary Information:							
Corresponding Author's Institution:	University of Canterbury						
Corresponding Author's Secondary Institution:							
First Author:	Daniel Mark Blake						
First Author Secondary Information:							
Order of Authors:	Daniel Mark Blake Thomas McDonald Wilson Christopher Gomez						
Order of Authors Secondary Information:							
Funding Information:	<table border="1"> <tr> <td>New Zealand Earthquake Commission (EQC)</td> <td>Mr Daniel Mark Blake</td> </tr> <tr> <td>Determining Volcanic Risk in Auckland (DEVORA) Project</td> <td>Mr Daniel Mark Blake</td> </tr> <tr> <td>University of Canterbury Mason Trust Scheme</td> <td>Mr Daniel Mark Blake</td> </tr> </table>	New Zealand Earthquake Commission (EQC)	Mr Daniel Mark Blake	Determining Volcanic Risk in Auckland (DEVORA) Project	Mr Daniel Mark Blake	University of Canterbury Mason Trust Scheme	Mr Daniel Mark Blake
New Zealand Earthquake Commission (EQC)	Mr Daniel Mark Blake						
Determining Volcanic Risk in Auckland (DEVORA) Project	Mr Daniel Mark Blake						
University of Canterbury Mason Trust Scheme	Mr Daniel Mark Blake						
Abstract:	<p>Coverage of road markings by volcanic ash is one of the most commonly reported impacts to surface transportation networks during volcanic ashfall. Even minimal accumulation can obscure markings, leading to driver disorientation, diminished flow capacity and an increase in accidents. Such impacts may recur due to repeated direct ashfall (i.e. during prolonged eruptions) and/or due to the re-suspension of ash by wind, water, traffic or other human activities, and subsequent secondary deposition on the road surface. Cleaning is thus required to restore and maintain road network functionality. Previous studies have not constrained ash accumulation measurements to inform road cleaning initiation or plans for safe road operations in environments containing ash. This study uses a laboratory approach with digital image analysis to quantify the percentage of white road marking coverage by three types of volcanic ash with coarse, medium and fine particle size distributions. We find that very small accumulations of ash are responsible for road marking coverage and suggest that around 8% visible white paint or less would result in the road markings being hidden. Road markings are more easily covered by fine-grained ash, with ash area densities of ~30 g m⁻² (estimated at less than 0.1 mm surface thickness) potentially causing markings to be obscured. For the coarse ash in our study, road marking coverage occurs at area densities of ~1,000 - 2,200 g m⁻² (~1.0 - 2.5 mm depth) with ash colour and line paint characteristics causing some of the variation. We suggest that risk management measures such as vehicle speed reduction and the initiation of road cleaning activities, should be taken at or before the lower thresholds as our experiments are conducted at a relatively short distance and the ability to observe road markings when driving will be comparatively reduced.</p>						
Suggested Reviewers:	Susanna Jenkins, PhD Research Fellow, University of Bristol School of Earth Sciences susanna.jenkins@bristol.ac.uk						

	Volcanic hazard and impact quantification background
	Christina Magill, PhD Senior Research Fellow, Macquarie University christina.magill@mq.edu.au Hazard science and physical impacts of volcanic eruptions background
	Thomas Cova, PhD Director/Professor, University of Utah cova@geog.utah.edu Environmental hazards and transportation background
	David Johnston, PhD Director/Professor, Massey University, New Zealand d.m.johnston@massey.ac.nz Disaster management background with physical and social science focus
	Thomas Walter, PhD Priv Doz, University of Postdam thomas.walter@gfz-potsdam.de Co-author of paper investigating solar panel coverage by ash. Shares some similarities with this manuscript.
Opposed Reviewers:	

Department of Geological Sciences
Volcanic Ash Testing Lab
University of Canterbury
Private Bag 4800
Christchurch 8140
New Zealand



Tuesday 09 February 2016

Dear Editor,

Please find enclosed the research manuscript: ***Road marking coverage by volcanic ash: an experimental approach***

By Daniel M Blake, Thomas M Wilson and Christopher Gomez

For consideration for publication in the Journal of Environmental Earth Sciences.

Thank you for your consideration and I look forward to hearing back soon.

Yours faithfully,

A handwritten signature in black ink that reads 'DBlake' with a stylized flourish underneath.

Daniel Blake (corresponding author)

Road marking coverage by volcanic ash: an experimental approach

Daniel M Blake^{1*}, Thomas M Wilson¹, Christopher Gomez²

¹ Department of Geological Sciences, University of Canterbury, Private Bag 4800, Christchurch, New Zealand

² Department of Geography, University of Canterbury, Private Bag 4800, Christchurch, New Zealand

*Corresponding author

Email: daniel.blake@pg.canterbury.ac.nz

1
2
3
4
5
6
7
8
9
10
11
12
13
14
15
16
17
18
19
20
21
22
23
24
25
26
27
28
29
30
31
32
33
34
35
36
37
38
39
40
41
42
43
44
45
46
47
48
49
50
51
52
53
54
55
56
57
58
59
60
61
62
63
64
65

Abstract

Coverage of road markings by volcanic ash is one of the most commonly reported impacts to surface transportation networks during volcanic ashfall. Even minimal accumulation can obscure markings, leading to driver disorientation, diminished flow capacity and an increase in accidents. Such impacts may recur due to repeated direct ashfall (i.e. during prolonged eruptions) and/or due to the re-suspension of ash by wind, water, traffic or other human activities, and subsequent secondary deposition on the road surface. Cleaning is thus required to restore and maintain road network functionality. Previous studies have not constrained ash accumulation measurements to inform road cleaning initiation or plans for safe road operations in environments containing ash. This study uses a laboratory approach with digital image analysis to quantify the percentage of white road marking coverage by three types of volcanic ash with coarse, medium and fine particle size distributions. We find that very small accumulations of ash are responsible for road marking coverage and suggest that around 8% visible white paint or less would result in the road markings being hidden. Road markings are more easily covered by fine-grained ash, with ash area densities of $\sim 30 \text{ g m}^{-2}$ (estimated at less than 0.1 mm surface thickness) potentially causing markings to be obscured. For the coarse ash in our study, road marking coverage occurs at area densities of $\sim 1,000 - 2,200 \text{ g m}^{-2}$ ($\sim 1.0 - 2.5 \text{ mm}$ depth) with ash colour and line paint characteristics causing some of the variation. We suggest that risk management measures such as vehicle speed reduction and the initiation of road cleaning activities, should be taken at or before the lower thresholds as our experiments are conducted at a relatively short distance and the ability to observe road markings when driving will be comparatively reduced.

Highlights

- Image analysis to quantify road marking coverage by volcanic ash.
- Road markings may be obscured when covered by only $\sim 30 \text{ g m}^{-2}$ ash.
- Light-coloured ash reduces marking visibility more than dark-coloured ash.
- Thick line paint and retroreflective beads increase susceptibility to coverage.
- Road cleaning is recommended at $\sim 0.1 - 1.0 \text{ mm}$ ash surface depths.

Keywords

Stone Mastic Asphalt, visibility, image analysis, road safety, transportation, hazard, impact.

1. Introduction

As populations grow worldwide, more people are residing in volcanically active areas, generally with associated development and expansion of infrastructure including transportation networks (Loughlin et al. 2015). Volcanic ash is the most widely dispersed of all volcanic hazards, often affecting road transport potentially hundreds to thousands of kilometers from its source. Common impacts include reduced skid resistance and visual range, and engine air filter blockage (Wilson et al. 2014). However, perhaps the most frequent and greatest impact during initial ash accumulation is the coverage of road markings. Road marking coverage is also recognised as a substantial impact in areas affected by duststorms, as experienced for example in parts of the Middle East (Aljassar et al. 2006) and North America (ADOT 2015). It is of concern, as much of the visual information needed by a driver to navigate roads safely is provided by continuous road markings (Gibbons et al. 2004). Coverage can lead to driver disorientation (Durand et al. 2001, T. Wilson et al. 2012, USGS 2013) and cascading effects on vehicle movement across the road network, such as diminished flow capacity and an increase in traffic accidents (Wolshon 2009). Indeed, the Australian Automobile Association estimate that if 'average standard' road markings are maintained, the percentage of crash rates is reduced by between 10 and 40%, depending on the crash type (Carnaby 2005).

Road marking coverage by volcanic ash is by no means transient. Impacts may recur due to repeated ashfall (i.e. during prolonged eruptions) and/or due to the re-suspension of ash by wind, water, traffic or other human activities, and subsequent secondary deposition on the road surface. Road cleaning may thus be required to restore and maintain road network functionality. Some authorities (e.g. Kagoshima City Office near Sakurajima volcano, Japan) use road marking coverage as a prompt to mobilise road sweepers and commence ash removal. In 2014 alone when there were 450 eruptions, this led to the removal of 1,274 m³ of ash from the region's roads (Kagoshima City Office, personal communication, June 08 2015).

Road marking coverage by volcanic ash has been recorded on road networks following a number of eruptions, such as Mt St Helens, USA (1980), Hudson, Chile (1991), Ruapehu, New Zealand (1995-96), Reventador, Ecuador (2002), and during the many ashfall events on Kagoshima City (Japan) from Sakurajima volcano (1955-2015) (Becker et al. 2001, Cole et al. 2005, Leonard et al. 2005, Barnard 2009, Wilson et al. 2009, Magill et al. 2013). However, a review of available sources reveals only limited estimates of volcanic ash thickness that have caused complete coverage, ranging from trace amounts to 5 mm. We suggest that other characteristics, such as the size of ash particles, colour of ash and road surface texture may account for the range to some extent. At such small accumulations however, depths of ash are difficult to measure accurately and other measurements such as the area density of ash may be more appropriate.

In this study at the University of Canterbury's Volcanic Ash Testing Laboratory (VATLab), we adopt a method to replicate volcanic ash deposition on road surfaces by using asphalt slabs painted with two thicknesses of line paint. We employ image classification and segmentation techniques to quantify the extent of road marking coverage by ash and to determine ash depth and surface area density when markings are visually obscured. Based on our findings, suggestions to maintain road safety are made, particularly thresholds for road cleaning initiation.

2. Methods

2.1 Ash and road surface type

Stone Mastic Asphalt (SMA), constructed as 300 x 300 x 45 mm slabs (with aggregate particle size <13.2 mm and a bitumen content of 5.9 %) by the Road Science Laboratory in Tauranga, New Zealand, were placed directly beneath an ash delivery system (section 2.2). Three ash types (a basalt of dark colouration, an andesite of medium colouration, and a rhyolite of light colouration) were sourced from different ash deposits in New Zealand (Table 1) to provide a means of contrast comparison. All samples were dried and then processed using a rock pulveriser and/or sieving to achieve three distinct clusters of particle size distributions (Figure 1). Spatial distributions of particle sizes from ashfall events are often

complex. However, ash particle sizes are typically larger closer to the vent with smaller particles carried further downwind (Jenkins et al. 2014).

Particle sizes (Figure 1) were determined using a Micrometrics Saturn DigiSizer II Laser-Sizer (three runs per sample). We note that the maximum particle sizes for some samples are substantially less than the size of the disc measure used for pulverisation or sieve mesh aperture. This is likely due to the process of pulverisation and mechanism of breakage. Conversely, the maximum particle sizes for some samples are greater than the size of the sieve mesh aperture used. This is due to the tabulate form of some ash particles and their orientation when passing through the sieve.

Table 1. Ash samples used for testing and their characteristics following processing. Note that there is no coarse particle group for the Hatepe rhyolite ash type due to the smaller particle sizes of the raw field sample.

	Pupuke, Auckland Volcanic Field			Poutu, Tongariro			Hatepe, Taupo	
Time of eruption	~200,000 years BP			~11,000 - 12,000 BP			~1,770 years BP	
Ash type	Basalt			Andesite			Rhyolite	
Colour (determined from Munsell Rock Colour Chart)	N4: Medium Dark Grey			5Y 6/1: Light Olive Grey (with a small 10YR 6/6 Dark Yellowish Orange component when coarse)			5Y 8/1: Yellowish Grey	
SiO₂ content (determined by Philips PW2400 XRF analysis)	44% (mafic)			52% (intermediate)			70% (felsic)	
Dominant minerals (determined by Philips XRD analysis)	Diopside, Forsterite, Anorthite			Albite, Augite			Sanidine, Quartz	
Particle size group	<u>coarse</u>	<u>medium</u>	<u>fine</u>	<u>coarse</u>	<u>medium</u>	<u>fine</u>	<u>medium</u>	<u>fine</u>
Modal particle size (µm) (see Figure 1)	680	220	40	540	200	40	180	35
Dry bulk density (g cm⁻³)	1.1	1.5	1.1	1.3	1.2	0.9	0.9	0.7

Mafic ash such as the Pupuke samples, along with intermediate ash such as Poutu, is relatively common from eruptions globally. Eruptions of felsic ash such as Hatepe, are less common (Wicander and Monroe 2006), but the high concentration and quantity of lighter elements, high explosivity and generally high eruption columns, means that the ash can be dispersed up to hundreds of kilometers from the vent (Woo 2009).

Paint is the most common and widespread form of road marking material in most countries worldwide. In this study, Downer Group applied a Damar Bead Lock Oil Based Paint, which contains 63% solids, using a standard machine on the asphalt concrete slabs. The side of one slab was painted with a single coat 180-200 µm thick, and the other side with four coats (720-800 µm thick in total) to replicate markings that have been exposed to different abrasion or multiple paint applications. The other slab was painted with the same thickness lines but with retroreflective glass beads incorporated in the paint mix.

Fig. 1 Mean particle size distributions of samples used in experimentation and their designated classification discussed in this article (i.e. coarse, medium and fine).

2.2 Ash application and measurement

The ash delivery system used comprises of a 400 x 400 x 100 mm sieve box with an adaptable mesh base (of 1 mm, 500 μm or 125 μm aperture depending on the particle size distribution of the ash) and manual-striking hammer which causes ash to fall through when struck. The set-up has been used in previous experiments including by G. Wilson et al. (2012) and Hill (2014). The ash delivery system produces ash in a consistent and repeatable manner and is calibrated to replicate ash settling velocities and accumulation rates that would be expected from real ashfalls. The delivery system has been designed using formulas derived from Bonadonna et al. (1998) (equations 1-3) to ensure that the majority of ash particles dispensed from the sieve box reach terminal velocity well before ground level (Hill 2014):

$$V_t \approx (3.1 g \rho d / \sigma)^{1/2} \quad (1)$$

$$V_t \approx (g \rho d^2 / 18 \mu) \quad (2)$$

$$V_t \approx d (4\rho^2 g^2 / 225 \mu \sigma)^{1/3} \quad (3)$$

Where V_t is the terminal velocity, g is the acceleration due to gravity (9.81 m s^{-2}), ρ is the density of the particles, d is the particle diameter, σ is the density of the air and μ is the dynamic viscosity of the medium (Bonadonna et al. 1998, Hill 2014).

In this study, we incorporate the ash delivery system to investigate failure thresholds (i.e. when road markings become obscured by ash). Petri dishes were placed on the asphalt surface at the end of each road marking line to enable measurements of ash thickness from a flat surface (using a calliper). Ash thicknesses within asphalt aggregate pores of both average and distinctively large depth, and from the top of aggregate grains were also recorded (averaged from 5 measurements for each). Furthermore, the mass of ash collected in the petri dishes was measured at each stage in order to calculate the area density throughout experimentation. This was conducted to allow a more accurate measure of ash deposition, particularly as the thickness of ash at low accumulations is difficult to measure, and also the quantity of ash released by the delivery system experiences slight variations between ash types and as the experiment progresses and sieve mesh becomes clogged.

Fig. 2 Experimental set-up for road marking visibility testing.

2.3 Image collection

A Fuji Finepix S100 (FS) digital SLR camera was mounted on a tripod 1.5 m horizontally and 1.08 m vertically away from the slab (Figure 2), 1.08 m being the height of the driver's eye above the road in measuring stopping sight distances (Fambro et al. 1997). A digital photograph was taken at a focal length of 200 mm (under consistent camera and light conditions) and observations were noted following strikes of the ash delivery system after the ash had settled. This was conducted until five photos after the ash visually appeared to the observer to completely cover the markings. The number of strikes between each photo was varied depending how readily the ash sample passed through the sieve mesh. The mean depths of ash in the asphalt pores and on the surfaces of both the asphalt slab and petri dishes, along with the mass of petri dishes containing ash were measured and recorded in conjunction with each photo.

Other research involving road marking visibility has been conducted in the past, often involving participant drivers in simulated driving conditions (e.g. Brooks et al. 2011) or on the road at specialised road research facilities (e.g. Gibbons et al. 2004, Gibbons and Williams 2012). Specialised technical equipment has also been developed to measure the retroreflective luminance of markings (e.g. Carlson and Miles 2011). Most previous experiments have assessed the effectiveness of road markings where atmospheric conditions such as rainfall and fog present a hazard to driving. In these experiments, the distance between participants or equipment from road markings is often in the order of tens of meters. Our experimental set-up enables precise analysis of ash accumulation on the road surface and detailed measurements under controlled conditions. We investigate road markings at close range (1.5 m horizontal distance) and, due to spatial laboratory constraints, do not directly account for viewing road markings >1.5 m away. Additionally, we do not account for visibility interference due to airborne volcanic ash, which requires separate investigation. Therefore, our results for road marking coverage are

conservative, and at greater viewing distances or where the atmosphere contains ash, road marking visibility will likely be even less than portrayed.

2.4 Image analysis

Each image file was opened using Ilastik version 0.5.12 software (Sommer et al. 2011) to conduct supervised segmentation by pixel colour; one class was created for the white paint, and another class for ash or asphalt (Figure 3). After segmentation (which displayed the white paint as red, and asphalt and ash as green), Adobe Photoshop version CS6 was used for image registration, and to ensure that each image was cropped automatically without the geometry of objects changing between images. The photographs were intentionally not nadir, and the images were not orthorectified as the viewing angle and associated properties of visibility were of particular interest in the study. The mean pixel resolution was 1 pixel to 0.088 mm for the cropped area of the photographs. A fuzziness setting of 200 was selected to account for the range of colours in the ash, asphalt and line paint. This selects all pixels that are the exact same colour as the pixels clicked on, as well as all pixels that are within 200 brightness values lighter or darker. The 'histogram' function was then used to observe and record the pixel count for the white paint (red pixels). The number of pixels for the ash/asphalt was then calculated by subtracting the number for the white paint from the total pixel count. A total of 142 photographs (i.e. 284 cropped line images) were analysed with a mean of nine images analysed for each sample of specific particle size distribution and ash type.

Fig. 3 Generalised steps for the image analysis process.

3. Results and discussion

Following initial dispersal of all ash samples through the delivery system and accumulation on the slabs, the percentage of pixels representing white road marking paint was found to decrease substantially (Figure 4). This suggests that only very small ash accumulations are required for an impact on road marking visibility reduction. With further ash accumulation, the road markings continue to become obscured but at a decreasing rate. Through physical visual observations in the laboratory and comparisons with raw and analysed images (section 2.4), it was decided that when 8% white line paint or less is visible that it would be unlikely that drivers could effectively view road markings when driving. Therefore, the measurements of ash area density and depth at this threshold are of interest. It appeared particularly difficult to delineate the edges of the markings around this value, although we note that the 8% threshold is somewhat subjective and that there are few comparative studies; most others adopt instruments such as retroreflectometers which are used over several tens of meters (e.g. Dravitzki et al. 2003, Babic et al. 2014).

Fig. 4 Percentage of white road marking paint visible and ash area densities for the andesite sample with mode particle size of a) 600 μm , b) 200 μm , and c) 40 μm . The results for asphalt slabs covered by one and four coats of paint with and without retroreflective glass beads incorporated in the paint mix are shown. Also displayed are the thresholds for 8% visible road marking paint (horizontal black dashed lines). We suggest that it would be difficult for drivers to view road markings at or below this threshold.

The 8% threshold of pixels for white paint (i.e. 92% pixels for ash/asphalt) was evident through image analysis at ash area densities of between 30 g m^{-2} and 2,150 g m^{-2} for all ash samples used in experimentation (Table 2). This equates to ash depths of between trace amounts (taken to be <0.1 mm in our study) and 2.2 mm, measured from the surface of the asphalt aggregate. The large range in measurements is largely due to the influence of particle size, but also ash type and road paint characteristics to some degree (sections 3.1 – 3.3).

Our findings correspond well with the ash characteristics and observations of road marking coverage at Sakurajima volcano in Kyushu, Japan. In June 2015, the Kagoshima City Office reported that area densities were currently $\sim 300\text{-}400 \text{ g m}^{-2}$ when road markings could not be seen and cleaning was required

(Kagoshima City Office, personal communication, June 08 2015). The ash is typically of andesitic type, typically with a SiO₂ content of ~59%, and mode particle sizes of 150-200 μm at this distance (4-5 km) for recent eruptions from the Showa crater (Yamanoi et al. 2008, Matsumoto et al. 2013, Nanayama et al. 2013, Miwa et al. 2015). Our summarised results (Table 2) suggest that ash depths on the roads, measured from the surface of the asphalt aggregate, would have been approximately 0.5 mm at the time.

Table 2. Measurements of ash area density and depths when it would be difficult for drivers to see road markings (i.e. when 8% white line marking paint was visible), determined through image analysis for all of the ash samples tested. The range of values is largely due to differences in paint thickness (i.e. number of coats) and retroreflective bead content of the paint (see section 3.3), as well as unavoidable but natural variations in surface texture across the asphalt slabs.

		ASH TYPE		
		Basalt	Andesite	Rhyolite
MODE PARTICLE SIZE DISTRIBUTION	Coarse (600 – 700 μm)	Area density: 1350 – 2150 g m ⁻² Depth on surface: 1.0 – 2.2 mm Depth in voids: 3.3 – 7.5 mm	Area density: 1050 – 2100 g m ⁻² Depth on surface: 1.0 – 1.4 mm Depth in voids: 3.2 – 7.5 mm	(No data as sample not possible at this particle size)
	Intermediate (200 – 260 μm)	Area density: 240 – 450 g m ⁻² Depth on surface: 0.3 – 0.8 mm Depth in voids: 0.9 – 1.5 mm	Area density: 80 – 350 g m ⁻² Depth on surface: 0.2 – 0.5 mm Depth in voids: 0.4 – 1.5 mm	Area density: 40 – 180 g m ⁻² Depth on surface: 0.2 – 0.4 mm Depth in voids: 0.2 – 0.7 mm
	Fine (35 – 45 μm)	Area density: 45 – 80 g m ⁻² Depth on surface: trace – 0.1 mm Depth in voids: trace – 0.1 mm	Area density: 35 – 80 g m ⁻² Depth on surface: trace – 0.1 mm Depth in voids: trace – 0.1 mm	Area density: 30 – 65 g m ⁻² Depth on surface: trace – 0.1 mm Depth in voids: trace – 0.1 mm

We highlight the importance of outlining the specifics for depth type measured on road surfaces for ash accumulations less than ~10 mm. Depths within the asphalt aggregate voids were found to be over five times greater than those measured from the surface of the aggregate in some cases (e.g. for the coarse andesite, ash depths within voids were ~7.5 mm when surface depths were ~1.4 mm).

3.1 Road marking type

The thickness of surface paint appears to have some influence on road marking coverage. Figure 4 illustrates that the lines with four coats of paint generally become covered more easily than a single

1 coated line. This is intuitive because the greater quantity of paint acts to reduce the macrotexture of the
2 asphalt surface, causing the voids to fill sooner with the same mass of ash.

3 The markings of paint that incorporate retroreflective glass beads in the mix are generally more easily
4 obscured. This is perhaps due to the retroreflective beads adding to the overall volume of paint, thus
5 reducing the macrotextural depth of the asphalt voids. The rougher microtexture may cause more ash to
6 remain on the surface than for road markings without beads (caused by retroreflective beads 'trapping'
7 individual ash particles as they fall). Crystalline ash particles will also act to reflect light, potentially
8 reducing the effectiveness of the added retroreflective beads. Therefore, although retroreflective beads
9 are added to paint with the overall intention of improving road safety, they act to reduce the visibility of
10 road markings when volcanic ash accumulates, reducing road safety in such environments.

11
12 The ranges of ash area densities and ash depths shown in Table 2 are mainly due to the variations in road
13 marking characteristics. Generally, the higher values reflect conditions where there is less paint and/or
14 where the paint mix does not contain retroreflective beads, and the lower values in the table correspond
15 to road markings formed of multiple paint layers (with little wear) and/or where the paint incorporates
16 retroreflective beads.

17 18 19 **3.2 Ash particle size**

20
21 It is evident that road marking coverage is highly dependent on the particle size distribution of volcanic
22 ash falling on textured road surfaces such as SMA. Ash depth measurements in petri dishes and on
23 different locations of the asphalt surfaces, and through visual observations when the ash was falling,
24 revealed that this is largely due to the behaviour of individual particles upon impact (Figure 5).

25
26 A mass of fine ash particles is more effective at covering road markings than the same mass of coarse
27 particles. This is largely because coarser particles bounce into the macrotextural voids of the asphalt
28 aggregate and initially accumulate in these spaces, with white road marking paint on the upper asphalt
29 surface remaining uncovered and visible to drivers. Even as the ash in the void spaces accumulates to the
30 upper surface of the asphalt, ash particles settling on the surface of the aggregate have a tendency to be
31 displaced by further ash that falls and collect in areas immediately above the voids where the thicker
32 existing ash limits movement. This results in very small mounds of ash immediately above the voids (with
33 white line paint still visible in-between) before ash spreads across the entire surface of the asphalt.

34
35 Fine ash particles pack more densely wherever they settle, causing the surface to be easily covered. This
36 process is observed on the asphalt and on the flat surfaces of our petri dish bases. It has also recently
37 been attributed to the vulnerability of horizontally placed photovoltaic modules and power-output
38 reduction (Zorn and Walter 2016). Furthermore, the fine ash particles appear to exhibit electrostatic
39 properties and adhere more readily to the asphalt surface, successfully covering the line-covered
40 aggregate at various orientations. Ash with finer particle size distributions, and sometimes more
41 triboelectrically charged particles (Aplin et al. 2014) are relatively common in distal volcanic plumes.
42 Therefore, our findings indicate that road marking coverage, especially in distal locations from volcanic
43 vents, should not be overlooked.

44
45
46
47 *Fig. 5 The process of ash accumulation on textured road surfaces showing the difference between ash
48 containing predominantly fine and coarse particles.*

49 50 51 **3.3 Ash type and contrast**

52
53 Although the mean dry bulk densities for the light-coloured ash were less than those of the darker
54 material, less ash is required at intermediate and coarse particle sizes to cover the same percentage of
55 road markings. For example, at intermediate particle sizes (i.e. 200-260 μm modal distributions), 8% of
56 line paint is visible at mean asphalt surface accumulations of 0.55 mm for the basalt (dark-coloured), 0.35
57 mm for the andesite (mid-coloured), and 0.30 mm for the rhyolite (light-coloured) (Figure 6). This
58 suggests that white road markings covered by light-coloured deposits such as the rhyolite may become
59 obscured at smaller depths than dark-coloured deposits such as the basalt. Although the same trend is
60
61
62
63
64
65

1 suspected for fine ash particle sizes, it is not verified here due to the very small accumulations it took for
2 surfaces to be covered (≤ 0.1 mm) and difficulties in measuring and estimating ash depths.

3 Some of the difference between ash colour types may be due to errors in the image analysis process
4 whereby the ash and markings are more difficult to classify when the ash is of lighter colour. However,
5 the image analysis findings correspond with the visual observations recorded during experimentation in
6 that it was more difficult to distinguish road markings when covered by light-coloured ash compared to
7 the same depths of dark-coloured ash. The findings also align with the mere definition of visual contrast
8 (i.e. the difference in colour or brightness between objects that makes them distinguishable). With light-
9 coloured ash covering the dark asphalt either side of white road markings; the markings will be less
10 distinguishable. We also note that contrast requirements are greater the farther the object is from the
11 driver (Gibbons et al. 2004). Therefore a driver's ability to see road markings with distance may be less
12 for light-coloured than dark-coloured ash.

13
14
15 **Fig. 6** Road markings painted on a SMA slab as one coat (left lines) and four coats (right lines), both
16 containing no retroreflective beads in the paint mix. a) shows the markings with no volcanic ash on the
17 surface. b), c) and d) show when $\leq 8\%$ of line paint is visible (i.e. when it would be difficult for drivers to see
18 the lines) for basaltic, andesitic and rhyolitic ash of 200-260 μm modal particle size distributions
19 respectively. This corresponds to mean thicknesses on the surface of the asphalt aggregate of 0.55 mm for
20 the basalt, 0.35 mm for the andesite, and 0.30 mm for the rhyolite.
21
22
23
24

25 4. Conclusion

26
27 Our experimental findings demonstrate that very low levels of volcanic ash accumulation can cause
28 substantial road marking coverage. If ash particles are predominantly fine (i.e. mode particle sizes ≤ 45
29 μm), then road markings may become obscured for drivers when ash area densities are between 30 and
30 80 g m^{-2} . This is equivalent to ≤ 0.1 mm of ash accumulation on the surface of the asphalt.
31

32 Ash particle size distribution is likely the most important characteristic for road marking coverage at
33 small depths and a mass of fine particles is much more effective at covering a surface than the same mass
34 of coarse particles. This is largely attributed to the ash particle behaviour upon initial impact, with coarse
35 particles bouncing into voids between the asphalt aggregate and fine particles generally settling where
36 they initially land. For coarse (i.e. mode particle sizes $\geq 600 \mu\text{m}$) ash, depths ≥ 1.0 mm, measured from the
37 surface of the aggregate, or ≥ 3.2 mm, measured within the asphalt voids, lead to road marking coverage.
38 This represents ash area densities at least 13 times greater than for fine ash of the same type.
39 These thresholds assume dry and near-pristine atmospheric conditions (i.e. no airborne ash) and further
40 work is required to determine the extent of visual range impairment by suspended ash particles.
41
42

43 Road markings covered by light-coloured ash of the same thickness as dark-coloured ash are more
44 difficult to distinguish (due to low contrast). Multiple paint layers (assuming little wear) and paint mix
45 that incorporates retroreflective glass beads also make markings more difficult to distinguish when
46 covered by ash. Although crucial to consider on all road networks that include line painted surfaces in
47 volcanically active regions, our findings especially highlight the susceptibility of road markings being
48 covered in distal areas from the vent.
49

50 We recommend thresholds for when road cleaning should occur on asphalt surfaces in order to maintain
51 road safety and network functionality. Note that the values assume 'worse-case conditions' for volcanic
52 ash coverage in terms of paint characteristics:
53

- 54 • For fine ($\sim 30 - 45 \mu\text{m}$ mode particle size) ash of all types and felsic ash such as rhyolite up to a
55 size dominated by $\sim 300 \mu\text{m}$ particles, road cleaning should be conducted at or before ash area
56 densities of $30 - 45 \text{ g m}^{-2}$. Depths will be extremely difficult to measure at such accumulations but
57 will likely be around $0.1 - 0.2$ mm from the surface of the upper aggregate.
58
59
60
61
62
63
64
65

- For intermediate size (up to $\sim 300 \mu\text{m}$ mode particle size) andesite, road cleaning should be conducted at ash area densities of $\sim 100 \text{ g m}^{-2}$. For mafic ash such as basalt of the same size, it should be conducted at $\sim 250 \text{ g m}^{-2}$. Surface depths will be around 0.2 – 1.0 mm at this stage.
- For coarse (mode particle sizes up to $\sim 800 \mu\text{m}$) andesite and basalt, road cleaning should occur at ash area densities of $\sim 1,000$ and $1,500 \text{ g m}^{-2}$ respectively, which is equivalent to surface depths of approximately 1.0 – 2.5 mm.

Due to road safety considerations in environments when there is no volcanic ash, it seems counterintuitive to suggest changes to road marking paint mix properties such as changes in retroreflective glass bead concentrations or design, so that visibility of road markings is maintained at a higher standard solely during ashy conditions. Therefore, we do not suggest that any major changes to physical road marking properties should be made in areas prone to volcanic ashfall. Applying new coats of paint should only be conducted if existing paint is sufficiently worn and if it is required to improve road safety in normal conditions. This is because thicker paint can lead to road markings becoming more easily obscured by ash. Changes to the physical structure of the road surface itself, such as the application of an aerodynamic profile to promote particle removal from the carriageway by wind-driven saltation (as achieved in Kuwait (Aljassar et al. 2006)), may be cost-effective in some regions frequently affected by volcanic ash. However, perhaps the simplest technique to improve road safety in all areas when road markings become covered is for all drivers to travel at a reduced speed, or to avoid driving until the ash is cleared.

Acknowledgements

We thank the University of Canterbury Mason Trust scheme, New Zealand Earthquake Commission (EQC) and Determining Volcanic Risk in Auckland (DEVORA) project for their financial support towards the study through the provision of funding for authors Daniel Blake and Thomas Wilson. We also express thanks for the support towards laboratory assistance and equipment provided by several people, whose help was vital to the success of this study. In particular we wish to thank Janet Jackson and Howard Jamison of Downer Group for coordinating the painting of the asphalt concrete slabs, and Kerry Swanson, Matt Cockcroft, Chris Grimshaw, Stephen Brown, Alec Wild, Connor Jones and Brigitt White for their assistance with sample preparation and conducting experiments at the University of Canterbury's Volcanic Ash Testing Lab. Daniel Blake would also like to thank his PhD co-supervisors, Jim Cole (University of Canterbury), Jan Lindsay (The University of Auckland) and Natalia Deligne (GNS Science) for their edits, guidance and support throughout the project.

References

- ADOT (2011) Dusty roads. Arizona Department of Transportation Blog. <http://www.azdot.gov/media/blog/posts/2011/04/18/dusty-roads> Accessed 13/10/2015.
- Aljassar, A.H. Al-Kulaib, A. Ghoneim, A.N. Metwali, E-S. (2006) A cost effective solution to the problem of sand accumulation on a desert road in Kuwait. Third Gulf Conference on Roads, March 6-8, 2006. www.dr.aljassar.net/text/t0026.doc Accessed 13/10/2015.
- Aplin, K. Houghton, I. Nicoll, K. Humphries, M. Tong, A. (2014) Electrical charging of volcanic ash. Proceedings ESA Annual Meeting on Electrostatics. http://www.electrostatics.org/images/ESA_2014_G_Aplin_et_al.pdf Accessed 20/01/2016.
- Babic, D. Fiolic, M. Prusa, P. (2014) Evaluation of road markings retroreflection measuring methods. European Scientific Journal, 3, pp.105-114.
- Barnard, S.T. (2009) The vulnerability of New Zealand lifelines infrastructure to ashfall. Doctor of Philosophy Thesis, Department of Geological Sciences, University of Canterbury, Christchurch, New Zealand.

1 Becker, J. Smith, R. Johnston, D. Munro, A. (2001) Effects of the 1995-1996 Ruapehu eruptions on
2 communities in central North Island, New Zealand, and people's perceptions of volcanic hazards after the
3 event. *The Australasian Journal of Disaster and Trauma Studies*, 2001-1.

4
5 Carlson, P. Miles, J. (2011) Nighttime visibility of in-service pavement markings, pavement markers, and
6 guardrail delineation in Alaska (with and without continuous lighting). Alaska Department of
7 Transportation, Statewide Research Office, Juneau, Alaska.
8 http://www.dot.state.ak.us/stwddes/research/assets/pdf/fhwa_ak_rd_11_04.pdf Accessed 26/09/2015.
9

10 Carnaby, B. (2005) Road marking is road safety. Conference paper by Potters Asia Pacific, presented at
11 the New Zealand Roadmarkers Federation Conference 2005, Christchurch, New Zealand.

12
13 Cole, J.W. Sabel, C.E. Blumenthal, E. Finnis, K. Dantas, A. Barnard, B. Johnston, D.M. (2005) GIS-based
14 emergency and evacuation planning for volcanic hazards in New Zealand. *Bulletin of the New Zealand
15 Society for Earthquake Engineering*, 38:2, pp.149-164.

16
17 Dravitzki, V.K. Wood, C.W.B. Laing, J.N. Potter, S. (2003) Guidelines for performance of New Zealand
18 markings, Opus Central Laboratories Report 03-527605,
19 [http://www.nzta.govt.nz/assets/resources/guidelines-for-performance-of-nz-road-
20 markings/docs/guidelines-for-performance-of-nz-road-markings.pdf](http://www.nzta.govt.nz/assets/resources/guidelines-for-performance-of-nz-road-markings/docs/guidelines-for-performance-of-nz-road-markings.pdf) Accessed 25/01/2016.
21

22 Durand, M. Gordon, K. Johnston, D. Lorden, R. Poirot, T. Scott, J. Shephard, B. (2001) Impacts and
23 responses to ashfall in Kagoshima from Sakurajima Volcano – lessons for New Zealand. *GNS Science
24 Report 2001/30*, 53 p.

25
26 Fambro, D.B. Fitzpatrick, K. Rodger, J.K. (1997) Determination of stopping sight distances. National
27 Cooperative Highway Research Program Report 400, Transportation Research Board National Research
28 Council, Washington D.C.

29
30 Gibbons, R.B. Hankey, J. Pashaj, I. (2004) Wet night visibility of pavement markings: executive summary.
31 Virginia Tech Transportation Institute, Virginia Polytechnic Institute and State University, Charlottesville,
32 Virginia. <https://vtechworks.lib.vt.edu/bitstream/handle/10919/46697/05-cr4.pdf?sequence=1>
33 Accessed 26/09/2015.
34

35
36 Gibbons, R.B. Williams, B.M. (2012) Assessment of the durability of wet night visible pavement markings:
37 wet visibility project phase IV. Virginia Centre for Transportation Innovation and Research,
38 Charlottesville, Virginia. http://www.virginiadot.org/vtrc/main/online_reports/pdf/12-r13.pdf Accessed
39 26/09/2015.
40

41 Hill, D.J. (2014) Filtering out the ash: mitigating volcanic ash ingestion for generator sets. Master of
42 Science Thesis, Department of Geological Sciences, University of Canterbury, Christchurch, New Zealand.

43
44 Jenkins, S.F. Wilson, T.M. Magill, C.R. Miller, V. Stewart, C. Marzocchi, W. Boulton, M. (2014) Volcanic ash
45 fall hazard and risk: technical background paper for the UN-ISDR 2015 Global Assessment Report on
46 Disaster Risk Reduction. Global Volcano Model and IAVCEI. www.preventionweb.net/english/hyogo/gar
47 Accessed 08/01/2016.
48

49 Leonard, G.S. Johnston, D.M. Williams, S. Cole, J.W. Finnis, K. Barnard, S. (2005) Impacts and management
50 of recent volcanic eruptions in Ecuador: lessons for New Zealand. *GNS Science Report 2005/20*, 52 p.

51
52 Loughlin, S.C. Sparks, R.S.J. Brown, S.K. Jenkins, S.F. Vye-Brown C. (2015) *Global Volcanic Hazards and
53 Risk*, Cambridge University Press, UK.

54
55 Matsumoto, A. Nakagawa, M. Amma-Miyasaka, Iguchi, M. (2013) Temporal variations of the petrological
56 features of the juvenile materials during 2006 to 2010 from Showa crater, Sakurajima volcano, Kyushu,
57 Japan. *Bulletin of Volcanology*, 58:1, pp.191-212.
58
59
60
61
62
63
64
65

1 Miwa, T. Shimano, T. Nishimura, T. (2015) Characterization of the luminance and shape of ash particles at
2 Sakurajima volcano, Japan, using CCD camera images. *Bulletin of Volcanology*, 77:5, 13p.

3 Magill, C. Wilson, T. Okada, T. (2013) Observations of tephra fall impacts from the 2011 Shinmoedake
4 eruption, Japan. *Earth Planets Space*, 65, pp.677-698.

5
6 Nanayama, F. Furukawa, R. Ishizuka, Y. Yamamoto, T. Geshi, N. Oishi, M. (2013) Characterization of fine
7 volcanic ash from explosive eruption from Sakurajima volcano, South Japan, American Geophysical Union
8 Fall Meeting 2013, December 2013.

9
10 Sommer, C. Strähle, C. Köthe, U. Hamprecht, F.A. (2011) Ilastik: interactive learning and segmentation
11 toolkit. BibTex file, Technical Report, In: Eighth IEEE International Symposium on Biomedical Imaging
12 Proceedings, pp.230-233.

13
14 USGS (2013) Volcanic ash: effects and mitigation strategies. United States Geological Survey
15 <http://volcanoes.usgs.gov/ash/trans/> Accessed 21/09/2015.

16
17 Wilson, T.M. Cole, J.W. Stewart, C. Cronin, S.J. Johnston, D.J. (2011) Ash storms: impacts of wind-
18 remobilised volcanic ash on rural communities and agriculture following the 1991 Hudson eruption,
19 southern Patagonia, Chile. *Bulletin of Volcanology*, 73, pp.223-239.

20
21 Wilson, G. Wilson, T. Cole, J. Oze, C. (2012) Vulnerability of laptop computers to volcanic ash and gas.
22 *Natural Hazards*, 63:2, pp.711-736.

23
24 Wilson, T.M. Stewart, C. Sword-Daniels, V. Leonard, G.S. Johnston, D.J. Cole, J.W. Wardman, J. Wilson, G.
25 Barnard, S.T. (2012) Volcanic ash impacts on critical infrastructure. *Physics and Chemistry of the Earth*,
26 45-46, pp.5-23.

27
28 Wolshon, B. (2009) *Transportation's role in emergency evacuation and re-entry: a synthesis of highway*
29 *practice*. National Cooperative Highway Research Program, Transportation Research Board Synthesis
30 392, Washington D.C.

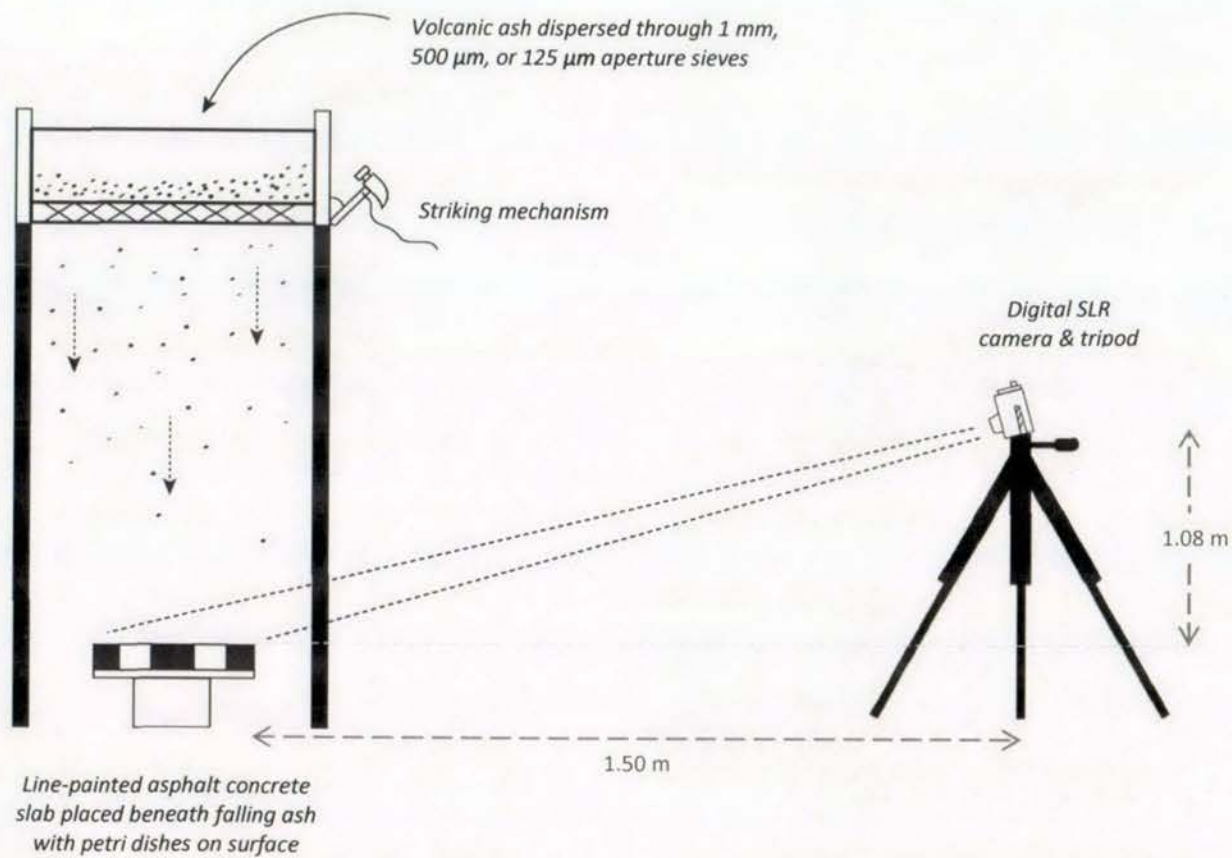
31
32 Wicander, R. Monroe, J. (2006) *Essentials of Geology: fourth edition*. Thomson Brooks/Cole, United States
33 of America.

34
35 Woo, G. (2009) *A new era of volcano risk management: RMS special report*. Risk Management Solutions,
36 Inc. London, UK.

37
38 Yamanoi, Y. Takeuchi, S. Okumura, S. Nakashima, S. Yokoyama, T. (2008) Color measurements of volcanic
39 ash deposits from three different styles of summit activity at Sakurajima volcano, Japan: conduit
40 processes recorded in color of volcanic ash. *Journal of Volcanology and Geothermal Research*, 178, pp.81-
41 93.

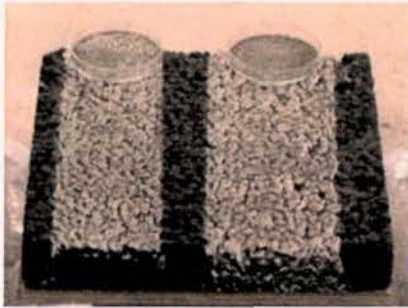
42
43 Zorn, E. Walter, T.R. (2016) Influence of volcanic tephra on photovoltaic (PV)-modules: an experimental
44 study with application to the 2010 Eyjafjallajökull eruption, Iceland. *Journal of Applied Volcanology*, 5:2,
45 pp.1-14.

46
47
48
49
50
51
52
53
54
55
56
57
58
59
60
61
62
63
64
65



1. Photography

Image of ash-covered slab taken



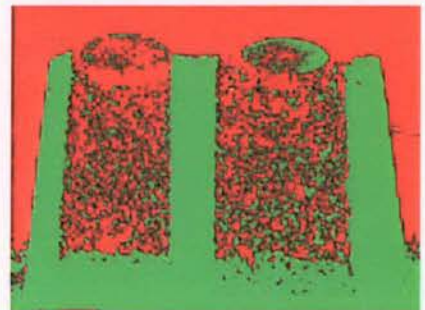
2. Classification

*One class for white paint
One class for ash and asphalt*



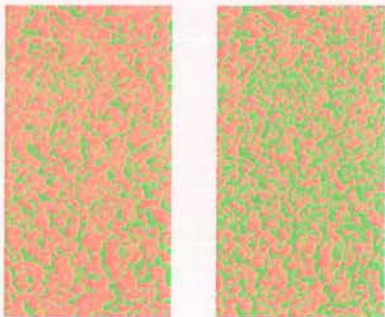
3. Pixel segmentation

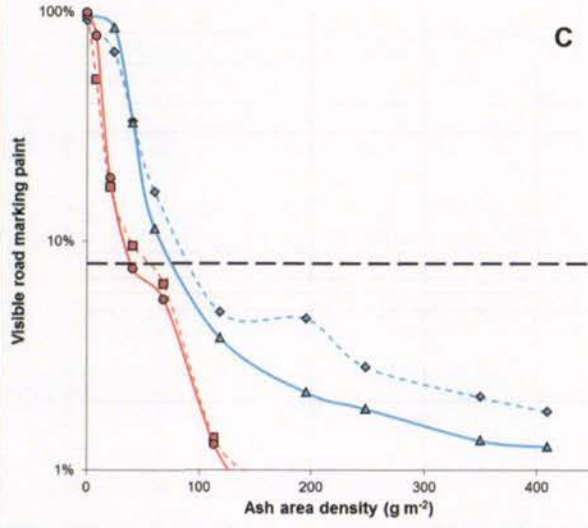
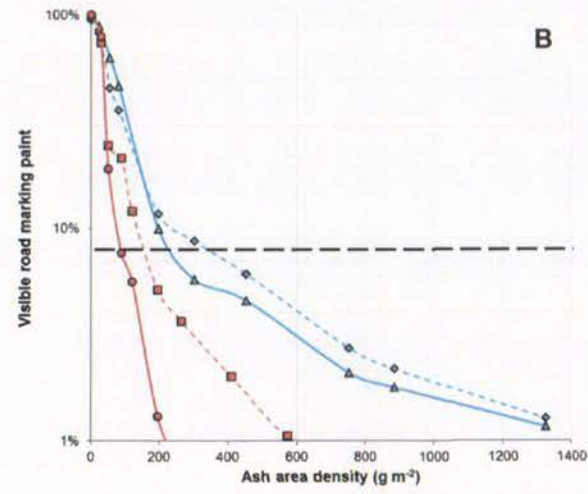
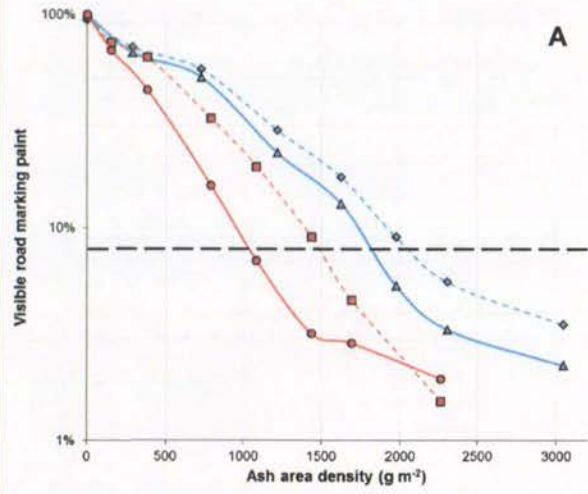
*Red pixels = white paint
Green pixels = ash / asphalt*



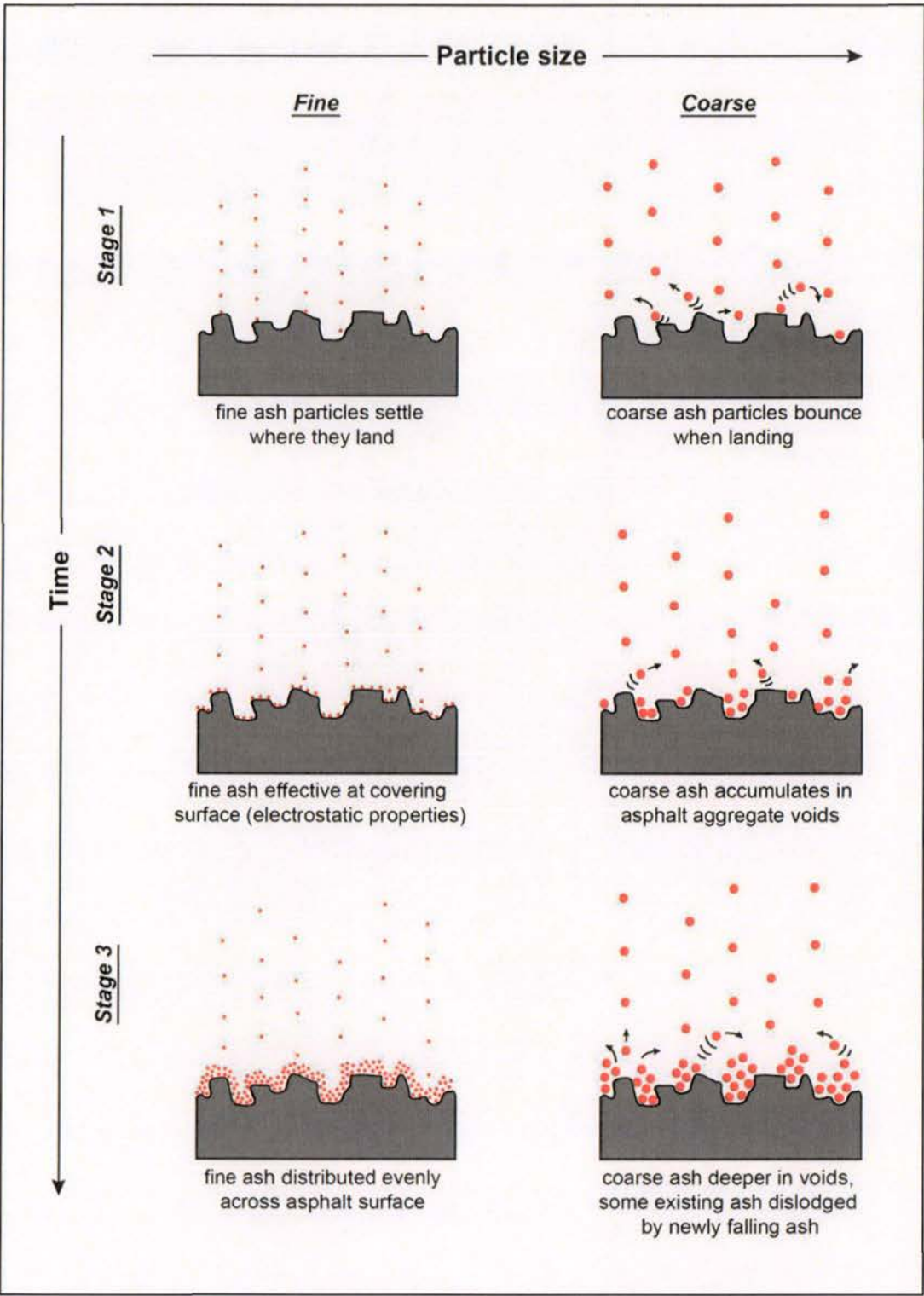
4. Image processing

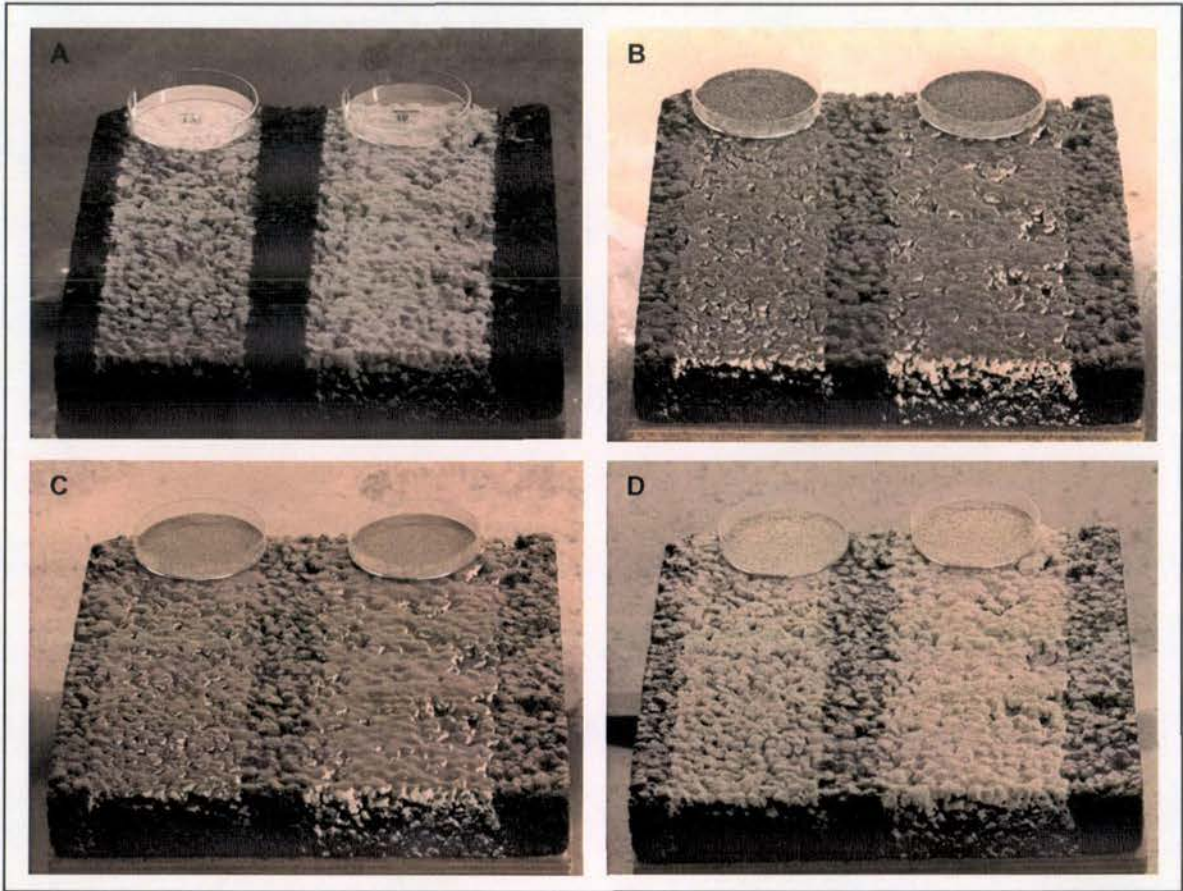
*Fuzziness value selected
Percentage cover calculation*





- ◇— No retroreflective beads (1 coat)
- △— No retroreflective beads (4 coats)
- - -□- - - With retroreflective beads (1 coat)
- With retroreflective beads (4 coats)





Article

Impact of Volcanic Ash on Road and Airfield Surface Skid Resistance

Daniel M. Blake ^{1,*}, Thomas M. Wilson ¹, Jim W. Cole ¹, Natalia I. Deligne ² and Jan M. Lindsay ³

¹ Department of Geological Sciences, University of Canterbury, Private Bag 4800, Christchurch 8041, New Zealand; thomas.wilson@canterbury.ac.nz (T.M.W.); jim.cole@canterbury.ac.nz (J.W.C.)

² GNS Science, 1 Fairway Drive, Avalon 5010, P.O. Box 30-368, Lower Hutt 5040, New Zealand; n.deligne@gns.cri.nz

³ School of Environment, The University of Auckland, Private Bag 92019, Auckland 1142, New Zealand; j.lindsay@auckland.ac.nz

* Correspondence: daniel.blake@pg.canterbury.ac.nz; Tel.: +64-21-050-1450

Received: 14 July 2017; Accepted: 31 July 2017; Published: 6 August 2017

Abstract: Volcanic ash deposited on paved surfaces during volcanic eruptions often compromises skid resistance, which is a major component of safety. We adopt the British pendulum test method in laboratory conditions to investigate the skid resistance of road asphalt and airfield concrete surfaces covered by volcanic ash sourced from various locations in New Zealand. Controlled variations in ash characteristics include type, depth, wetness, particle size and soluble components. We use Stone Mastic Asphalt (SMA) for most road surface experiments but also test porous asphalt, line-painted road surfaces, and a roller screed concrete mix used for airfields. Due to their importance for skid resistance, SMA surface macrotexture and microtexture are analysed with semi-quantitative image analysis, microscopy and a standardised sand patch volumetric test, which enables determination of the relative effectiveness of different cleaning techniques. We find that SMA surfaces covered by thin deposits (~1 mm) of ash result in skid resistance values slightly lower than those observed on wet uncontaminated surfaces. At these depths, a higher relative soluble content for low-crystalline ash and a coarser particle size results in lower skid resistance. Skid resistance results for relatively thicker deposits (3–5 mm) of non-vesiculated basaltic ash are similar to those for thin deposits. There are similarities between road asphalt and airfield concrete, although there is little difference in skid resistance between bare airfield surfaces and airfield surfaces covered by 1 mm of ash. Based on our findings, we provide recommendations for maintaining road safety and effective cleaning techniques in volcanic ash environments.

Keywords: volcanic ash; asphalt; concrete; runway; highway; traction; British Pendulum Tester; safety

1. Introduction

1.1. Background

Functional transport networks are critical for society both under normal operating conditions and in emergencies. During volcanic eruptions, transport networks may be required for the evacuation of residents, to allow sufficient access for emergency services or military personnel to enter affected areas and for regular societal activities. Once direct threats have subsided, transport networks are crucial for both immediate and long-term recovery, including the clean-up and disposal of material, and restoration of services and commerce. It is thus imperative that effective and realistic transport management strategies are incorporated into volcanic contingency planning in areas where society

and infrastructure are at risk (e.g., Auckland, New Zealand; Kagoshima, Japan; Mexico City, Mexico; Naples, Italy; Yogyakarta, Indonesia).

Volcanic eruptions produce many hazards. Damage to transport from proximal hazards such as lava flows, pyroclastic density currents and lahars is often severe, leaving ground routes impassable and facilities such as airports closed or inoperable. Volcanic ash (ejected material with particle sizes <2 mm in diameter) is widely dispersed and, although not necessarily damaging to static transport infrastructure, is generally the most disruptive of all volcanic hazards [1,2]. Even relatively small eruptions are capable of widespread disruption on ground transport and aviation, which may continue for months due to the remobilisation and secondary deposition of ash by wind, traffic or other human activities, even after an eruption has subsided.

To date studies on the impacts of volcanic hazards to society have focussed on the effects of ash [2–13]. These studies and reports suggest four frequently occurring types of volcanic ash impacts on surface transport:

1. Reduction of skid resistance on roads and runways covered by volcanic ash
2. Coverage of road and airfield markings by ash
3. Reduction in visibility during initial ashfall and any ash re-suspension
4. Blockage of engine air intake filters which can lead to engine failure.

Despite much anecdotal evidence, detailed work to quantify the impact of ash on surface transport including roads and airfields is in its infancy [12,14]. Quantitative, empirical evidence can inform management strategies in syn-eruptive and post-ashfall environments such as evacuation planning, safe travel advice in the recovery phase and recommended clean-up operations.

Most studies of exposed critical infrastructure have generally focussed on very large eruptions and ashfall deposits >10 mm thick, rarely reporting the effects from ashfall <10 mm thick [10]. This presents a source of uncertainty for emergency management planning and loss assessment models, which is important, as thin deposits are more frequent and often cover larger areas [15]. Some notable eruptions that have led to reported reduced skid resistance on roads in the past are highlighted in Table 1. It has been suggested that impacts start at ~2–3 mm ash thickness [2], although there have been few studies that have quantified such impacts in detail. Indeed, the limited quantitative data available from historic observations generally relates impacts to approximate depths of ash, which may not be the best metric: ash characteristics such as particle size, ash type, degree of soluble components and wetness, may influence or even control the level of skid resistance. We investigate the importance of these alternative characteristics in this paper.

Here, we present experimental methods and results from the University of Canterbury's Volcanic Ash Testing Laboratory (VAT Lab) on the reduction of skid resistance on surfaces covered by volcanic ash. We test the skid resistance on road and airfield surfaces using the British Pendulum Tester (BPT), a standard instrument used by road engineers for surface friction testing since its development in the 1950s [16], and still used in many countries, particularly at problematic road sites. Despite the widespread and frequent use of the BPT by road engineers, we are unaware of other studies that have utilised the instrument on ash-covered surfaces. We note that other instruments are available to measure skid resistance on paved surfaces, including the Dynamic Friction Tester, GripTester, Sideways force Coefficient Routine Investigation Machine (SCRIM) and the Road Analyser and Recorder (ROAR) [16]. However, after an assessment of the literature, we decided that these would not be suitable for this study due to likely complications associated with testing surfaces covered in loose ash material by machines with fast-moving components, difficulties in obtaining enough volcanic ash to cover necessary travel paths, and/or potential damage to expensive components.

Table 1. Historical reports of reduced skid resistance following volcanic eruptions. There may be other instances described as ‘general impacts to transportation’ or which have not been recorded in the literature.

Volcano and Country	Year	Ash Thickness (mm)	Observations Related to Skid Resistance
St Helens, United States of America	1980	17	Ash became slick when wet [17–19]
Hudson, Chile	1991	not specified	Traction problems from ash on road [7,20]
Tavurvur and Vulcan, Papua New Guinea	1994	1000	Vehicles sunk and stuck in deep ash, although passable if hardened [21–23]
Sakurajima, Japan	1995	>1	Roads slippery [22,24]
Ruapehu, New Zealand	1995–1996	“thin”	Slippery sludge from ash-rain mix (roads closed) [22,25]
Soufrière Hills, United Kingdom (overseas territory)	1997	not specified	Rain can turn particles into a slurry of slippery mud [26]
Etna, Italy	2002	2–20	Traction problems, although damp and compacted ash easier to drive on [22]
Reventador, Ecuador	2002	2–5	Vehicles banned due to slippery surfaces [22,27]
Chaitén, Chile	2008	not specified	Reduced traction caused dam access problems [28,29]
Merapi, Indonesia	2010	not specified	Slippery roads caused accidents and increased journey times [30]
Pacaya, Guatemala	2010	20–30	Slippery roads with coarse ash [9]
Puyehue-Cordón Caulle, Chile	2011	>100	2WDs experienced traction problems (wet conditions) [31]
Shinmoedake, Japan	2011	not specified	Ladders very slippery [32]
Kelud, Indonesia	2014	1–100	Roads slippery with increased accident rate [33]
Sinabung, Indonesia	2014	80–100	Road travel impracticable in wet muddy ash [34]

1.2. Skid Resistance

Skid resistance (i.e., the force developed when a tyre that is prevented from rotating slides along a pavement surface [35]) is a fundamental component of road safety and should be managed so that it is adequate to enable safe operation [36]. Skid resistance is also essential for airfields to enable sufficient acceleration, deceleration and change in direction of aircraft on the surface [37]. It has become particularly important since the advent of turbojet aircraft with their greater weight and high landing speeds [38,39]. Skid resistance is essentially a measure of the Coefficient of Friction (CoF) obtained under standardised conditions in which the many variables are controlled so that the effects of surface characteristics can be isolated [40].

Skid resistance of surfaces changes over time, typically increasing in the first two years following pavement construction for roads due to the wearing by traffic, and rough aggregate surfaces becoming exposed, then decreasing over the remaining pavement life as aggregates become polished [41].

1.2.1. Surface Macrotexture and Microtexture

Surface friction is primarily a result of the macrotexture and microtexture of road and airfield pavements; these are thus intrinsically linked to skid resistance. As defined by the World Road Association-PIARC in 1987 [42]:

- Macrotexture defines the amplitude of pavement surface deviations with wavelengths from 0.5 to 50 mm.
- Microtexture is the amplitude of pavement surface deviations from the plane with wavelengths less than or equal to 0.5 mm, measured at the micron scale [43].

Microtexture, a property of each individual aggregate chip, contributes in particular to skid resistance for vehicles at low speed (i.e., the tyre rubber locally bonds to the surface through adhesion). Microtexture varies from harsh to polished. When a pavement is newly constructed, microtexture is particularly rough; however, once in service, microtexture changes due to the effects of traffic and weather conditions [43]. Macrotexture, the coarse texture of pavement surface aggregates, helps to reduce the potential for aquaplaning and provides skid resistance at high speeds through the effect of hysteresis (caused by the surface projections deforming the tyre) [36,40]. Typically, if the surface binder and aggregate chips have been appropriately applied, macrotexture levels should very gradually and linearly decrease over time as the aggregate surface slowly abrades [16].

1.2.2. Road Skid Resistance

The minimum recommended values of skid resistance and calculated corresponding CoFs for different sites on road networks that are measured with the BPT under typical wet conditions are shown in Table 2 and are reported in various literature sources internationally [41,44,45].

Table 2. Minimum recommended Skid Resistance Values for different road network sites, under wet conditions and measured using the British Pendulum Tester [41,44,45].

Type of Site	Minimum Recommended Skid Resistance Value	Corresponding Coefficient of Friction
Difficult sites such as:		
(a) Roundabouts	65.0	0.74
(b) Bends with radius less than 150 m on unrestricted roads		
(c) Gradients, 1 in 20 or steeper, of lengths >100 m		
(d) Approaches to traffic lights on unrestricted roads		
Motorways and heavily trafficked roads in urban areas (with >2000 vehicles per day)	55.0	0.60
All other sites	45.0	0.47

Rain, snow and ice are common hazards that compromise the quality of road surfaces [46–48] by interfering with surface macrotexture and microtexture. In 2003, Bennis and De Wit quantified how surface friction varies with time during a short rain shower following a reasonable period of no rain (Figure 1) [49]. The measured skid resistance significantly reduces immediately after rainfall and then recovers to a more typical wet skid resistance. However, the effect of individual contaminants, such as vehicle residues and atmospheric dust, on surface friction is poorly understood [16].

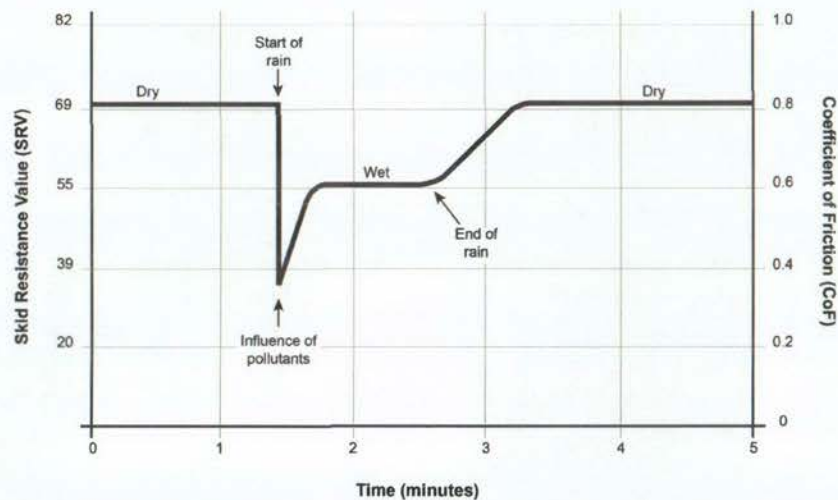


Figure 1. Variation in Coefficient of Friction (CoF) during a rain event [16,49–51].

Many studies have focused on snow- and rain-related crashes in northern states of the U.S. [52–55]. We propose that parallels may be drawn between such hazards and the hazard presented by ashfall on roads. Following a review of the literature, Aström and Wallman (2001) summarise typical CoFs for different road conditions (Table 3) [56]. The effect of hazards such as ice and snow can be substantial with most skid resistance values under such conditions falling below the minimum recommended levels (Table 2). Skid resistance is very limited under black ice conditions.

Table 3. Skid Resistance Values (SRVs) and calculated corresponding CoFs for different road conditions (adapted from [56]). The two measures of friction are related by the Equation: $CoF = (3 \times SRV) / (330 - SRV)$ [57].

Type of Site	Typical Skid Resistance Value	Corresponding Coefficient of Friction
Dry, bare surface	69.5–82.5	0.8–1.0
Wet, bare surface	62.4–69.5	0.7–0.8
Packed snow	20.6–30.0	0.20–0.30
Loose snow/slush	20.6–47.1 (higher value when tyres in contact with pavement)	0.20–0.50
Black ice	15.7–30.0	0.15–0.30
Loose snow on black ice	15.7–25.4	0.15–0.25
Wet black ice	5.4–10.6	0.05–0.10

1.2.3. Airfield Skid Resistance

In addition to the contaminants mentioned in Section 1.2.2, a common and important contaminant on airport runway surfaces is tyre rubber. With repeated aircraft landings, rubber from tyres can cover the entire surface of landing areas, filling the surface voids and reducing macrotexture and microtexture, resulting in loss of aircraft braking capacity and directional control, especially when runways are wet [38,39]. The extent of rubber tyre contaminant accumulation on runways is dependent on the volume and type of aircraft that use the airport [38].

Unfortunately, there is no common index for ground friction measurements on airfields. Currently, individual airport operating authorities are responsible for providing any take-off and landing performance data as a function of a braking coefficient with ground speed, and relating this data to a friction index measured by a ground device [58]. CoF values measured by Continuous Friction

Measuring Equipment (CFME) can be used as guidelines for evaluating friction deterioration of runway pavements [38]. The CoFs for three classification levels for Federal Aviation Administration (FAA) qualified CFME operated at 65 and 95 km h⁻¹ test speeds are shown in Table 4. There are no airfield guideline thresholds for the BPT as it only provides spot friction measurements of the surface (and is not classified as CFME). However, BPTs are sometimes used on runways and we thus summarise BPT results for airfield concrete surfaces in Section 3.

Table 4. Guideline friction values for three classification levels for Federal Aviation Administration (FAA) qualified Continuous Friction Measuring Equipment (CFME) operated at 65 and 95 km h⁻¹ test speeds [38]. Note that there are no airfield guideline thresholds for the British Pendulum Tester (BPT) which is not CFME and only provides spot friction measurements.

	65 km h ⁻¹			95 km h ⁻¹		
	Minimum	Maintenance Planning	New Design/Construction	Minimum	Maintenance Planning	New Design/Construction
Mu Meter	0.42	0.52	0.72	0.26	0.38	0.66
Runway Friction Tester (Dynatest Consulting, Inc.)	0.50	0.60	0.82	0.41	0.54	0.72
Skiddometer (Airport Equipment Co.)	0.50	0.60	0.82	0.34	0.47	0.74
Airport Surface Friction Tester	0.50	0.60	0.82	0.34	0.47	0.74
Safegate Friction Tester (Airport Technology USA)	0.50	0.60	0.82	0.34	0.47	0.74
Griptester Friction Meter (Findlay, Irvine, Ltd.)	0.43	0.53	0.74	0.24	0.36	0.64
Tatra Friction Tester	0.48	0.57	0.76	0.42	0.52	0.67
Norsemeter RUNAR (operated at fixed 16% slip)	0.45	0.52	0.69	0.32	0.42	0.63

1.2.4. Volcanic Ash and Skid Resistance

Due to its rapid formation, volcanic ash particles comprise various proportions of vitric (glassy, non-crystalline), crystalline or lithic (non-magmatic) particles [10] which are usually hard and highly angular. Volcanic ash properties are influenced by various factors, including the magma source type, distance from the vent, weather conditions and time since the eruption. Important volcanic ash properties include:

1. Particle size and surface area
2. Composition and degree of soluble components
3. Hardness and vesicularity
4. Angularity and abrasiveness
5. Wetness.

Since coarser and denser particles are deposited close to the source, fine glass and pumice shards are relatively enriched in ash fall deposits at distal locations [59]. Newly erupted ash has coatings of soluble components [60,61] resulting from interactions with volcanic gases and their new surfaces. Mineral fragment composition is dependent on the chemistry of the magma from which it was erupted, with the most explosive eruptions dispersing high silica rhyolite rich in hard quartz fragments [62,63]. Volcanic ash is very abrasive [3,25,64–67] with the degree of abrasiveness dependent on the hardness of the material forming the particles and their shape; high angularity leads to greater abrasiveness [10]. Most abrasion occurs from particles <500 µm in diameter, with a sharp increase in the abrasion rate from 5 to 100 µm [67].

Skid resistance from volcanic ash may be different to that expected from other contaminants due to cementitious and vesicular properties of the ash. There is also potential for large thicknesses to develop on ground surfaces or contamination to reoccur once cleaned due to re-suspension and

re-deposition. There have been several instances where road line markings have become obscured by settled volcanic ash (e.g., Mt Reventador 2002 [27], Mt Hudson 1991 [7]). An ash thickness of only ~0.1 mm can lead to road marking coverage in some cases [12]. Drivers can unintentionally drive over road markings, which may have different skid resistance properties to unmarked road surfaces. Additionally, with ash accumulation, the vibrations that drivers receive from rumble strips incorporated in some markings will likely be subdued or even eliminated, decreasing road safety further. Vehicle accidents during or after ashfall (e.g., Figure 2) are a particular concern where no road closures occur, due to decreased braking ability and increased stopping distances caused by low skid resistance.



Figure 2. Vehicle accident attributed to reduced skid resistance after ashfall from Merapi volcano, Indonesia, 2010 [68].

At airports, any observed or detected ash accumulation usually requires closure and the removal of ash from airfields before full operations can resume, both of which incur considerable expense [4]. For example, the eruption of Mt. Redoubt volcano in Alaska in 1989 resulted in a minimum loss of US \$21 million at Anchorage International airport [69]. Many airports face closure even before ash settles on the airfield due to potential damage to aircraft by airborne ash, or solely the threat of ash in the vicinity. As such there are limited observations of ash resulting in reduced skid resistance on airfields, although it has been noted that slippery runways are one of the primary hazards to airports from volcanic eruptions [4].

2. Methods

2.1. Sample Preparation

2.1.1. Volcanic Ash

Volcanic ash samples derived from four different volcanic sources in New Zealand were used in this study to investigate two volcanic ash types (basalt and rhyolite) and to span a range of hardness and mineral components. The locations and ash types are shown in Table 5. Compositions and characteristics were selected as they are representative of ash likely to be encountered in the future in New Zealand, but are also common worldwide. For logistical and supply reasons, experimentation on basaltic ash was focussed on a proxy ash sourced from locally abundant basaltic lava blocks from the Lyttelton Volcanic Group at Gollans Bay Quarry in the Port Hills of Christchurch, New Zealand. Ash was physically produced from the blocks by splitting, crushing and pulverisation as described by

Broom (2010) and Wilson et al. (2012) [70,71], a method generally found to provide good correlations with real volcanic ash grain sizes. Some of the proxy Lyttelton basaltic ash produced was pulverised and sieved to 1000 μm and some to 106 μm to investigate the effect of grain size on skid resistance. In addition, further basaltic ash was sourced from deposits originating from the Pupuke eruption in the Auckland Volcanic Field and Punatekahi eruptions in the Taupo Volcanic Zone. Rhyolitic ash was sourced from deposits from the Hatepe eruption in the Taupo Volcanic Zone. These three samples were pulverised (splitting and crushing was not necessary due to their smaller original sizes) and sieved to 1000 μm (Table 5). The grain size distributions for all samples are shown in Figure 3. We note that the maximum particle sizes for all four samples sieved to 1000 μm are in fact <500 μm , likely due to the pulverisation process. Some particles for the LYT-BAS4 sample (sieved to 106 μm) exceed 106 μm due to the often-tabular nature of volcanic ash particles and their ability to pass through the sieve mesh when vertically orientated.

Table 5. Ash samples prepared for testing. Note: RCL = Ruapehu Crater Lake, WICL = White Island Crater Lake.

Ash Source	Ash Type	Sieve Size (μm)	Soluble Components Added	Sample ID
Lyttelton Volcanic Group	Hard Basalt	1000	No	LYT-BAS1
			Yes (RCL)	LYT-BAS2
		106	Yes (WICL)	LYT-BAS3
			No	LYT-BAS4
Punatekahi cone, Taupo	Scoriaceous Basalt	1000	No	PUN-BAS1
			Yes (RCL)	PUN-BAS2
			Yes (WICL)	PUN-BAS3
Hatepe ash, Taupo	Pumiceous Rhyolite	1000	No	HAT-RHY
Pupuke, Auckland Volcanic Field	Scoriaceous Basalt	1000	No	PUP-BAS1
			Yes (WICL)	PUP-BAS3

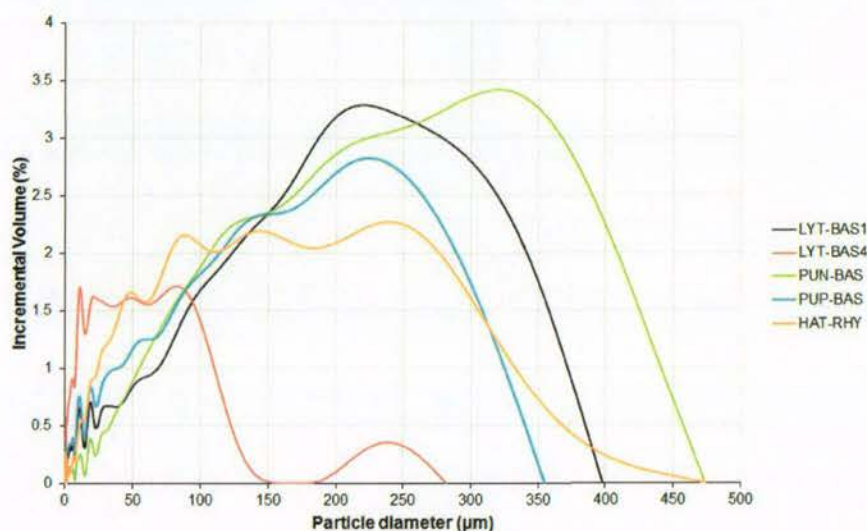


Figure 3. Mean particle size distribution analysed using a Micromeritics Saturn DigiSizer II Laser-Sizer (3 \times runs per sample).

As fresh ash contains adhered soluble components, we dosed a portion of our ash samples with fluid from volcanic crater lakes to mimic the volatile adsorption processes which occur in volcanic plumes, thus enabling the effects of soluble components on skid resistance to be studied. A dosing method using fluids from the crater lakes of Ruapehu and White Island volcanoes, New Zealand, described by Broom (2010) and Wilson et al. (2012) [70,71], was used for a portion of the 1000 μm

Lyttelton and Punatekahi basaltic ash samples for road testing, and Pupuke basaltic ash sample for airfield testing. The following dosing solutions were used as previous work established that they produce samples representative of real fresh volcanic ash [70,71]:

- 100% strength Ruapehu Crater Lake fluid (Table A1), i.e., no dilution, mixed at a ratio of 1:1 (ash to dosing agent)
- 20% strength White Island Crater Lake fluid (Table A1), i.e., 4 parts de-ionised water to 1 part White Island Crater Lake fluid, mixed at a ratio of 4:1 (ash to dosing agent).

We undertook a water leachate test using the method outlined by Stewart et al. (2013) [11] to measure the concentration of dissolved material in solution for all of the samples used and verify the effectiveness of dosing. Both 1:20 and 1:100 ratios of ash (g) to de-ionised water (mL) were used. The water leachate test findings (Figure A1) revealed that the soluble components in the samples we dosed (LYT-BAS2, LYT-BAS3, PUN-BAS2, PUN-BAS3, PUP-BAS3) were considerably higher than those that were not dosed and confirms that the samples used provide a suitable means of testing the effects of this characteristic on skid resistance. Additionally, the lowest pH values were generally recorded for the dosed samples.

Due to limitations in dosing fluids and possible interference caused by the crystalline characteristics of the LYT-BAS samples, most testing was undertaken using the PUN-BAS samples. Large quantities of freshly dosed ash samples were required for each thick ash test under wet conditions, hence only dry conditions were analysed for the 5 and 7 mm thick testing rounds.

2.1.2. Test Surfaces

Stone Mastic Asphalt (SMA) surfaces are commonly used on modern motorways, such as in parts of the UK and on the Auckland State Highway Network in New Zealand [72]. However, concerns have been raised about its use, as initial skid resistance may be low until the thick binder film is worn down: it sometimes takes up to two years for the material to offer an acceptable level of skid resistance [73–75]. The desire to have good macrotexture led to the development of Open Graded Porous Asphalt (OGPA) [72].

For this study, we focus mainly on tests of skid resistance for SMA surfaces using $300 \times 300 \times 45$ mm slabs, newly constructed by the Road Science Laboratory in Tauranga, New Zealand. We also conducted some comparative tests on OGPA also constructed by the Road Science Laboratory, and on concrete surfaces constructed as $220 \times 220 \times 40$ mm slabs by Firth Concrete. The concrete mix was compiled with the same specifications as used for placement via manual labour and a roller screed on the airfield (i.e., runways, taxiways and hardstand areas) at Auckland Airport, although we note that airfield surfaces vary between countries and airports. However, unless otherwise specified, we refer to SMA surfaces in this paper.

2.1.3. Painted Road Markings

Under typical conditions, road markings reduce accident rates [76] as they provide continuous visual guidance of features such as road edges and centres. However, when non-mechanical markings such as paint and thermoplastics are applied, the microtexture of the road surface changes and, with thicker non-mechanical markings, the macrotexture also alters as voids in the asphalt become filled. Consequently, localised skid resistance can be substantially reduced. The skid resistance of the markings is generally lower than that for the bare pavement, although the addition of retroreflective glass beads to the surface can increase skid resistance to more acceptable levels [76]. As little as 0.1 mm of volcanic ash may obscure road markings [12], meaning that drivers may unintentionally travel over marked road surfaces (e.g., such as crossing centre lines). Further accumulation may inhibit the effectiveness of rumble strips which normally cause vibrations within the vehicle.

Paint is the most common form of road marking material used in many countries, including New Zealand, and is typically applied by spraying in dry film with thicknesses varying from 70 μm to

500 μm [77]. In New Zealand, retroreflective glass beads are often applied to longitudinal centre line paint but not to paint on the road margins [78]. Road lines are usually re-painted once or twice a year to account for abrasion, with skid resistance decreasing as the paint fills more voids in the asphalt surface. With a typical asphalt lifespan of ~ 10 years, marking paint accumulation can be substantial in places [78]. In this study we test skid resistance on SMA slabs, machine painted by Downer Group with typical road paint (Damar Bead Lock Oil Based Paint containing 63% solids), in four forms:

- 1 \times application (180–200 μm thick) without retroreflective glass beads
- 1 \times application (180–200 μm thick) with retroreflective glass beads
- 4 \times applications (720–800 μm thick) without retroreflective glass beads
- 4 \times applications (720–800 μm thick) with retroreflective glass beads.

The asphalt with one application of paint is used to replicate markings that have been heavily abraded, whereas that with four applications mimics typical marking thickness found on New Zealand roads [78].

2.2. Skid Resistance Testing

The test procedure for the BPT (Figure 4) is standardised in the ASTM E303 (2013) method [76]. It is a dynamic pendulum impact type test, based on the energy loss occurring when a rubber slider is propelled across the test surface. The method is intended to correlate with the performance of a vehicle with patterned tyres braking with locked wheels on a wet road at 50 km h^{-1} [45]. Since the BPT is designed to test the skid resistance of extensive surfaces in-situ, care was taken to ensure that the instrument was stable and slabs were aligned before conducting our testing in the laboratory environment. Both 3.00" rubber mounted TRL (55) sliders (used for road testing) and 3.00" CEN sliders (used for airfield testing), purchased from Cooper Technology UK, were used in our study.

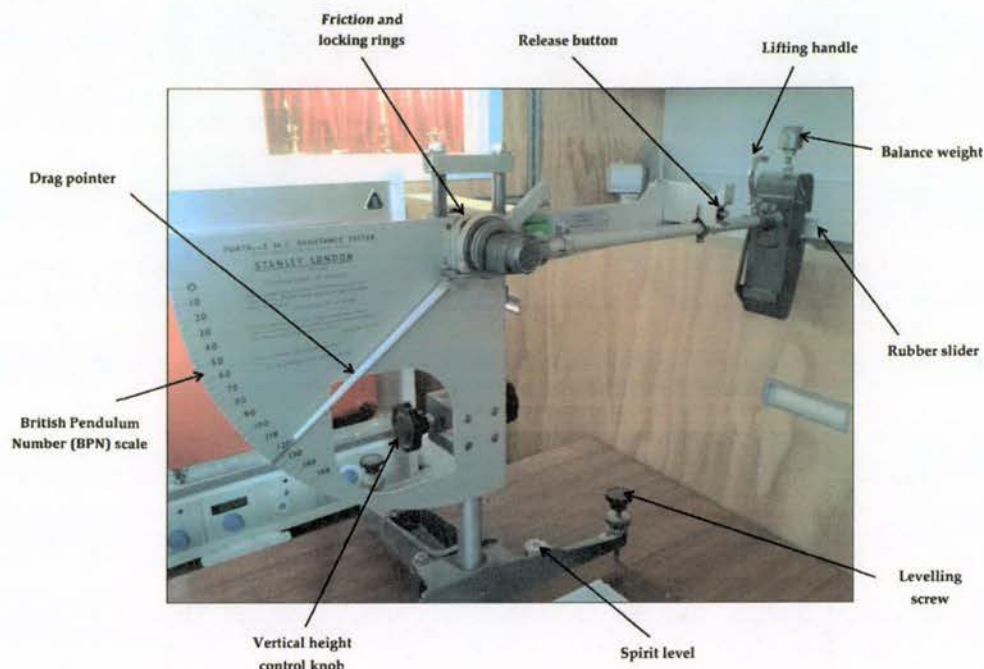


Figure 4. British Pendulum Tester (BPT) used for surface friction testing.

2.2.1. Surfaces Not Covered by Ash

As the ASTM E303 (2013) [76] method states, the direct values are measured as British Pendulum (Tester) Numbers (BPNs) [79]. Typically, tests using the BPT are conducted on wet surfaces. However,

as we are also investigating the effects of dry volcanic ash on skid resistance, we also ran the experiments under dry conditions. For surfaces not covered in ash, we adopted the same technique as used by the New Zealand Transport Agency (NZTA) [80], whereby for each test surface area, results of a minimum of five successive swings which do not differ by more than 3 BPNs are recorded. The mean of the 5 BPNs is then calculated to give a value representing skid resistance (i.e., the Skid Resistance Value (SRV)). The tests were conducted on every side of each slab to retrieve four SRVs (later averaged) for each condition. CoFs for each mean SRV are calculated using the following equation [57]:

$$\text{CoF} = (3 \times \text{SRV}) / (330 - \text{SRV}) \quad (1)$$

2.2.2. Surfaces Covered by Ash

The ash characteristics analysed during experimentation and production techniques are summarised in Figure A2 [81]. For the surfaces covered in ash, we use two test methods to replicate different ash settling conditions in combination with vehicle movement effects:

1. A similar procedure as adopted by the NZTA [80] whereby five successive swings are recorded, which do not differ by more than 3 BPNs and the SRV calculated. Between each swing, ash which has been displaced by the pendulum movement is replenished with new ash of the same type (and re-wetted if applicable) to maintain a consistent depth (and wetness). This test method mimics to some degree the effect of vehicles driving during ash fall, with ash settling on a paved surface and filling any voids left by vehicle tyres before the next vehicle passes. A mean SRV is calculated by repeating the test on all four sides of each asphalt slab. Skid resistance was tested using 1, 3, 5 and 7 mm thick wet and dry samples on SMA, and 1, 3, 5, 7 and 9 mm thick samples on airfield concrete. Limitations in the quantity of samples prevented testing at 9 mm thick on SMA, and limitations in the quantity of rhyolite (HAT-RHY) in particular meant that testing was only conducted at 1 and 5 mm thickness on SMA for this ash type.
2. Eight successive swings of the pendulum are taken over each ash-covered test surface area but ash is not replenished between each swing. For each swing, the BPN is taken to be the SRV, allowing the change in skid resistance to be observed through analysis of the individual results. If the original surface has been wetted, further water is applied between each swing. To some degree, this method represents vehicle movement over an ash-covered surface in dry or wet conditions, where ashfall onto the road surface has ceased. A mean SRV is calculated for each successive swing by repeating the test on all four sides of each asphalt slab where possible.

In dry field conditions, the impact of remobilised ash might be more substantial than captured in the laboratory tests. However, some remobilisation during experimentation is achieved as a result of the pendulum arm movement and associated ash disturbance.

2.2.3. Cleaning

Following testing, the ash was cleaned from the asphalt concrete slabs by brushing and using compressed air if dry, or a combination of compressed air, water and light scrubbing if wet. Wetted slabs were then left to air-dry for 3–4 days before any further dry tests were conducted.

2.3. Macrotexture

2.3.1. Sand Patch Method

This volumetric technique is standardised in the ASTM E965 (2006) method [82] and summarised in Figure A3. It involves a procedure for determining the average depth of pavement macrotexture by careful application of a known volume of spherical glass beads on the surface and subsequent

measurement of the total area covered. The average pavement macrotexture depth is calculated using the following equation:

$$\text{MTD} = 4V / \pi D^2 \quad (2)$$

where MTD = mean texture depth of pavement macrotexture (mm), V = sample volume (mm³) and D = average diameter of the area covered by the material (mm).

We use this approach to determine the macrotexture of new non-contaminated SMA surfaces and SMA surfaces that were contaminated by ash but have undergone testing (10× BPT swings) and cleaning (see Section 2.2.3). The method is not suitable for the airfield concrete slabs due to there being considerably fewer voids at the macrotexture scale and thus a much larger area would be required to conduct the test.

2.3.2. Image Analysis

In addition to the ASTM sand patch method, a visual technique involving digital photography and image analysis was adopted to distinguish between ash and asphalt at a macrotextural level on the SMA slabs. This provides a proxy for surface macrotexture and allows the relative success of cleaning techniques in relation to ash removal and skid resistance reduction to be quantitatively assessed through the calculation of remaining ash coverage. The light-coloured rhyolitic volcanic ash (sample ID: HAT-RHY) was used to allow easy visual interpretation between the ash and dark-coloured asphalt concrete.

1. White paint was marked on the edge of the slabs in order to identify the same segment of the slab between each testing round.
2. A Fuji Finepix S100 (FS) digital SLR camera (with settings: Manual, ISO 800, F6.4, 10-s timer) was mounted on a tripod directly above the asphalt slab.
3. Halogen tripod worklights were used to illuminate the surface of the slab and all ambient light was blocked out using black sheeting before images were taken to keep lighting levels consistent between photos.
4. Images were analysed for percentage coverage of ash by means of 'training' and 'segmentation' using 'Ilastik' and 'Photoshop' software.

2.4. Microtexture–Microscopy

A Meiji EMZ-8TRD (0.7–4.5 zoom) stereomicroscope and Lumenera Infinity 1 digital camera were used to capture images of 10 × 10 mm areas on the asphalt slabs and thus enable visual identification of remaining ash particles at a microtextural level. The microscope was mounted directly above the slab and Leica CLS 100 LED fibre-optic lighting was used to illuminate the Section of interest, with all ambient light blocked using black sheeting. A portable (300 × 300 mm internal dimension) grid (with 10 mm squares) was constructed to fit securely over the slab and allow easy identification of specific segments between each testing round (Figure A4).

3. Results and Discussion

3.1. Consistent Depth

When ash was replenished between each swing, the skid resistance remained relatively constant with time, permitting calculation of a mean SRV for each condition. The mean SRVs and corresponding CoFs for the non-contaminated SMA (new and cleaned) and for the SMA covered by three samples sieved to 1000 µm are shown in Figure 5. Similarly, the SRVs and CoFs for the airfield concrete, both clean and covered by two samples sieved to 1000 µm are shown in Figure 6. The Pupuke volcano sample (PUP-BAS1) was found to have very similar values to the Punatekahi (PUN-BAS1) sample. This was expected as they are both scoriaceous (highly vesiculated) basaltic rock. Due to limitations in

available ash and time constraints, full testing was only conducted with one of the scoriaceous samples on the SMA and airfield concrete.

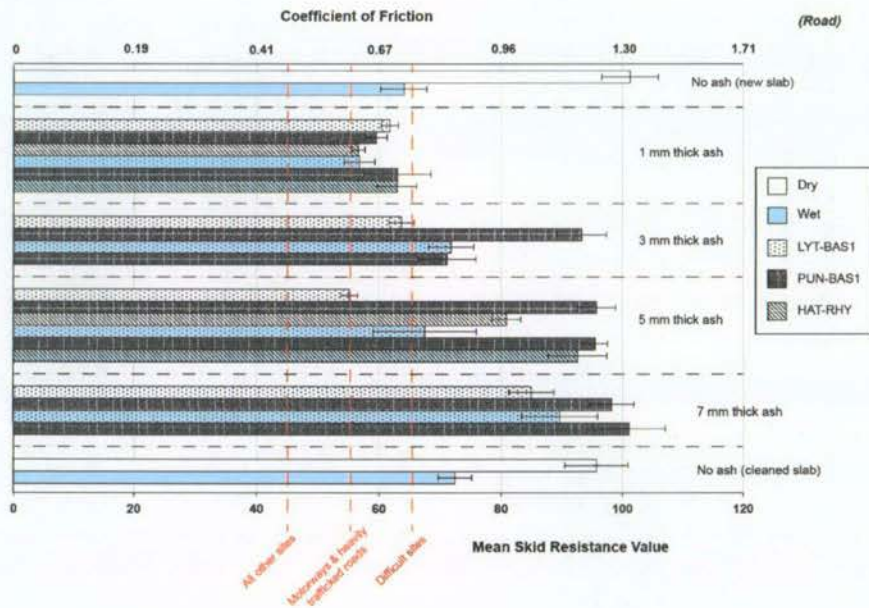


Figure 5. Mean SRVs and CoFs for the non-contaminated Stone Mastic Asphalt (SMA) and SMA covered in the three ash types sieved to 1000 μm . The error bars represent the standard deviation for each data set. Also displayed (as red dashed lines) are the minimum recommended SRVs for different road network sites (Table 2).

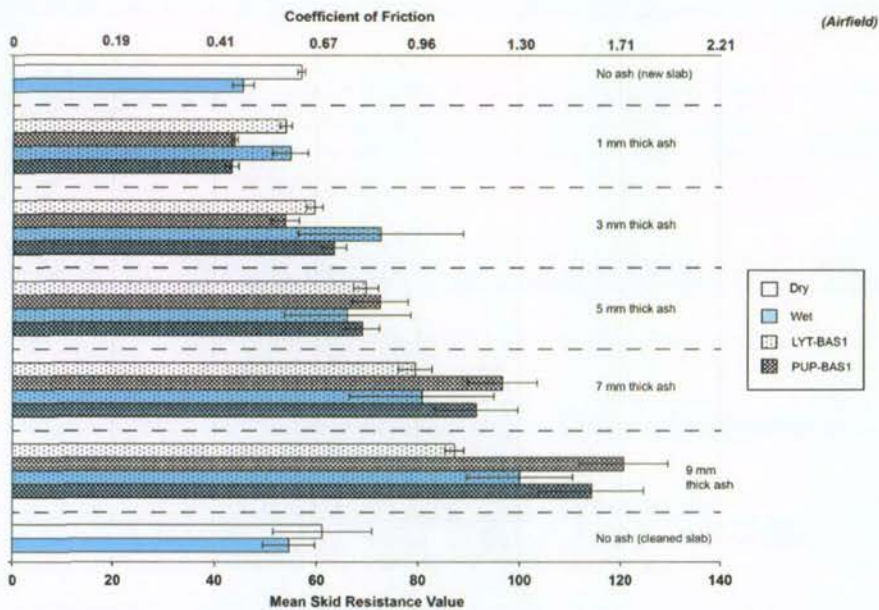


Figure 6. Mean SRVs and COFs for the non-contaminated airfield concrete and airfield concrete covered in the two ash types sieved to 1000 μm . The error bars represent the standard deviation for each data set.

3.1.1. Ash Type and Wetness

Anecdotal observations during historical eruptions suggest that skid resistance on roads is reduced following dry unconsolidated ash accumulation. This is consistent with our results, which also reveal that reduced SRVs are particularly pronounced under dry conditions for a 1 mm thick ash layer on asphalt (Figure 5). Mean SRVs for all 1 mm thick ash types fall below the minimum recommended SRV for difficult sites (an SRV of 65). Wet 1 mm ash-covered surfaces are not necessarily more slippery than dry 1 mm ash-covered surfaces and the wet surfaces covered in 1 mm thick ash are only slightly more slippery than the wet asphalt without ash contamination.

For the 3 and 5 mm thick ash-covered asphalt surfaces, we observe different trends. The LYT-BAS1 sample has similar SRVs to the 1 mm thick ash layer and the mean SRV for 5 mm is near the recommended minimum SRV for motorways (SRV 55). Samples PUN-BAS1 and HAT-RHY however, have greater SRVs than those for 1 mm of ash, suggesting that these ash types are perhaps less slippery when thicker, especially sample PUN-BAS1. The wetted PUN-BAS1 and HAT-RHY >1 mm samples have increasing SRVs as thickness increases. SRV values exceed those for bare wet asphalt surfaces and are similar to those for dry bare asphalt surfaces when ash is >5 mm thick. The vesicular nature of these two samples may play a role in increasing SRVs with the individual particles perhaps able to effectively interlock with one another and with the asphalt aggregate beneath. The pumiceous HAT-RHY sample is more friable than the PUN-BAS1 sample, which may explain the difference in mean SRVs (of up to 20) between the two. We note that the pendulum arm may be slowed upon initial impact with the thicker deposits, producing higher than true representative SRVs. However, the comparatively low SRVs for the 5 mm thick LYT-BAS1 sample suggest that other ash characteristics besides ash thickness (such as hardness and vesicularity) are also important.

Compared to asphalt, there is less difference between SRVs for bare airfield concrete surfaces and those covered by 1 mm of ash (Figure 6), perhaps due to the initially smooth surface when bare. However, as with the asphalt, results suggest little difference in slipperiness (difference in mean SRVs of <5) between wet and dry surfaces with 1 mm of ash deposition. The scoriaceous and vesicular sample PUP-BAS1 exhibits especially large SRVs as thickness is increased, reinforcing our hypothesis that ash of this type is less slippery when thicker. The apparent increase in skid resistance with the addition of ash to SRV values greater than those for bare surfaces may be a function of the pendulum arm slowing upon contact.

3.1.2. Soluble Components

There are no clear differences in SRVs observed between non-dosed and dosed LYT-BAS ash at 1 mm thick (Figure 7). However, the highly crystalline properties of this ash type may reduce the impact that dosing has on SRVs. SRVs for the dosed scoriaceous PUN-BAS ash used on road asphalt (Figure 7) and dosed scoriaceous PUP-BAS ash used on airfield concrete (Figure 8) are generally less than those which are not dosed. For all ash thicknesses, the PUN-BAS3 sample (i.e., that dosed in WICL fluid) produce mean SRVs 2-20 lower than the PUN-BAS2 sample (i.e., that dosed in RCL fluid), suggesting that the skid resistance of non-crystalline ash-covered road surfaces decreases if the soluble component of the ash increases. This corresponds with findings for other road contaminants [50], demonstrating a friction drop at the transition between no rain and rain due to the high-viscosity mix of rainwater and road debris. As such, only WICL fluid was used to dose the PUP-BAS sample (used for airfield concrete) to assess results representative of a 'likely worse-case' SRV scenario.

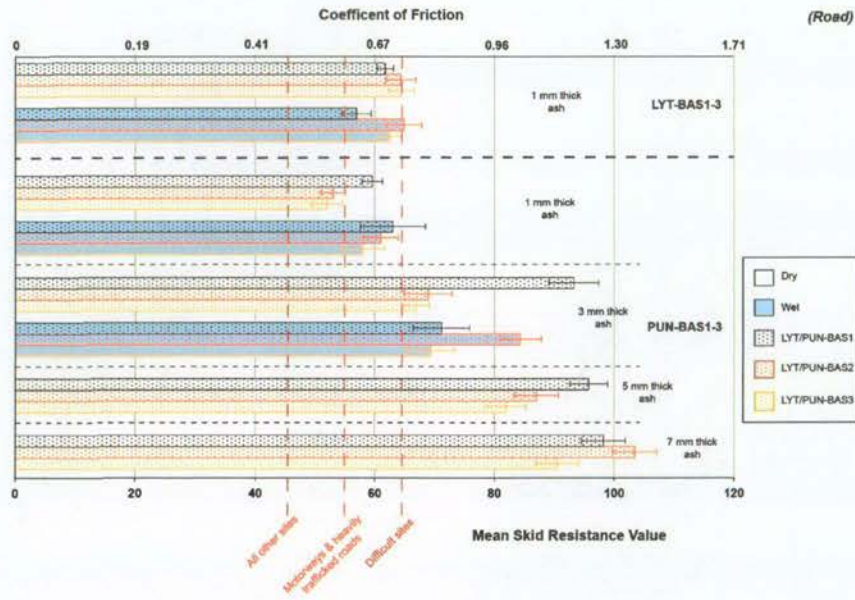


Figure 7. Mean SRVs and CoFs for the road asphalt covered in non-dosed and dosed LYT-BAS and PUN-BAS ash sieved to 1000 μm . Both samples dosed in RCL and WICL fluid under dry and wet conditions are displayed. Red dashed lines indicate the minimum recommended SRVs for different road network sites (Table 2).

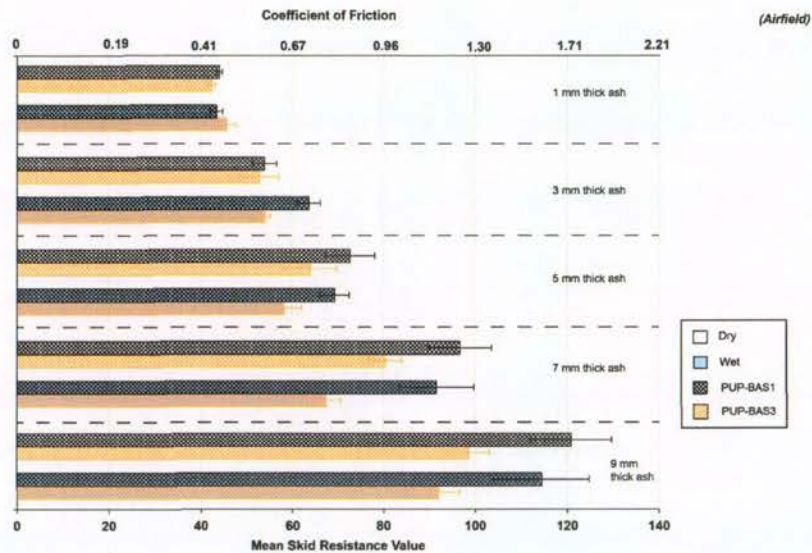


Figure 8. Mean SRVs and CoFs for the airfield concrete covered in non-dosed and dosed PUP-BAS ash sieved to 1000 μm . The samples dosed in WICL fluid under both dry and wet conditions are displayed.

3.1.3. Ash Particle Size

The mean SRVs for fine-grained basaltic ash (LYT-BAS4) are slightly higher than those for the coarse-grained ash of the same type (LYT-BAS1) when at 1 mm thickness on roads, with mean values for both wet and dry samples above the minimum recommended SRVs for difficult sites (Figure 9). This concurs with field observations made by the Kagoshima City Office staff following frequent volcanic ash deposition on roads from the multiple eruptions of Sakurajima volcano, Japan (since 1955). These observations suggest that the finer ash from the recent eruptions at the Showa crater resulted in less slippery roads than the generally coarser-grained ash produced during past eruptions from the

Minami-daki summit area [83]. We hypothesise that this difference between fine- and coarse-grained ash is due to the finer particles being more easily mobilised and displaced at the tyre-asphalt interface, allowing improved contact between the tyre and asphalt. However, no clear correlations exist between the fine- and coarse-grained ash when at 5 mm thick, perhaps due to both types covering the asphalt surface when the tyre makes contact.

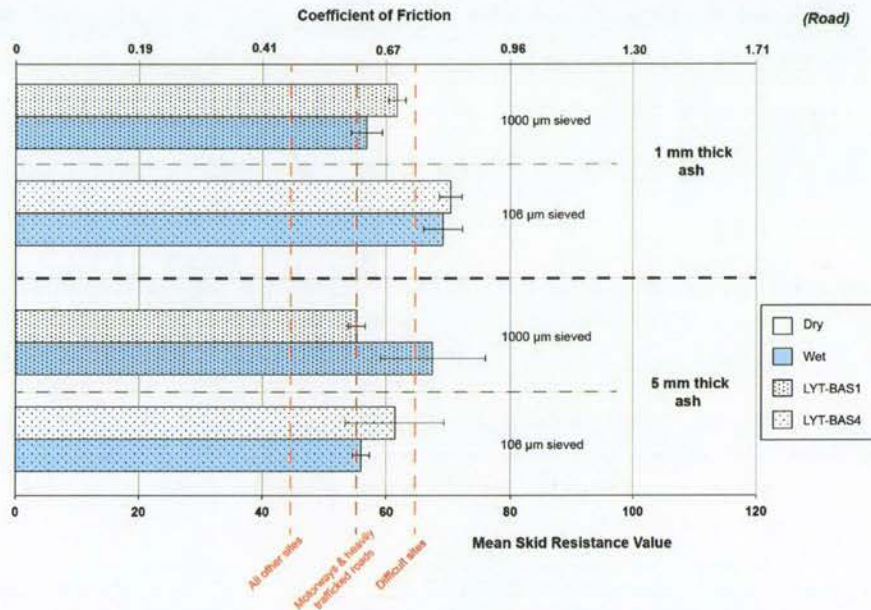


Figure 9. Mean SRVs and CoFs for the asphalt covered in coarse-grained (i.e., LYT-BAS1, 1000 µm sieved) and fine-grained (i.e., LYT-BAS4, 106 µm sieved) samples at 1 mm and 5 mm ash thickness under both dry and wet conditions. Also displayed (as red dashed lines) are the minimum recommended SRVs for different road network sites (Table 2).

3.1.4. Line-Painted Asphalt Surfaces

SRVs can be reduced substantially as a result of road markings, although the addition of retroreflective glass beads can increase values to more acceptable levels [76]. This is demonstrated in our findings for wet conditions, in which BPT analysis is typically conducted, with mean SRVs on line-painted asphalt surfaces with no beads and no ash the lowest of all our results. SRVs for these wet surfaces range from 40 to 46, and lie below the minimum recommended skid resistance for ‘all other sites’ when 4× coats of line paint have been applied (Figure 10). The addition of glass beads does increase SRVs (by around 5), although values are still relatively low. SRVs for ‘clean’ and dry line-painted asphalt surfaces are very high, but as with non-painted surfaces, the addition of a 1 mm ash layer decreases SRVs substantially. Conversely, the SRVs for wet asphalt concrete increase with a 1 mm ash layer to similar levels as for dry conditions. With the thicker (5 mm) ash layer on top of line-painted surfaces, SRVs increase further by around 20 (Figure 10).

3.1.5. Asphalt Comparison

Because of increased macrotexture of the surface, higher SRVs (~5) were measured on the bare OGPA than the SMA slabs when wet. Similar differences in SRVs existed between the two asphalt types covered by wet volcanic ash (both at 1 mm and 5 mm depths). However, no major differences in SRVs were observed between the two asphalt types when dry, whether surfaces were covered by ash or not.

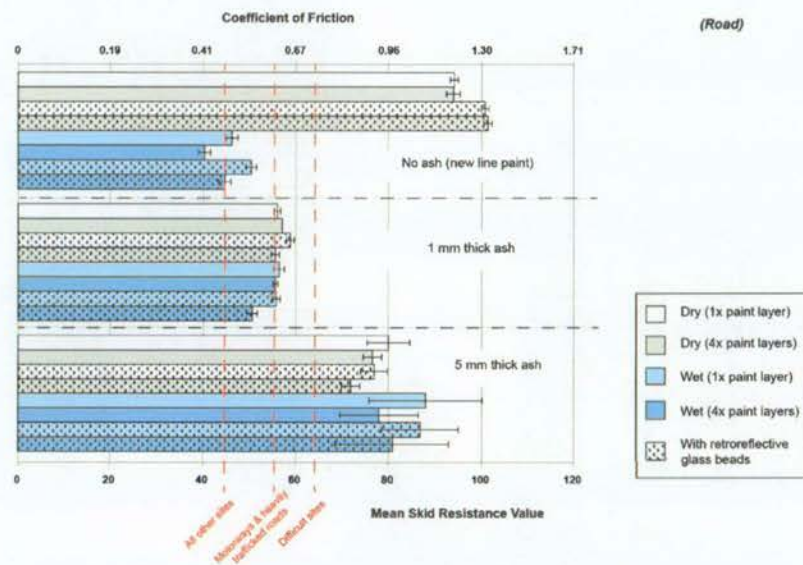


Figure 10. Mean SRVs and CoFs for the road asphalt with line-painted surfaces. Conditions of no ash, 1 mm thick ash, and 5 mm thick ash (using the LYT-BAS1 ash type) were analysed under both wet and dry conditions. Also displayed (as red dashed lines) are the minimum recommended SRVs for different road network sites (Table 2).

3.2. Inconsistent Depth

Where ash was not replenished between each swing, SRVs represent those expected for surfaces where ashfall has ceased but where there is some traffic movement.

3.2.1. Ash Types and Wetness

SRV results obtained for the samples sieved to 1000 μm (at 1 mm and 5 mm ash thickness) and deposited on road asphalt are shown in Figure 11. Note that tests of other thicknesses (3, 7 and 9 mm) were also conducted but these have been omitted from the figure for clarity.

Despite the large standard deviations, the 5 mm thick PUN-BAS1 and HAT-RHY samples initially produced high SRVs. However, the SRVs recorded for the first 2–3 swings of the pendulum over 5 mm thick ash should be interpreted with caution. This is due to possible interference of the thicker deposit when the pendulum slider first impacts the surface; similar circumstances may occur in the field when initial vehicles are driven into thicker ash deposits. When wet however, the SRVs are higher than the mean recorded on the bare asphalt surface, particularly for the PUN-BAS1 sample, suggesting that thicker layers of vesiculated (and especially harder) volcanic ash are perhaps initially less slippery than thin layers of ash of those ash types. Observations during our experimentation revealed that the wet 5 mm thick vesiculated deposits (PUN-BAS1 and HAT-RHY) consolidated, thus resisting major ash displacement more than for dry ash (Figure 12), even following several swings of the pendulum arm. The consolidated deposits were very firm to touch and, although further work is required to test this, it is suggested that light vehicles would be able to drive over the surface without sinking substantially.

Very similar patterns in skid resistance were observed for the airfield concrete surfaces where ash was not replenished between swings. The main difference was that the initially high SRVs for the scoriaceous sample (PUP-BAS) decreased more quickly with pendulum swings, most likely due to the ash being more easily displaced from the smoother concrete surface than for asphalt.

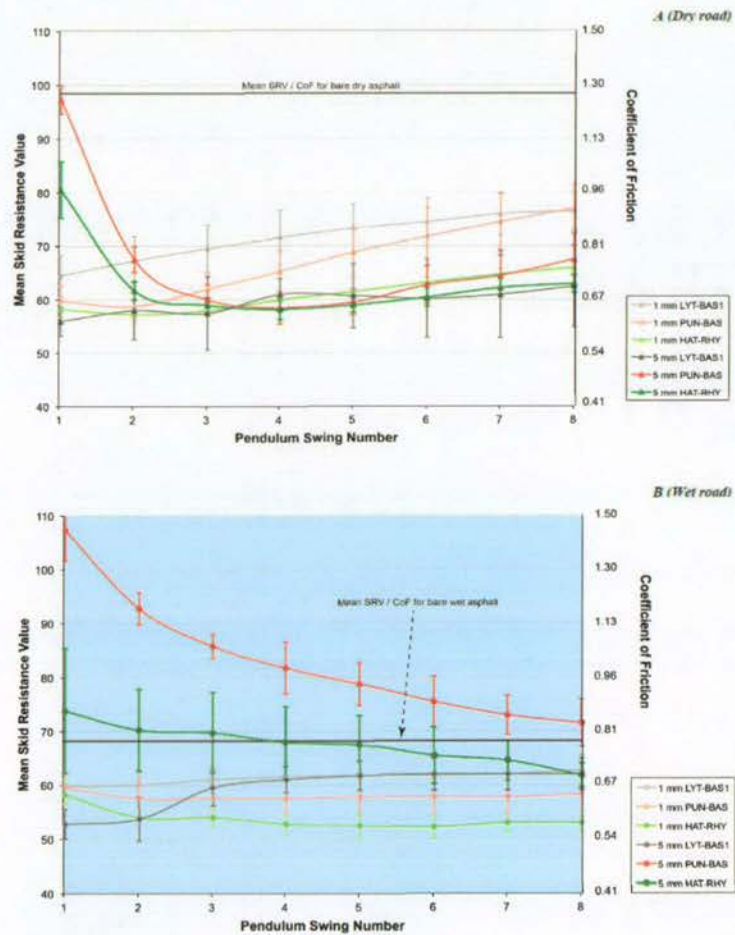


Figure 11. SRVs and corresponding CoFs on asphalt covered by ash sieved to 1000 μm , under (A) dry and (B) wet conditions. Also shown are the mean SRVs for bare asphalt, taken from Section 3.1. Error bars display the standard deviations for each pendulum swing number for the different sample types.



Figure 12. Dry ash displacement from the BPT slider-surface interface after $8 \times$ swings of the pendulum arm for (A) SMA and (B) airfield concrete. Dry ash was displaced from the surface more readily than wet ash. Note that white lines indicate length of slider contact path (i.e., 125 mm).

3.2.2. Ash Particle Size

No major changes were observed for the fine-grained basaltic ash samples (LYT-BAS4) over the course of the eight pendulum swings on asphalt, other than a gradual increase in SRVs over time, particularly for the dry ash at 1 mm thickness as observed for the coarse-grained samples (Figure 11A). As with the testing where ash was replenished, here SRVs for the fine-grained ash samples were

generally slightly higher than those for coarse-grained samples, suggesting that fine-grained ash is a little less slippery than coarser material.

3.2.3. Soluble Components

The testing involving non-replenished dosed ash confirmed the key finding already discussed during replenished testing (Section 3.1.2); non-crystalline ash containing a higher soluble component content generally produces lower SRVs than undosed ash. However, with an increasing number of swings of the pendulum, this trend becomes less pronounced, particularly under wet conditions where the effect of adding water between each test leaches the samples, thus reducing the soluble component content of the ash.

3.2.4. Line-Painted Asphalt Surfaces

Line-painted asphalt surfaces covered in ash (Figure 13) produce relatively low SRVs. Although the first 2–3 swings involving 5 mm thick ash are not considered, it is evident that wet painted surfaces are generally slightly more slippery than painted dry surfaces. The trend of quick SRV recovery (as seen in Section 3.2.1) is also evident under dry line-painted conditions, when compared to wet conditions which remain slippery for longer. Under dry conditions, the addition of retroreflective glass in the line-paint appears to aid the recovery of skid resistance over time (as shown by the rising green and orange lines for the latter swings in Figure 13A). However, this trend is not evident for wet conditions.

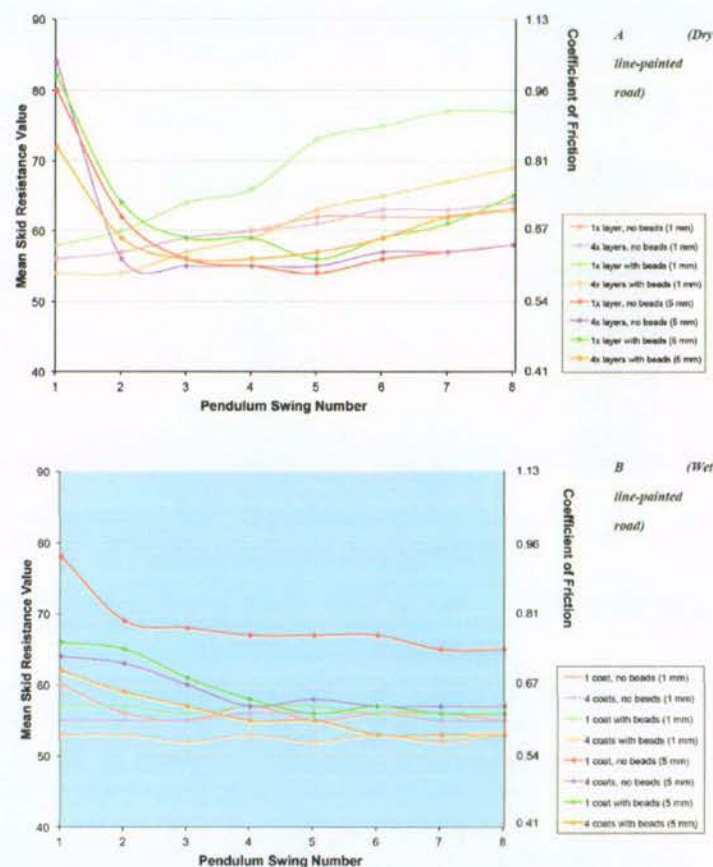


Figure 13. SRVs and corresponding CoFs for line-painted asphalt surfaces covered in 1 mm or 5 mm thick LYT-BAS1, under (A) dry, and (B) wet conditions. The initial 2–3 swings over the 5 mm deposits should be treated with caution (see text). No standard deviations are provided as only one test was conducted on each surface type due to the availability of line-painted slabs.

3.3. Surface Macro and Microtexture

3.3.1. Ash Displacement and Removal

The results for mean macrotexture depth calculated using the sand patch method for the bare, clean, new asphalt surface and the asphalt surface following dry testing and brushing, and cleaning with compressed air after contamination are shown in Table 6.

Table 6. Mean macrotexture depth of asphalt slab before and after testing/cleaning, calculated using the ASTM sand patch method, and percentage ash surface coverage.

Asphalt Concrete Slab Condition	Mean Macrotexture Depth (mm)	Ash Surface Coverage (%)
Bare, clean and new	1.37	0
Ashed, 10× BPT swings	-	81
Ashed, 10× BPT swings and brushed (10× strokes)	0.99	40
Cleaned with compressed air	1.29	<1

The results for the new slab and pre-contaminated slab after cleaning with compressed air suggest that there is little difference in macrotexture depth after cleaning using this method. However, cleaning using only brush strokes shows a mean macrotexture depth reduction of 0.38 mm, 28% less depth than the original new surface. This suggests that cleaning of dry road surfaces using only brushes may not be entirely effective and that alternative methods should be considered where possible. To confirm this, after brushing and 10× swings of the BPT, some HAT-RHY ash remains - as shown in the digital photography macrotexture image sequence (Figure 14) and semi-quantitative analysis of these images using *Ilastik* and *Adobe Photoshop* gives results of surface coverage (Table 6).

Cleaning using high-pressure water spraying and brushing was more effective than brushing alone at removing ash (<1% surface ash coverage afterwards). However, this approach requires large quantities of water and the microscope imagery revealed that some small particles of ash remain on the surface, which would perhaps still reduce skid resistance somewhat. Field observations from Kagoshima, Japan, where high quantities of only low-pressure water are used to clean road surfaces indicates that some ash remains on the road surfaces even immediately after cleaning [83]. Furthermore, clearing ash from roads using water may cause some drainage systems to become blocked [22], potentially resulting in surface water flooding.

3.3.2. Temporal Change of Skid Resistance on Bare Asphalt Surfaces

In normal conditions, the skid resistance of bare asphalt surfaces changes over time [41]. The initial trend of increasing skid resistance was confirmed during our testing of the bare wet asphalt and concrete slabs before and after contamination with ash (but following cleaning), particularly so for the asphalt (Figure 5). We suggest that the abrasive properties of volcanic ash accelerates these processes, especially for our testing as all ash particles were <500 µm in diameter (see Section 1.2.4). Following testing, the SRV of bare wet asphalt had increased by around 5. The microscopy imagery showed that the lustrous film on the new asphalt slabs had been removed during BPT experimentation (Figure 15).

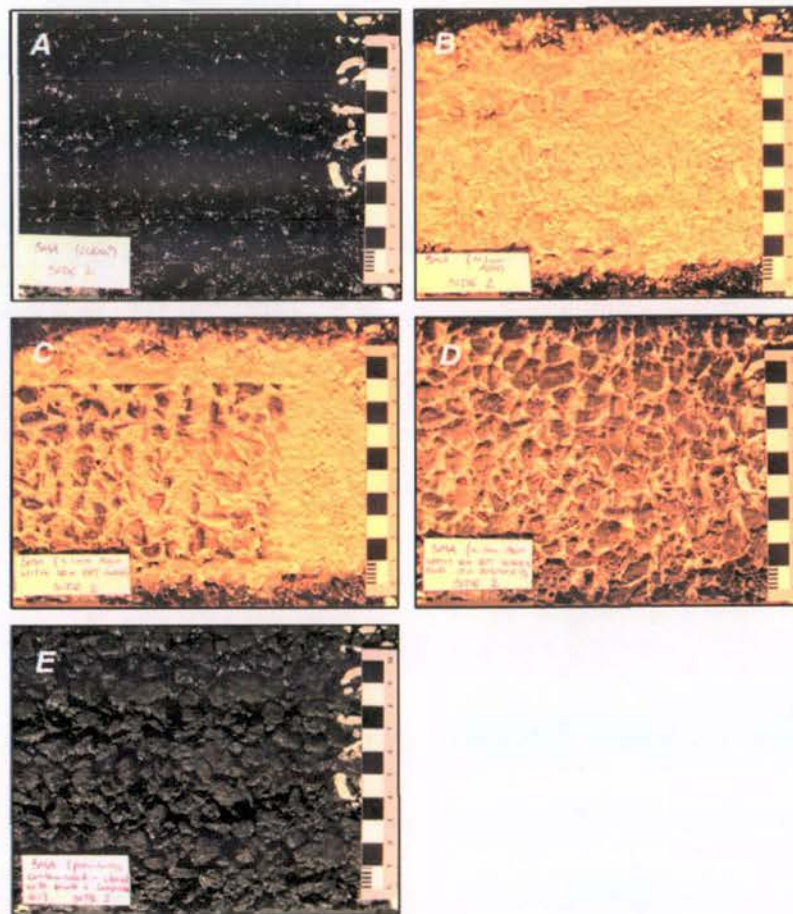


Figure 14. Macrotexture image sequence for asphalt. (A) Clean new slab; (B) covered with 1 mm rhyolitic ash (100% surface coverage); (C) after 10× BPT swings (81% surface ash coverage); (D) after cleaning with 10× brush strokes (40% surface ash coverage); (E) after cleaning with compressed air (<1% surface ash coverage). The macrotexture of the surface is visibly affected in images B–D with much ash remaining between the asphalt’s aggregate pore spaces, even after 10× BPT swings and cleaning using a brush.

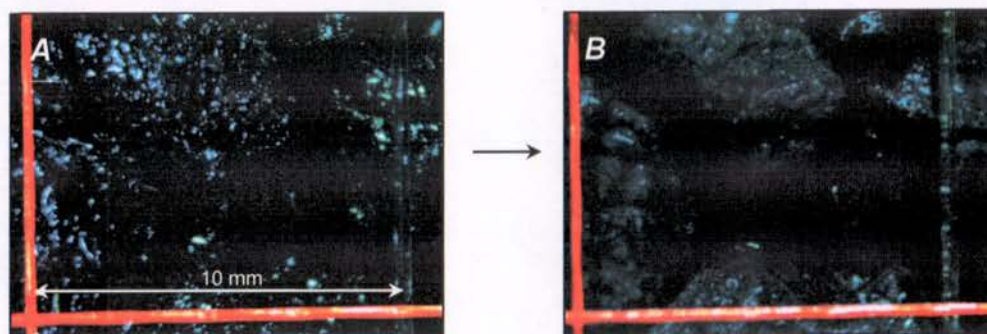


Figure 15. Microscope images on the same segment of asphalt, (A) on the new slab and (B) after contamination with volcanic ash and cleaning with compressed air. Much of the shiny film visible on the surface of the new asphalt has been removed. Note that the length of the white lines is 10 mm and that lighting conditions and microscope settings were consistent for both images.

4. Conclusions

4.1. Key Findings

Our experiments suggest that the following lead to particularly reduced skid resistance on asphalt road surfaces and may thus lead to slippery surfaces following volcanic ashfall:

- Thin (~1 mm deep) layers of relatively coarse-grained ash, with ash type having little effect at this depth (average SRVs of 55–65).
- Thicker (~5 mm deep) layers of hard, non-vesiculated ash (average SRVs of 55–60).
- Ash of low crystallinity or containing a high degree of soluble components (average SRVs ~5 lower than for ash that has undergone substantial leaching).
- Line-painted surfaces that are either dry or wet but covered by thin layers of ash, particularly when paint does not incorporate retroreflective glass beads (average SRVs of ~55).

Importantly, the largest change in skid resistance for surfaces that became covered by ash occurs during dry conditions, where SRVs fall to levels just below those for wet non-contaminated surfaces, with similar SRVs as the wet contaminated surfaces. This large reduction in skid resistance may not be expected by motorists who may consequently not adjust driving, potentially resulting in high accident rates. As time goes on, wet ash deposits on roads are most likely to lead to reduced skid resistance, particularly for thicker deposits as these remain slippery for longer (typical SRVs of around 55).

Similarities exist for airfield surfaces and the second and third bullet points above are especially true for the concrete surface type. The following additional key findings are also drawn:

- There is little difference in skid resistance between bare airfield surfaces and those covered by ~1 mm of ash.
- Low crystalline ash containing high soluble components may result in SRVs of up to 20 less than non-dosed samples, particularly if the ash is thicker (~7–9 mm depth).
- Ash is more readily displaced on smoother airfield concrete than road asphalt causing SRVs to recover to 'typical non-contaminated' values at a faster rate with consistent traffic flow.

4.2. Recommendations for Road Safety

Based on skid resistance analysis, we make the following recommendations to increase road safety in areas with volcanic ashfall exposure of ≤ 5 mm depth:

- During initial ash fall, vehicle speed (or advisory speed) should immediately be reduced to levels below those advised for driving in very wet conditions on that road, whether the surface is wet or dry. Wet ash is not necessarily more slippery than dry ash, at least initially.
- Fresh ash contains more soluble components, which results in lower skid resistance values than for leached ash. Therefore, it is important to advise motorists promptly of any restrictions.
- Particular caution should be taken on dry surfaces that become covered by coarse-grained ash as skid resistance will reduce substantially from what occurs on dry non-contaminated surfaces. The slipperiness of dry surfaces with such contamination may not be expected by motorists (skid resistance values will be similar as for wet fresh ash and slightly less than for wet non-contaminated conditions).
- Road markings may be hidden from view, impacting road safety through lack of visual and audio guidance of road features. Areas of road that are line-painted and covered in thin ash are especially slippery. Motorcyclists and cyclists in particular should take extreme care.

It is unlikely that road closures will be necessary for thin ash accumulations based on loss of skid resistance alone. SRVs rarely fall below the minimum recommended threshold for motorways and heavily trafficked roads (i.e., SRV 55) although many values fall between this and the threshold for minimum

recommended skid resistance for difficult sites (i.e., SRV 65). These results are conservative however, because of the typical reduction in skid resistance over the later stages of the pavement life. Based on observations from previous eruptions and field studies [22], physical obstruction to road vehicles may occur once ash deposits reach ~100 mm and road closures may be necessary at and above this depth. It should be stressed however, that all recommendations given ignore other impacts from volcanic ashfall such as visibility impairment, local road authority decisions, breakdowns and driver behaviour which often introduce further complexities associated with driving in volcanic ashfall. For example, lower thresholds for road closures and lower speed restrictions may be required where visibility is reduced.

4.3. Airport Safety

We do not make any specific recommendations for airport safety related to concrete airfield surfaces, although it is highlighted that extensive efforts may be required to clean airfield surfaces as has occurred following historical eruptions (e.g., Chaitén 2008 [29], Kelud 2014 [33]). It is likely that airports will remain closed until all ash has been cleared from runways due to other potential impacts such as damage to aircraft turbine engines. Our results suggest that residual ash of minimal depths on concrete airfield surfaces is likely to have little effect on skid resistance. However, airport managers should be aware that freshly erupted ash or ash that has not been leached (i.e., containing higher soluble components) will likely be more slippery than that which has persisted in the environment for some time. As with road asphalt, wet ash is not necessarily more slippery than dry ash on airfield concrete and any restrictions implemented should thus be in place for both conditions.

4.4. Recommendations for Cleaning

The following advice for road cleaning is given based on our studies of macrotexture and microtexture and from the observations during small-scale cleaning conducted on our slabs between skid resistance tests:

- Brushing alone will not restore surfaces to their original condition in terms of skid resistance. Following simple brushing practices on asphalt roads, the macrotexture depth may be around one third less than the original depth and ~40% ash coverage may occur on the surface.
- If surfaces are dry and contaminated with dry ash, air blasting combined with suction and capture of loosened ash, is an effective way to remove ash from macrotextural pores. Minor quantities of ash may remain at the microtextural level although this is deemed too low to substantially affect skid resistance.
- If surfaces are wet, a combination of water spraying and brushing and/or air blasting (with suction and ash capture) is an effective way to remove most ash and restore surface skid resistance. However, large quantities of water are required and some ash will remain in the asphalt pore spaces, especially if low-pressure water is used. Care should be taken if using water for ash removal due to the potential for blockage of some drainage systems.

Ash remobilisation should be carefully considered prior to cleaning. Extensive (and often expensive) cleaning efforts may be useless if ash continues to fall or is remobilised from elsewhere and deposited onto roads and airfields.

Acknowledgments: We thank the University of Canterbury Mason Trust scheme, New Zealand Earthquake Commission (EQC), Determining Volcanic Risk in Auckland (DEVORA) project, Natural Hazard Research Platform (research contract: C05X0907), and GNS Science for their support towards the study through the provision of funding to researchers. We also express thanks to the organisations and people who helped source equipment that was vital to the project. In particular, we would like to thank Alan Nicholson and John Kooloos of the Civil and Natural Resources Engineering department at the University of Canterbury for the loan of the BPT, and Janet Jackson, Howard Jamison and the wider laboratory and road teams at Downer Group for their support towards coordinating the construction and line-painting of asphalt slabs and for providing Daniel Blake with BPT training. We thank Roy Robertson (Auckland Airport) and Robert McKinnon (Firth Concrete) for their advice on airfield surfaces and for providing the airfield concrete slabs used in this study. Particular thanks also go to the

people who provided support with the laboratory set-up at various stages, including technician support from Rob Spiers, Matt Cockcroft, Chris Grimshaw and Sacha Baldwin-Cunningham. We also thank researchers Emily Lambie, Rinze Schuurmans, Alec Wild and Alistair Davies for their assistance with sample preparation and skid resistance testing.

Author Contributions: All authors contributed to the manuscript. D.M.B. conducted the majority of the planning, research and laboratory testing, and also led the writing and editing of the article. T.M.W. assisted D.M.B. in the development of the methodology including potential experimental approaches. T.M.W., J.W.C., N.I.D. and J.M.L. conducted multiple reviews of the article prior to submission.

Conflicts of Interest: The authors declare no conflicts of interest.

Appendix A

Table A1. Concentration of elements in the Ruapehu and White Island Crater Lake fluids at the strength used to dose the ash (after Broom 2010, Wilson 2012 [70,71]).

Element	Concentration (mg/L)	
	Ruapehu Crater Lake (100% Strength)	White Island Crater Lake (20% Strength)
Aluminium (Al)	370	965
Boron (B)	17.2	28.6
Bromine (Br)	10.8	44.2
Calcium (Ca)	909	823
Chlorine (Cl)	5568	19,452
Fluorine (F)	133	1518
Iron (Fe)	424	179
Potassium (K)	90	686
Lithium (Li)	0.77	5.60
Magnesium (Mg)	1067	1325
Sodium (Na)	660	3372
Ammonia (NH ₃)	13.0	24.8
Sulphate (SO ₄ ²⁻)	7988	4952
pH	1.13	0.07

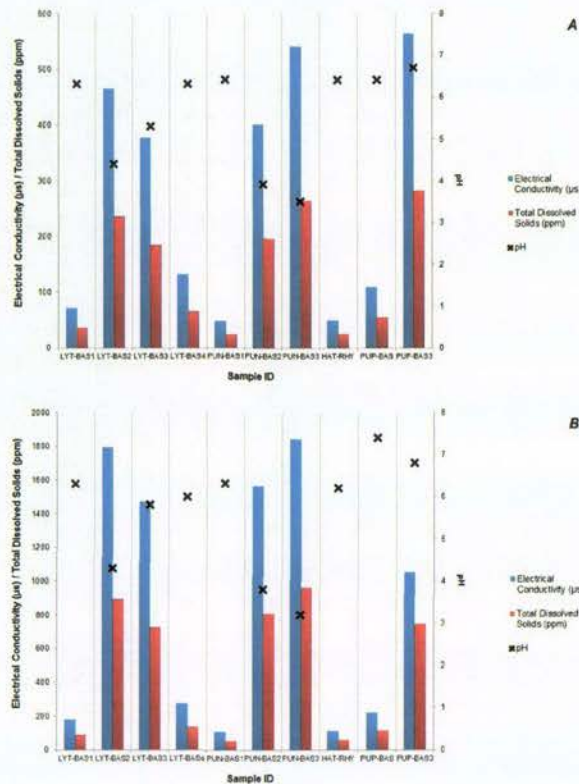


Figure A1. Water leachate results showing relative soluble components (expressed as Electrical Conductivity (EC) and Total Dissolved Solids (TDS)), and pH. (A) 1:100 ash to de-ionised water; (B) 1:20 ash to de-ionised water.

Characteristic	Variables	Method Summary
Ash type	Hard basalt, scoriaceous basalt, pumiceous rhyolite	Different volcano source locations in New Zealand
Ash grain size	<1000 µm, <106 µm	Rock splitting, crushing and pulverisation (as required), then sieving
 <p>Hydraulic press [81] Jaw crusher [81] Disk pulverisor [81] Rock sieves</p>		
Ash thickness	1-2 mm, 5 mm	Manual sprinkling (1-2 mm), Metal spacer across ash surface (5 mm)
 <p>1-2 mm 5 mm</p>		
Soluble components	Non-dosed, dosed with Ruapehu Crater Lake fluid, dosed with White Island Crater Lake fluid	Established laboratory dosing technique (see section 2.1.1)
		
Wetness	Wetted to saturation, dry (no added moisture)	Hand-held water sprayer (water at room temperature)
 <p>Dry Wet</p>		

Figure A2. Ash characteristics analysed during experimentation and illustrations to show production of each characteristic.

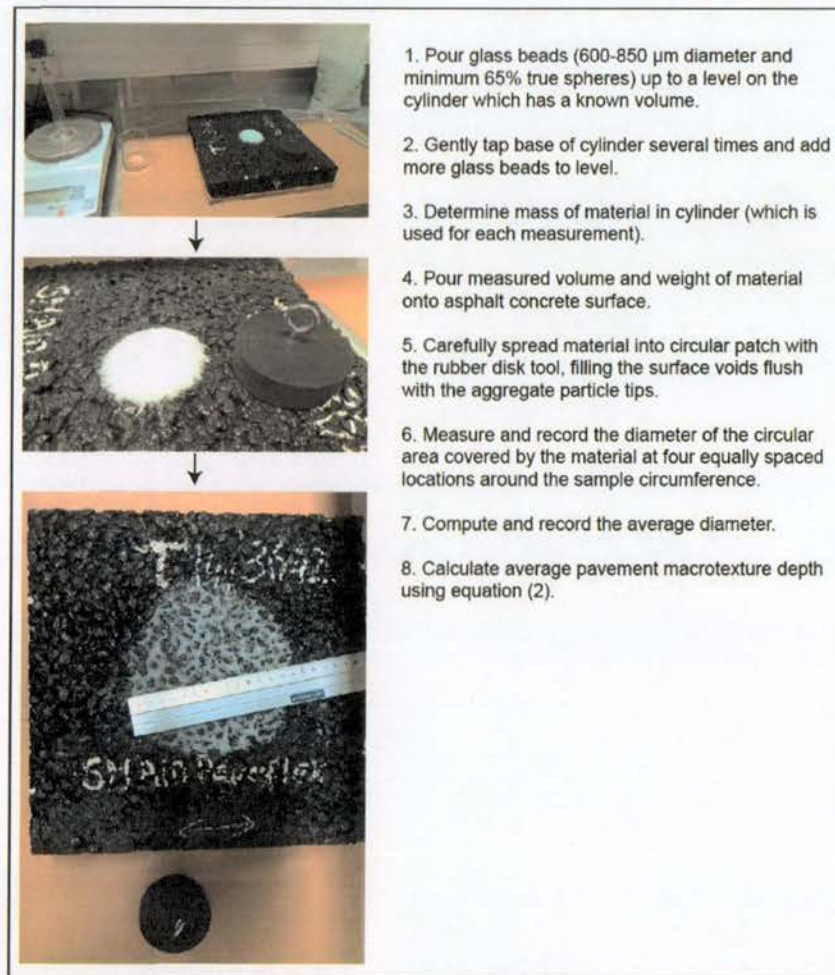


Figure A3. Summary of sand patch volumetric technique used to calculate the average pavement macrotexture depth (adapted from [82]).

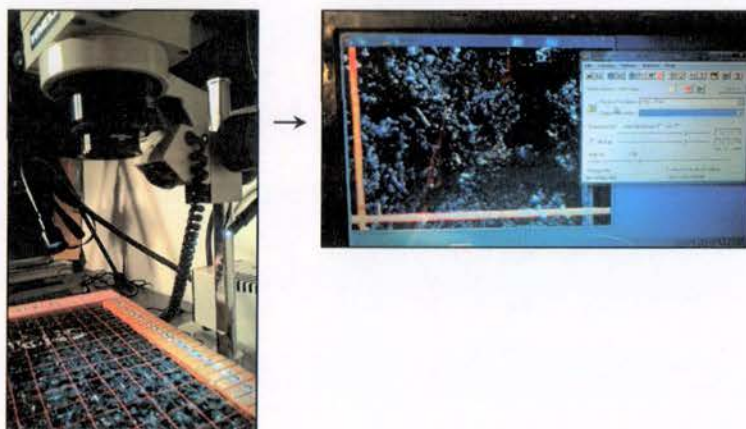


Figure A4. Image capture using stereo-microscope to analyse asphalt at a microtextural scale. Note that the grid squares are spaced at 10 mm intervals.

References

1. Johnston, D.M.; Daly, M. Auckland erupts!! *N. Z. Sci. Mon.* **1995**, *8*, 6–7.
2. Wilson, G.; Wilson, T.M.; Deligne, N.I.; Cole, J.W. Volcanic hazard impacts to critical infrastructure: A review. *J. Volcanol. Geotherm. Res.* **2014**, *286*, 148–182. [CrossRef]
3. Blong, R.J. *Volcanic Hazards: A Sourcebook on the Effects of Eruptions*; Academic Press Inc.: Sydney, Australia, 1984.
4. Guffanti, M.; Mayberry, G.C.; Casadevall, T.J.; Wunderman, R. Volcanic hazards to airports. *Nat. Hazards* **2009**, *51*, 287–302. [CrossRef]
5. Wilson, T.; Daly, M.; Johnston, D. *Review of Impacts of Volcanic Ash on Electricity Distribution Systems, Broadcasting and Communication Networks*; Technical Publication No. 051; Auckland Engineering Lifelines Group, Auckland Regional Council: Auckland, New Zealand, 2009.
6. Horwell, C.J.; Baxter, P.J.; Hillman, S.E.; Damby, D.E.; Delmelle, P.; Donaldson, K.; Dunster, C.; Calkins, J.A.; Fubini, B.; Hoskuldsson, A.; et al. *Respiratory Health Hazard Assessment of Ash from the 2010 Eruption of Eyjafjallajökull Volcano, Iceland: A Summary of Initial Findings from a Multi-Centre Laboratory Study*; International Volcanic Health Hazard Network (IVHHN), Durham University: Durham, UK, 2009.
7. Wilson, T.M.; Stewart, C.; Cole, J.W.; Dewar, D.J.; Johnston, D.M.; Cronin, S.J. *The 1991 Eruption of Volcan Hudson, Chile: Impacts on Agriculture and Rural Communities and Long-Term Recovery*; GNS Science Report 2009/66; GNS Science: Lower Hutt, New Zealand, 2011; p. 77.
8. Dunn, M.G. Operation of gas turbine engines in an environment contaminated with volcanic ash. *J. Turbomach.* **2012**, *134*, 051001. [CrossRef]
9. Wardman, J.; Sword-Daniels, V.; Stewart, C.; Wilson, T. *Impact Assessment of the May 2010 Eruption of Pacaya Volcano, Guatemala*; GNS Science Report 2012/09; GNS Science: Lower Hutt, New Zealand, 2012.
10. Wilson, T.M.; Stewart, C.; Sword-Daniels, V.; Leonard, G.S.; Johnston, D.M.; Cole, J.W.; Wardman, J.; Wilson, G.; Barnard, S.T. Volcanic ash impacts to critical infrastructure. *Phys. Chem. Earth* **2012**, *45–46*, 5–23. [CrossRef]
11. Stewart, C.; Horwell, C.; Plumlee, G.; Cronin, S.; Delmelle, P.; Baxter, P.; Calkins, J.; Damby, D.; Mormon, S.; Oppenheimer, C. Protocol for Analysis of Volcanic Ash Samples for Assessment of Hazards from Leachable Elements. Available online: http://www.ivhhn.org/images/pdf/volcanic_ash_leachate_protocols.pdf (accessed on 2 August 2017).
12. Blake, D.M.; Wilson, T.M.; Gomez, C. Road marking coverage by volcanic ash. *Environ. Earth Sci.* **2016**, *75*, 1–12. [CrossRef]
13. Hayes, J.; Wilson, T.M.; Deligne, N.I.; Cole, J.; Hughes, M. A model to assess tephra clean-up requirements in urban environments. *J. Appl. Volcanol.* **2017**, *6*. [CrossRef]
14. Blake, D.M.; Wilson, T.M.; Stewart, C. Visibility in airborne volcanic ash: Considerations for surface transportation using a laboratory-based method. *Nat. Hazards*. in review.
15. Pyle, D.M. The thickness, volume and grain size of tephra fall deposits. *Bull. Volcanol.* **1989**, *51*, 1–15. [CrossRef]
16. Wilson, D.J. An Analysis of the Seasonal and Short-Term Variation of Road Pavement Skid Resistance. Ph.D. Thesis, Department of Civil and Environmental Engineering, University of Auckland, Auckland, New Zealand, 2006.
17. Warrick, R.A. *Four Communities under Ash*; Institute of Behavioural Science, University of Colorado: Boulder, CO, USA, 1981.
18. Cole, J.; Blumenthal, E. Evacuate: What an evacuation order given because of a pending volcanic eruption could mean to residents of the Bay of Plenty. *Tephra* **2004**, *21*, 46–52.
19. Cole, J.W.; Sabel, C.E.; Blumenthal, E.; Finnis, K.; Dantas, A.; Barnard, B.; Johnston, D.M. GIS-based emergency and evacuation planning for volcanic hazards in New Zealand. *Bull. N. Z. Soc. Earthq. Eng.* **2005**, *38*, 149–164.
20. Wilson, T.M. *Unpublished Field Notes from the Hudson Eruption Field Visit*; University of Canterbury: Christchurch, New Zealand, 2009.
21. Nairn, I.A. *The Effects of Volcanic Ash Fall (Tephra) on Road and Airport Surfaces*; GNS Science Report 2002/13; GNS Science: Lower Hutt, New Zealand, 2002; p. 32.

22. Barnard, S. The Vulnerability of New Zealand Lifelines Infrastructure to Ashfall. Ph.D. Thesis, Hazard and Disaster Management, University of Canterbury, Christchurch, New Zealand, 2009.
23. Stammers, S.A.A. The Effects of Major Eruptions of Mt Pinatubo, Philippines and Rabaul Caldera, Papua New Guinea, and the Subsequent Social Disruption and Urban Recovery: Lessons for the Future. Master's Thesis, University of Canterbury, New Zealand, 2000.
24. Durand, M.; Gordon, K.; Johnston, D.; Lorden, R.; Poirot, T.; Scott, J.; Shephard, B. *Impacts and Responses to Ashfall in Kagoshima from Sakurajima Volcano—Lessons for New Zealand*; GNS Science Report 2001/30; GNS Science: Lower Hutt, New Zealand, 2001; p. 53.
25. Johnston, D.M. Physical and Social Impacts of Past and Future Volcanic Eruptions in New Zealand. Ph.D. Thesis, Massey University, Palmerston North, New Zealand, 1997.
26. Small Explosion Produces Light Ash Fall at Soufriere Hills Volcano, Montserrat. United States Geological Survey. Available online: <https://volcanoes.usgs.gov/ash/ashfall.html#eyewitness> (accessed on 20 October 2015).
27. Leonard, G.S.; Johnston, D.M.; Williams, S.; Cole, J.W.; Finnis, K.; Barnard, S. *Impacts and Management of Recent Volcanic Eruptions in Ecuador: Lessons for New Zealand*; GNS Science Report 2005/20; GNS Science: Lower Hutt, New Zealand, 2006.
28. Wilson, T.M.; Cole, J.; Johnston, D.; Cronin, S.; Stewart, C.; Dantas, A. Short- and long-term evacuation of people and livestock during a volcanic crisis: Lessons from the 1991 eruption of Volcán Hudson, Chile. *J. Appl. Volcanol.* **2012**, *1*, 1–11. [CrossRef]
29. Wilson, T.M. *Unpublished Field Notes from the Chaitén Eruption Field Visit*; University of Canterbury: Christchurch, New Zealand, 2008.
30. Jamaludin, D. BORDA Respond to Merapi Disaster. Bremen Overseas Research and Development Association, South East Asia, 2010. Available online: <http://www.borda-sea.org/news/borda-sea-news/article/borda-respond-to-merapi-disaster.html> (accessed on 20 October 2015).
31. Wilson, T.; Outes, V.; Stewart, C.; Villarosa, G.; Bickerton, H.; Rovere, E.; Baxter, P. *Impacts of the June 2011 Puyehue-Cordón Caulle Volcanic Complex Eruption on Urban Infrastructure, Agriculture and Public Health*; GNS Science Report 2012/20; GNS Science: Lower Hutt, New Zealand, 2013; p. 88.
32. Wilson, T.M. *Unpublished Field Notes from the Shinmoedake Eruption Field Visit*; University of Canterbury: Christchurch, New Zealand, 2011.
33. Blake, D.M.; Wilson, G.; Stewart, C.; Craig, H.M.; Hayes, J.L.; Jenkins, S.F.; Wilson, T.M.; Horwell, C.J.; Andreastuti, S.; Daniswara, R.; et al. *The 2014 Eruption of Kelud Volcano, Indonesia: Impacts on Infrastructure, Utilities, Agriculture and Health*; GNS Science Report 2015/15; GNS Science: Lower Hutt, New Zealand, 2015; p. 139.
34. The Sub-Plinian Eruption of Mt Kelut Volcano on 13 Feb 2014. *Volcano Discovery*. 2014. Available online: <http://www.volcanodiscovery.com/kelut/eruptions/13feb2014plinian-explosion.html> (accessed on 31 October 2016).
35. Highway Research Board. *National Cooperative Highway Research Program Synthesis of Highway Practice 14: Skid Resistance*; National Academy of Sciences: Washington, DC, USA, 1972.
36. Dookeeram, V.; Nataadmadja, A.D.; Wilson, D.J.; Black, P.M. The skid resistance performance of different New Zealand aggregate types. In Proceedings of the IPENZ Transportation Group Conference, Shed 6, Wellington, New Zealand, 23–26 March 2014.
37. International Civil Aviation Organisation, Regional Aviation Safety Group (Asian and Pacific Region). *Industry Best Practices Manual for Timely and Accurate Reporting of Runway Surface Conditions by ATS/AIS to Flight Crew*. 2013. Available online: <http://www.icao.int/APAC/Documents/edocs/FS-07IBP%20Manual%20on%20Reporting%20of%20Runway%20Surface%20Condition.pdf> (accessed on 2 October 2015).
38. U.S. Department of Transportation, Federal Aviation Administration. *Measurement, Construction and Maintenance of Skid-Resistant Airport Pavement Surfaces*. Advisory Circular 150/5320-12C. 1997. Available online: http://www.faa.gov/documentLibrary/media/advisory_circular/150-5320-12C/150_5320_12c.PDF (accessed on 3 October 2015).
39. *Airport Runways: Skid Resistance and Rubber Removal*. *Blastrac*. 2015. Available online: <http://pdf.aeroexpo.online/pdf/blastrac/airport-runways-skid-resistance-rubber-removal/168551-3763.html> (accessed on 2 August 2017).
40. Wilson, D.J.; Chan, W. *The Effects of Road Roughness (and Test Speed) on GripTester Measurements*; New Zealand Transport Agency Research Report 523; Clearway Consulting Ltd.: Auckland, New Zealand, 2013.
41. Asi, I. Evaluating skid resistance of different asphalt concrete mixes. *Build. Environ.* **2007**, *42*, 325–329. [CrossRef]

42. World Road Association-PIARC. Technical committee report on road surface characteristics, Permanent International Association of Road Congress. In Proceedings of the 18th World Congress, Brussels, Belgium, 13–19 September 1987.
43. Ergun, M.; Iyınam, S.; Iyınam, F. Prediction of road surface friction coefficient using only macro- and microtexture measurements. *J. Transp. Eng.* **2005**, *131*, 311–319. [CrossRef]
44. Manual, B.P. *Operation Manual of the British Pendulum Skid Resistance Tester*; Wessex Engineering Ltd.: Victoria, BC, Canada, 2000.
45. Skid Tester: AG190. Impact Test Equipment Ltd. Available online: http://www.impact-test.co.uk/docs/AG190_HB.pdf (accessed on 4 November 2014).
46. Benedetto, J. A decision support system for the safety of airport runways: The case of heavy rainstorms. *Transp. Res. Part A Policy Pract.* **2002**, *8*, 665–682. [CrossRef]
47. Andrey, J. Relationships between weather and traffic safety: Past, present and future directions. *Climatol. Bull.* **1990**, *24*, 124–136.
48. Cova, T.; Conger, S. Transportation hazards. In *Transportation Engineers' Handbook*; Kutz, M., Ed.; Centre for Natural and Technological Hazards, University of Utah: Salt Lake City, UT, USA, 2003.
49. Bennis, T.A.; De Wit, L.B. PIARC State-of-the-Art on Friction and IFI. In Proceedings of the 1st Annual Australian Runway and Roads Friction Testing Workshop, Sydney, Australia, 5 August 2003.
50. Persson, B.N.J.; Tartaglino, U.; Albohr, O. Rubber friction on wet and dry road surfaces: The sealing effect. *Phys. Rev. B* **2005**, *71*, 035428. [CrossRef]
51. Do, M.T.; Cerezo, V.; Zahouani, H. Laboratory test to evaluate the effect of contaminants on road skid resistance. *Proc. Inst. Mech. Eng. Part J J. Eng. Tribol.* **2014**, *228*, 1276–1284. [CrossRef]
52. Qin, X.; Noyce, D.; Lee, C.; Kinar, J.R. Snowstorm event-based crash analysis. *Transp. Res. Rec.* **2006**, *1948*, 135–141. [CrossRef]
53. Khattak, A.J.; Knapp, K.K. Interstate highway crash injuries during winter snow and non-snow events. *Transp. Res. Board* **2001**, *1746*, 30–36. [CrossRef]
54. Oh, S.; Chung, K.; Ragland, D.R.; Chan, C. Analysis of wet weather related collision concentration locations: Empirical assessment of continuous risk profile. In Proceedings of the 88th Annual Meeting of the Transportation Research Board, Washington, DC, USA, 11–15 January 2009.
55. Abdel-Aty, M.; Ekram, A.-A.; Huang, H.; Choi, K. A study on crashes related to visibility obstruction due to fog and smoke. *Accid. Anal. Prev.* **2011**, *43*, 1730–1737. [CrossRef] [PubMed]
56. Aström, H.; Wallman, C. *Friction Measurement Methods and the Correlation between Road Friction and Traffic Safety: A Literature Review*; Swedish National Road and Transport Research Institute (VTI): Linköping, Sweden, 2001.
57. Lester, T. *Pedestrian Slip Resistance Testing: AS/NZS 3661.1:1993*; Opus International Consultants Ltd.: Lower Hut, New Zealand, 2014.
58. European Aviation Safety Agency. *RuFAB—Runway Friction Characteristics Measurement and Aircraft Braking: Volume 3, Functional Friction*; Research Project EASA 2008/4; BMT Fleet Technology Limited: Kanata, ON, Canada, 2010; Available online: <https://easa.europa.eu/system/files/dfu/Report%20Volume%203%20-%20Functional%20friction.pdf> (accessed on 5 October 2015).
59. Sarna-Wojcicki, A.M.; Shipley, S.; Waitt, R.B.; Dzurisin, D.; Wood, S.H. Areal distribution, thickness, mass, volume, and grain size of air-fall ash from the six major eruptions of 1980. In *The 1980 Eruptions of Mount Saint Helens*; USGS Numbered Series 1250; Lipman, P.W., Mullineaux, D.R., Eds.; U.S. Government Publishing Office: Washington, DC, USA, 1981; pp. 577–600.
60. Matsumoto, H.; Okabyashi, T.; Mochihara, M. Influence of eruptions from Mt. Sakurajima on the deterioration of materials. In Proceedings of the Kagoshima International Conference on Volcanoes, Kagoshima, Japan, 19–23 July 1988; pp. 732–735.
61. Delmelle, P.; Villiéras, F.; Pelletier, M. Surface area, porosity and water adsorption properties of fine volcanic ash particles. *Bull. Volcanol.* **2005**, *67*, 160–169. [CrossRef]
62. Heiken, G.; Wohletz, K. *Volcanic Ash*; University of California Press: Berkeley, CA, USA, 1985.
63. Wardman, J.B.; Wilson, T.M.; Bodger, P.S.; Cole, J.W.; Johnston, D.M. Investigating the electrical conductivity of volcanic ash and its effect on HV power systems. *Phys. Chem. Earth* **2012**, *45–46*, 128–145. [CrossRef]

64. Labadie, J.R. Volcanic Ash Effects and Mitigation. Adapted from a Report Prepared in 1983 for the Air Force Office of Scientific Research and the Defence Advanced Research Projects Agency. 1994. Available online: https://volcanoes.usgs.gov/vsc/file_mgr/file-126/Doc%209691_3rd%20ed_Appendix-A.pdf (accessed on 6 August 2017).
65. Heiken, G.; Murphy, M.; Hackett, W.; Scott, W. *Volcanic Hazards to Energy Infrastructure-Ash Fallout Hazards and Their Mitigation*; World Geothermal Congress: Florence, Italy, 1995; pp. 2795–2798.
66. Miller, T.P.; Casadevall, T.J. Volcanic ash hazards to aviation. In *Encyclopedia of Volcanoes*, 1st ed.; Sigurdsson, H., Houghton, B., Rymer, H., Stix, J., McNutt, S., Eds.; Academic Press: San Diego, CA, USA, 1999; pp. 915–930.
67. Gordon, K.D.; Cole, J.W.; Rosenberg, M.D.; Johnston, D.M. Effects of volcanic ash on computers and electronic equipment. *Nat. Hazards* **2005**, *34*, 231–262. [CrossRef]
68. Van Traffic Accident on Slippery Road, iStock Photograph 14892158, Andersen, O., 2010. Available online: <http://www.istockphoto.com/photo/van-traffic-accident-on-slippery-road-gm183542417-14892158?st=a141548> (accessed on 1 February 2016).
69. Tuck, B.H.; Huskey, L.; Talbot, L. *The Economic Consequences of the 1989–1990 Mt. Redoubt Eruptions*; Institute of Social and Economic Research, University of Alaska: Anchorage, Alaska, 1992.
70. Broom, S.J. Characterisation of “Pseudo-Ash” for Quantitative Testing of Critical Infrastructure Components with a Focus on Roofing Fragility. Bachelor’s Thesis, University of Canterbury, Christchurch, New Zealand, 2010.
71. Wilson, G.; Wilson, T.; Cole, J.; Oze, C. Vulnerability of laptop computers to volcanic ash and gas. *Nat. Hazards* **2012**, *63*, 711–736. [CrossRef]
72. Boyle, T. *Skid Resistance Management on the Auckland State Highway Network*; Transit New Zealand: Wellington, New Zealand, 2005. Available online: <http://www.nzta.govt.nz/resources/surface-friction-conference-2005/8/docs/skid-resistance-management-auckland-state-highway-network.pdf> (accessed on 15 June 2015).
73. Bastow, R.; Webb, M.; Roy, M.; Mitchell, J. *An Investigation of the Skid Resistance of Stone Mastic Asphalt Laid on a Rural English County Road Network*; Transit New Zealand: Wellington, New Zealand, 2004; pp. 1–16. Available online: <http://www.nzta.govt.nz/resources/surface-friction-conference-2005/7/docs/investigation-skid-resistance-stone-mastic-asphalt-laid-rural-english-county-road-network.pdf> (accessed on 16 June 2015).
74. ‘Hidden Menace’ on UK’s Roads. *BBC News*. 2015. Available online: http://news.bbc.co.uk/2/hi/programmes/file_on_4/4278419.stm (accessed on 12 February 2015).
75. Get a Grip: Motorcycle Road Safety. *Daily Telegraph*. 2008. Available online: <http://www.telegraph.co.uk/motoring/motorbikes/2750422/Motorcycle-road-safety-Get-a-grip.html> (accessed on 12 February 2015).
76. NZRF (The New Zealand Roadmarkers Federation Inc.). Road Marking is Road Safety. In Proceedings of the 2005 New Zealand Road Marking Federation Inc. Conference, Christchurch, New Zealand, 17–19 August 2005; Potters Asian Pacific: Dandenong, Australia, 2005.
77. NZRF. *NZRF Roadmarking Materials Guide*; New Zealand Roadmarkers Federation Inc.: Auckland, New Zealand, 2009.
78. Downer Group. (Christchurch, New Zealand). Personal communication (by email) with roading supervisor. December 2014–January 2015.
79. ASTM International. *ASTM E303. Standard Test Method for Measuring Surface Frictional Properties Using the British Pendulum Tester*; ASTM E303-93 (Reapproved 2013); ASTM International: West Conshohocken, PA, USA, 2013.
80. TNZ (Transit New Zealand). *Standard Test Procedure for Measurement of Skid Resistance Using the British Pendulum Tester*; Report TNZ T/2:2003; Transit New Zealand: Wellington, New Zealand, 2003.
81. Hill, D.J. Filtering out the Ash: Mitigating Volcanic Ash Ingestion for Generator Sets. Master’s Thesis, Hazard and Disaster Management, University of Canterbury, Christchurch, New Zealand, 2014.
82. ASTM International. *ASTM E965. Standard Test Method for Measuring Pavement Macrotexture Depth Using a Volumetric Technique*; ASTM E965-96 (Reapproved 2006); ASTM: West Conshohocken, PA, USA, 2006.
83. Kagoshima City Office (Kagoshima, Japan). Personal communication (by meeting) with road network and volcanic ash clean-up managers. 8 June 2015.



RESEARCH

Open Access

Evacuation planning in the Auckland Volcanic Field, New Zealand: a spatio-temporal approach for emergency management and transportation network decisions

Erik Tomsen^{1,4}, Jan M Lindsay^{1*}, Mark Gahegan², Thomas M Wilson³ and Daniel M Blake³

Abstract

Auckland is the largest city in New Zealand (pop. 1.5 million) and is situated atop an active monogenetic volcanic field. When volcanic activity next occurs, the most effective means of protecting the people who reside and work in the region will be to evacuate the danger zone prior to the eruption. This study investigates the evacuation demand throughout the Auckland Volcanic Field and the capacity of the transportation network to fulfil such a demand. Diurnal movements of the population are assessed and, due to the seemingly random pattern of eruptions in the past, a non-specific approach is adopted to determine spatial vulnerabilities at a micro-scale (neighbourhoods). We achieve this through the calculation of population-, household- and car-to-exit capacity ratios. Following an analysis of transportation hub functionality and the susceptibility of motorway bridges to a new eruption, modelling using dynamic route and traffic assignment was undertaken to determine various evacuation attributes at a macro-scale and forecast total network clearance times. Evacuation demand was found to be highly correlated to diurnal population movements and neighbourhood boundary types, a trend that was also evident in the evacuation capacity ratio results. Elevated population to evacuation capacity ratios occur during the day in and around the central city, and at night in many of the outlying suburbs. Low-mobility populations generally have better than average access to public transportation. Macro-scale vulnerability was far more contingent upon the destination of evacuees, with favourable results for evacuation within the region as opposed to outside the region. Clearance times for intra-regional evacuation ranged from one to nine hours, whereas those for inter-regional evacuation were found to be so high, that the results were unrealistic. Therefore, we conclude that, from a mobility standpoint, there is considerable merit to intra-regional evacuation.

Keywords: Emergency management; Geospatial analysis; Transportation modelling; Vulnerability; Hazard; Risk

Introduction

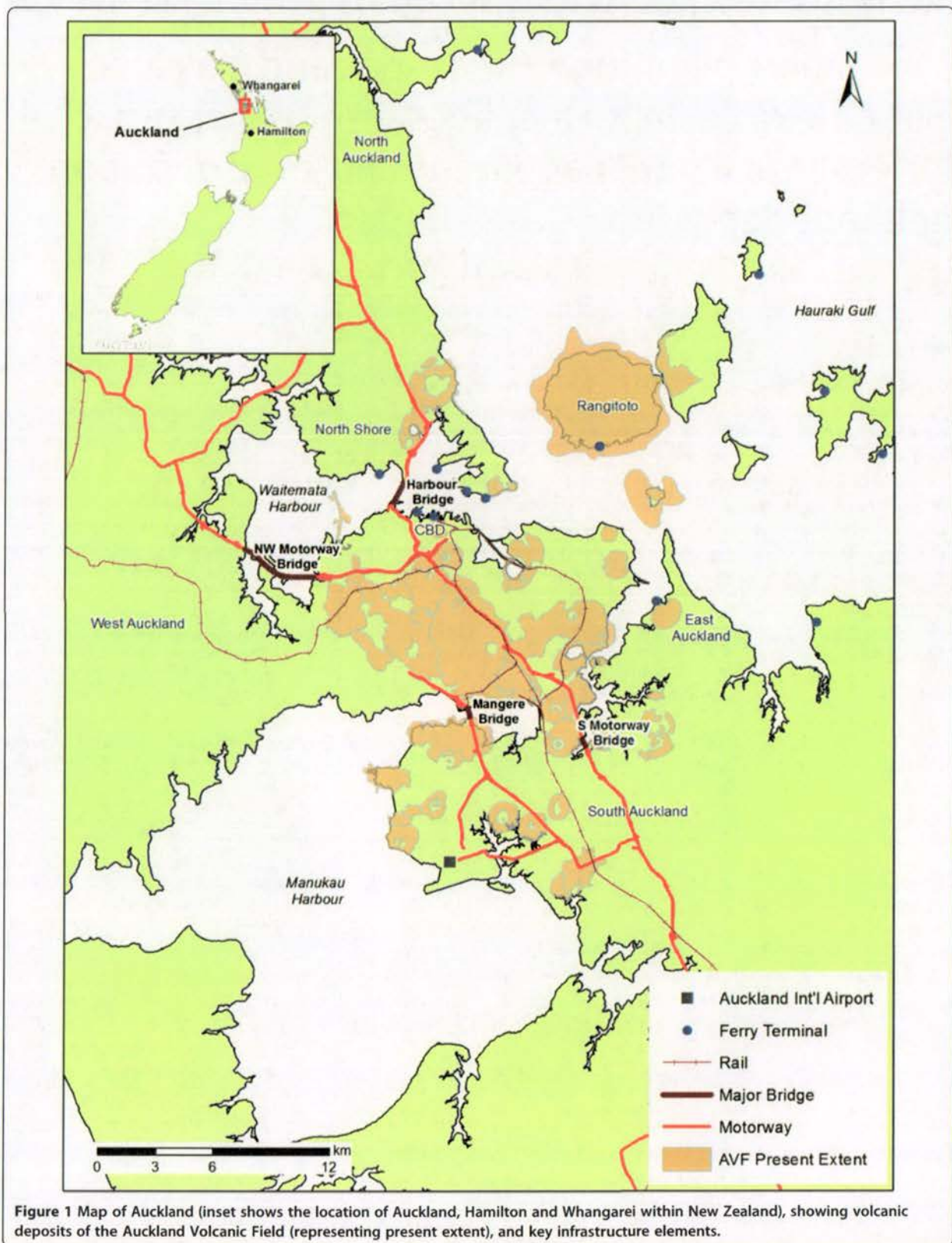
Evacuations are, and most likely will continue to be, the most common and efficient emergency management strategy when a hazardous event threatens and puts at risk the safety of those within the area (Moriarty et al. 2007). Evacuations are also becoming increasingly frequent worldwide as humans continue to develop in hazardous areas and improved technology in many countries allows for prior warnings and the movement

of people before a disaster strikes (Sparks 2003, Woo and Grossi 2009). However, evacuations can produce long-term negative effects such as psychological trauma, and disruption of community cohesion and employment and economic continuity (e.g. Mileti et al. 1991, Lindell and Perry 1992, Cola 1996, Tobin and Whiteford 2002, Perry and Lindell 2003). Poorly managed evacuations tend to lead to a strong resentment of government which, in turn, decreases the ability of emergency management organisations to act effectively in the future (MCDEM 2008). Therefore, effective planning of an evacuation is essential.

* Correspondence: j.lindsay@auckland.ac.nz

¹School of Environment, The University of Auckland, Private Bag 92019, Auckland, New Zealand

Full list of author information is available at the end of the article



Volcanic eruptions are capable of producing a spectrum of hazards which are harmful to humans. These hazards range from highly destructive phenomena such as pyroclastic density currents, debris avalanches, lava flows and lahars that typically destroy everything in their path, to less destructive yet highly disruptive phenomena such as ash fall, volcanic tremor and gas release. As many volcanoes and volcanic regions around the world are already heavily populated, the most effective means of risk reduction will be to identify the most hazardous areas and evacuate the population from the danger zone prior to an eruption (Marzocchi and Woo 2007, Lindsay et al. 2011, Sandri et al. 2012).

The city of Auckland, New Zealand, with a population of ~1.5 million as of December 2012, is built within the 360 km² potentially active basaltic Auckland Volcanic Field (AVF) (Figure 1), with the last eruption occurring just 550 years ago (Needham et al. 2011). Auckland's geography poses significant constraints for evacuation planning. The city is located on an isthmus bounded by the Waitemata Harbour to the northeast and Manukau Harbour to the southwest. As a result, all land-based transport into and out of the city is constricted through narrow stretches of land serviced by four motorway bridges which form critical links in Auckland's transportation network (Figure 1). To date, there has been no major modelling-based study conducted on the mass evacuation capacity of Auckland. Previous evacuation planning has been mainly strategic and lacking in geospatial analysis and physical evacuation procedures that can be used operationally (Auckland CDEM Group 2008a, Auckland CDEM Group 2008b, Tomsen 2010).

In this study we adopt a novel, non-specific approach (Shulman 2008) in considering the spatial and temporal distribution of population and transport networks across Auckland and how they affect mass evacuation planning. Spatial network analysis is used to determine the geographic functionality of major transport origin and destination points and we determine the relative vulnerabilities of the key motorway bridges to new AVF eruptions. We then assess micro-evacuation vulnerability by combining spatial network analysis with population evacuation demand to calculate evacuation capacity ratios for individuals, households and vehicles. Finally, we employ modelling using dynamic route and traffic assignment to measure evacuation attributes at a macro-scale and forecast total network clearance times. This quantitative study thus serves to fill the informational void and provides emergency management officials with a more holistic understanding of the local variations in susceptibility to mass evacuations, particularly those related to volcanic activity in the AVF.

Evacuation planning

There is a broad body of literature on effective evacuation planning. Many studies have attempted to classify

evacuations into various types (e.g. Baker 1991, Ketteridge et al. 1996, Wolshon et al. 2001, Marrero et al. 2010) and others have focussed on emergency response activities (e.g. Cova 1999, Cutter 2003, Marzocchi and Woo 2007, Moriarty et al. 2007, Shaluf 2008). The core components to this evacuation planning can be summarised as: 1) conditions under which an evacuation may be necessary; 2) 'at risk' people/communities who may require evacuation; 3) evacuation routes and destinations; and 4) the resources and time required to evacuate 'at risk' people/communities (MCDEM, 2008).

Identifying when an evacuation is necessary

Evacuation can be classified as an "organised, phased, and supervised withdrawal, dispersal, or removal of civilians from dangerous or potentially dangerous areas, and includes their reception and care in safe areas" (U.S. Department of Transportation 2006, p.2-1). Evacuation becomes necessary when the benefits of leaving significantly outweigh the risk of other options, such as 'sheltering-in-place'. In a volcanic context, evacuation is a response strategy – an effort to preserve human life (Marzocchi and Woo 2007, Auckland CDEM 2013). In order to assist with evacuations, plans are created in advance, identifying key personnel, areas at risk, and mitigation measures to enact (Moriarty et al. 2007). In New Zealand, the Mass Evacuation Plan (MCDEM 2008) is the key sub-national level plan which aims to detail a range of considerations and actions for the mass evacuation of people from a hazardous environment to a relative place of safety (Auckland CDEM Group 2008b). The Auckland Volcanic Field Contingency Plan is more specific and includes planning arrangements for evacuations resulting from an eruption within the AVF (Auckland CDEM 2013). According to the plan, an evacuation will be called by the Auckland CDEM Group if hazard assessment indicates urban or strategic areas may lie within 5 kilometres of the inferred eruption centre and/or there is a potential risk to life.

'At risk' people and communities

There is varied focus in the literature about which group or groups tend to be the most 'at risk'. Low-income populations are studied in detail by some (e.g. Morrow 1999, Chakraborty et al. 2005), while others (e.g. Bascetta 2006, Dosa et al. 2007) focus on the elderly and disabled. The *low-mobility population* (i.e. those without access to a private vehicle), however, are discussed by many and we examine this group further as they will require public modes of transport (Leonard 1985, Hushon et al. 1989, Wolshon et al. 2001). Ideally, people within an evacuation zone evacuate and people resident outside the zone shelter in place. However, evacuations are typically far more complex, with some choosing to remain

within a zone, and others outside the evacuation zone voluntarily evacuating (termed *shadow evacuation*, Baker 1991).

Uncertainty as to who will stay and go (the *population evacuation demand*) makes it difficult to establish credible time estimates for those evacuating, although this is fundamental for evacuation planning. The population evacuation demand is dependent on numerous variables including external conditions such as weather, location of the hazard source and time, as well as human behavioural characteristics inherent in the population (Wolshon 2006, Tomsen 2010). Research on evacuation response rates for hurricane-based evacuations in the United States found that evacuation rates ranged between 33-97% during the same hurricane, with an average of 47.5% (Baker 1991). People in high-risk areas, on average, were found to be more than twice as likely to evacuate when compared to low-risk areas. This was attributed to two factors: people residing in high-risk areas are aware of the hazardousness of their location and/or public officials go to greater lengths to evacuate the residents of these areas (Baker 1991). Less data is available for non-compliance to shelter-in-place orders, a factor that often causes emergency management officials the most difficulty. Two recent surveys regarding such *unofficial evacuees* reported nearly 60% of respondents leaving before evacuation orders were given during Hurricanes Lili and Katrina (Lindell et al. 2005, Lindell and Prater 2006).

Evacuation routes and destinations

Evacuation route choice is a complex decision-making process. Some researchers believe that in emergency situations, evacuees will take any possible egress route (Moriarty et al. 2007). However, others contend that people will take the most familiar routes (predominantly motorways), which often become overloaded while capacity on alternative routes remains unused (Prater et al. 2000, Dow and Cutter 2002). During Hurricane Katrina, drivers were more influenced by familiarity with the route than traffic conditions they experienced en route (Lindell and Prater 2006). As stated in the Mass Evacuation Plan for New Zealand (MCDEM 2008, p.56), "the planning process should decide upon primary and secondary evacuation routes from an anticipated affected area", and "evacuation routes should be designed with due consideration to local area hazard maps to ensure that selected routes are appropriate for anticipated hazards". Any potential bottlenecks in traffic movement should also be identified (MCDEM 2008). Many studies in the U.S. have shown that, despite the enormous demand during hurricane evacuations, many roads carry flows well below the predicted maximums (Wolshon 2008). However, contraflow systems are frequently used

for evacuations in the U.S. and plans are often well engineered and publicised (Wolshon 2002). Indeed, although studies on hurricane-based evacuations provide valuable information, many differences in characteristics such as risk perception, familiarity and cultural geography, mean that the results cannot be easily extrapolated to other hazards or locations (Marrero et al. 2010). Transportation modelling can be used to help with specific planning objectives, and allow the testing of various assumptions and alternatives.

During evacuations people tend to favour temporary re-location in second homes, hotel/motel accommodation or with family and friends, rather than seeking public shelter (Quarantelli 1985). However, in a mass evacuation, many of the low mobility population and those without social networks or financial resources will require assistance with accommodation from emergency management authorities. For smaller events, 'all-in-one welfare facilities' may be all that are required to service evacuees. However, when the volume of evacuees is likely to be large, separate evacuation and recovery centres may need to be established (MCDEM 2008).

Evacuation resources and time

The ability of a community to respond to a disaster and cope with its consequences largely depends on its level of preparedness. However, the impact on an evacuated community is reduced when evacuation is carried out in a well-managed and organised manner. During a mass evacuation, transportation networks are the most critical components of a region's infrastructure network, as they facilitate the mobility of the human population. In developed countries, private vehicles have often been the predominant form of mass evacuation (Quarantelli 1980, Drabek 1986, Lindell and Perry 1992, Tierney et al. 2001, Cole and Blumenthal 2004). This is likely due to their prominence in today's society, the flexibility of route and destination choice they allow, as well as their asset value, which many evacuees seek to retain. A survey conducted in 2008 by the New Zealand Ministry of Civil Defence and Emergency Management with regard to evacuation behaviour in Auckland, confirmed this tendency. Of the 2,050 people in the survey, 91.3% would choose to leave with their own vehicle if required to evacuate due to an AVF eruption (Horrocks 2008b). Alternative forms of transportation such as trains and buses can also be used for evacuation purposes and are particularly beneficial to the low mobility population who may strongly rely on their provision.

When considering the time and resources required for evacuation, it is important to acknowledge the regular diurnal population shift which occurs in most developed countries when people travel to places of work and learning during the day and return home again at night.

A national telephone survey conducted by Klepeis et al. (2001) across the U.S. demonstrated that while more than 90% of people are at home and indoors between the hours of 11 pm and 5 am, less than 35% are there from 10 am to 3 pm. We expect similar trends to occur in New Zealand, particularly in city environments, although there is little data for comparison at present. In addition to the standard diurnal shift, other spatio-temporal movement patterns exist in urban areas. On weekends and during school holidays, when many residents leave for recreational activities and travel, the population in the urban area sinks compared to its weekday highs. At other times, such as during major concerts, sporting events and conventions, the urban population may grow substantially. When evacuation time estimates are available, emergency management officials can determine how far in advance evacuation orders should be issued. This allows authorities to balance the competing demands of enduring public safety and unnecessary costs associated with imprecise or unnecessary evacuations, i.e. false alarms. Because running evacuation drills is difficult due to the large areas and populations involved, computer simulations based on various traffic analysis models offer the next best option (Franzese and Liu 2008). Current emergency management planning in Auckland assumes that a major evacuation (such as for an impending volcanic eruption) would require 48 hours for authorities to implement (this includes a pre-evacuation-call planning period). This was illustrated in the lead up to the simulated evacuation during a major 2008 exercise based on an Auckland Volcanic Field eruption, *Exercise Ruaumoko*, when civil authorities wanted to know when the 48 hour 'time window' before outbreak had been entered (Lindsay et al. 2010).

The Auckland Volcanic Field

When considering evacuation planning for a volcanic field eruption the following factors related to the hazard must be considered: the likelihood; the number of vents expected; the location(s) of the new vent; the area impacted by volcanic hazards (hazard footprint), which is dependent on the style and size of eruptive activity produced during vent opening; and how much warning will be provided by volcano monitoring systems. The two most important factors are the hazard footprint and the location of the eruption, which together allow determination of the necessary spatial extent of the evacuation zone. This section reviews the past known eruptive history of the AVF with particular focus on these two factors.

The AVF (Figure 1) is a geologically young, generally monogenetic, intraplate volcanic field made up of over 50 small basaltic volcanoes, which has been active for

250,000 years with the last eruption ~550 years ago (Lindsay et al. 2010, Needham et al. 2011, Shane et al. 2013). Being generally monogenetic in nature, each vent is typically only active for a single eruption sequence and new eruptions usually occur in a different location from those before. To date there have been no spatio-temporal trends identified for vents in the AVF. Recent algorithmic analysis by Bebbington and Cronin (2011) has discounted earlier studies that suggested spatio-temporal clustering in the AVF. Instead the spatial and temporal aspects appear independent; hence the location of the last eruption provides no information about the next location.

Previous AVF eruptions have typically been small in volume (<0.1 km³, Allen and Smith 1994), However the last two eruptions, Rangitoto (2 km³) and Mt. Wellington (0.17 km³) are two of the largest in volume, suggesting a possible change in future eruptive behaviour (Lindsay 2010).

The eruption style during vent opening is typically phreatomagmatic, due to rising magma interacting with groundwater and/or seawater (if a vent occurs in the ocean). Some eruptions cease after this stage, leaving broad maars or explosion craters typically 1-2 kilometres in diameter. Where the eruptions continue beyond this stage, subsequent activity is of magmatic Hawaiian style, which produces scoria cones and lava flows. The explosive phreatomagmatic AVF eruptions have generated volcanic hazards such as base surges, a type of pyroclastic density current (denser-than-air flows which can travel at 200-300 km h⁻¹ and be >200 °C; Browne 1958, Belousov et al. 2007), shock-waves and ballistics (material >64 mm erupted from the vent) which are highly destructive to areas up to 3 kilometre radius of the vent. Secondary hazards, such as earthquakes, tephra fall and gas release, would also be noticed throughout the entire region. The footprint of these hazards from previous AVF eruptions and those of other analogous volcanoes have been used to calculate evacuation zones for future events. Current contingency and mass evacuation plans call for areas of 3 kilometres ("Primary Evacuation Zone") and 5 kilometres ("Secondary Evacuation Zone") radius from the erupting vents to account for base surges (Beca Carter Hollings and Ferner Ltd. 2002, Auckland CDEM Group 2008b, Auckland CDEM 2013).

Finally, It is likely that civil authorities and area residents will only be provided with at most a few weeks and as little as a few days of warning time prior to an eruption (Beca Carter Hollings and Ferner Ltd. 2002). This is based on the expected fast magma ascent rates (1-10 cm s⁻¹) that basaltic volcanic fields are known to exhibit (Blake et al. 2006, Sherburn et al. 2007). Early detection of precursory activity is therefore critical. However, the factors contributing to a decision by emergency

management officials to call a mass evacuation bring significant levels of uncertainty to mass evacuation planning in Auckland. Furthermore, the exact vent area is likely to be unknown until shortly before outbreak (Blake et al. 2006). One attempt to address this uncertainty was presented by Sandri et al. (2012), who developed a cost-benefit analysis model for evacuation planning by weighing the cost of issuing evacuation warnings for geographic areas (represented by lost work potential, warning costs, movement costs etc.) against the benefit of evacuating (represented by the number of lives saved). When the benefits of evacuating a certain area exceed the associated costs, an evacuation is deemed warranted. The point of changeover is the ideal boundary to use as the time to call for evacuation. Sandri et al. (2012) calculated probability threshold values for a range of magnitudes: small effusive, moderate phreatomagmatic and large phreatomagmatic eruptions. Evacuation radii for these three scenarios were established at 3.5, 5 and 8 kilometres respectively. These are somewhat consistent with the primary (3 km radius) and secondary (5 km radius) evacuation zones in the AVF contingency plan, but crucially suggest an additional larger radius of 8 km should be considered in evacuation demand analysis. The evacuation area was also found to change in size with time in the lead-in period, due to a reduction in the uncertainty in the vent location and increase in the probability of an eruption. Thus, there is a trade-off between these two factors (area and time) that dictates which cells must be evacuated, and when (Sandri et al. 2012). Given the uncertainty in vent location (and the subsequent need to wait until close to outbreak to define the evacuation area) it is likely that the evacuation will need to be carried out quickly, i.e. within the 48-hour evacuation time required by civil authorities.

Data sources

Two primary types of data are used in this study: population data and infrastructure data. Population data from Statistics New Zealand, which provides data in its *Census of Population and Dwellings*, was sourced from the results of the 2006 census. Census areas are arranged hierarchically with *regions* representing the most extensive geographical areas, and *meshblocks* representing the smallest areas. The more detailed meshblock scale is used for determining evacuation demand in this research. We also use *neighbourhood areas*; defined here as areas bounded by major and arterial roads, motorways, or saltwater inlets. Census data utilised in the research includes night-time population, average household sizes, ages, income levels, vehicle availability per household, and business demography. Data regarding school attendance was obtained from the Ministry of Education. The majority of infrastructure data employed

was provided by the former Auckland Regional Council and were current as of October 2009. This included geospatial road data files, which contained comprehensive attributes for the Auckland region such as road hierarchy, designated speed limits and directionality. In order to facilitate macro-evacuation studies covering areas outside Auckland, major and arterial road and motorway data for Northland and Waikato, produced by NZ Open GPS Maps (2009), was added to the database. Since our study a new Census has been carried out in New Zealand, and we note that it would be worthwhile repeating this study with post-2009 infrastructure data together with the new (2013) Census data once it becomes available.

Methods

Constraining the study area

Various size estimates have been employed to represent the size of the AVF. For this study we adopt the same bounding limits used by Lindsay et al. (2010), reflecting the continuity of the underlying geology and recognising the possibility of eruptions taking place outside the current extent of the AVF. However, we employ an ellipse rather than a rectangular area since established volcanic fields are more often ovalar in shape (Spörl and Eastwood 1997). The resulting ellipsoid (Figure 2) represents the large conservative 'future geologic extent' of the AVF and is used as the theoretical boundary of the field in this study. Subsequent to our study, further work by Le Corvec et al. (2013a,b) has provided new insights into a smaller quantitative boundary for the AVF. Were such a smaller, less-conservative ellipsoid representing the current extent of the AVF used, all of our calculated probabilities would be much larger, as the total area (much of which is water) is reduced. Also, the chance of zero evacuation demand would likely be minimal, particularly if evacuations resulting from tsunami generated by offshore eruptions were incorporated into the study.

Population evacuation demand

Traditional census data in New Zealand reports the population according to their night-time residence but does not cover daytime population figures. Business demographics data from Statistics New Zealand (2008) and school enrolment data for 2009 provided by the Ministry of Education were thus used to estimate Auckland's daytime population. Using employing units with a Goods and Services Tax turnover of \$30,000 or more, there were 593,276 people employed *in* Auckland and 601,638 people employed *from* Auckland, suggesting that roughly 1.4% of Aucklanders leave the region for work. The number of students enrolled in Auckland schools was 244,449. As the Ministry of Education do not code their data to show where students reside, a proxy value

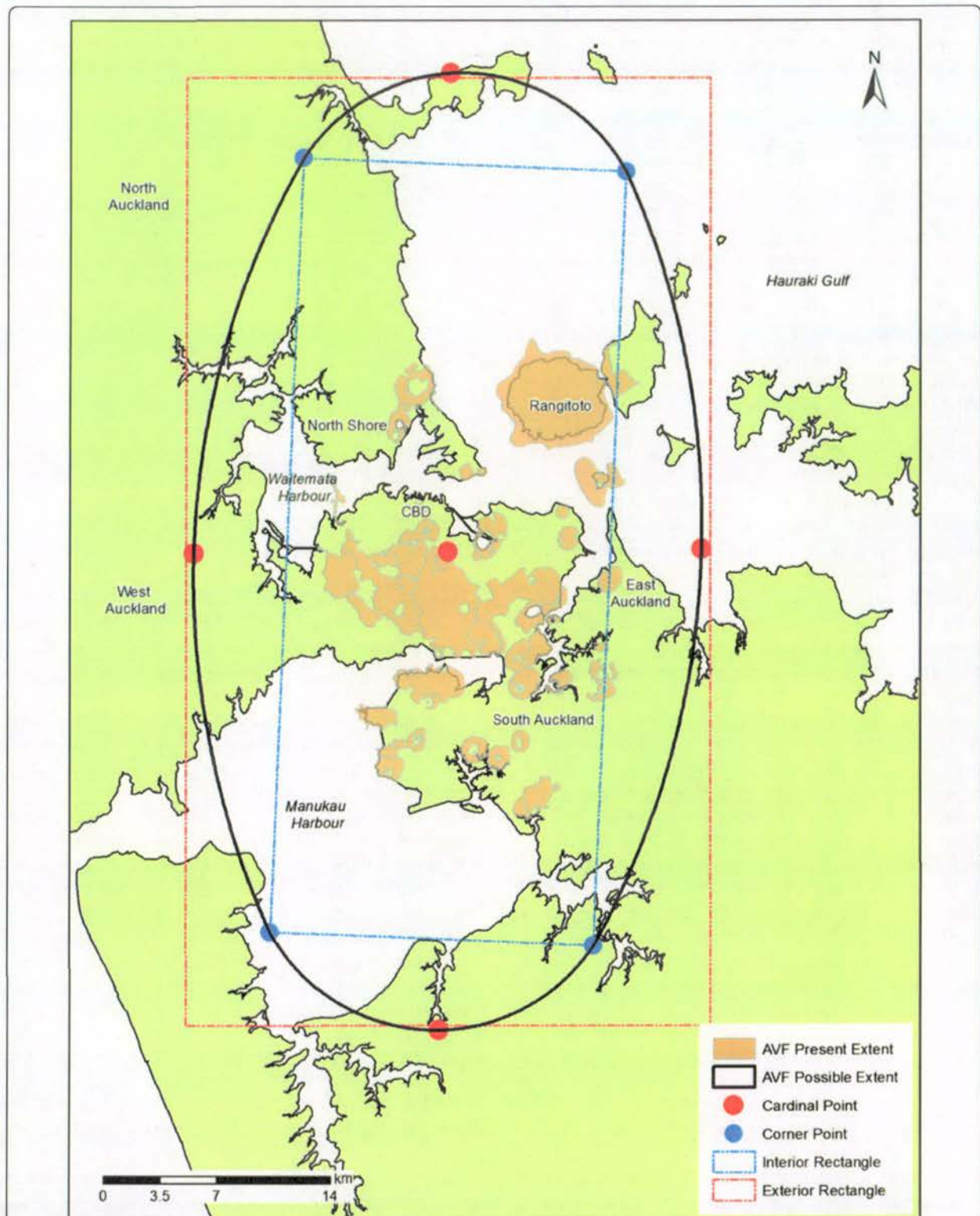


Figure 2 Geometry of the Auckland Volcanic Field. The ellipsoid represents the possible future geologic extent of the AVF and is used in this study as the presumed theoretical boundary of the field.

based on age cohorts from the census data was obtained (sum of age 5-9, 10-14 and 15-19 cohorts). However, as not all people in this range attend school, the proxy value (281,460) overestimates the enrolment generation by 15%. Equation 1, which was used to generate daytime population, used the night-time population as a baseline measure and added the inflows of workers and students, then subtracted their outflows:

$$\text{Day pop.} = \text{Census night pop.} + \text{workers in} \\ + \text{school in} - \text{workers out} - \text{school out} \quad (1)$$

Using the night-time and daytime statistics together allows the magnitude of diurnal movement of Auckland's populations to be calculated. However, although diurnal trends in population are thoroughly assessed in this study, these are largely based on scenarios for a typical weekday. Further work to obtain detailed estimates of population distribution over space and time would greatly assist evacuation planning in Auckland.

To calculate population evacuation demand, we assumed that all evacuees in the danger areas would evacuate, and that there is no shadow evacuation outside of those areas. While these assumptions are simplistic and unlikely to represent the true human dynamics of a mass evacuation, they allow for the creation of baseline values. We also assumed an equal probability distribution of a new vent forming anywhere in the AVF and calculated population evacuation demand (at 100-metre resolution) during day and night for every point in the AVF. This was accomplished first by determining the population density of each census meshblock and transforming the densities into aerial-based population values in ArcGIS (2009). Then, the AVF extent ellipsoid was buffered by the evacuation radius values. This was done to reflect the reality that eruptions occurring on the edge of the AVF will impact those within the evacuation radius even if they are outside the AVF boundary. In the final step of the process, the population evacuation demand was calculated for each 100 m² cell by summing the values of the individual cells within designated neighbourhood distances. The three evacuation radii proposed by Sandri et al. (2012), 3.5, 5 and 8 kilometres, were used as the neighbourhood distances in successive calculations, thus producing three models. Each model was clipped to match the extent of the AVF study area and contour lines were created at intervals of 50,000 people to enable improved visualisation of the data. The cells were also reclassified into 50,000 unit intervals, allowing the results to be displayed numerically as 11 classes. For ease of comparison, we focus our results on the 5 kilometre evacuation radii, which is also the larger of the 'most probable' evacuation radii used in the current AVF contingency plan.

In addition to total number of evacuees, the low-mobility population evacuation demand is also of concern for public authorities, particularly as they may rely on public transportation. Both census and school enrolment data were used to determine the spatial and numeric extent of the population without a vehicle for each meshblock using Equations 2 and 3 for night and day respectively.

$$\text{Low mobility pop. (night)} = \text{no motor vehicle households} \\ \times \text{average household size} \quad (2)$$

$$\text{Low mobility pop. (day)} = (\text{\#motor vehicle households} \\ \times \text{av. household size}) \\ + \text{school enrolment} \quad (3)$$

It was assumed that no school children drive to school. Therefore, all school children are considered low-mobility during the day, but not at night when they return home to their families. Population evacuation demand figures for the low-mobility population were calculated using a similar technique as for the general population, the major alteration being that low-mobility meshblock statistics, rather than total meshblock statistics, were adopted as the inputs. The statistical results were reclassified into 12 classes at 10,000 unit intervals.

Network analysis

Two types of network analysis were conducted in this study: Spatial analysis to determine the geographic functionality of different transport hubs and evacuation destinations; and vulnerability analysis for the four major motorway bridges which are integral to Auckland's transportation network. ArcGIS (2009) was employed, with constraining values such as movement restrictions and distances adopted to calculate populations that reside within easy reach of different transportation assets. Such assets included public transport stops (bus stations, ferry terminals and train stations), boat ramps, marinas and welfare facilities. It should be noted that public transportation in Auckland is more limited at certain times such as at night and at weekends, and that the functionality of such transport depends on the reliability of its workers and their ability and willingness to travel to work, no matter what the timing.

All roads and footpaths in Auckland were used to create the network dataset and the daytime and night-time populations for meshblocks within transport service areas were summed. We chose 30 minutes as the maximum time that evacuees would be willing to walk to a departure point and, based on a consistent walking rate of 5 km h⁻¹, a time interval representing accessibility was set correspondingly. As most boat owners access

boat ramps using motor vehicles, we adopted an accessibility time interval of 15 minutes, based on average rush hour speeds for different road types (Auckland Regional Council 2009b) for this asset type.

The four primary motorway bridges that form essential links in Auckland's transportation network are the Auckland Harbour Bridge and Northwest Motorway Bridge at the north end of the isthmus, and the Southern Motorway Bridge and Mangere Bridge at the south end (Figure 1). For the purpose of this study, the vulnerability of these bridges was based on the likelihood of the structures lying within each of the designated evacuation radii. Geospatial buffers were created for each bridge to match the extent of the three evacuation radii and these were subsequently clipped to the extent of the AVF. The resulting areas were then divided by the total area of the AVF. This provided the probability that any bridge would intersect the evacuation zone and thus would likely be damaged or made unusable by the eruption. The directional vulnerability (i.e. that either bridge in one direction would be impacted) and combined vulnerability of any of the four bridges being impacted was also assessed. We achieved this by merging and intersecting the existing bridge-evacuation radii areas with one another in ArcGIS (2009) and dividing the new areas by the total area of the AVF.

Evacuation vulnerability

Evacuation vulnerability was analysed at both the micro- and macro-scale. In order to assess evacuation difficulty at the micro-scale, we employed a method using population to exit capacity (P/EC) ratios, first pioneered by Cova and Church (1997). Neighbourhoods, which are commonly used for transportation modelling, were used as a key unit of analysis for this study. This was deemed appropriate, as evacuation zones need to be easily differentiated by the public and neighbourhood boundaries (i.e. major and arterial roads, motorways and saltwater inlets) are easily distinguishable by eye. Although there is no mention of boundary delineation in the current mass evacuation plan for Auckland, clear geographic and functional features were used to determine evacuation zones during Exercise Ruaumoko (see Lindsay et al. 2010). Therefore we used saltwater inlets, motorways, and major and arterial roads to define the neighbourhoods and thus evacuation zone boundaries in this study. This ensures that the majority of traffic will flow towards the periphery of the neighbourhood from the onset of evacuation, rather than to a point within the zone, and then outwards. After determining the neighbourhood zones, the points where each road intersected the neighbourhood boundary were designated as exits. Exits were coded according to the neighbourhood they serviced and their capacity, and half of all one-way

streets were removed, as the direction of flow for these was indiscernible. The total exit capacity for each neighbourhood was generated and daytime and night-time populations were calculated based on the neighbourhood areas. Dividing the populations by the total exit capacities thus produced the P/EC ratios.

To statistically test correlations between P/EC ratios and neighbourhoods with different constricting boundary types (i.e. motorways and water), we employed a two-tailed t-test with a 95% confidence interval. The null hypothesis stated that there was statistically no difference between the mean of the first data set (μ_1) and the second data set (μ_2). The alternative hypothesis claimed that the difference is statistically significant. Four t-tests were performed. The first three assessed each of the two constricting boundary types individually and in combination against the neighbourhoods with neither boundary type. The final assessment compared neighbourhoods with neither boundary type against all data values in aggregate.

As most evacuees in developed countries prefer to evacuate by private vehicle, we assumed that each household leaves in one vehicle, and, following the same procedure used to calculate P/EC ratios, household to exit capacity (HH/EC) ratios were calculated. Sensitivity analysis on this assumption was also conducted by assuming that all available vehicles per household are used during evacuation. This was achieved first by using Equation 4, followed by the same method that was used to calculate P/EC ratios, thus determining Car/EC ratios.

$$\text{Cars} = n_{HH}(\text{one car}) \times 1 + n_{HH}(\text{two cars}) \times 2 + n_{HH}(\text{three or more cars}) \times 3 \quad (4)$$

where n_{HH} represents the number of households in each census meshblock.

Equation 4 slightly underestimates the number of cars per meshblock, because it is based on the assumption that no household has more than three cars, which some likely do, though data that would resolve this is unavailable at present.

TransCAD models were built to assess the feasibility of overland movements along the regional roadway network in Auckland and to test various independent variables on a macro-scale to determine the degree to which they impact the network clearance time (TransCAD, developed by Caliper Corporation, is a GIS with highly specialised transportation modelling capabilities). Such models dissect the transportation network as a set of links (roads) and nodes (intersections or endpoints). Centroids are a special set of nodes representing the geographic centre of a Traffic Analysis Zone (TAZ). Centroids begin and end every modelled trip and therefore represent both origin (neighbourhood) and

destination (welfare facility) locations. They are connected by the Auckland road network, which is generalised to improve processing. A generalised road network also has the advantage of more realistically modelling evacuation flows because the public's knowledge of the road network will be imperfect and they are most likely to remain on more familiar routes such as major roads and motorways (Tomsen 2010).

Designated Auckland Civil Defence and Emergency Management welfare facilities were chosen as the destination locations for intra-regional evacuation studies on the macro-scale. This is because, in an ideal situation, all evacuees would go to such a facility to register with emergency management officials before heading to their final destination. For inter-regional analysis, two major welfare facilities outside the Auckland region, one in Hamilton (south) and the other in Whangarei (north) were chosen as the destination locations (Figure 1). For the purpose of this study, the road network outside of the Auckland region was generalised in two ways: motorways only, and motorways in combination with major arterial roads. However, within the Auckland region, all major and arterial roads were utilised, forming the intricate lattice of TAZ boundaries. In macro-evacuation models, TAZs do not contain intra-zonal roads; therefore, secondary roads in Auckland were removed by definition. Vehicle capacity values were assigned to each road type in the models. As capacity values were not available for Auckland, estimates provided in the Brisbane Strategic Transport Model (Brisbane City Council 2007) were adopted. These values range from 1,100 vehicles per lane per hour for arterial roads to 2,100 vehicles per lane per hour for 4-lane motorways. The number of centroid connectors determines the number of neighbourhood exits that are utilised. While this has no impact on intra-zonal movement, the effects of congestion begin as soon as the first non-centroid node is reached. To determine the effect of this congestion, the number of centroid connectors was varied as a form of sensitivity analysis. Other forms of sensitivity analysis included modification for time of day, evacuation radii, vent locations, welfare facility locations, shadow evacuations and various levels of road network detail.

TransCAD models were run for AVF vent locations with minimum and maximum population evacuation demand values using the 5 kilometre evacuation radius (determined from results of the micro-vulnerability work). Since there were multiple locations with no evacuation demand, vent locations furthest from the coast in both Waitemata and Manukau Harbours were selected as the minima. The maximum population evacuation demand value was generated from a vent location one kilometre south of Mount Eden. Additionally, the vent used for Exercise Ruaumoko, 0.7 kilometres

west of Mangere Bridge in the Manukau Harbour (see Lindsay et al. 2010), was also selected as a scenario.

Outputs from TransCAD models include total flows over the entire network, Volume-Over-Capacity (VOC) ratios and total network clearance times. Flows indicate the total volume of traffic passing over each network link, which in turn provides data on which links are most heavily used and thus the most critical during evacuations. Total flows over the entire network equalled the total number of vehicles involved in the evacuation. Flows alone, though useful in visualising movement, cannot predict congestion, because they do not account for the capacity of the road segments. VOC ratios excel at this and are a common measure of assessing movement difficulty (Cova and Church 1997, Church and Cova 2000, Shulman 2008, Marrero et al. 2010). VOC ratios examine the volume of traffic on each lane of the road divided by the lane's capacity (similar to Car/EC ratios, except VOC ratios are based on links rather than zones). High ratios are indicative of congestion and when the VOC approaches 1, the velocity of traffic approaches 0. The clearance time (i.e. the time required to evacuate Auckland) was calculated for different inter- and intra-regional evacuation scenarios by linking the network travel times to the original road network.

TransCAD models, like all other evacuation models, rely on the accuracy of the data they employ and the underlying assumptions within the models. While the baseline datasets of population and road infrastructure are accurate, the derivative datasets used to produce origin-to-destination functions are highly dependent on the validity of numerous assumptions. Some assumptions, including evacuation compliance, shadow evacuation and vehicle use rates can be measured indirectly through questionnaires and tested in models with sensitivity analysis; others, such as the destination of evacuees, can only be presumed and aggregated. Further assumptions are built into the model and cannot be altered. For instance, TransCAD models rely on a constant road network and consistent driver interaction. This ignores the possibility of traffic accidents, network alterations due to ongoing damage, and the possibility of panic or "road rage" on the part of drivers. A further limitation with TransCAD is its click-and-run start-up method, which prevents evacuees from being added to the model at successive time intervals. Essentially, the number of evacuees the model begins with is how many it processes to completion. No variation in preparation time is accounted for. Models are also limited to egress population movements, disregarding background traffic. Background traffic is a legitimate concern if little forewarning is provided (Urbanik 2000); yet, when sufficient forewarning is provided (as is expected with an AVF

eruption), background traffic is unlikely to pose significant issues (Lindell and Prater 2007).

Results

Population evacuation demand

The total night-time population of Auckland, based on the raw census data (2006) was 1,264,011. The daytime population based on typical worker and student migration was calculated to be 1,218,638. Thus, a loss of 3.6% of the population is noted in the statistics and used as the basis of further analysis for this study. Geographic analysis of diurnal movement in Auckland showed that areas of greatest population gain during the day were business areas, whereas areas of greatest population loss were residential areas. The Central Business District (CBD) had nearly three times the population influx of any of Auckland's other 238 neighbourhoods and thus is likely to be much more difficult to evacuate during the day than night.

The numeric results of the population evacuation demand model outputs are presented in Table 1. Two outputs of this model, utilising the 5 kilometre evacuation radii and the two time variables, are shown in Figure 3. The percentage values reflect the proportion of the cells in the AVF that fall into each category. Because this study employs an equal probability distribution of an eruption occurring at any location in the AVF, the percentage values also represent the likelihood that a future AVF eruption will generate the number of evacuees listed in each class. For instance, using a 5 kilometre evacuation radius, there is a 56.4% chance that 1-50,000 evacuees will result from a daytime eruption.

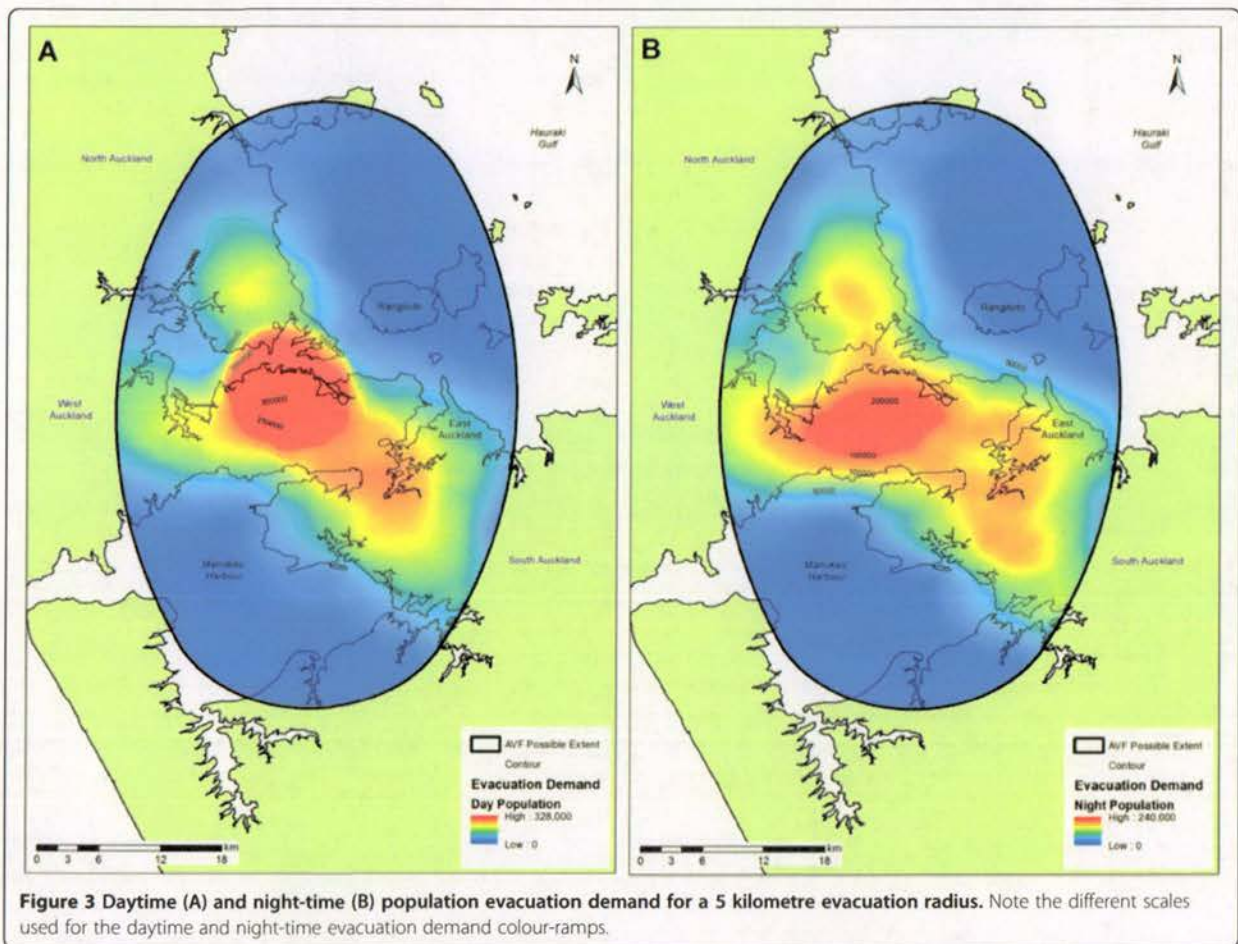
Table 1 Population evacuation demand statistics

Evacuation Demand	Day			Night		
	3.5 km	5 km	8 km	3.5 km	5 km	8 km
0	11.8%	3.9%	0.0%	11.7%	3.9%	0.0%
1 - 50,000	65.5%	56.4%	37.3%	62.3%	50.8%	32.4%
50,000-100,000	18.7%	18.0%	13.0%	23.6%	20.9%	13.7%
100,000-150,000	2.1%	11.2%	12.1%	2.3%	19.5%	11.7%
150,000-200,000	1.2%	5.7%	10.4%	0.0%	3.8%	13.4%
200,000-250,000	0.8%	2.5%	5.9%	0.0%	1.1%	9.7%
250,000-300,000	0.0%	1.7%	5.0%	0.0%	0.0%	7.2%
300,000-350,000	0.0%	0.6%	4.9%	0.0%	0.0%	5.8%
350,000-400,000	0.0%	0.0%	4.3%	0.0%	0.0%	6.0%
400,000-450,000	0.0%	0.0%	4.7%	0.0%	0.0%	0.0%
450,000-500,000	0.0%	0.0%	2.5%	0.0%	0.0%	0.0%
Average	27,210	55,077	137,317	27,088	55,346	134,268
Minimum	0	0	6	0	0	6
Maximum	237,405	327,937	505,677	131,841	239,895	397,549

Larger evacuation radii were found to substantially increase the average and maximum population evacuation demands and diminish the initial spike in evacuation demands present for smaller radii. During daytime, evacuation demand values are high around the CBD area but become more widely dispersed as the radius increases or during night-time. Correspondingly, the maximum evacuation demand values are substantially smaller for night-time than daytime evacuations (the average maximum daytime value is 357,000 using all three radii, while the average maximum night-time value is 256,000). The results show that there are some locations in the AVF that would generate no evacuation demand, because the vents are located sufficiently far offshore (reflected as zero values in Table 1). Using the 3.5 kilometre radius, there is a 12% chance that an eruption will generate no evacuees. Using the 5 kilometre radius, this figure is reduced to 4%, and with an 8 kilometre radius to 0%, though the minimum values remain quite low. However, it should be noted that we do not consider evacuation need due to tsunami generated by offshore volcanic eruptions in our study. Such an event may result in increased evacuation demand in coastal areas.

Low-mobility population evacuation demand

Based on school enrolment figures and households with no vehicles, there are 321,162 people with low-mobility in Auckland during the day and 76,713 people at night. This represents 25.4% and 6.1% of Auckland's total population, respectively. These calculations may overestimate the daytime low-mobility population, since low-mobility groups increasingly use social networks to obtain rides with friends or neighbours rather than relying on public transportation (Lindell and Prater 2007). Additionally, an unknown percentage of school children come from low-mobility households and thus would be double-counted during the day, and some parents may pick up children from school during an evacuation. A proportion of older students may also drive to school, although we expect that this is more prevalent in rural communities than urban centres such as Auckland. All of these variables however, are somewhat counterbalanced by an underestimation of the number of households with no access to motor vehicles, which result from the meshblock level census data for car ownership providing no data for some areas (due to small sample sizes being deemed confidential by Statistics New Zealand). Also, other low-mobility groups such as the hospitalised and institutionalised are omitted from the calculations. The former Auckland Regional Council calculated that 7.4% of Aucklanders have no access to a motor vehicle - a figure comparative to the 6.1% value used in this study, justified as the council's calculations are based on a regional rather than meshblock scale



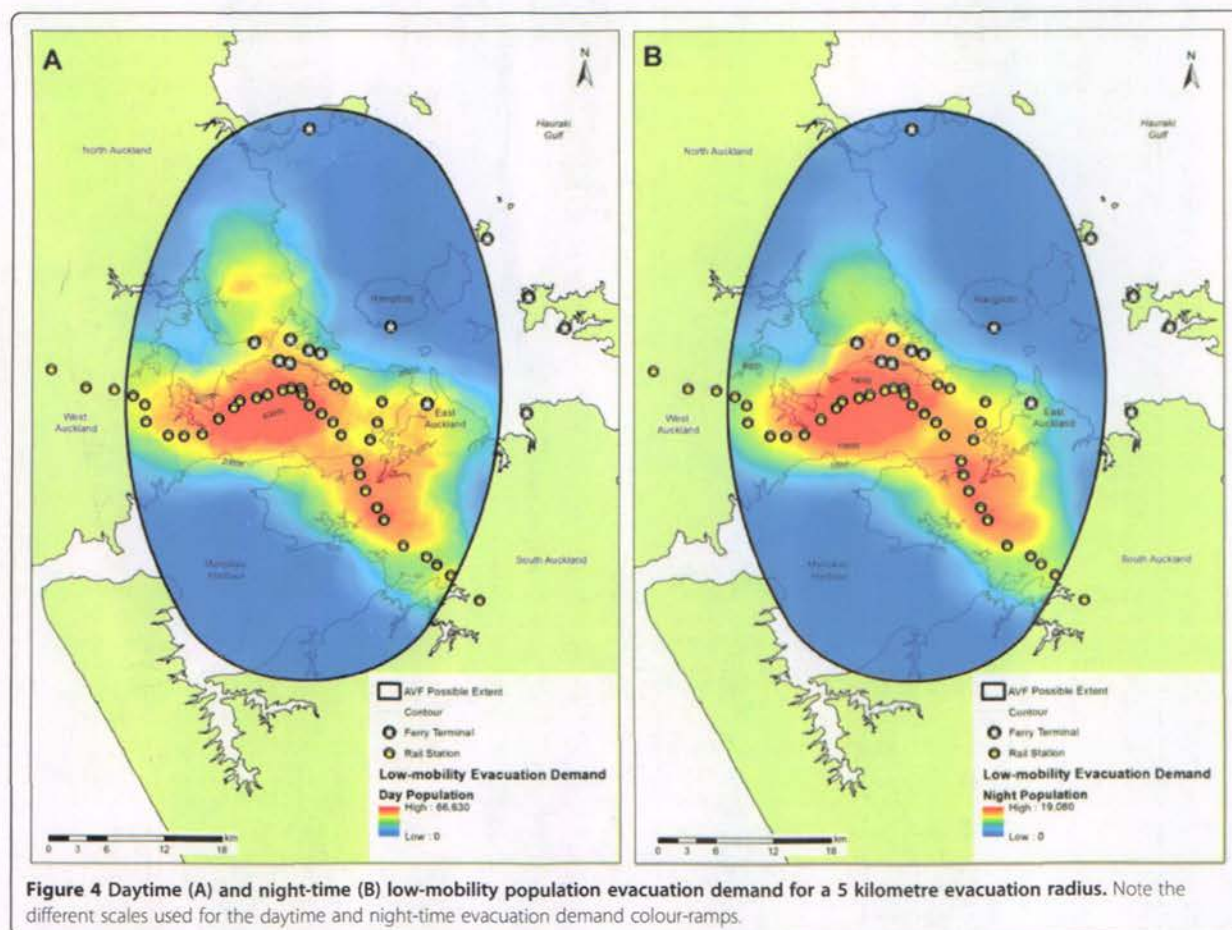
(Auckland Regional Council 2009a). The statistical results for the low-mobility population evacuation demand are presented in Table 2 and two outputs of the geographic model utilising the 5 kilometre evacuation radii and two time variables, are shown in Figure 4, overlaid atop the ferry and rail station stops.

Network analysis

Geospatial network analysis showed that the bus network, with a high number of stops and wide geographic distribution, was accessible to the majority of the Auckland population. Based on a standardised walking rate of 5 km h⁻¹, over 92% of Aucklanders can reach a bus stop within a 30 minute walk regardless of the time of day. Other networks such as trains and ferries, were significantly less accessible; The number of Aucklanders who can reach train stations or ferry terminals within a 30 minute walk were 37% (night-time) to 47% (daytime) and those who can reach ferry terminals in the same time were 5% (night-time) to 12% (daytime). The percentage of people living within a 15-minute drive, based on typical rush hour traffic speeds (Auckland Regional Council

Table 2 Low-mobility population evacuation demand statistics

Evacuation Demand	Day			Night		
	3.5 km	5 km	8 km	3.5 km	5 km	8 km
0	20.6%	11.8%	4.0%	21.0%	11.8%	4.0%
1-10,000	47.7%	40.2%	26.9%	78.7%	77.7%	59.3%
10,000-20,000	22.5%	15.0%	10.9%	0.4%	10.5%	22.9%
20,000-30,000	7.3%	14.1%	8.6%	0.0%	0.0%	13.5%
30,000-40,000	1.9%	12.7%	9.2%	0.0%	0.0%	0.4%
40,000-50,000	0.0%	4.5%	10.0%	0.0%	0.0%	0.0%
50,000-60,000	0.0%	1.3%	7.1%	0.0%	0.0%	0.0%
60,000-70,000	0.0%	0.5%	7.0%	0.0%	0.0%	0.0%
70,000-80,000	0.0%	0.0%	5.2%	0.0%	0.0%	0.0%
80,000-90,000	0.0%	0.0%	4.0%	0.0%	0.0%	0.0%
90,000-100,000	0.0%	0.0%	5.7%	0.0%	0.0%	0.0%
100,000-110,000	0.0%	0.0%	1.5%	0.0%	0.0%	0.0%
Average	6,945	13,993	34,672	1,722	3,473	8,652
Minimum	0	0	0	0	0	0
Maximum	39,283	66,629	108,455	11,375	19,073	31,610



2009b), of the nearest marina is relatively low (31-37%), whereas the percentage within 15 minutes of a boat ramp is high (90-92%).

Individual vulnerable bridge probability values for the three evacuation radii range from 3.1% to 14.7%. Combined bridge vulnerability statistics are listed in Table 3. The maximum probability of either one of the north or south bridges being impacted nearly doubles as the radius is increased. For the 5 kilometre evacuation radius, there is a 1.7% chance that both north bridges, and a 1.5% chance that both south bridges, will be impacted but 0% chance that three bridges will be impacted by the

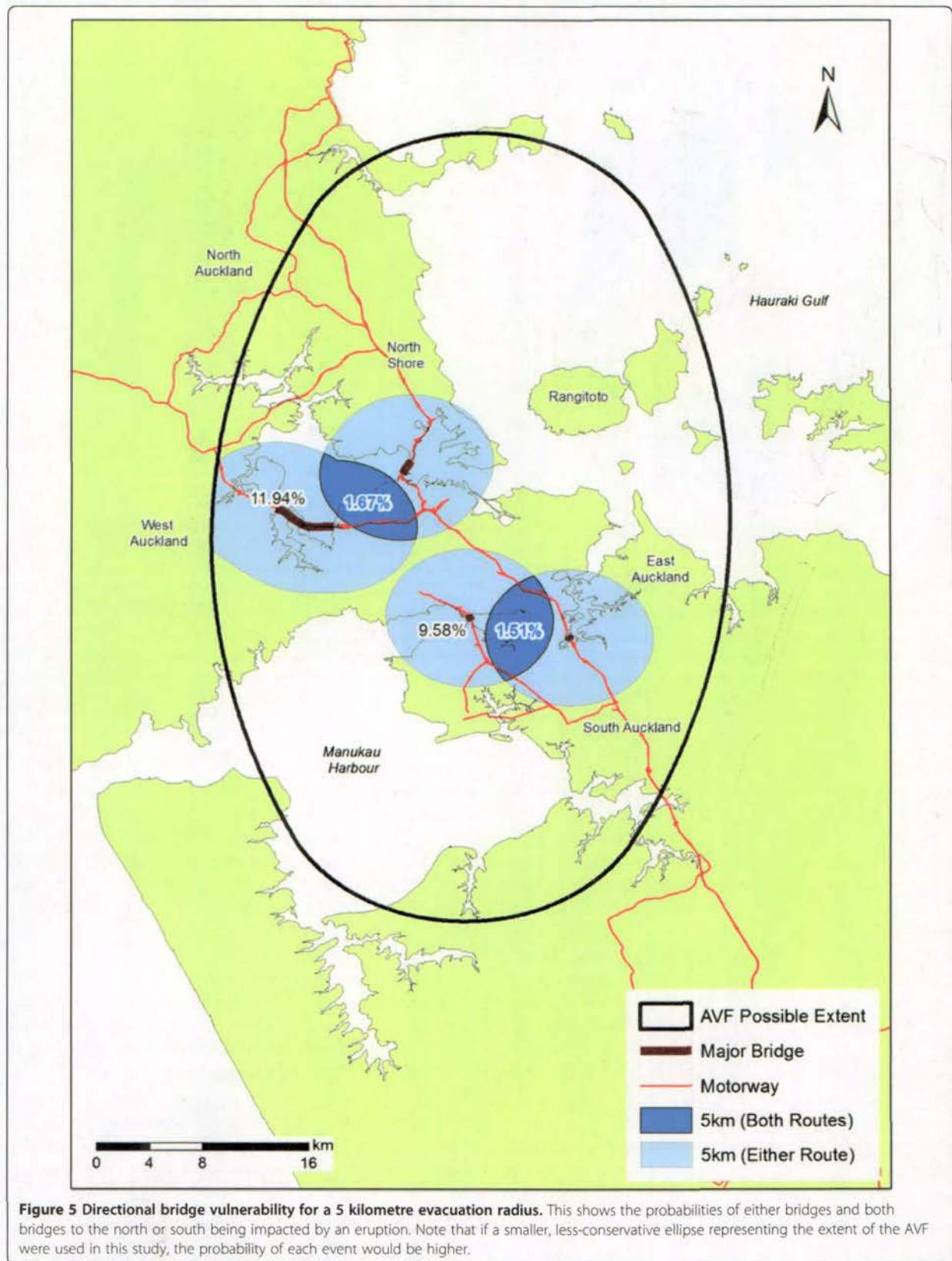
Table 3 Combined bridge vulnerability statistics

Bridges	3.5 km	5 km	8 km
Any	12.7%	21.5%	38.7%
Either North	7.3%	11.9%	21.8%
Either South	5.4%	9.6%	20.6%
Both North	0.2%	1.7%	7.7%
Both South	0.2%	1.5%	7.3%
NW, Harbour & Mangere	0.0%	0.0%	1.7%

eruption (Figure 5). In the event of an 8 kilometre evacuation radius however, there is a 1.7% chance that three bridges could be simultaneously impacted. It should be stressed that if the overall size of the AVF were reduced to include a more restricted (less conservative) ellipse around the existing volcanic cones (Figure 1), the probability of each event described above would be dramatically increased.

Micro-scale evacuation vulnerability

Diurnal changes in population evacuation demand are reflected in the calculated P/EC ratio values (population/exit capacity, described above). Although no data exists for threshold P/EC ratios for different roads in Auckland, a comparison of values provides a first-hand relative assessment of potential congestion areas. There is a high concentration of areas with elevated P/EC ratios during the day in and around the CBD, which at night is dramatically reduced. The reverse is true for many outlying suburbs, particularly those in West Auckland and the North Shore, which experience much higher ratios at night. This makes intuitive sense as many people



travel from the suburbs to the CBD for work each day. Table 4 lists the five neighbourhoods with the highest and five neighbourhoods with the lowest P/EC ratios. Two of the five neighbourhoods with the greatest net population gain during the day, the CBD and Auckland Airport, also have the two highest P/EC ratios during the day (1,819 and 1,574 people per exit lane, respectively). Night-time P/EC ratios for many of these neighbourhoods are significantly lower. Neighbourhoods with the greatest net population losses during the day also have some of the highest night-time P/EC ratios. Overall, the highest P/EC ratios during the night are far lower than the highest P/EC ratios during the day. Only two neighbourhoods, both in south Auckland, have P/EC ratios over 1,000 at night.

When graphically comparing daytime and night-time P/EC ratios, the prevalence of neighbourhoods with lower P/EC ratios is very clear. Based on the Brisbane Strategic Transport Model (Brisbane City Council 2007) access roads, such as those connecting neighbourhoods to primary roads, can facilitate the movement of up to 600 vehicles per hour. Therefore P/EC ratios > 600 are very likely to cause congestion and the value was used as a benchmark. In our study, the number of neighbourhoods with P/EC values greater than 600 is very small both at day and night (Figure 6).

Geographic features are of great consequence when assessing P/EC ratios. Neighbourhoods with both motorway and water boundaries have higher P/EC ratios. This is to be expected, as boundaries work as constraining geographic features limiting the number of exits. The results of statistical analysis of neighbourhood boundaries are shown in Table 5. All p-values, with two exceptions, were less than 0.05 and thus statistically significant.

These results show that there is a significant difference between neighbourhoods with only motorways as

boundaries and neighbourhoods with neither water nor motorways as boundaries during the day (i.e. when people are at work). However, at night there is no statistically significant difference. Contrastingly, neighbourhoods with only water boundaries are significantly different during the night (i.e. when those people return home), but not during the day. This is likely due to more residential neighbourhoods being located close to water features which provide both aesthetic and recreational value. Neighbourhoods containing businesses are more likely to occur close to motorway on- and off-ramps, which enable easy access for workers and goods. Therefore, when either of these neighbourhood types reach their peak population, they usually become more difficult to evacuate.

The numeric results of the HH/EC ratio and Car/EC ratio calculations are presented in Table 6. Results of both studies were found to be similar to those of the night-time P/EC ratios. HH/EC ratios were generally one third that of the P/EC ratios; this correlates with the fact that the mean Auckland household has three residents (Statistics New Zealand 2006). Car/EC ratios were around half as large as P/EC ratios, which correlates with there being roughly twice as many people as cars in Auckland (Statistics New Zealand 2006, New Zealand Transport Agency 2009). The minima Car/EC ratios at or bordering zero are suspect and likely due to the fact that such areas have very low residential populations. When compared to P/EC ratios and Car/EC ratios, HH/EC ratios represent the best-case scenario, as they minimise the overall number of evacuating units and thus the ratio, thereby producing fewer units per exit lane.

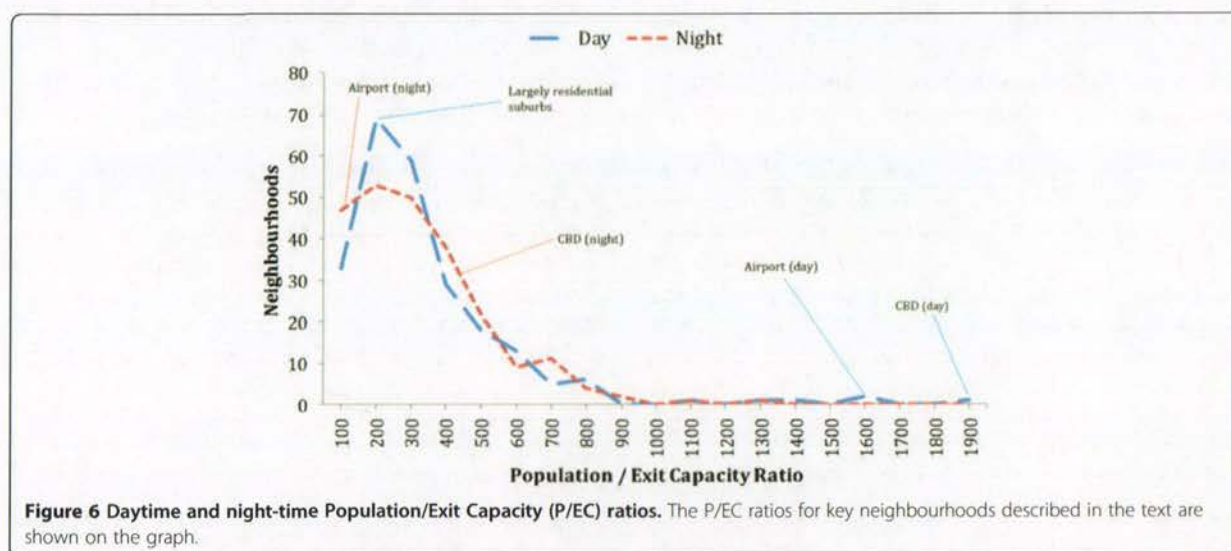
Macro-scale evacuation vulnerability

For inter- and intra-regional evacuations, flows often exceeded 50,000 vehicles along motorway sections, but

Table 4 Neighbourhoods with highest and lowest Population/Evacuation Capacity (P/EC) ratios for day and night

DAY*				NIGHT*			
Rank	Neighbourhood	P/EC Day	P/EC Night	Rank	Neighbourhood	P/EC Night	P/EC Day
1	Puhoi	10.3	28.5	1	Druces West	4.3	710.9
2	Gardens East	11.3	42.9	2	Manukau South	6.5	361.3
3	Glenbrook	15.1	34.6	3	Sylvia Park	10.3	1292.4
4	Ormiston North	18.9	41.9	4	Hampton Park	10.8	595.1
5	Greenhithe	23.6	84.2	5	Pukekohe North	16.2	123.9
234	Sylvia Park	1292.4	10.3	234	Wattle Farm	778.6	450.0
235	Rosedale	1362.5	267.0	235	Sunnynook	842.1	376.3
236	Hingaia	1567.9	685.3	236	Gulf Harbour	886.0	448.3
237	Akld Airport	1574.3	89.9	237	E Howick Beaches	1000.6	653.8
238	Akld CBD	1818.9	447.0	238	Mt. Mangere	1291.4	753.4

*The highest and lowest ranked P/EC ratios are shown in bold font. These are compared with the corresponding P/EC ratios for the contrasting diurnal time shown in normal font. For location of neighbourhoods please visit: <http://www.stats.govt.nz/StatsMaps/Home.aspx>.



rarely exceeded 20,000 vehicles for arterial and major roads. Symbolising flows along different routes by means of varying line thickness allows these differences in flows to be visualised (Figure 7).

In scenarios run for Auckland, the maximum VOC ratio for inter-regional evacuation was 92, which was established for a daytime evacuation with multiple vehicles, based on the maxima vent location and a large shadow evacuation. This suggests that the volume of traffic greatly exceeded the lane's capacity. VOC ratios were highest along motorways and in inter-regional evacuation models. In such cases, speeds were reduced to miniscule fractions of a km h^{-1} , i.e. traffic had come to a virtual standstill. The maximum VOC ratios for intra-regional evacuations however, were much lower (maximum = 6.56), a trend which was also depicted in the total network travel times (i.e. the cumulative time for all drivers to reach their final destinations). For the inter-regional evacuations modelled, clearance time was found to be in the order of days to years. Intra-regional evacuation clearance times were found to be much lower, ranging from one to nine hours. This was regardless of the level of network detail or number of connectors employed.

Table 5 Statistical t-test comparison of neighbourhood boundary types

μ_1	μ_2	p-value (day)	p-value (night)
Both	Neither	0.020	0.012
Motorway Only	Neither	0.020	0.632
Water Only	Neither	0.623	0.004
Neither	All	0.020	0.034

Discussion

Impact of diurnal population shifts on evacuation demand

Neighbourhoods with large daily population influxes are likely to be more difficult to evacuate during the day than at night because a greater demand will be placed on a static infrastructure network. Neighbourhoods with net losses will become easier to evacuate during the day (Tomsen 2010). A key finding of the population evacuation demand results is that demand values are high around the CBD during the day but become more widely dispersed at night. This can be attributed to a diurnal population shift, which is likely due to commuters moving away from the CBD toward peripheral, residential areas during the evening.

Night-time evacuation demand figures are significantly lower for the low-mobility population than the general population. In terms of geographic distribution, the North Shore has much less of a low-mobility evacuation demand as residents living there have greater access to motor vehicles. The reverse is true for South Auckland, which, when utilising the smaller two evacuation radii, nearly rivals the CBD as the peak evacuation demand centre. Daly et al. (2007) estimated that the maximum combined capacity of the Auckland public transportation system for an initial outward movement, assuming all public resources could be mustered, was just under 50,000 passenger seats. This capacity is more than sufficient for all night-time low-mobility evacuation models in our study, but not the 5 kilometre and 8 kilometre daytime low-mobility evacuation models. With a 5 kilometre evacuation radius, there is roughly a 2% chance this capacity will be exceeded during a daytime evacuation. This probability grows to roughly 35% with an 8 kilometre evacuation radius. Similar issues associated

Table 6 Neighbourhoods with highest and lowest Household/EC Ratios and Car/EC Ratios

Household/Evacuation Capacity (HH/EC)*					Car/Evacuation Capacity (Car/EC)*				
Rank	Neighbourhood	HH/EC	Car/EC	P/EC Night	Rank	Neighbourhood	Car/EC	HH/EC	P/EC Night
1	Manukau South	0.5	0.7	6.5	1	Druces West	0.0	2.1	4.3
2	Druces West	2.1	0.0	4.3	2	Sylvia Park	0.0	3.2	10.3
3	Sylvia Park	3.2	0.0	10.3	3	Manukau South	0.7	0.5	6.5
4	Hampton Park	4.9	6.2	10.8	4	Pukekohe North	5.5	5.3	16.2
5	Hobsonville	5.2	9.6	16.7	5	Hampton Park	6.2	4.9	10.8
234	West Tamaki	246.4	361.4	771.5	234	Hingaia	454.5	229.0	685.3
235	Sunnynook	280.1	472.9	842.1	235	Sunnynook	472.9	280.1	842.1
236	Gulf Harbour	313.1	540.0	886.0	236	Gulf Harbour	540.0	313.1	886.0
237	E Howick Beaches	328.2	628.1	1000.6	237	E Howick Beaches	628.1	328.2	1000.6
238	Mt. Mangere	411.6	643.2	1291.4	238	Mt. Mangere	643.2	411.6	1291.4

*The highest and lowest ranked Household/EC ratios and Car/EC ratios are shown in bold font. These are compared with the corresponding Car/EC ratios and Household/EC ratios, and also P/EC ratios, which are shown in normal font. For location of neighbourhoods please visit: <http://www.stats.govt.nz/StatsMaps/Home.aspx>.

with evacuating low-mobility populations are frequently encountered worldwide. For example, during Hurricane Katrina, there were some clear failures, particularly when it came to evacuating low-mobility groups in New Orleans (Wolshon 2006).

Bridge vulnerability and importance of maritime transport

In terms of transportation networks, a worst-case scenario for Auckland is a volcanic eruption impacting both bridges connecting the isthmus in the same direction; a 1.7% and 1.5% chance for both north and both south bridges respectively, for a 5 kilometre evacuation radius. Such an event would virtually sever all motor vehicle movement into and out of Auckland in that direction. Values for public transport network accessibility for the population with no access to a private vehicle were always greater than night-time values for the entire population. This makes intuitive sense, as people without a vehicle would likely live closer to public transportation assets to fulfil any day-to-day transportation requirements. It should be noted that while motorways and public transit routes are likely to become jammed, not helped by the constraining geography in Auckland, the likelihood of such congestion on the waters of the Waitemata and Manukau Harbours is low. Boats, unlike most cars and buses, are capable of transporting extensive cargo and are often kept stocked with essential survival materials including food, water and clothes. Therefore, although non-traditional, a part-maritime based evacuation may hold several advantages in Auckland. In 2008, such an evacuation was successfully demonstrated in Chaitén, Chile where over 5,000 people were evacuated by boat shortly before the town was inundated by lahars originating from the nearby volcano (Major and Lara 2013, Wilson et al. 2009). Marinas and ferry terminals

are more limited in numbers than boat ramps in Auckland and the accessibility figures reflect this. Boat ramps however, have the major disadvantage of additional preparation time required as many boat owners would initially have to return home from work during the day to collect boats for an evacuation, perhaps via congested roads. Despite this, the potential for maritime evacuation by private boats and ferries should not be underestimated in Auckland.

Relative evacuation difficulty as revealed by P/EC ratios

Micro-scale vulnerability analysis using P/EC ratios can be produced anywhere that population and road network data are available. In this study, such ratios were found to be effective in determining which areas, due to their infrastructure design, pose greater difficulties for evacuation. A comparison of daytime and night-time P/EC ratios (Figure 6) shows that the number of neighbourhoods with relatively large P/EC ratios is low. However, these neighbourhoods are of greatest concern as they will likely be more difficult to evacuate on a micro-scale. Two of the five neighbourhoods with the greatest net population gain during the day, the CBD and Auckland Airport, also have the two highest P/EC ratios during the day. This indicates that neighbourhoods experiencing the largest daytime population influx are some of the most difficult to evacuate during the day because of the inflexible infrastructure setup. A similar trend is observed for neighbourhoods with high night-time population influx. Neighbourhoods such as Wattle Farm in South Auckland and Eastern Howick Beaches in East Auckland (Figure 1), with the greatest net population losses during the day, also have some of the highest night-time P/EC ratios. This is most likely attributed to the return of school children and workers during evening hours. This suggests that residential neighbourhoods

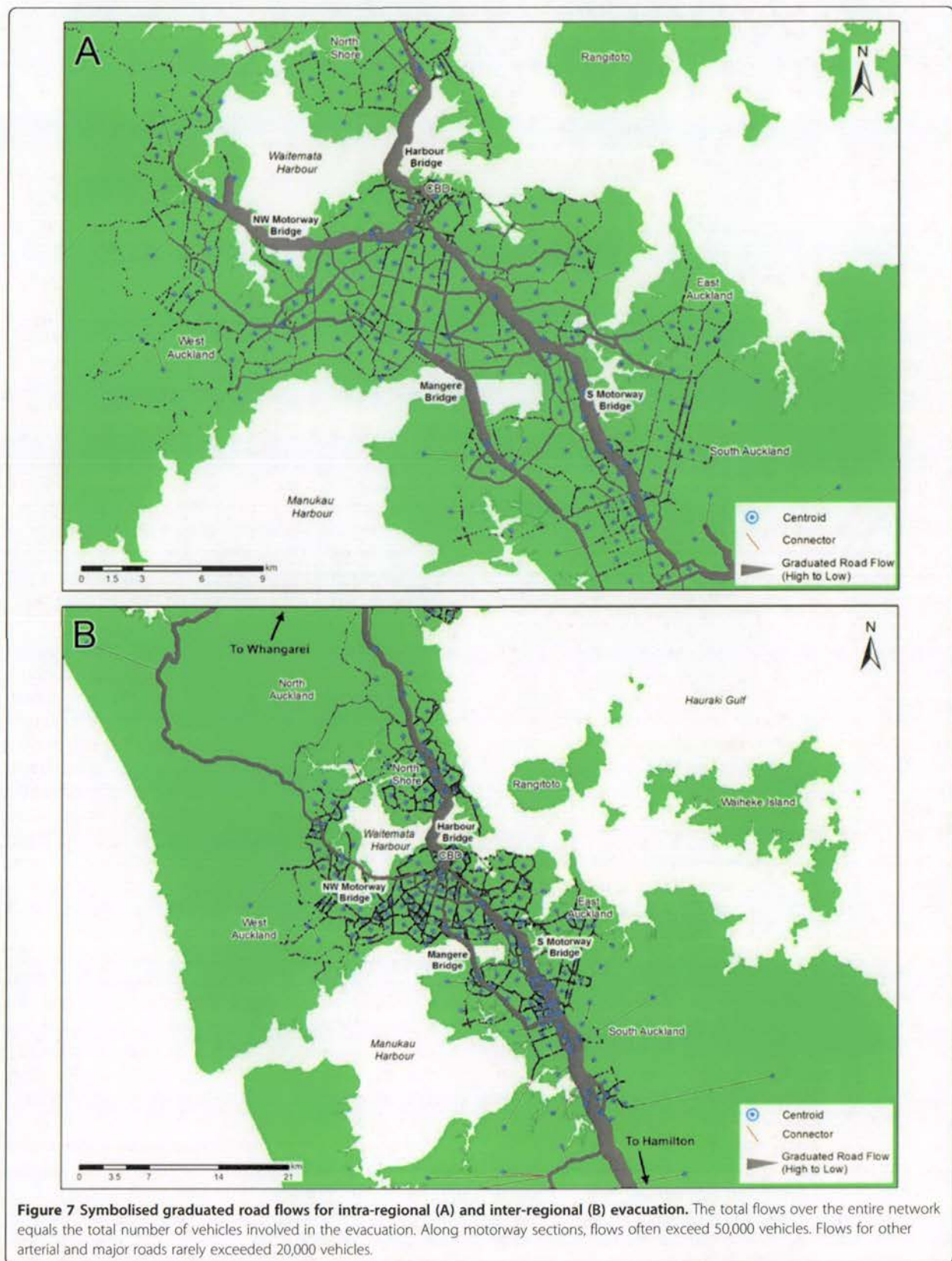


Figure 7 Symbolised graduated road flows for intra-regional (A) and inter-regional (B) evacuation. The total flows over the entire network equals the total number of vehicles involved in the evacuation. Along motorway sections, flows often exceed 50,000 vehicles. Flows for other arterial and major roads rarely exceeded 20,000 vehicles.

that experience the greatest net population influxes at night are also some of the most difficult to evacuate at night as a result of infrastructure setup. Overall, however, the highest P/EC ratios during the day are far higher than the highest P/EC ratios during the night. This indicates that evacuations in the top-five most challenging neighbourhoods are much more challenging during the day than at night. This can be attributed to the larger number of residential neighbourhoods than business and industrial neighbourhoods in Auckland. This reflects a metropolitan standard; in order to support an urban core, multiple feeder (i.e. residential) neighbourhoods are required.

Vulnerability trends related to boundary types also emerged during the study. Significantly higher P/EC ratios were experienced by neighbourhoods with both water and motorway boundaries than neighbourhoods with neither. Contrasting P/EC ratios observed for neighbourhoods with the different boundary types (i.e. high P/EC ratios for those with motorways and low P/EC ratios for those with water during the day) are likely attributable to the neighbourhood type. Business and industrial neighbourhoods are more likely to be located near motorways to enable easy access for workers and goods. Residential neighbourhoods, in contrast, are more likely to be located close to water features as they provide aesthetic and recreational value. Motorways offer neither of these. The minima Car/EC ratios at or bordering zero for some neighbourhoods may be due to the fact that some areas, such as Druces West and Sylvia Park (both in South Auckland), have virtually no residential population and are primarily used for business purposes. Such areas will likely be easy to evacuate at night but will be difficult to evacuate during business hours when there are high populations and limited capacities.

Intra-regional vs. inter-regional evacuation

The preference for Auckland Civil Defence and Emergency Management is to localise evacuations as much as possible, moving evacuees outside the danger zone (via a welfare facility for registration purposes) but keeping them close to home and within the region (MCDEM 2008). There were 151 Civil Defence and Emergency Management designated welfare facilities at the time of this study, including schools, churches and sports stadiums. More than half of Auckland's population were located within 5 minutes driving distance of the nearest facility and virtually all Aucklanders can access one within a 15-minute drive. However, the nearest welfare facility will not always be available or suitable for evacuation purposes (for example it might lie in the evacuation zone or be impacted by localised critical infrastructure disruption). In such cases it will be

necessary for evacuees to travel greater distances until they reach an alternative welfare facility in a safe location before heading to their final destination, wherever that may be. During a large phreatomagmatic eruption, critical infrastructure across Auckland may be crippled and an inter-regional evacuation may be necessary. Prior to this study, the best estimate of an evacuation clearance time for Auckland was developed during Exercise Ruaumoko in 2008. During this exercise, civil defence authorities allowed less than 24 hours in order to evacuate a 5 kilometre radius zone (Horrocks 2008a). However, this clearance time was only postulation and lacked any scientific backing. Though a conclusive figure will be unavailable until an actual evacuation is conducted, the next best solution, deriving scientifically backed estimates by means of evacuation modelling, was undertaken in this study.

Marco-scale evacuation vulnerability analysis showed that clearance time for inter-regional evacuation was in the order of days to years. This indicates that congestion is not limited to specific links, but rather endemic in the network due to limited capacities and excessive demand. Evacuees would most likely walk rather than wait in traffic congestion for such prolonged periods and the capabilities of the TransCAD model can therefore be deemed somewhat limited for computing movement times over such large distances especially with heavy congestion. In essence however, it can be concluded that the Auckland road network is ill suited for large-scale egress movements at present. Despite this, one major trend was identified from the inter-regional modelling: as more detail is added to the road network, thus allowing evacuees more route choice flexibility, clearance times are reduced. In the future it would be worthwhile recalculating macro-scale evacuation vulnerability using an evacuation modelling program specifically designed to accommodate high congestion levels, which could also be used to validate intra-regional evacuation results.

The relatively short clearance times for intra-regional evacuations mean that there is considerable merit to intra-regional over inter-regional evacuation from a mobility standpoint. The reasons for lower intra-regional clearance times are heavily associated with path lengths. While inter-regional evacuees commonly traversed roughly 150 kilometres of road network, intra-regional evacuees seldom travelled further than 10 kilometres. Network capacity is another contributing factor. VOC analysis confirmed that motorways would be congested in all evacuation scenarios, regardless of the amount of network detail. Yet, intra-regional evacuations are less dependent on the motorway network than inter-regional evacuations, as there are more alternate routes due to dense urban development in the city. It should be noted that all of the clearance time figures represent the

movement times once evacuees have reached the Traffic Analysis Zone boundary and do not include preparation times (estimated to be 1 to 2 days in Auckland (Auckland CDEM Group 2008b)) or intra-zonal movement times.

Conclusions

This study has numerically demonstrated a future eruption in the AVF will almost certainly create considerable evacuation demands, which require considerable planning. Although the locations of new eruptions are unknown, adopting a non-specific eruption vent approach has allowed the impacts at all locations, and population and infrastructure vulnerability to be modelled and assessed. Our key conclusions and recommendations are:

- Eruptions in the central Auckland isthmus area are likely to generate high evacuation demand, peaking at just over half a million evacuees in places. This is particularly relevant given that rapid evacuation is likely to be needed, i.e. within 48 hours. High P/EC ratios in the same regions indicate that transportation infrastructure may struggle to cope. Based on a 5 kilometre evacuation radius, there is just a 4% chance that an eruption would generate no evacuation demand.
- Daytime eruptions near Auckland Airport and in business districts, particularly the CBD, will generate high population evacuation demand. Daytime maximum population evacuation demand figures are around three times higher than night-time eruptions in these areas due to the large population influx from residential suburbs during the day. There is also a substantial low-mobility population in the central Auckland area during the day, largely attributable to the number of students. Indeed the predicted daytime maximum low-mobility evacuation demand may be more than twice the seating capacity of Auckland's total public transportation assets meaning that return trips may be required to accommodate such demand. Large daytime increases in population evacuation demand combined with high P/EC ratios may favour an evacuation at night in some areas (such as the CBD) to avoid severe congestion (although this needs to be counterbalanced by the limited visibility and other constraints of evacuation by night). Delaying the call to evacuate until the majority of people are home, or advising people to remain at home to await an evacuation decision, should be considered. This supports the consideration in the current mass evacuation plan for Auckland which favours evacuation from home due to likely reduced preparation time (Auckland CDEM Group 2008b).
- The bus network is accessible by foot to nearly the entire Auckland population but, as with private transport, is subject to road congestion that commonly plagues evacuations. There is a moderate chance (13-39% depending on the eruptive magnitude) that one of the four motorway bridges would be impacted and an up to 8% chance that multiple bridges facilitating evacuation in the same direction are impacted. Any impacts to bridges will likely increase congestion and further disrupt evacuation. Transportation by boat and rail is significantly less accessible but these modes rarely experience major congestion in Auckland. For this reason, the value of maritime evacuation by ferries, and private boats using boat ramps and marinas, should not be underestimated. This could be particularly beneficial in neighbourhoods with high population/exit capacity that have both water and motorway boundaries. Maritime evacuation would play to Auckland's geographic strength: its double harbour access, and would likely ease congestion on available motorways. In addition, the Ports of Auckland east coast seaport (adjacent to the CBD) provides an opportunity for people to be evacuated by a non-traditional mode of maritime transport, namely cargo vessels.
- Each of the modelled TransCAD scenarios experienced massive congestion, as thousands of evacuees flooded a limited number of evacuation routes. Congestion was not limited to specific links, but rather endemic in the network due to limited capacities and excessive demand. Intra-regional, rather than inter-regional, evacuations were favoured, reducing total network clearance times by multiple orders of magnitude (from days to between one and nine hours). This suggests that evacuation to destinations within the Auckland region should be given preference over evacuation to destinations outside the region if possible.
- TransCAD results also suggest that route choice flexibility will likely reduce the clearance time for evacuation. Such choices may be critical for inter-regional evacuations to be completed within manageable timeframes. However for this to work, evacuees must either have prior knowledge of the various network connections or be informed of them using signage and/or other communication methods.
- The survivability of Auckland's critical infrastructure during volcanic activity is an important unknown. Functional transportation networks are fundamental for evacuation purposes. Whether infrastructure assets, including bridges, tunnels, traffic lights, signs and motorways will be functional following volcanic activity such as tremors and ash fall determines

which routes are available to evacuees and radically impacts egress movements. Further study is required in this field.

Abbreviations

AVF: Auckland Volcanic Field; P/EC: Population to exit capacity; HH/EC: Household to exit capacity; nHH: Number of households; Car/EC: Car to exit capacity; TAZ: Traffic Analysis Zone; CBD: Central Business District; VOC: Volume-Over-Capacity.

Competing interests

The authors declare that they have no competing interests.

Authors' contribution

Supported by the expertise and direction of JML and MG, ET acquired data, planned and conducted the research and undertook all statistical analysis for the study. TMW contributed knowledge and skills, particularly regarding the modelling component of the work and DMB participated through the writing and editing of this manuscript. All authors have read, reviewed and approved the final manuscript.

Acknowledgements

We are grateful to the Rotary Foundation for providing funding for ET to conduct the research. We thank Statistics New Zealand, the Ministry of Education and the former Auckland Regional Council for the supply of data. We also thank Associate Professor André Dantas, in Civil Engineering at the University of Canterbury at the time of the research, for his support with the TransCAD studies. JML gratefully acknowledges support from the New Zealand Earthquake Commission.

Author details

¹School of Environment, The University of Auckland, Private Bag 92019, Auckland, New Zealand. ²Centre for eResearch & Department of Computer Science, University of Auckland, Private Bag 92019, Auckland, New Zealand. ³Centre for Risk, Resilience and Renewal, Department of Geological Sciences, University of Canterbury, Private Bag 4800, Christchurch, New Zealand. ⁴Present address: CMR 464, Box 2361, APO, AE 09226, USA.

Received: 16 August 2013 Revised: 27 November 2013

Accepted: 14 February 2014

Published: 31 Mar 2014

References

- Allen SR, Smith IEM (1994) Eruption styles and volcanic hazard in the Auckland Volcanic Field, New Zealand. *Geoscience Reports of Shizuoka University* 205–14
- ArcGIS (2009) GIS software: version 9.3.1. Environmental Systems Research Institute (ESRI), Redlands, California
- Auckland CDEM (2013) Auckland Volcanic Field contingency plan. Available from: <http://www.aucklandcivildefence.org.nz/About-Us/Document-Library/Supporting-Plans/>. Accessed 22 June 2013
- Auckland CDEM Group (2008a) Final exercise report: exercise Ruamoko '08. Auckland Regional Council, Auckland, New Zealand
- Auckland CDEM Group (2008b) Mass evacuation plan: group functional plan P2. Auckland Regional Council, Auckland, New Zealand
- Auckland Regional Council (2009a) Monitor Auckland: tracking our progress. Auckland Regional Council, Auckland, New Zealand
- Auckland Regional Council (2009b) Trends and issues (transport challenges): regional land transport strategy working report. Auckland Regional Council, Auckland, New Zealand
- Baker EJ (1991) Hurricane evacuation behavior. *International Journal of Mass Emergencies and Disasters* 9:287–310
- Baschetta C (2006) Disaster preparedness preliminary observations on the education of vulnerable populations due to hurricanes and other disasters testimony. In: United States Government Accountability Office (ed) Testimony before the special committee on aging. U.S. Senate, Washington D.C
- Bebbington MS, Cronin SJ (2011) Spatio-temporal hazard estimation in the Auckland volcanic field, New Zealand, with a new event-order model. *Bull Volcanol* 73(1):55–72
- Beca Carter Hollings and Ferner Ltd (2002) Contingency plan for the Auckland Volcanic Field. Auckland, New Zealand, [http://www.arc.govt.nz/albany/fms/main/Documents/Council/Civil%20defence%20emergency%20management/Publications%208%20factsheets/Auckland%20Volcanic%20Plan%20\(VCP\).pdf](http://www.arc.govt.nz/albany/fms/main/Documents/Council/Civil%20defence%20emergency%20management/Publications%208%20factsheets/Auckland%20Volcanic%20Plan%20(VCP).pdf). Accessed 16 June 2013
- Belousov A, Voight B, Belousova M (2007) Directed blasts and blast-generated pyroclastic density currents: a comparison of the Bezymianny 1956, Mount St Helens 1980, and Soufrière Hills, Montserrat 1997 eruptions and deposits. *Bull Volcanol* 69(7):701–740, 10.1007/s00445-006-0109-y
- Blake S, Smith I, Wilson C, Leonard G (2006) Lead times and precursors of eruptions in the Auckland Volcanic Field, New Zealand: indications from historical analogues and theoretical modelling. Consultancy Report 2006/34, GNS Science, Lower Hutt, New Zealand
- Brisbane City Council (2007) Brisbane Strategic Transport Model (BSTM) version 6.0. Brisbane City Council, Brisbane, Australia
- Browne FL (1958) Theories of the combustion of wood and its control: a survey of the literature. Forest Products Laboratory, U.S. Forest Service Research Legacy, Report 2136
- Chakraborty J, Tobin GA, Montz BE (2005) Population evacuation: assessing spatial variability in geophysical risk and social vulnerability to natural hazards. *Natural Hazards Review* 6:23–33
- Church RL, Cova TJ (2000) Mapping evacuation risk on transportation networks using a spatial optimization model. *Transportation Research Part C: Emerging Technologies* 8:321–336
- Cola RM (1996) Responses of Pampanga households to lahar warnings: lessons from two villages in the Pasig-Patrero River watershed. In: Newhall CG, Punongbayan RS (eds) Fire and Mud. Philippine Institute of Volcanology and Seismology and University of Washington Press, Quezon City and Seattle
- Cole J, Blumenthal E (2004) Evacuate: what an evacuation order given because of a pending volcanic eruption could mean to residents of the Bay of Plenty. *Tephra* 21:46–52
- Cova TJ (1999) GIS in emergency management. *Geographical Information Systems: Principles, Techniques, Applications and Management*. John Wiley and Sons, New York
- Cova TJ, Church RL (1997) Modelling community evacuation vulnerability using GIS. *Int J Geogr Inf Sci* 11:763–784
- Cutter CL (2003) GI science, disasters, and emergency management. *Trans GIS* 7:439–446
- Daly M, Hoskin K, Leonard G (2007) Physical evacuation workshop, 2007 (facilitator comments). Auckland Regional Council, Auckland, New Zealand
- Dosa DM, Grossman N, Wetle T, Mor V (2007) To evacuate or not to evacuate: lessons learned from Louisiana nursing home administrators following Hurricanes Katrina and Rita. *Journal of the American Medical Directors Association* 8:142–149
- Dow K, Cutter SL (2002) Emerging hurricane evacuation issues: Hurricane Floyd and South Carolina. *Natural Hazards Review* 3:267–285
- Drabek TE (1986) Human system responses to disaster. Springer, New York
- Franzese O, Liu C (2008) Emergency evacuations, transportation networks. In: Shekhar S, Xiong H (eds) *Encyclopaedia of GIS*. Springer, New York
- Horrocks J (2008a) Evacuation progression script summary, Exercise Ruamoko 2008. Ministry of Civil Defence and Emergency Management, New Zealand
- Horrocks J (2008b) Learning from Exercise Ruamoko, Exercise Ruamoko 2008. Ministry of Civil Defence and Emergency Management, New Zealand
- Hushon J, Kelly RB, Rubin C (1989) Identification and analysis of factors affecting emergency evacuations. Nuclear Management and Resources Council Inc. (NUMARC), Washington D.C
- Ketteridge AM, Clarke L, Fordham M (1996) EUROflood: evacuation 1996, technical annex 14 for the evacuation module. Flood Hazard Research Centre, University of Middlesex, Enfield, United Kingdom
- Klepeis NE, Nelson WC, Ott WR, Robinson JP, Tsang AM, Switzer P, Behar JV, Hern SC, Engelmann WH (2001) The National Human Activity Pattern Survey (NHAPS): a resource for assessing exposure to environmental pollutants. *J Expo Anal Environ Epidemiol* 11:231–252
- Le Corvec N, Bebbington MS, Lindsay JM, McGee LE (2013a) Age, distance and geochemical evolution within a monogenetic volcanic field: analyzing patterns in the Auckland Volcanic Field eruption sequence. *Geochemistry, Geophysics, Geosystems* 14(9):3648–3665
- Le Corvec N, Spörli KB, Rowland J, Lindsay J (2013b) Spatial distribution and alignments of volcanic centers: clues to the formation of monogenetic volcanic fields. *Earth Sci Rev* 124:96–114
- Leonard R (1985) Mass evacuation is disasters. *J Emerg Med* 2:279–286

- Lindell MK, Perry RW (1992) Behavioral foundations of community emergency planning. Hemisphere Publishing, Washington D.C
- Lindell MK, Prater CS (2006) Evacuation from Hurricane Katrina: Jefferson and St. Charles parishes. National Hurricane Conference, Orlando, Florida
- Lindell MK, Prater CS (2007) Critical behavioural assumptions in evacuation time estimate analysis for private vehicles: examples from hurricane research and planning. *Journal of Urban Planning and Development* 133:18–29
- Lindell MK, Lu J-C, Prater CS (2005) Household decision making and evacuation in response to Hurricane Lili. *Natural Hazards Review* 6:171–179
- Lindsay JM (2010) Volcanoes in the big smoke: a review of hazard and risk in the Auckland Volcanic Field. Institute of Earth Science and Engineering and School of Environment. University of Auckland, Auckland, New Zealand
- Lindsay JM, Marzocchi W, Jolly G, Constantinescu R, Selva J, Sandri L (2010) Towards real-time eruption forecasting in the Auckland volcanic field: application of BET_EF during the New Zealand national disaster Exercise 'Ruau-moko'. *Bull Volcanol* 72:185–204
- Lindsay JM, Leonard GS, Smid ER, Hayward BW (2011) Age of the Auckland Volcanic Field: a review of existing data. *N Z J Geol Geophys* 54(4):379–401
- Major JJ, Lara LE (2013) Overview of Chaitén volcano. *Andean Geology* 40(2):196–215
- Marrero JM, García A, Llinares A, Rodríguez-Losada JA, Ortiz R (2010) The Variable Scale Evacuation Model (VSEM): a new tool for simulating massive evacuation processes during volcanic crises. *Natural Hazards and Earth Systems Sciences* 10:747–760
- Marzocchi W, Woo G (2007) Probabilistic eruption forecasting and the call for an evacuation. *Geophysical Research Letters* 34:1–4
- MCDEM (2008) Mass evacuation planning: director's guidelines for civil defence emergency management (CDEM) groups, DGL 07/08. Ministry of Civil Defence and Emergency Management, [http://www.civildefence.govt.nz/memwebsite.nsf/Files/Director_Guidelines/\\$file/Mass-evacu-planningDGL07-08.pdf](http://www.civildefence.govt.nz/memwebsite.nsf/Files/Director_Guidelines/$file/Mass-evacu-planningDGL07-08.pdf). Accessed 12 May 2013
- Mileti DS, Bolton PA, Fernandez G, Updike RG (1991) The eruption of Nevado Del Ruiz volcano Colombia, South America, November 13, 1985. Commission on Engineering and Technical Systems (National Academy Press), Washington, D.C
- Moriarty K, Ni D, Collura J (2007) Modelling traffic flow under emergency evacuation situations: current practices and future directions. 86th Transportation Research Board Annual Meeting, Transportation Research Board, Washington, D.C
- Morrow BH (1999) Identifying and mapping community vulnerability. *Disasters* 23:1–18
- Needham AJ, Lindsay JM, Smith IEM, Augustinus P, Shane PA (2011) Sequential eruption of alkaline and sub-alkaline magmas from a small monogenetic volcano in the Auckland Volcanic Field, New Zealand. *J Volcanol Geotherm Res* 201:126–142
- New Zealand Transport Agency (2009) Motor vehicle registration statistics 2008. MVR Statistics, Wellington, New Zealand
- NZ Open GPS Maps (2009) Improved NZ road centrelines. Coordinates, <https://coordinates.com/layer/183-improved-nz-road-centrelines-august-2011/>. Accessed 10 November 2009
- Perry RW, Lindell MK (2003) Preparedness for emergency response: guidelines for the emergency planning process. *Disasters* 27(4):336–350
- Prater C, Wenger D, Grady K (2000) Hurricane Bret post storm assessment: a review of the utilisation of hurricane evacuation studies and information dissemination. College Station, TX, Hazard Reduction and Recovery Centre, A&M University, Texas
- Quarantelli EL (1980) Evacuation behaviour and problems: findings and implications from the research literature. Ohio State University Disaster Research Centre, Columbus, Ohio
- Quarantelli EL (1985) Social support systems: some behavioural patterns in the context of mass evacuation activities. *Disasters and Mental Health: Selected Contemporary Perspectives* 178:122–136
- Sandri L, Jolly G, Lindsay J, Howe T, Marzocchi W (2012) Combining probabilistic hazard assessment with cost-benefit analysis to support decision making in a volcanic crisis from the Auckland volcanic field, New Zealand. *Bull Volcanol* 74:705–723
- Shaluf IM (2008) Technological disaster stages and management. *Disaster Prevention and Management* 17:114–126
- Shane P, Gehrels M, Zawalna-Geer A, Augustinus P, Lindsay J, Chaillou I (2013) Longevity of a small shield volcano revealed by crypto-tephra studies (Rangitoto volcano, New Zealand): change in eruptive behaviour of a basaltic field. *J Volcanol Geotherm Res* 257:174–183
- Sherburn S, Scott B, Olsen J, Miller C (2007) Monitoring seismic precursors to an eruption from the Auckland Volcanic Field, New Zealand. *N Z J Geol Geophys* 50:1–11
- Shulman HML (2008) Estimating evacuation vulnerability of urban transportation systems using GIS. Department of Geography, Queen's University, Kingston, Canada
- Sparks RSJ (2003) Forecasting volcanic eruptions. *Earth Planet Sci Lett* 210:1–15
- Spörli KB, Eastwood VR (1997) Elliptical boundary of an intraplate volcanic field, Auckland, New Zealand. *J Volcanol Geotherm Res* 79(3–4):169–179
- Statistics New Zealand (2006) Census of population and dwellings. Wellington, New Zealand
- Statistics New Zealand (2008) Business demographic statistics Table 11: business demography tables. Wellington, New Zealand
- Tierney KJ, Lindell MK, Perry RW (2001) Facing the unexpected: disaster preparedness and response in the United States. Joseph Henry, Washington, D.C
- Tobin GA, Whiteford LM (2002) Community resilience and volcano hazard: the eruption of Tungurahua and evacuation of the Faldas in Ecuador. *Disasters* 26(1):28–48
- Tomsen E (2010) GIS-based mass evacuation planning for the Auckland volcanic field. Masters Dissertation, School of Environment, University of Auckland, Auckland, New Zealand
- U.S. Department of Transportation (2006) Catastrophic hurricane evacuation plan evaluation: a report to congress (in corporation with the U.S. Department of Homeland Security), http://www.fhwa.dot.gov/reports/hurricaneevacuation/rtc_chep_eval.pdf. Accessed 01 August 2013
- Urbanik T (2000) Evacuation time estimates for nuclear power plants. *J Hazard Mater* 75:165–180
- Wilson T, Leonard G, Stewart C, Johnston D (2009) Rhyolitic eruption of Vulkan Chaitén, Chile. HAZM 401 – Geological Uncertainty, University of Canterbury, Christchurch, New Zealand
- Wolshon B (2002) Planning for the evacuation of New Orleans. *Institute of Transportation Engineers* 72(2):44–49
- Wolshon B (2006) The aftermath of Katrina. *The Bridge*, National Academy of Engineering, Washington D.C, 36(1):27–34
- Wolshon B (2008) Empirical characterisation of mass evacuation traffic flow. *J Transp Res Board* 2041:38–48
- Wolshon B, Urbina E, Levitan M (2001) National review of hurricane evacuation plans and policies. Louisiana State University Hurricane Centre, Baton Rouge, LA
- Woo G, Grossi P (2009) A new era of volcano risk management. Risk Management Solutions Inc, Stanford, CA, https://support.rms.com/publications/Volcano_Risk_Management.pdf. Accessed 20 June 2013

10.1186/2191-5040-3-6

Cite this article as: Tomsen et al.: Evacuation planning in the Auckland Volcanic Field, New Zealand: a spatio-temporal approach for emergency management and transportation network decisions. *Journal of Applied Volcanology* 2014, 3:6

Submit your manuscript to a SpringerOpen® journal and benefit from:

- Convenient online submission
- Rigorous peer review
- Immediate publication on acceptance
- Open access: articles freely available online
- High visibility within the field
- Retaining the copyright to your article

Submit your next manuscript at ► springeropen.com

IMPACTS OF VOLCANIC ASH ON ROAD TRANSPORTATION: CONSIDERATIONS FOR RESILIENCE IN CENTRAL AUCKLAND

Daniel Blake: PhD Candidate (BSc, MSc) daniel.blake@pg.canterbury.ac.nz

Hazard and Disaster Management, Department of Geological Sciences, University of Canterbury, Private Bag 4800, Christchurch 8140

Thomas Wilson: Senior Supervisor (BSc, PhD)

Senior Lecturer in Hazard and Disaster Management, Department of Geological Sciences, University of Canterbury, Private Bag 4800, Christchurch 8140

Natalia Deligne: Co-supervisor (BSc, MRes, PhD)

Volcanic Hazard and Risk Modeller, GNS Science, 1 Fairway Drive, Avalon 5010, PO Box 30368, Lower Hutt 5040

Jan Lindsay: Co-supervisor (BSc, MSc, PhD)

Senior Lecturer, School of Environment, The University of Auckland, Private Bag 92019, Auckland 1142

Jim Cole: Co-supervisor (BSc, PhD)

Professor of Geology, Department of Geological Sciences, University of Canterbury, Private Bag 4800, Christchurch 8140

ABSTRACT

Auckland is built on an active volcanic field. During a future volcanic eruption, functional transport networks will be critical for evacuations, as well as for immediate and long-term recovery once direct threats have subsided. Ash is generally the most disruptive and widely dispersed volcanic hazard, potentially impacting road transport networks for months to years. In Auckland ash may originate from both local eruptions and those further afield in the North Island.

Common ash impacts on roads include:

- Skid resistance reduction
- Road marking coverage
- Visual range reduction

Few studies have attempted to quantify these impacts in detail, particularly for ash <10 mm thick. This research involves the conception and implementation of a series of experiments in the Volcanic Ash Testing Laboratory (VAT Lab) at the University of Canterbury to provide quantitative data relating ash characteristics to road transport impact types.

The results, along with empirical evidence and expert advice from staff at transport organisations, are being used to inform models of disruption across Auckland's road network following hypothetical eruptive scenarios. Findings can be used to improve evacuation planning and clean-up strategies, and provide safe operating thresholds and specific travel advice for future ashfall events, increasing transport system resilience.

1. INTRODUCTION

Functional transport networks are critical for society both under normal operating conditions and in emergencies. During volcanic eruptions, transport networks may be required for the evacuation of residents and to allow sufficient access for emergency services to enter affected areas. Once direct threats have subsided, transport networks are crucial for both immediate and long-term recovery including the clean-up and disposal of pyroclastic material, and restoration of services. To increase resilience to volcanic hazards, it is thus imperative that effective transport management strategies are incorporated into contingency planning in areas where society and infrastructure are at risk (e.g., Auckland, New Zealand; Kagoshima, Japan; Mexico City, Mexico; Naples, Italy; Yogyakarta, Indonesia).

Volcanic eruptions produce many hazards. Damage to transport from proximal hazards such as lava flows, pyroclastic density currents and lahars is often severe, leaving routes impassable and facilities closed. Volcanic ash (ejected material with particle sizes <2 mm in diameter) is widely dispersed and, although not necessarily damaging to the static transport infrastructure, is generally the most disruptive of all volcanic hazards (Johnston & Daly 1997). Even relatively small eruptions are capable of widespread disruption, which may continue for months due to the remobilisation and secondary deposition of ash by wind, water, traffic or other human activities, even after an eruption has subsided.

To date, studies on the impacts of volcanic hazards to society have focussed on the effects of ash (e.g. Blong 1984; Wilson, Daly & Johnston 2009a; Wilson et al. 2011; Wardman et al. 2012a; Wilson et al. 2012a; Wilson et al. 2014). These studies and reports suggest three frequently occurring types of volcanic ash impacts on surface transport, with notable eruptions that have led to such impacts highlighted in Table 1:

1. Reduction of skid resistance on roads covered by volcanic ash.
2. Coverage of road markings by ash.
3. Reduction in visual range during initial ashfall and any ash re-suspension.

Despite much anecdotal evidence, there has been little work to quantify the impacts of ash on surface transport. Quantitative, empirical evidence could inform road management strategies in syn-eruptive and post-ashfall environments such as evacuation planning, safe travel advice in the recovery phase and recommended clean-up operations.

Existing studies of exposed critical infrastructure have generally focussed on very large eruptions and ashfall deposits >10 mm thick, rarely reporting the effects from ashfall <10 mm thick (Wilson et al. 2012a). This presents a source of uncertainty for emergency management planning and loss assessment models, which is important, as thin deposits are more frequent. Indeed, the limited quantitative data available from historic observations generally relates impacts to approximate depths of ash, which may not be the best metric: ash characteristics such as particle size, ash type, degree of soluble components and wetness, may influence or even control surface transport impacts. We investigate the importance of these alternative characteristics in this study.

Here, we present experimental methods and results to date from the University of Canterbury's Volcanic Ash Testing Laboratory (VAT Lab) on the three frequently occurring impacts to surface transportation. All laboratory techniques have been developed in the context of Auckland's motorway and arterial road network and results can be used to provide safe operating thresholds and specific travel advice during future ashfall, thus increasing overall transportation system resilience. We briefly summarise how the findings are being used to inform models of disruption and recovery across Auckland's road network following hypothetical eruptive scenarios in the Auckland Volcanic Field.

Volcano	Year	Ash depth (mm)	Skid resistance observations	Road marking coverage observations	Visibility observations
Ruapehu	1945				Bus headlamps blacked out by thick ash ¹
Ruapehu	1945				Re-suspended ash similar to dust produced on unsealed roads ¹
St Helens	1980	>1		Drivers disorientated due to loss of markings ²	
St Helens	1980	17	Ash became slick when wet ^{3,4,5}		
St Helens	1980	40			Flares used to guide people ⁶
Hudson	1991		Traction problems from ash on road ⁷	Road markings obscured ⁷	
Hudson	1991	20-50			-1 m visual range a week after eruption ("transport virtually closed down") ^{7,8}
Hudson	1991	200-300			People couldn't drive partly due to visibility ⁷
Spurr	1992	3			Visibility reduced until rain alleviated issues ^{1,9}
Unzen	1992				Visibility reduced by suspended ash ^{9,10}
Tavurvur and Vulcan	1994	1000	Vehicles stuck in deep ash, passable if hardened ^{8,11,12}		
Ruapehu	1995-96	"thin"	Slippery sludge from ash-rain mix ^{1,9}	Road markings obscured ^{1,9}	Reduced visibility (roads closed) ^{1,9}
Montserrat	1997		Rain can turn particles into slurry of slippery mud ¹³		
Etna	2002	0-2			Ash remobilisation by traffic and wind caused reduced visibility ⁹
Etna	2002	2-20	Traction problems, damp & compacted easier to drive on ⁹		
Reventador	2002	2-5	Vehicles banned due to slippery surfaces ^{9,14}	Vehicles banned due to covered road markings ^{9,14}	
Chaitén	2008		Reduced traction caused dam access problems ^{15,16}		Reduced visibility caused dam access problems ¹⁶
Chaitén	2008	~300			10-15 m visibility (people drove cautiously) ¹⁵
Merapi	2010		Slippery roads caused accidents & increased journey times ¹⁷		
Pacaya	2011	20-30	Slippery roads with coarse ash ¹⁸		Difficult to drive due to impaired visibility ¹⁸
Puyehue-Cordon Caulle	2011	>100	2WDs experienced traction problems (wet conditions) ¹⁹		"No visibility" ¹⁹
Shinmoedake	2011				Reduced visibility (roads closed) ²⁰
San Cristóbal	2013				Visibility greatly reduced ~15 km from vent (headlights used) ²¹
Sinabung	2014	80-100	Road travel impracticable in wet muddy ash ²²		Reduced visibility ²³
Kelud	2014				Visibility reduced to 500 m around 100 km from vent ²⁴
Calbuco	2015	~50			
Sakurajima	1955-2015	>1	Roads slippery, perhaps less so with recent fine ash ^{7,25,26}	Road markings obscured ^{25,26,27,28}	

Table 1. Examples of reduced skid resistance, road marking coverage and reduced visibility following volcanic eruptions (¹Johnston 1997; ²USGS 2013; ³Warrick et al. 1981; ⁴Cole & Blumenthal 2004; ⁵Cole et al. 2005; ⁶Blong 1984; ⁷Wilson et al. 2009b; ⁸Wilson 2009 (unpublished field notes); ⁹Barnard 2009; ¹⁰Yanagi, Okada & Ohta 1992; ¹¹Stammers 2000; ¹²Nairn 2002; ¹³USGS 2009; ¹⁴Leonard et al. 2005; ¹⁵Wilson 2008 (unpublished field notes); ¹⁶Wilson et al. 2012b; ¹⁷Jamaludin 2010; ¹⁸Wardman et al. 2012b; ¹⁹Wilson et al. 2013; ²⁰Magill, Wilson & Okada 2013; ²¹GVP 2013; ²²Volcano Discovery 2014; ²³Blake et al. 2015; ²⁴AccuWeather 2015; ²⁵Durand et al. 2001; ²⁶Kagoshima City Office (2015, pers comm)). There may be other instances described as 'general impacts to transportation' or which have not been recorded in available records.

2. STUDY AREA – AUCKLAND

Auckland, with a population of 1.42 million as of June 2013 (Statistics NZ, 2013), is the largest city in New Zealand and a vital link in the country's economy. A smoothly operating transport network in Auckland is important for both the regional and national economy (AELP-1, 1999). However, central Auckland is built on a narrow isthmus between the Waitemata Harbour to the north-east, and Manukau Harbour to the south-west. This forms a major geographical feature of the city, constraining the location of many lifeline utilities including electricity, communication and transportation networks, and limiting land-based evacuation routes (Auckland CDEM 2015). Many utilities running through the Auckland isthmus service high populations and consequences of any disruption may be widespread.

Auckland is built on the 360 km² active intra-plate Auckland Volcanic Field (AVF) (Figure 1a-b). The geologically recent eruption of Rangitoto (~600 years ago), comparison with lifespans of analogue volcanic fields and the presence of a mantle anomaly at depths of about 70 – 90 km beneath Auckland that has been interpreted as a zone of partial melting (Horspool, Savage & Bannister 2006) all suggest the field will erupt again (Lindsay 2010). Critical infrastructure including road transportation in the city may be affected by many volcanic hazards from both future eruptions in the AVF and volcanic ash from eruptions at any of the large andesitic to rhyolitic volcanic centres located >190 km away in the central North Island (Auckland CDEM 2015; Lindsay & Peace 2005; Steele et al. 2009) (Figure 1a).

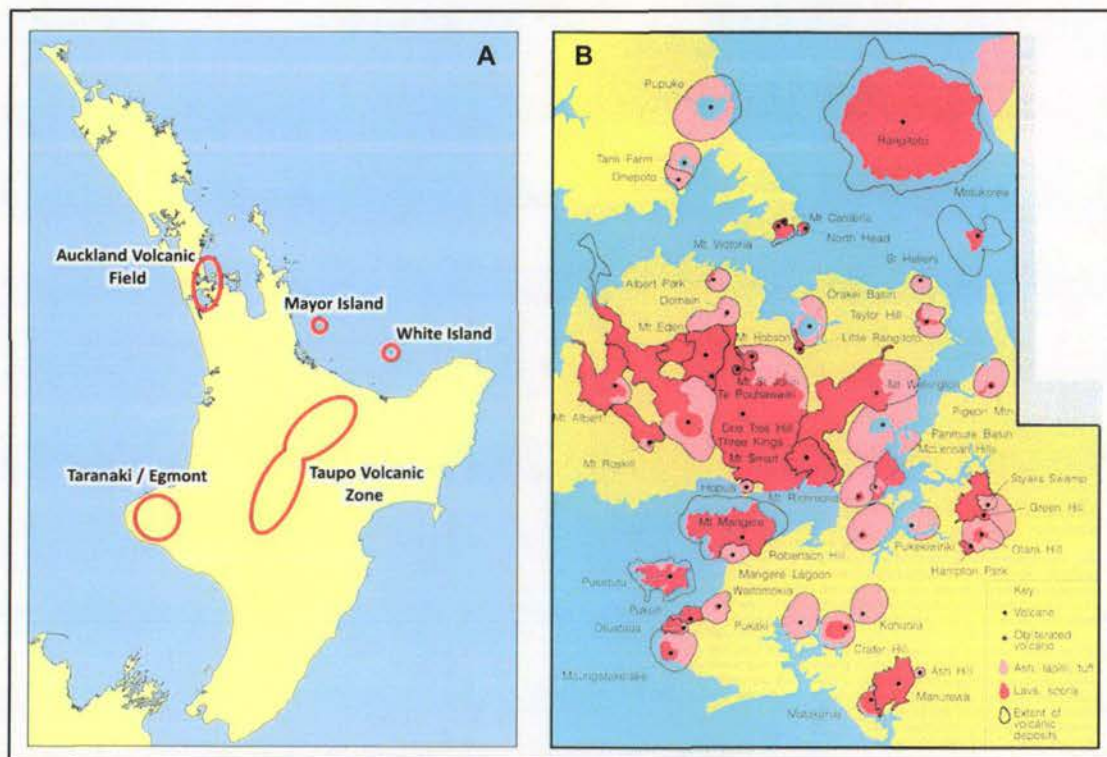


Figure 1. Potential sources of volcanic ash in Auckland including (a) volcanoes in the central North Island of New Zealand and Auckland Volcanic Field (AVF), (b) the AVF showing historic erupted material (Kermode 1992). Note that a new eruption in the AVF will likely occur from a new vent location anywhere within the approximate extent shown on the map.

3. METHODOLOGY

3.1 Skid Resistance

Skid resistance (i.e. the cumulative effects of water, snow, ice, other contaminants and the surface texture on the traction produced by the wheels of a vehicle) is a fundamental component of road safety and should be managed so that it is adequate (Dookeeram et al. 2014). It is essentially a measure of the Coefficient of Friction (CoF) obtained under standardised conditions in which the many variables are controlled so that the effects of surface characteristics can be isolated (Wilson & Chan 2013). We test the skid resistance on road surfaces using the British Pendulum Tester (BPT) (Figure 2), a standard instrument used by road engineers for surface friction testing since its development in the 1950s (Wilson 2006), and still used in many countries, particularly at problematic road sites. Despite the widespread and frequent use of the BPT by road engineers, we are unaware of other studies that have utilised the instrument on ash-covered surfaces.

The test procedure for the BPT is standardised in the ASTM E303 (2013) method. It is a dynamic pendulum impact type test, based on the energy loss occurring when a rubber slider edge is propelled across the test surface. Since the BPT is designed to test the skid resistance of extensive surfaces in-situ, care was taken to ensure that the instrument was stable before conducting our testing in the laboratory environment. We focus our testing on Stone Mastic Asphalt (SMA) concrete, a common surface on the Auckland State Highway network in New Zealand (Boyle 2005), in the form of slabs constructed by the Road Science Laboratory in Tauranga, New Zealand. The skid resistance of line-painted asphalt concrete was also tested using the BPT, after the slabs were machine painted by Downer Group (using a Damar Bead Lock Oil Based Paint containing 63% solids) in four forms (either 1 or 4 applications, with or without retroreflective glass beads).

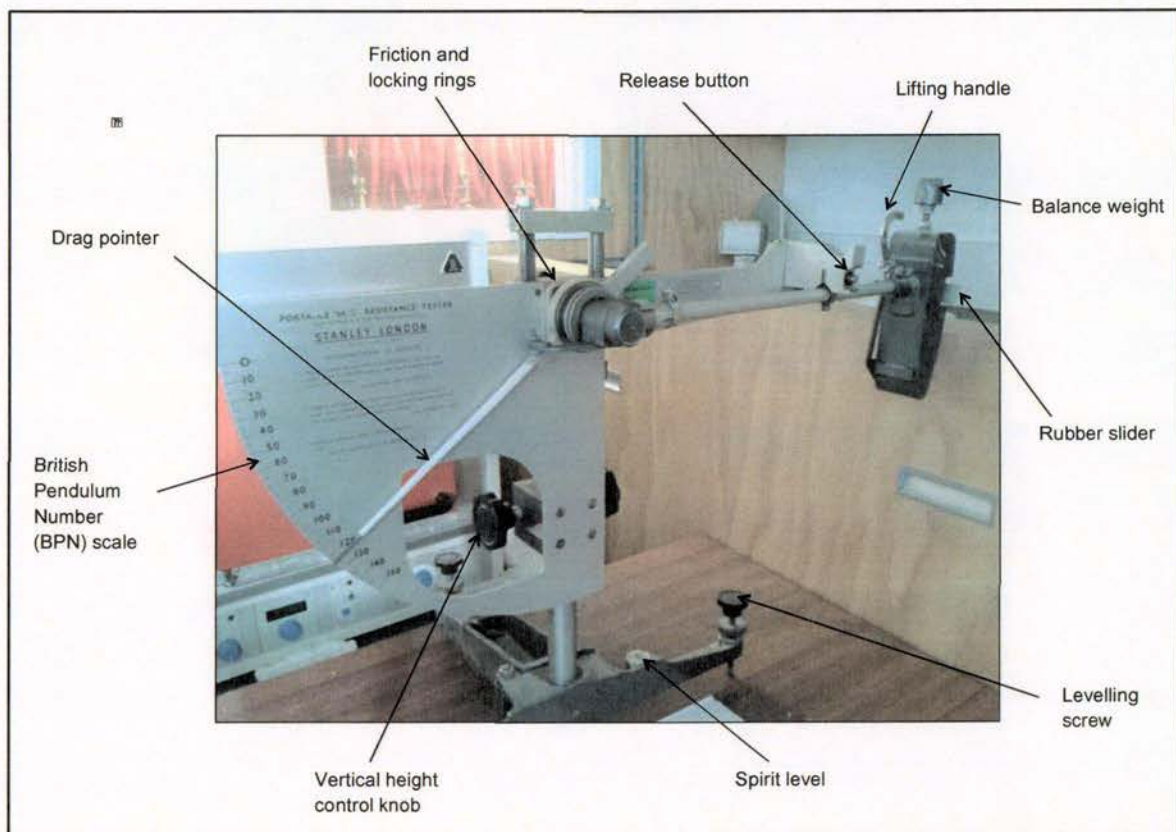


Figure 2. British Pendulum Tester (BPT) used for surface friction testing.

Three volcanic ash types (hard basalt, scoriaceous basalt and pumiceous rhyolite), sourced from different locations in New Zealand, were used in this study to investigate the effects of hardness and mineral components. Both dry and wet ash conditions were investigated for each type with the majority of ash sieved to 1000 μm but some sieved to 106 μm to also study the influence of particle size. Some ash was dosed with fluid from Ruapehu and White Island crater lakes in order to examine the effects of soluble components, which typically adhere to fresh volcanic ash, on skid resistance.

We adopted the same technique as used by the New Zealand Transport Agency (NZTA) (TNZ 2003), whereby for each test surface area, results of a minimum of five successive swings which do not differ by more than three British Pendulum Numbers (BPNs) are recorded. When analysing surfaces covered by ash, any ash that was displaced by the pendulum movement between each swing was replenished with new ash and re-wetted if applicable. The mean of the five BPNs was calculated to give a value representing skid resistance (i.e. the Skid Resistance Value (SRV)). The tests were conducted on every side of each slab to retrieve four SRVs for each condition, which were later averaged.

3.2 Road Marking Coverage

Road marking coverage by volcanic ash is of concern as markings typically provide much of the visual information needed by a driver to navigate roads safely (Gibbons, Hankey & Pashaj 2004). Coverage can lead to driver disorientation (Durand et al. 2001; Wilson et al. 2012a; USGS 2013) and cascading effects on vehicle movement across the road network, such as diminished flow capacity and an increase in traffic accidents (Wolshon 2009). Indeed, the Australian Automobile Association estimate that if 'average standard' road marking is maintained, the percentage of crash rates are reduced by between 10 and 40%, depending on the crash type (Carnaby 2005).

We adopt a method to replicate volcanic ash deposition on road surfaces in the VAT Lab by using the same SMA slabs painted with two thicknesses of line paint as described in section 3.1. The slabs were placed directly beneath an ash delivery system (Figure 3) to investigate thresholds for when road markings become obscured by ash. Samples included ash of three types; one of dark colouration (basalt), one of intermediate colouration (andesite), and one of light colouration (rhyolite), with three modal particle size distributions; fine (34-45 μm), intermediate (200-260 μm), and coarse (600-700 μm). Each sample was deposited onto the surface separately to provide means of contrast and particle size comparisons. Ash depths, measured from the surface of the asphalt concrete aggregate and within the aggregate voids using a caliper, and area density, calculated from the weight of ash in petri dishes, were recorded as the ash accumulated.

A series of digital images were taken in conjunction with the ash measurements using a camera mounted on a tripod 1.5 m horizontally and 1.08 m vertically away from the slab (Figure 3), 1.08 m being the typical height of a driver's eye above the road (Fambro, Fitzpatrick & Rodger 1997). Each image file was opened using Ilastik version 0.5.12 software (Sommer et al. 2011) and one class created for the white paint, and another class for ash or asphalt. After pixel segmentation, Adobe Photoshop version CS6 was used to ensure that each image was cropped to the same dimensions and the number of pixels for the ash/asphalt was calculated by subtracting the number for the white paint from the total pixel count in order to determine the percentage of visible white road markings throughout the experiment.

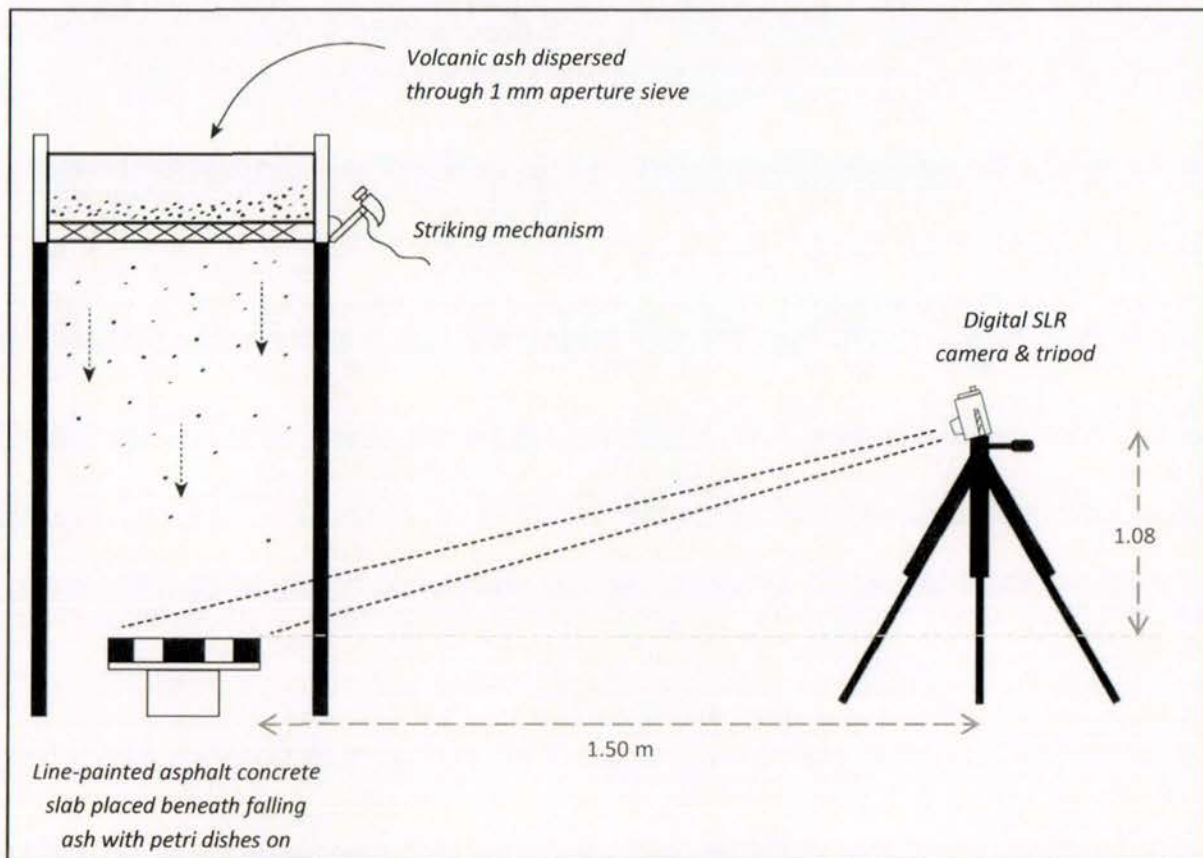


Figure 3. Experimental set-up for road marking coverage experiments.

3.3 Visual Range

Particles and gases interact with light to affect visibility and the interactions consist of light absorption and light scattering. The amount of light redirected from its original path is referred to as the total extinction coefficient (b_{ext}). Light scattering by particles is the dominant cause of reduced visibility in most areas because particles scatter light more efficiently than gases (van de Hulst 1957; White 1990; Hyslop 2009). Once b_{ext} is determined, the corresponding Visual Range (VR), which is often used to quantify visibility, can be calculated:

$$\text{VR} = 3.912 / (b_{\text{ext}} + 0.01) \quad (1)$$

Where the value of the numerator is constant and 0.01 is the Rayleigh coefficient corresponding to a "pristine" environment used to normalise the estimation (Barsotti et al. 2010).

VR is defined as the longest distance that a large, black object can be seen against the sky at the horizon with the unaided eye (Hyslop 2009). VR and b_{ext} are inversely related by the Koschmieder equation.

We investigate the VR through airborne volcanic ash using a set-up incorporating a Dual Pass Opacity Meter (Dynoptic DSL-460 MkII), and a Solid Aerosol Generator (Topas SAG

410) which replicates precise and consistent ash flow rates in a purpose-built enclosed cylindrical container (Figure 4). The opacity meter was calibrated to measure and record b_{ext} so that VRs could be calculated using equation 1.

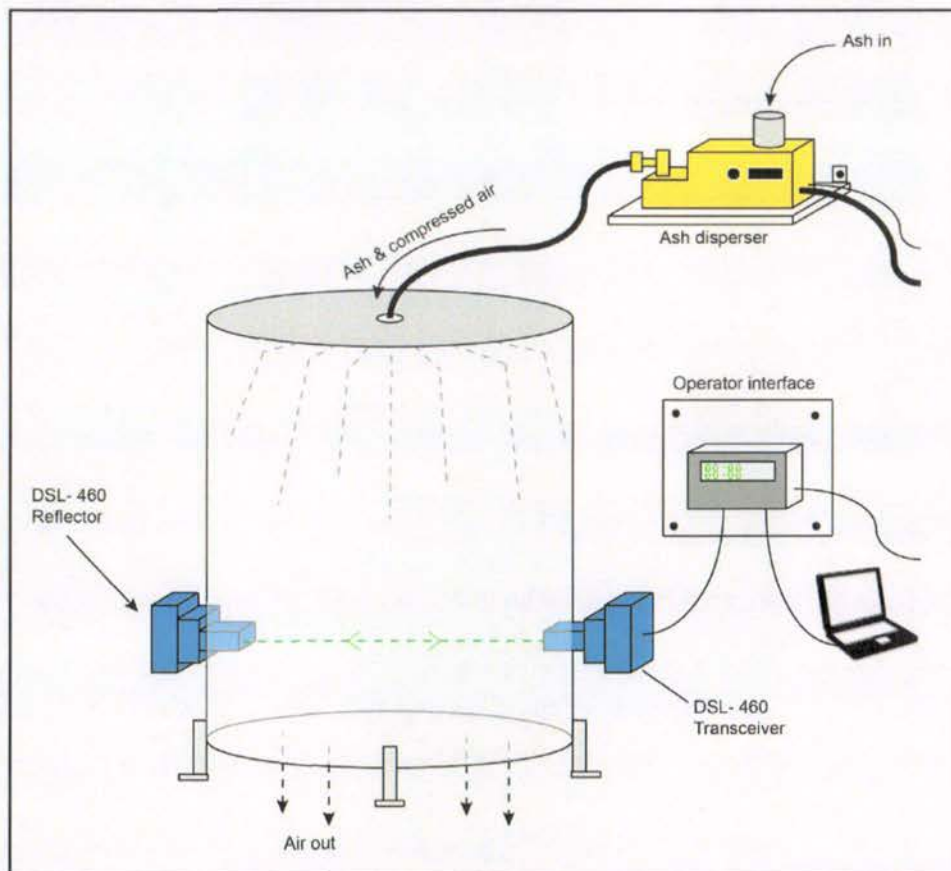


Figure 4. Experimental set-up to investigate visual range in airborne volcanic ash.

Experiments to calculate the visual range in different airborne concentrations of volcanic ash were ongoing during the write-up of this paper. As with the road marking coverage experiment (section 3.2), three types of ash of different colouration will be used in this study. A range of particle sizes (with mode diameters between $\sim 10 \mu\text{m}$ and $\sim 100 \mu\text{m}$) will be incorporated in order to investigate the effect of particle size on visual range.

4. RESULTS

4.1 Skid Resistance

Mean Skid Resistance Values (SRVs) and the corresponding Coefficients of Friction (CoFs) for the non-contaminated SMA concrete (new and cleaned) and the SMA concrete covered by three samples sieved to $1000 \mu\text{m}$ are shown in Figure 5. Our results confirm suggestions from anecdotal observations that skid resistance is reduced following unconsolidated ash accumulation. They also reveal that reduced SRVs are particularly pronounced under dry conditions for a 1 mm thick ash layer on SMA concrete. Mean SRVs for all 1 mm thick ash types fall below the typical minimum recommended SRV for difficult road sites (i.e., an SRV of 65). Wet 1 mm ash-covered surfaces are not necessarily more slippery than dry 1 mm ash-covered surfaces and the wet surfaces covered in 1 mm thick ash are only slightly more slippery than the wet asphalt without ash contamination.

Different trends are observed for SMA concrete covered by ash >1 mm thick. The hard basalt has similar SRVs to the 1 mm thick layer but the scoriaceous basalt and pumiceous rhyolite have greater SRVs than those for 1 mm of ash, suggesting that these ash types are perhaps less slippery when thicker. We note that the pendulum arm may be slowed upon initial impact with the thicker deposits, producing higher than true representative SRVs. However, the comparatively low SRVs for the 5 mm thick hard basaltic sample suggest that other ash characteristics are also important.

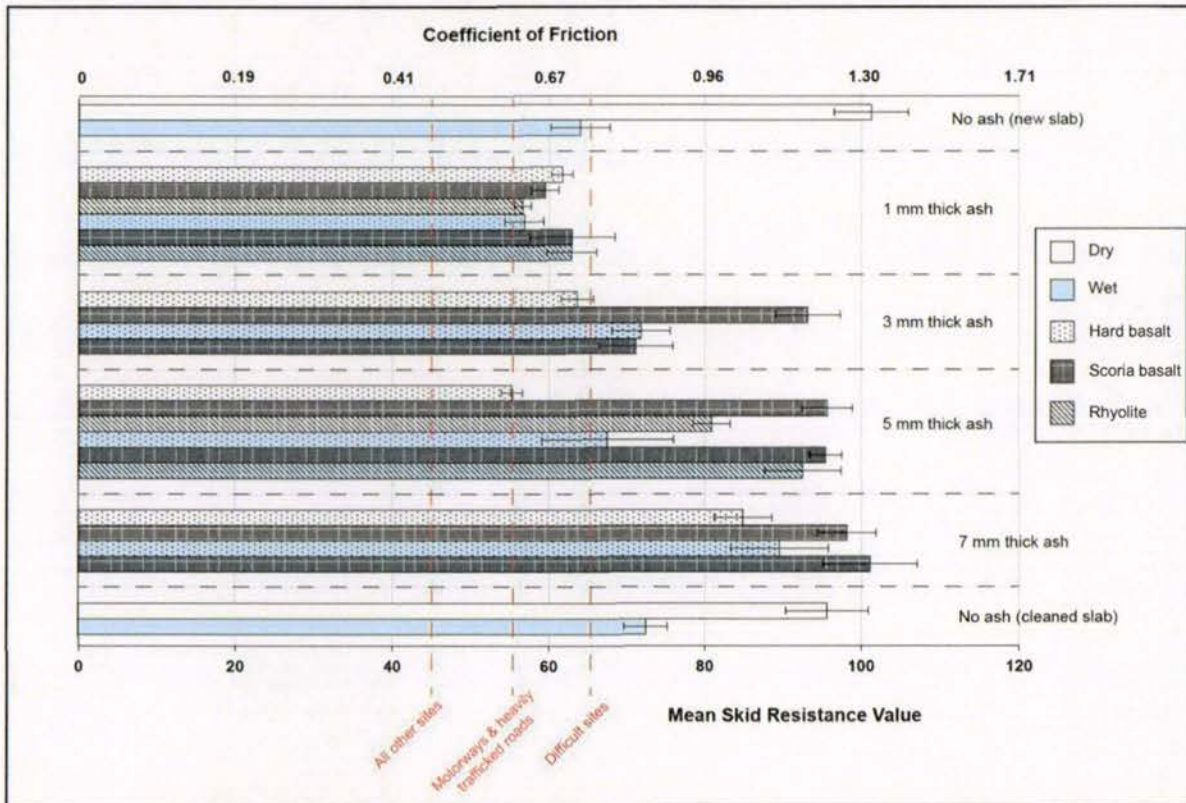


Figure 5. Mean SRVs and CoFs for the non-contaminated SMA and SMA covered in the three ash types sieved to 1000 μm . Wet and dry samples at 1, 3, 5 and 7 mm thicknesses are shown although limitations in the quantity of rhyolite meant that testing was only conducted at 1 and 5 mm thickness for this ash type. The error bars represent the standard deviation for each data set. Also displayed (as red dashed lines) are the minimum recommended SRVs for different road network sites (British Pendulum Manual 2000; Asi 2007; Impact 2010).

SRVs for the scoriaceous basalt containing adhered soluble components (i.e. the samples dosed with crater lake fluid) were generally less than those that were not dosed. Furthermore, as the degree of soluble components was increased, the SRVs decreased. However, no change was evident for the hard basaltic samples, perhaps due to the highly crystalline properties of this ash type reducing soluble component adherence.

Mean SRVs for the fine-grained ash samples were slightly higher than those for the coarse-grained ash of the same type when at 1 mm thickness, with mean values for both wet and dry samples above the minimum recommended SRVs for difficult sites. We suggest that this is due to the finer particles being more easily mobilised and displaced at the tyre-asphalt concrete interface at such ash depths, allowing improved contact between the tyre and road surface.

The mean SRVs on wet line-painted asphalt concrete surfaces with no retroreflective beads and no ash were the lowest of all our results (SRVs of 40-46 when wet). The addition of

glass beads does increase SRVs (by around 5), although values are still relatively low. SRVs for 'clean' and dry line-painted asphalt surfaces are very high, but as with non-painted surfaces, the addition of a 1 mm ash layer decreases SRVs substantially. Conversely, the SRVs for wet asphalt concrete increase with a 1 mm ash layer to similar levels as for dry conditions. With a thicker (5 mm) ash layer on top of line-painted surfaces, SRVs increase.

4.2 Road Marking Coverage

Following initial ash dispersal events, the percentage of pixels representing white road marking paint was found to decrease substantially, suggesting that only very small surface depths are required for an impact on road marking visibility. Indeed, $\leq 8\%$ of pixels for white paint (taken to be the threshold when it would be difficult for drivers to observe markings) without retroreflective beads was evident at area densities of $35\text{--}80\text{ g m}^{-2}$ for fine-grained ash. Although measurements of thickness proved difficult at such low accumulations, these area densities were estimated to correspond to depths of just $\sim 0.1\text{ mm}$ measured from the surface of the asphalt concrete aggregate. Ash particle size distribution is likely the most influential characteristic for marking coverage at small depths and a mass of fine particles is much more effective at covering a surface than the same mass of coarse particles.

Multiple paint layers (assuming little wear) and paint that incorporates retroreflective glass beads make markings more difficult to distinguish when ash accumulates. Road markings covered by light-coloured ash of the same thickness as dark-coloured ash are also more difficult to distinguish due to low contrast (Figure 6). We also note that contrast requirements are greater the farther the object is from the driver (Gibbons, Hankey & Pashaj 2004). Therefore a driver's ability to see road markings with distance may be also be hindered by light-coloured ash more than ash of dark colouration. These findings especially highlight the susceptibility of road markings being covered in distal areas from volcanic vents where fine-grained and light-coloured ash is more likely.

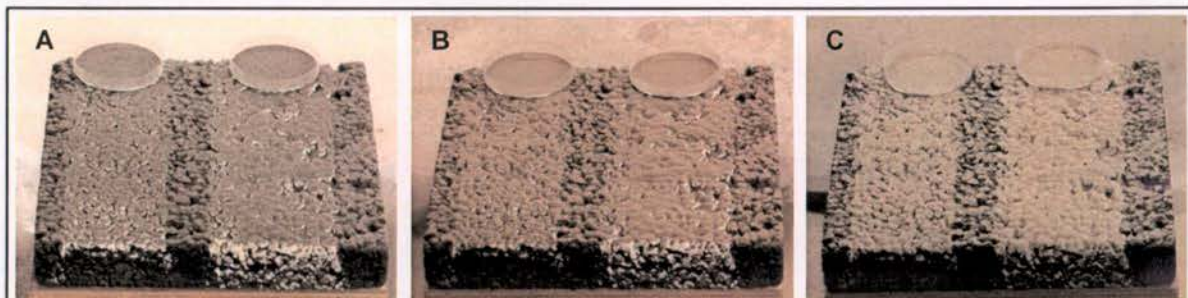


Figure 6. Road markings containing no retroreflective beads in the paint mix when $\leq 8\%$ of line paint was visible for (a) basaltic, (b) andesitic, and (c) rhyolitic, ash of $200\text{--}260\text{ }\mu\text{m}$ modal particle size distributions. This corresponds to mean thicknesses on the surface of the asphalt aggregate of 0.55 , 0.35 and 0.30 mm respectively.

We highlight the importance of outlining the specifics for depth type measured on road surfaces for ash accumulations less than $\sim 10\text{ mm}$. Depths within the asphalt aggregate voids were found to be over five times greater than those measured from the surface of the aggregate in some cases.

4.3 Visual Range

Preliminary results for the visual range experiments are for the basaltic ash sieved to $212\text{ }\mu\text{m}$ (with a particle size range of $1\text{--}280\text{ }\mu\text{m}$ and mode size of $105\text{ }\mu\text{m}$) and dispersed into the cylindrical container at a flow rate of 69 g h^{-1} (Figure 7a) and 137 g h^{-1} (Figure 7b). Such characteristics represent approximately the mean particle size that can be expected from

Auckland Volcanic Field eruptions when at locations of ~4-11 km from a vent (Hopkins pers comm, 2014), and likely lie towards the lower end of ash settling rates that can be expected based on data from historical eruptions worldwide.

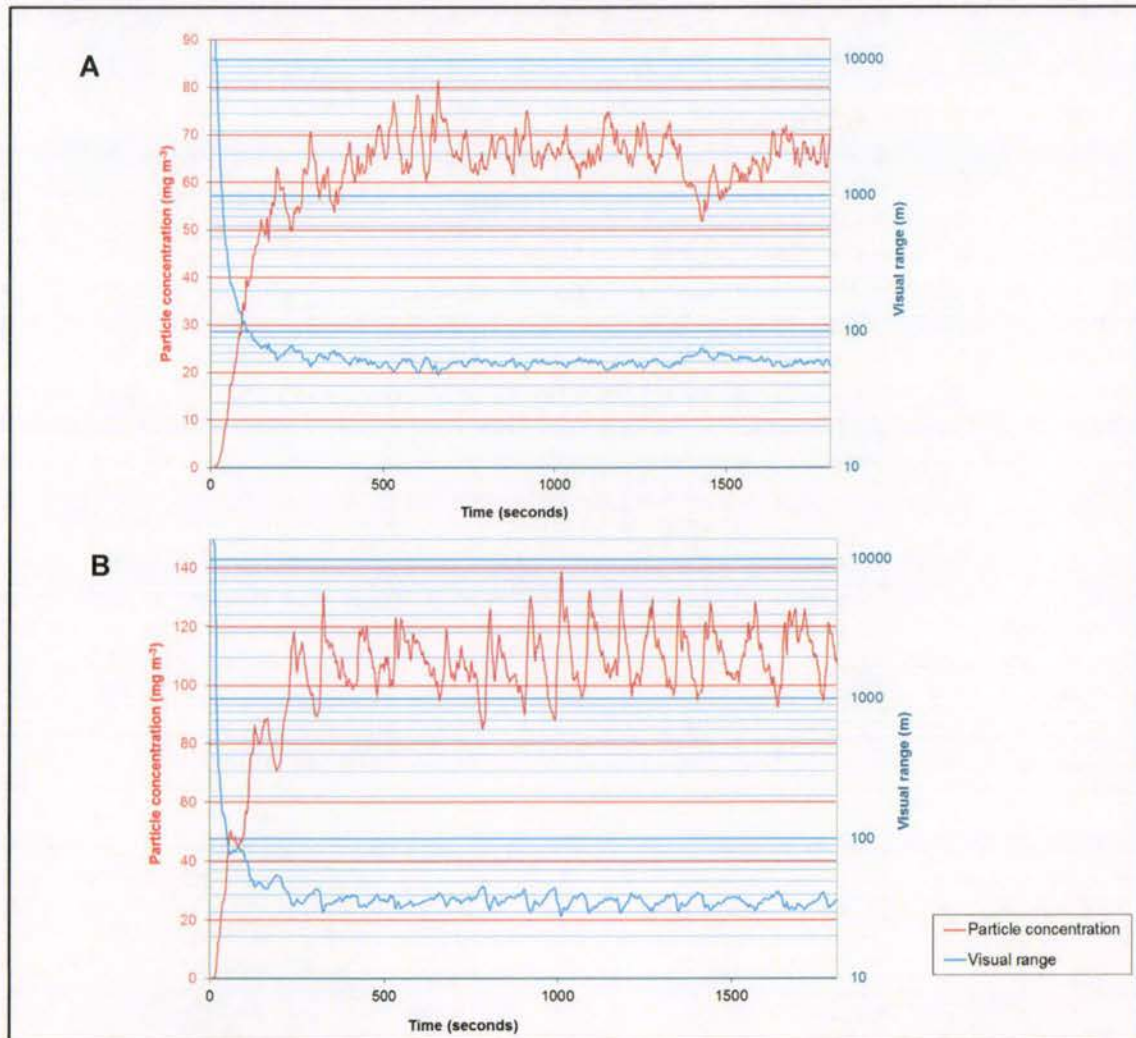


Figure 7. Visual range and particle concentration with ash sieved to 212 μm dispersed at (a) a flow rate of 69 g h^{-1} and (b) a flow rate of 137 g h^{-1} .

The visual range (calculated using equation 1) was found to decrease over around 300 seconds for both tests, albeit at a decreasing rate, reflecting the increase in airborne particle concentration. After this time, equilibrium between ash settling rate and flow rate (into the container) appears to have been reached. After 300 seconds at the lower flow rate, following dispersion of 5.8 grams of ash into the container, a particle concentration of around 65 mg m^{-3} and corresponding visual range of ~60 m occurred. At the higher flow rate, following dispersion of 11.4 grams of ash into the container, a particle concentration of around 110 mg m^{-3} and corresponding visual range of ~35 m occurred.

In previous studies to determine how drivers react when driving in varying levels of fog using a driver-simulation method (Brooks et al. 2011), a visual range of 18 m resulted in participants decreasing their average speed by over 5 km h^{-1} (from 88.6 km h^{-1}). However, it was calculated that drivers would be incapable of stopping to avoid obstacles in the roadway at such speeds, a situation that corresponds to what has been recorded on actual roads in inclement weather (Edwards 1999). Lane-keeping ability was reduced when fog resulted in visual ranges <30 m (Brooks et al. 2011). Such visual ranges and associated disruption are

not anticipated for the same conditions as in our initial tests. However, it seems probable that they would occur at the mid-to-large range of ash settling rates that can be expected in Auckland with additional impacts on road safety including covered road markings and reduced skid resistance. Further testing will confirm the specifics.

5. DISCUSSION & CONCLUSIONS

5.1 Road transport resilience

The experiments and analysis demonstrate that very low quantities of volcanic ash (~0.1-1.0 mm surface depths) have the potential to cause substantial impacts to road transportation. It also appears likely that airborne ash can cause disruption at relatively high concentrations. Many ash characteristics are important to consider, not just the depth of ash. For example, the largest change in skid resistance for surfaces that become covered by ash occurs during dry conditions with ash type having a large influence on SRVs as the depth of deposits increases (i.e. thicker layers of hard basalt were found to be more slippery than scoriaceous ash at the same depth). Ash of low crystallinity containing a high degree of soluble components (i.e. replicating fresh deposits) was found to be more slippery than ash which had not been dosed, and road markings covered by fine-grained ash of the same thickness as coarse-grained ash are much more difficult to distinguish.

Based on findings so far, we make the following preliminary recommendations to increase road safety with volcanic ash exposure of ≤ 5 mm depth, therefore helping to increase the resilience of road transportation networks following eruptions:

- During initial ash fall, vehicle speed (or advisory speed) should immediately be reduced to levels below those when driving in very wet conditions on that road, whether the surface is wet or dry. Wet ash is not necessarily more slippery than dry ash, at least initially.
- Fresh ash generally contains more soluble components, which results in lower skid resistance values than for leached ash. Therefore, it is important to advise motorists promptly of any restrictions.
- Particular caution should be taken on dry surfaces that become covered by coarse-grained ash as skid resistance will reduce substantially from what occurs on dry non-contaminated surfaces. The slipperiness of dry surfaces with such contamination may not be expected by motorists.
- Road markings may be hidden from view with as little as 0.1 mm of ash if fine-grained, impacting road safety through lack of visual guidance of road features. Visual impairment of markings will be particularly problematic during rhyolitic ashfall due to lower visual contrast.
- Areas of road that are line-painted and covered in ash are also especially slippery. Motorcyclists and cyclists in particular should take extreme care.
- Visibility from direct ashfall will decrease quickly and likely fall to the lowest level after around 5 minutes of it arriving (assuming a consistent ashfall rate). Extreme caution should be taken as it may be difficult to avoid stopped vehicles and other obstacles, and lane-keeping ability may be reduced.

Our studies also allow thresholds and recommendations associated with road cleaning to be determined, which will improve road safety and network functionality during ashfall:

- Road cleaning should be conducted at or before ash area densities of 30-45 g m⁻² for fine-grained ash of all types, 100-250 g m⁻² for ash of intermediate size, and 1,000-1,500 g m⁻² for coarse-grained andesite or basalt.

- Brushing alone will not restore surfaces to their original condition in terms of skid resistance:
 - If surfaces are dry and contaminated with ash, air blasting combined with suction and capture of loosened ash, is an effective way to remove ash from surface voids and restore skid resistance to near-original levels.
 - If surfaces are wet, a combination of water spraying and brushing and/or air blasting (with suction and ash capture) is an effective way to remove most ash and restore surface skid resistance.

Ash re-suspension and subsequent secondary deposition should be carefully considered prior to cleaning. Extensive (and often expensive) cleaning efforts may be wasted if substantial ash is still present in the environment and continues to be deposited onto road surfaces.

5.2 Modelling disruption and recovery in Auckland

Our results are informing models of critical infrastructure disruption and recovery in central Auckland following hypothetical eruptive scenarios in the AVF. Modelling includes the recently extended Mt. Ruaumoko volcanic eruption scenario (Deligne et al. 2015), developed as part of the Economics of Resilient Infrastructure (ERI) research programme, a four-year project funded by the New Zealand government. Mt. Ruaumoko is a hypothetical volcano that first emerged during 'Exercise Ruaumoko' in 2007/08, the largest Civil Defence and Emergency Management exercise in New Zealand, which tested national arrangements for responding to a major disaster in Auckland. The extended scenario includes a sequence of time-series maps that convey infrastructure outages in terms of the change in 'level of service' experienced by the end-user during the course of the eruption. An example of road transportation 'level of service' experienced during this scenario is shown in Figure 8.

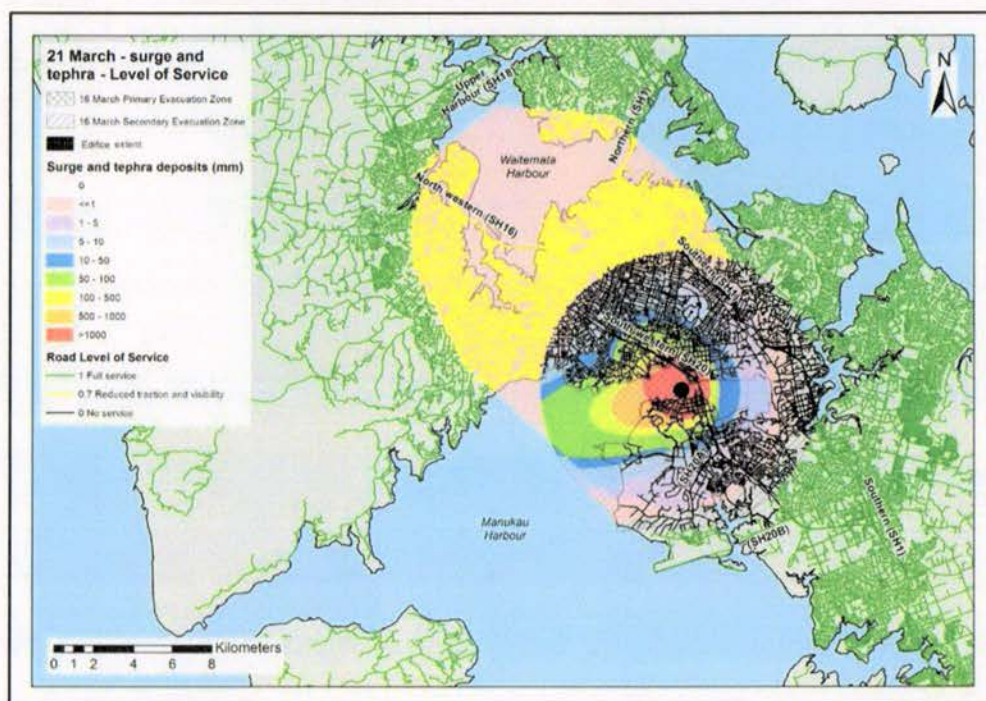


Figure 8. Level of service for road transportation experienced on 21 March during the hypothetical Mt. Ruaumoko eruption in the AVF (Deligne et al. 2015).

The anticipated level of service on central Auckland roads affected by ash fall deposits ≤ 1 mm is 0.7 (coloured in yellow on Figure 8), 1 conveying the 'typical' full service level and 0

describing 'no service'. This reduced level of service for roads was based on anecdotal evidence from previous eruptions worldwide, discussions with road transportation managers in Auckland, and the empirical evidence determined by laboratory studies described in this paper, which suggested that both skid resistance and visibility (of road markings and through airborne ash) will be reduced at such depths. Further work will analyse impacts to critical infrastructure including road transportation across the full extent of the AVF using a grid-based probabilistic method and incorporate a range of possible eruption styles and associated volcanic hazard 'rules'. This will enable the identification of road transport disruption 'hotspots' in Auckland, allowing further improvements in risk management for volcanic eruptions and an increase in overall transport system resilience.

REFERENCES

- AccuWeather (2015). *First Calbuco eruption in 42 years suspends flights in Buenos Aires*, AccuWeather.com, <http://www.accuweather.com/en/weather-news/more-than-4000-evacuated-after/46042985> Accessed 23/11/2015.
- AELP-1 (1999). *Auckland Engineering Lifelines Project: Final Report – Stage 1*. Auckland Regional Council Technical Publication No. 112, Auckland, New Zealand.
- ASTM E303 (2013). *Standard test method for measuring surface frictional properties using the British Pendulum Tester*. ASTM E303-93 (Reapproved 2013).
- Auckland CDEM (2015). *Auckland Volcanic Field Contingency Plan*. Civil Defence and Emergency Management, Auckland, New Zealand, <http://www.aucklandcivildefence.org.nz/about-us/document-library/supporting-plans/> Accessed 27/11/2015.
- Asi, I. (2007) Evaluating skid resistance of different asphalt concrete mixes. *Building and Environment*, 42:1, pp.325-329.
- Barnard, S. (2009). *The vulnerability of New Zealand lifelines infrastructure to ashfall*. PhD Thesis, Hazard and Disaster Management, University of Canterbury, Christchurch, New Zealand.
- Barsotti, S. Andronico, D. Neri, A. Del Carlo, P. Baxter, P.J. Aspinall, W.P. Hincks, T. (2010). Quantitative assessment of volcanic ash hazards for health and infrastructure at Mt. Etna (Italy) by numerical simulation, *Journal of Volcanology and Geothermal Research*, 192, pp.85-96.
- Blake, D.M. Wilson, G. Stewart, C. Craig, H.M. Hayes, J.L. Jenkins, S.F. Wilson, T.M. Horwell, C.J. Andreastuti, S. Daniswara, R. Ferdiwijaya, D. Leonard, G.S. Hendrasto, M. Cronin, S. (2015). The 2014 eruption of Kelud volcano, Indonesia: impacts on infrastructure, utilities, agriculture and health. *GNS Science Report 2015/15*, 139p.
- Blong, R.J. (1984). *Volcanic hazards: a sourcebook on the effects of eruptions*. New South Wales, Australia.
- Boyle, T. (2005). *Skid resistance management on the Auckland State Highway Network*. Transit New Zealand, <http://www.nzta.govt.nz/resources/surface-friction-conference-2005/8/docs/skid-resistance-management-auckland-state-highway-network.pdf> Accessed 16/06/2015.
- British Pendulum Manual (2000). *Operation manual of the British Pendulum Skid Resistance Tester*. Wessex Engineering Ltd., United Kingdom.
- Brooks, J.O. Crisler, M.C. Klein, N. Goodenough, R. Beeco, R.W. Guirf, C. Tyler, P.J. Hilbert, A. Miller, Y. Grygier, J. Burroughs, B. Martin, A. Ray, R. Palmer, C. Beck, C. (2011). Speed choice and driving performance in simulated foggy conditions. *Accident Analysis and Prevention*, 43, pp698-705.
- Carnaby, B. (2005). *Road marking is road safety*. Conference paper by Potters Asia Pacific, presented at the New Zealand Roadmarkers Federation Conference 2005, Christchurch, New Zealand.
- Cole, J. & Blumenthal, E. (2004). *Evacuate! Tephra Newsletter: June 2004*, New Zealand.
- Cole, J.W. Sabel, C.E. Blumenthal, E. Finnis, K. Dantas, A. Barnard, S. Johnston, D.M. (2005). GIS-based emergency and evacuation planning for volcanic hazards in New Zealand. *Bulletin of the New Zealand Society for Earthquake Engineering*, 38, pp149-164.
- Deligne, N.I. Blake, D.M. Davies, A.J. Grace, E.S. Hayes, J. Potter, S. Stewart, C. Wilson, G. Wilson, T.M. (2015). Economics of Resilient Infrastructure Auckland Volcanic Field scenario. *ERI Research Report 2015/03*, 151 p.
- Dookeeram, V. Nataadmadja, A.D. Wilson, D.J. Black, P.M. (2014). The skid resistance performance of different New Zealand aggregate types. *IPENZ Transportation Group Conference 23-26 March 2014*, Shed 6, Wellington, New Zealand.
- Durand, M. Gordon, K. Johnston, D. Lorden, R. Poirot, T. Scott, J. Shephard, B. (2001). Impacts and responses to ashfall in Kagoshima from Sakurajima Volcano – lessons for New Zealand, *GNS Science Report 2001/30*, 53 p.
- Edwards, J.B. (1999). Speed adjustment of motorway commuter traffic to inclement weather. *Transportation Research Part F*, 2, pp1-14.

- Fambro, D.B. Fitzpatrick, K. & Rodger, J.K. (1997). Determination of stopping sight distances. National Cooperative Highway Research Program Report 400, Transportation Research Board National Research Council, Washington D.C.
- Gibbons, R.B. Hankey, J. & Pashaj, I. (2004). *Wet night visibility of pavement markings: executive summary*. Virginia Tech Transportation Institute, Virginia Polytechnic Institute and State University, Charlottesville, Virginia. <https://vtechworks.lib.vt.edu/bitstream/handle/10919/46697/05-cr4.pdf?sequence=1> Accessed 26/09/2015.
- GVP (2013). *Report on San Cristobal (Nicaragua): January 2013*. Global Volcanism Program, <http://volcano.si.edu/showreport.cfm?doi=10.5479/si.GVP.BGVN201301-344020> Accessed 23/11/2015.
- Hopkins, J. (2015). Information and data obtained from Jenni Hopkins, Victoria University of Wellington, New Zealand. Personal Communication by Email, 19 July 2014.
- Horspool, N.A. Savage, M.K. & Bannister, S. (2006). Implications for intraplate volcanism and back-arc deformation in northwestern New Zealand, from joint inversion of receiver functions and surface waves. *Geophysical Journal International*, 166, pp.1466-1483.
- Hyslop, N.P. (2009). Impaired visibility: the air pollution people see. *Atmospheric Environment*, 43, pp.182-195.
- Impact (2010). Skid tester: AG190. Impact Test Equipment Ltd http://www.impact-test.co.uk/docs/AG190_HB.pdf Accessed 04/11/2014.
- Jamaludin, D. (2010). *BORDA respond to Merapi Disaster. Bremen Overseas Research and Development Association, Indonesia*, <http://www.borda-sea.org/news/borda-sea-news/article/borda-respond-to-merapi-disaster.html> Accessed 23/11/2015.
- Johnston, D.M. (1997). Physical and social impacts of past and future volcanic eruptions in New Zealand. PhD Thesis, Earth Science, Massey University, Palmerston North, New Zealand.
- Johnston, D.M. & Daly, M. (1997). Auckland erupts!! *New Zealand Science Monthly*, 8:10, pp.6-7.
- Kagoshima City Office (2015). Discussion with staff at the Kagoshima City Office, Kagoshima, Japan. Personal Communication, 08 June 2015.
- Leonard, G.S. Johnston, D.M. Williams, S. Cole, J.W. Finnis, K. Barnard, S. (2005). Impacts and management of recent volcanic eruptions in Ecuador: lessons for New Zealand. *GNS Science Report 2005/20*, 52 p.
- Lindsay JM (2010). Volcanoes in the big smoke: a review of hazard and risk in the Auckland Volcanic Field. Institute of Earth Science and Engineering and School of Environment, University of Auckland, Auckland, New Zealand.
- Lindsay, J. & Peace, C. (2005). Auckland Engineering Lifelines Group Project AELG-7: Health and safety issues in a volcanic ash environment. *Auckland Regional Council Technical Publication No. 290*, Auckland, New Zealand.
- Magill, C. Wilson, T. & Okada, T. (2013). Observations of tephra fall impacts from the 2011 Shinmoedake eruption, Japan. *Earths Planets and Space*, 65, pp.677-698.
- Nairn, I.A. (2002). The effects of volcanic ash fall (tephra) on road and airport surfaces. *Institute of Geological and Nuclear Science Report 2002/13*, Lower Hutt, New Zealand.
- Sommer, C. Strähle, C. Köthe, U. Hamprecht, F.A. (2011). Ilastik: interactive learning and segmentation toolkit. BibTex file, Technical Report, In: Eighth IEEE International Symposium on Biomedical Imaging Proceedings, pp.230-233.
- Stammers, S.A.A. (2000). The effects of major eruptions of Mount Pinatubo, Philippines and Rabaul Caldera, Papua New Guinea, and the subsequent social disruption: lessons for the future. Unpublished MSc Thesis, University of Canterbury, Christchurch, New Zealand.
- Statistics NZ (2013). *Auckland fastest-growing region since last census, and South Island districts grow most*. Statistics New Zealand, http://www.stats.govt.nz/browse_for_stats/population/census_counts/2013CensusUsuallyResidentPopulationCounts_MR2013Census.aspx Accessed 23/11/2015.
- Steele, A. Lindsay, J. Leonard, G. Smid, E. (2009). The DEVORA borehole database: initial report. Institute of Earth Science and Engineering, The University of Auckland, Auckland, New Zealand.
- TNZ (2003). Standard test procedure for measurement of skid resistance using the British Pendulum Tester, Report TNZ T/2:2003. Transit New Zealand, New Zealand.
- USGS (2009). *What's it like during ash fall: small explosion produced light ash fall at Soufriere Hills volcano, Montserrat*, <https://volcanoes.usgs.gov/ash/ashfall.html#eyewitness> Accessed 23/11/2015.
- USGS (2013) *Volcanic ash: effects and mitigation strategies*. United States Geological Survey <http://volcanoes.usgs.gov/ash/trans/> Accessed 21/09/2015.
- van de Hulst, H.C. (1957). *Light scattering by small particles*, John Wiley and Sons Inc, New York.
- Volcano Discovery (2014). *Sinabung eruption update: 13 January 2014*. Volcano Discovery, <http://www.volcanodiscovery.com/sinabung-eruptions.html> Accessed 16/01/2014.
- Wardman, J.B. Wilson, T.M. Bodger, P.S. Cole, J.W. Johnston, D.M. (2012a). Investigating the electrical conductivity of volcanic ash and its effect on HV power systems. *Physics and Chemistry of the Earth*, 45-46, pp.128-145.
- Wardman, J. Sword-Daniels, V. Stewart, C. Wilson, T. (2012b). Impact assessment of the May 2010 eruption of Pacaya volcano, Guatemala. *GNS Science Report 2012/09*, 90 p.
- Warrick et al. (1981). *Four communities under ash after Mount St. Helens*. Institute of Behavioural Science, University of Colorado.

- White, W.H. (1990). The components of atmospheric light extinction: a survey of ground-level budgets, *Atmospheric Environment*, 24A, pp.2673-2679.
- Wilson, D.J. (2006) An analysis of the seasonal and short-term variation of road pavement skid resistance. PhD Thesis, Department of Civil and Environmental Engineering, University of Auckland, Auckland, New Zealand.
- Wilson, D.J. & Chan, W. (2013). The effects of road roughness (and test speed) on GripTester measurements. NZ Transport Agency Research Report 523, Clearway Consulting Ltd., Auckland, New Zealand.
- Wilson, T.M. (2008). Unpublished field notes from the Chaiten eruption field visit, University of Canterbury, Christchurch, New Zealand.
- Wilson, T.M. (2009). Unpublished field notes from the Hudson eruption field visit, University of Canterbury, Christchurch, New Zealand.
- Wilson, T. Daly, M. & Johnston, D. (2009a) Review of impacts of volcanic ash on electricity distribution systems, broadcasting and communication networks. Auckland Engineering Lifelines Group, Auckland Regional Council Technical Publication No. 051.
- Wilson, T.M. Stewart, C. Cole, J.W. Dewar, D.J. Johnston, D.M. Cronin, S.J. (2009b). The 1991 eruption of Volcan Hudson, Chile: impacts on agriculture and rural communities and long-term recovery. *GNS Science Report 2009/66*. 99 p.
- Wilson, T.M. Stewart, C. Sword-Daniels, V. Leonard, G.S. Johnston, D.M. Cole, J.W. Wardman, J. Wilson, G. Barnard, S.T. (2012a) Volcanic ash impacts to critical infrastructure. *Physics and Chemistry of the Earth*, 45-46, pp.5-23.
- Wilson, T. Cole, J. Johnston, D. Cronin, S. Stewart, C. Dantas, A. (2012b) Short- and long-term evacuation of people and livestock during a volcanic crisis: lessons from the 1991 eruption of Volcan Hudson, Chile. *Journal of Applied Volcanology*, 1:2.
- Wilson, T. Stewart, C. Bickerton, H. Baxter, P. Outes, V. Villarosa, G. Rovere, E. (2013). Impacts of the June 2011 Puyehue-Cordon Caulle volcanic complex eruption on urban infrastructure, agriculture and public health. *GNS Science Report 2012/20*, 88 p.
- Wilson, G. Wilson, T.M. Deligne, N.I. Cole, J.W. (2014). Volcanic hazard impacts to critical infrastructure: a review. *Journal of Volcanology and Geothermal Research*, 286, pp.148-182.
- Wolshon, B. (2009). Transportation's role in emergency evacuation and re-entry: a synthesis of highway practice. National Cooperative Highway Research Program, Transportation Research Board Synthesis 392, Washington D.C.
- Yanagi, T. Okada, H. & Ohta, K. (1992). *Unzen volcano, the 1990-1992 eruption*. The Nishinippon and Kyushu University Press, Fukuoka, 137 p.

ACKNOWLEDGEMENTS

We thank the University of Canterbury Mason Trust scheme, New Zealand Earthquake Commission (EQC), Natural Hazards Research Platform (NHRP) and Determining Volcanic Risk in Auckland (DEVORA) project for their financial support towards the research. We also express thanks to the organisations and people who helped source equipment and provided advice that was vital to the project. In particular, we would like to thank Alan Nicholson and John Kooloos of the Civil and Natural Resources Engineering department at the University of Canterbury for the loan of the BPT, and Christopher Gomez from the Geography department at the University of Canterbury for advising on image processing methods. Additionally, thank you to Janet Jackson, Howard Jamison and the wider laboratory and road teams at Downer Group for their support towards coordinating the construction and line-painting of asphalt slabs and for providing Daniel Blake with BPT training. Special thanks to Jozua Taljaard and Andrew Blair of Ecotech NZ Environmental Ltd in Auckland, and Stephan Große of Topas GmbH in Dresden, Germany for their remote technical support before and following the supply of the opacity meter and solid aerosol generator respectively. Particular thanks also go to the people who provided support with the laboratory set-up at various stages, including University of Canterbury technician support from Rob Spiers, Matt Cockcroft, Chris Grimshaw and Sacha Baldwin-Cunningham. We also thank researchers Emily Lambie, Rinze Schuurmans, Connor Jones, Alec Wild and Alistair Davies for their assistance with sample preparation and skid resistance testing, and the wider University of Canterbury ash impacts team for their assistance with field sample collection.

We would like to highlight that much of the research outlined in this conference paper is intended for publication in a more detailed format within peer-reviewed academic journals.

Impact of volcanic ash on road and airfield surface skid resistance

Daniel M Blake^{1*}, Thomas M Wilson¹, Jim W Cole¹, Natalia I Deligne², Jan M Lindsay³

¹ Department of Geological Sciences, University of Canterbury, Private Bag 4800, Christchurch, New Zealand

² GNS Science, 1 Fairway Drive, Avalon 5010, PO Box 30-368, Lower Hutt 5040, New Zealand

³ School of Environment, The University of Auckland, Private Bag 92019, Auckland, New Zealand

*Corresponding author

Email: daniel.blake@pg.canterbury.ac.nz

Abstract

Volcanic ash deposited on paved surfaces during volcanic eruptions often compromises skid resistance, which is a major component of road and airfield safety. This can result in increased stopping distances for vehicles and higher accident rates. Impacts can be widespread and long lasting, particularly during eruptions that continue for weeks to months and where ash is readily dispersed or remobilised by wind, vehicles or other human activity. Despite numerous anecdotal observations to this effect, few detailed studies have quantified the impacts of volcanic ash on skid resistance. It is important to fill this gap, as the effects of thin ash deposits in particular present a source of uncertainty for impact and loss assessment models. We adopt the British pendulum test method in laboratory conditions to investigate the skid resistance of road asphalt and airfield concrete surfaces covered by ash sourced from various locations in New Zealand. Controlled variations in ash characteristics include type (rhyolite and basalt), depth (up to 9 mm thick), wetness, particle size and soluble components. We use Stone Mastic Asphalt (SMA) for most road surface tests. However, we also test porous asphalt and line-painted road surfaces, and a roller screed concrete mix used for airfields. Due to their importance for skid resistance, SMA surface macrotexture and microtexture are analysed with semi-quantitative image analysis, microscopy and a standardised sand patch volumetric test, which enables determination of the relative effectiveness of different cleaning techniques. We find that SMA surfaces covered by thin deposits (~1 mm) of ash result in skid resistance values slightly lower than those observed on wet uncontaminated surfaces. At these depths, a higher relative soluble content for low-crystalline ash and a coarser particle size results in lower skid resistance. Skid resistance results for relatively thicker deposits (3-5 mm) of non-vesiculated basaltic ash are similar to those for thin deposits. Although there is initially little difference in skid resistance between surfaces covered in dry or wet ash, testing indicates that surfaces covered by wet ash remain slippery for longer. There are similarities between road asphalt and airfield concrete, although there is little difference in skid resistance between bare airfield surfaces and airfield surfaces covered by 1 mm of ash. Based on our findings, we provide recommendations for maintaining road safety in a volcanic ash environment and suggest effective road cleaning techniques.

Highlights

- Laboratory tests of skid resistance for roads and airfields covered by volcanic ash
- Skid resistance can be reduced by only 1 mm of volcanic ash on the surface
- Several ash properties (e.g., grain size, soluble content) impact skid resistance
- Particular caution is required on roads covered by fresh, dry, coarse-grained ash
- Unlikely that skid resistance loss due to thin ash alone will warrant road closure

Keywords

Asphalt, concrete, runway, highway, traction, British Pendulum Tester.

1. Introduction

Functional transport networks are critical for society both under normal operating conditions and in emergencies. During volcanic eruptions, transport networks may be required for the evacuation of residents, to allow sufficient access for emergency services or military personnel to enter affected areas and for regular societal activities. Once direct threats have subsided, transport networks are crucial for both immediate and long-term recovery, including the clean-up and disposal of pyroclastic material, and restoration of services and commerce. It is thus imperative that effective and realistic transport management strategies are incorporated into volcanic contingency planning in areas where society and infrastructure are at risk (e.g., Auckland, New Zealand; Kagoshima, Japan; Mexico City, Mexico; Naples, Italy; Yogyakarta, Indonesia).

Volcanic eruptions produce many hazards. Damage to transport from proximal hazards such as lava flows, pyroclastic density currents and lahars is often severe, leaving ground routes impassable and facilities such as airports closed or inoperable. Volcanic ash (ejected material with particle sizes <2 mm in diameter) is widely dispersed and, although not necessarily damaging to static transport infrastructure, is generally the most disruptive of all volcanic hazards (Johnston and Daly 1997, Wilson et al. 2014). Even relatively small eruptions are capable of widespread disruption on ground transport and aviation, which may continue for months due to the remobilisation and secondary deposition of ash by wind, traffic or other human activities, even after an eruption has subsided.

To date studies on the impacts of volcanic hazards to society have focussed on the effects of ash (e.g. Blong 1984, Guffanti et al. 2009, Wilson et al. 2009, Horwell et al. 2010, Wilson et al. 2011, Dunn 2012, Wardman et al. 2012a, Wilson et al. 2012a, Stewart et al. 2013, Wilson et al. 2014). These studies and reports suggest four frequently occurring types of volcanic ash impacts on surface transport:

- (1) Reduction of skid resistance on roads and runways covered by volcanic ash
- (2) Coverage of road and airfield markings by ash
- (3) Reduction in visibility during initial ashfall and any ash re-suspension
- (4) Blockage of engine air intake filters which can lead to engine failure

Despite much anecdotal evidence, there has been little work to quantify the impact of ash on surface transport including roads and airfields. Quantitative, empirical evidence could inform management strategies in syn-eruptive and post-ashfall environments such as evacuation planning, safe travel advice in the recovery phase and recommended clean-up operations.

Existing studies of exposed critical infrastructure have generally focussed on very large eruptions and ashfall deposits >10 mm thick, rarely reporting the effects from ashfall <10 mm thick (Wilson et al. 2012a). This presents a source of uncertainty for emergency management planning and loss assessment models, which is important, as thin deposits are more frequent and often cover larger areas (Pyle 1989). Some notable eruptions that have led to reported reduced skid resistance on roads in the past are highlighted in Table 1. Wilson et al. (2014) suggest that impacts start at ~2-3 mm ash thickness, although there have been few studies that have quantified such impacts in detail. Indeed, the limited quantitative data available from historic observations generally relates impacts to approximate depths of ash, which may not be the best metric: ash characteristics such as particle size, ash type, degree of soluble components and wetness, may influence or even control the level of skid resistance. We investigate the importance of these alternative characteristics in this paper.

Here, we present experimental methods and results from the University of Canterbury's Volcanic Ash Testing Laboratory (VAT Lab) on the reduction of skid resistance on surfaces covered by volcanic ash. We test the skid resistance on road and airfield surfaces using the British Pendulum Tester (BPT), a standard instrument used by road engineers for surface friction testing since its development in the 1950s (Wilson 2006), and still used in many countries, particularly at problematic road sites. Despite the widespread and frequent use of the BPT by road engineers, we are unaware of other studies that have utilised the instrument on ash-covered surfaces.

Table 1. Historical reports of reduced skid resistance following volcanic eruptions. There may be other instances described as 'general impacts to transportation' or which have not been recorded in the literature.

Volcano and country	Year	Ash thickness (mm)	Observations related to skid resistance
St Helens, United States of America	1980	17	Ash became slick when wet ^{1,2,3}
Hudson, Chile	1991	<i>not specified</i>	Traction problems from ash on road ⁴
Tavurvur and Vulcan, Papua New Guinea	1994	1000	Vehicles sunk and stuck in deep ash, although passable if hardened ^{5,6,7}
Sakurajima, Japan	1995	>1	Roads slippery ^{8,9}
Ruapehu, New Zealand	1995-96	"thin"	Slippery sludge from ash-rain mix (roads closed) ^{6,9}
Soufrière Hills, United Kingdom (overseas territory)	1997	<i>not specified</i>	Rain can turn particles into a slurry of slippery mud ¹⁰
Etna, Italy	2002	2-20	Traction problems, although damp and compacted ash easier to drive on ⁶
Reventador, Ecuador	2002	2-5	Vehicles banned due to slippery surfaces ^{9,11}
Chaitén, Chile	2008	<i>not specified</i>	Reduced traction caused dam access problems ^{12,13}
Merapi, Indonesia	2010	<i>not specified</i>	Slippery roads caused accidents (Figure 2) and increased journey times ¹⁴
Pacaya, Guatemala	2010	20-30	Slippery roads with coarse ash ¹⁵
Puyehue-Cordón Caulle, Chile	2011	>100	2WDs experienced traction problems (wet conditions) ¹⁶
Shinmoedake, Japan	2011	<i>not specified</i>	Ladders very slippery ¹⁷
Sinabung, Indonesia	2014	80-100	Road travel impracticable in wet muddy ash ¹⁸

Information from ¹Warrick et al. 1981, ⁹Johnston 1997, ⁷Stammers 2000, ⁸Durand et al. 2001, ⁵Nairn 2002, ²Cole and Blumenthal 2004, ³Cole et al. 2005, ¹¹Leonard et al. 2006, ¹³Wilson (2009 unpublished field notes), ⁶Barnard 2009, ¹⁰USGS 2009, ⁴Wilson et al. 2009, ¹⁴Jamaludin 2010, ¹⁷Wilson (2011 unpublished field notes), ¹⁵Wardman et al. 2012a, ¹²Wilson et al. 2012b, ¹⁶Wilson et al. 2013, ¹⁸Volcano Discovery 2014.

2. Skid Resistance

Skid resistance (i.e. the force developed when a tyre that is prevented from rotating slides along a pavement surface (Highway Research Board 1972)) is a fundamental component of road safety and should be managed so that it is adequate to enable safe operation (Dookeeram et al. 2014). Skid resistance is also essential for airfields to enable sufficient acceleration, deceleration and change in direction of aircraft on the surface (ICAO 2013). It has become particularly important since the advent of turbojet aircraft with their greater weight and high landing speeds (FAA 1997, Blastrac 2015). Skid resistance is essentially a measure of the Coefficient of Friction (CoF) obtained under standardised conditions in which the many variables are controlled so that the effects of surface characteristics can be isolated (Wilson and Chan 2013).

Skid resistance of surfaces changes over time, typically increasing in the first two years following pavement construction for roads due to the wearing by traffic, and rough aggregate surfaces becoming exposed, then decreasing over the remaining pavement life as aggregates become polished (Asi 2007).

2.1 Surface macrotexture and microtexture

Surface friction is primarily a result of the macrotexture and microtexture of road and airfield pavements; these are thus intrinsically linked to skid resistance. As defined by the World Road Association-PIARC (1987):

- Macrotexture defines the amplitude of pavement surface deviations with wavelengths from 0.5 to 50 mm.
- Microtexture is the amplitude of pavement surface deviations from the plane with wavelengths less than or equal to 0.5 mm, measured at the micron scale (Ergun et al. 2005).

Microtexture, a property of each individual aggregate chip, contributes in particular to skid resistance for vehicles at low speed (i.e. the tyre rubber locally bonds to the surface through adhesion). Microtexture varies from harsh to polished. When a pavement is newly constructed, microtexture is particularly rough; however, once in service, microtexture changes due to the effects of traffic and weather conditions (Ergun et al. 2005). Macrotexture, the coarse texture of pavement surface aggregates, helps to reduce the potential for aquaplaning and provides skid

resistance at high speeds through the effect of hysteresis (caused by the surface projections deforming the tyre) (Wilson and Chan 2013, Dookeeram et al. 2014). Typically, if the surface binder and aggregate chips have been appropriately applied, macrotexture levels should very gradually and linearly decrease over time as the aggregate surface slowly abrades (Wilson 2006).

2.2 Road skid resistance

The minimum recommended values of skid resistance and calculated corresponding CoFs for different sites on road networks that are measured with the BPT under typical wet conditions are shown in Table 2 and are reported in various literature sources internationally (e.g. British Pendulum Manual 2000, Asi 2007, Impact 2010).

Table 2. Minimum recommended Skid Resistance Values for different road network sites, under wet conditions and measured using the British Pendulum Tester (British Pendulum Manual 2000, Asi 2007, Impact 2010).

Type of site	Minimum recommended skid resistance value	Corresponding Coefficient of Friction
Difficult sites such as: (a) Roundabouts (b) Bends with radius less than 150 m on unrestricted roads (c) Gradients, 1 in 20 or steeper, of lengths >100 m (d) Approaches to traffic lights on unrestricted roads	65.0	0.74
Motorways and heavily trafficked roads in urban areas (with >2000 vehicles per day)	55.0	0.60
All other sites	45.0	0.47

Rain, snow and ice are common hazards that compromise the quality of road surfaces (Benedetto 2002, Andrey 1990, Cova and Conger 2003) by interfering with surface macrotexture and microtexture. Bennis and De Wit (2003) and Persson et al. (2005) quantified how surface friction varies with time during a short rain shower following a reasonable period of no rain (Figure 1). The measured skid resistance significantly reduces immediately after rainfall and then recovers to a more typical wet skid resistance. However, the effect of individual contaminants, such as vehicle residues and atmospheric dust, on surface friction is poorly understood (Wilson 2006).

Many studies have focused on snow- and rain-related crashes in northern states of the U.S. (e.g., Qin et al. 2006, Khattak and Knapp 2001, Oh et al. 2009; Abdel-Aty et al. 2011). We propose that parallels may be drawn between such hazards and the hazard presented by ashfall on roads. Following a review of the literature, Aström and Wallman (2001) summarise typical CoFs for different road conditions (Table 3). The effect of hazards such as ice and snow can be substantial with most skid resistance values under such conditions falling below the minimum recommended levels (Table 2). Skid resistance is very limited under black ice conditions.

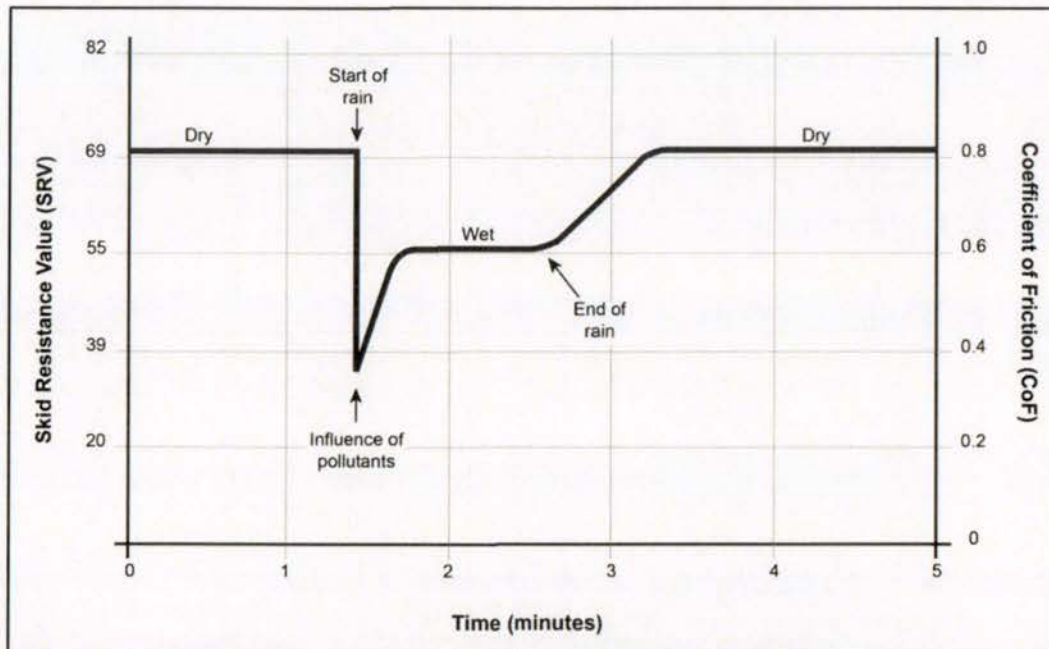


Figure 1. Variation in CoF during a rain event (after Bennis and De Wit 2003, Persson et al. 2005, Wilson 2006, Do et al. 2014).

Table 3. Skid Resistance Values (SRVs) and calculated corresponding CoFs for different road conditions (adapted from Aström and Wallman 2001). The two measures of friction are related by the equation: $CoF = (3 \times SRV) / (330 - SRV)$ (Lester 2014).

Type of Site	Typical Skid Resistance Value	Corresponding Coefficient of Friction
Dry, bare surface	69.5-82.5	0.8-1.0
Wet, bare surface	62.4-69.5	0.7-0.8
Packed snow	20.6-30.0	0.20-0.30
Loose snow / slush	20.6-47.1 (higher value when tyres in contact with pavement)	0.20-0.50
Black ice	15.7-30.0	0.15-0.30
Loose snow on black ice	15.7-25.4	0.15-0.25
Wet black ice	5.4-10.6	0.05-0.10

2.3 Airfield skid resistance

In addition to the contaminants mentioned in Section 2.2, a common and important contaminant on airport runway surfaces is tyre rubber. With repeated aircraft landings, rubber from tyres can cover the entire surface of landing areas, filling the surface voids and reducing macrotexture and microtexture, resulting in loss of aircraft braking capacity and directional control, especially when runways are wet (FAA 1997, Blastrac 2015). The extent of rubber tyre contaminant accumulation on runways is dependent on the volume and type of aircraft which use the airport (FAA 1997).

Unfortunately, there is no common index for ground friction measurements on airfields. Currently, individual airport operating authorities are responsible for providing any take-off and landing performance data as a function of a braking coefficient with ground speed, and relating this data to a friction index measured by a ground device (EASA 2010). CoF values measured by Continuous Friction Measuring Equipment (CFME) can be used as guidelines for evaluating

friction deterioration of runway pavements (FAA 1997). The CoFs for three classification levels for FAA qualified CFME operated at 65 and 95 km/h test speeds are shown in Table 4. There are no airfield guideline thresholds for the BPT as it only provides spot friction measurements of the surface (and is not classified as CFME). However, BPTs are sometimes used on runways and we thus summarise BPT results for airfield concrete surfaces in section 4.

Table 4. Guideline friction values for three classification levels for FAA qualified CFME operated at 65 and 95 km/h test speeds (FAA 1997). Note that there are no airfield guideline thresholds for the BPT which is not CFME and only provides spot friction measurements.

	65 km/h			95 km/h		
	Minimum	Maintenance Planning	New Design/ Construction	Minimum	Maintenance Planning	New Design/ Construction
Mu Meter	.42	.52	.72	.26	.38	.66
Dynatest Consulting, Inc. Runway Friction Tester	.50	.60	.82	.41	.54	.72
Airport Equipment Co. Skiddometer	.50	.60	.82	.34	.47	.74
Airport Surface Friction Tester	.50	.60	.82	.34	.47	.74
Airport Technology USA Safegate Friction Tester	.50	.60	.82	.34	.47	.74
Findlay, Irvine, Ltd. Griptest Friction Meter	.43	.53	.74	.24	.36	.64
Tatra Friction Tester	.48	.57	.76	.42	.52	.67
Norsemeter RUNAR (operated at fixed 16% slip)	.45	.52	.69	.32	.42	.63

2.4 Volcanic ash and skid resistance

Due to its rapid formation, volcanic ash particles comprise various proportions of vitric (glassy, non-crystalline), crystalline or lithic (non-magmatic) particles (Wilson et al. 2012a) which are usually hard and highly angular. Volcanic ash properties are influenced by various factors, including the magma source type, distance from the vent, weather conditions and time since the eruption. Important volcanic ash properties include:

- (1) Particle size and surface area
- (2) Composition and degree of soluble components
- (3) Hardness and vesicularity
- (4) Angularity and abrasiveness
- (5) Wetness.

Since coarser and denser particles are deposited close to the source, fine glass and pumice shards are relatively enriched in ash fall deposits at distal locations (Sarna-Wojcicki et al. 1981). Newly erupted ash has coatings of soluble components (Matsumoto et al. 1988, Delmelle et al. 2005) resulting from interactions with volcanic gases and their new surfaces. Mineral fragment composition is dependent on the chemistry of the magma from which it was erupted, with the most explosive eruptions dispersing high silica rhyolite rich in hard quartz fragments (Heiken and Wohletz 1985, Wardman et al. 2012b). Volcanic ash is very abrasive (Blong 1984, Labadie 1994, Heiken et al. 1995, Johnston 1997, Miller and Casadevall 2000, Gordon et al. 2005) with the degree of abrasiveness dependent on the hardness of the material forming the particles and their shape; high angularity leads to greater abrasiveness (Wilson et al. 2012a). Most abrasion occurs from particles <500 µm in diameter, with a sharp increase in the abrasion rate from 5 to 100 µm (Gordon et al. 2005).

Skid resistance from volcanic ash may be different to that expected from other contaminants due to cementitious and vesicular properties of the ash. There is also potential for large thicknesses to develop on ground surfaces or contamination to reoccur once cleaned due to re-suspension and re-deposition. There have been several instances where road line markings have become obscured by settled volcanic ash (e.g. Mt Reventador 2002, Leonard et al. 2006; Mt Hudson 1991, Wilson et al. 2009). An ash thickness of only ~0.1 mm can lead to road marking coverage in some cases (Blake et al. in prep). Drivers can unintentionally drive over road markings, which may have different skid resistance properties to unmarked road surfaces. Additionally, with ash accumulation, the vibrations that drivers receive from rumble strips incorporated in some markings will likely be subdued or even eliminated, decreasing road safety further. Vehicle accidents during or after ashfall (e.g. Figure 2) are a particular concern where no road closures occur, due to decreased braking ability and increased stopping distances caused by low skid resistance.



Figure 2. Vehicle accident attributed to reduced skid resistance after ashfall from Merapi volcano, Indonesia (2010). [Photo licence required from iStock](#)

At airports, ash accumulation above trace amounts usually requires closure and the removal of ash from airfields before full operations can resume, both of which incur considerable expense (Guffanti et al. 2009). For example, the eruption of Mt. Redoubt volcano in Alaska in 1989 resulted in a minimum loss of US \$21 million at Anchorage International airport (Tuck et al. 1992). Many airports face closure even before ash settles on the airfield due to potential damage to aircraft by airborne ash, or solely the threat of ash in the vicinity. As such there are limited observations of ash resulting in reduced skid resistance on airfields, although Guffanti et al. (2009) note that slippery runways are one of the primary hazards to airports from volcanic eruptions.

3. Methods

3.1 Sample preparation

3.1.1 Volcanic ash

Volcanic ash samples derived from four different volcanic sources in New Zealand were used in this study to investigate two volcanic ash types (basalt and rhyolite) and to span a range of hardness and mineral components. The locations and ash types are shown in [Table 5](#). Compositions and characteristics were selected as they are representative of ash likely to be encountered in the future in New Zealand, but are also common worldwide. For logistical and supply reasons, experimentation on basaltic ash was focussed on a proxy ash sourced from locally abundant basaltic lava blocks from the Lyttelton Volcanic Group at Gollans Bay Quarry in the Port Hills of Christchurch, New Zealand. Ash was physically produced from the blocks by

splitting, crushing and pulverisation as described by Broom (2010) and Wilson et al. (2012), a method generally found to provide good correlations with real volcanic ash grain sizes. Some of the proxy Lyttelton basaltic ash produced was pulverised and sieved to 1000 μm and some to 106 μm to investigate the effect of grain size on skid resistance. In addition, further basaltic ash was sourced from deposits originating from the Pupuke eruption in the Auckland Volcanic Field and Punatekahi eruptions in the Taupo Volcanic Zone. Rhyolitic ash was sourced from deposits from the Hatepe eruption in the Taupo Volcanic Zone. These three samples were pulverised (splitting and crushing was not necessary due to their smaller original sizes) and sieved to 1000 μm (Table 5). The grain size distributions for all samples are shown in Figure 3.

Table 5. Ash samples prepared for testing. Note RCL = Ruapehu Crater Lake, WICL = White Island Crater Lake.

Ash Source	Ash Type	Sieve Size (μm)	Soluble Components Added	Sample ID
Lyttelton Volcanic Group	Hard Basalt	1000	No	LYT-BAS1
			Yes (RCL)	LYT-BAS2
			Yes (WICL)	LYT-BAS3
		106	No	LYT-BAS4
Punatekahi cone, Taupo	Scoriaceous Basalt	1000	No	PUN-BAS1
			Yes (RCL)	PUN-BAS2
			Yes (WICL)	PUN-BAS3
Hatepe ash, Taupo	Pumiceous Rhyolite	1000	No	HAT-RHY
Pupuke, Auckland Volcanic Field	Scoriaceous Basalt	1000	No	PUP-BAS1
			Yes (WICL)	PUP-BAS3

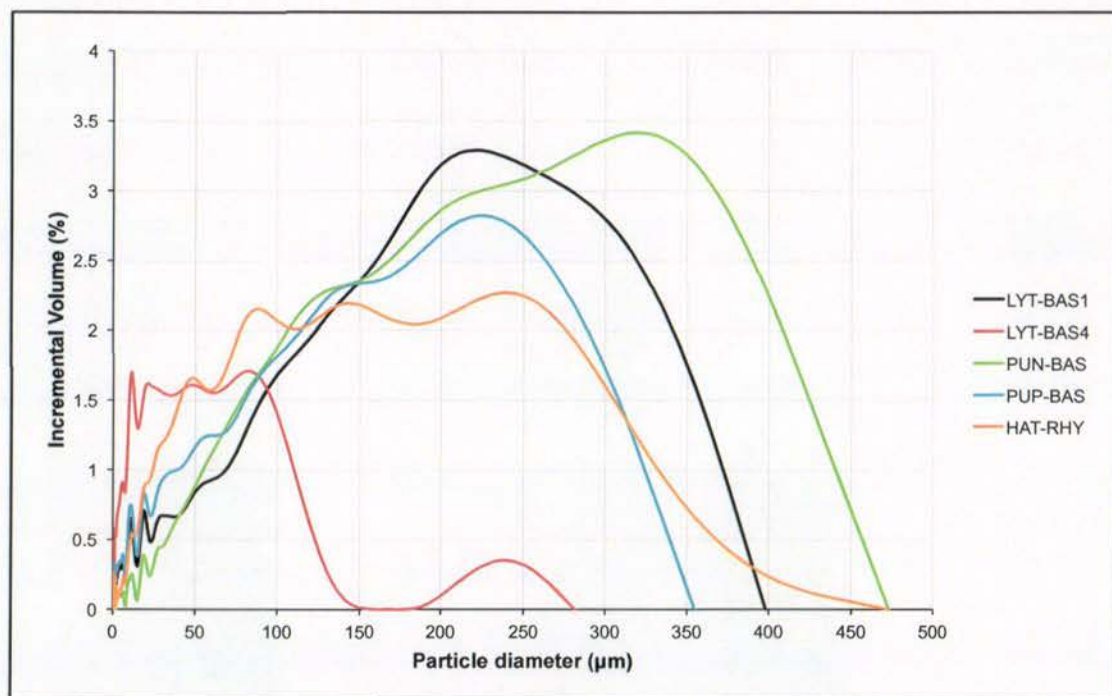


Figure 3. Mean particle size distribution analysed using a Micromeritics Saturn DigiSizer II Laser-Sizer (3x runs per sample). Note that the maximum particle sizes for the four samples that were sieved to 1000 μm are in fact <500 μm , likely due to the pulverisation process. Some particles for the LYT-BAS4 sample (sieved

to 106 μm) exceed 106 μm due to the often-tabular nature of volcanic ash particles and their ability to pass through the sieve mesh when vertically orientated.

As fresh ash contains adhered soluble components, we dosed a portion of our ash samples with fluid from volcanic crater lakes to mimic the volatile adsorption processes which occur in volcanic plumes, thus enabling the effects of soluble components on skid resistance to be studied. A dosing method using fluids from the crater lakes of Ruapehu and White Island volcanoes, New Zealand, described by Broom (2010) and Wilson et al. (2012), was used for a portion of the 1000 μm Lyttelton and Punatekahi basaltic ash samples for road testing, and Pupuke basaltic ash sample for airfield testing. The following dosing solutions were used as work by Broom (2010) and Wilson et al. (2012) established that they produce samples representative of real fresh volcanic ash:

- 100% strength Ruapehu Crater Lake fluid ([Appendix A](#)), i.e. no dilution, mixed at a ratio of 1:1 (ash to dosing agent)
- 20% strength White Island Crater Lake fluid ([Appendix A](#)), i.e. 4 parts de-ionised water to 1 part White Island Crater Lake fluid, mixed at a ratio of 4:1 (ash to dosing agent)

We undertook a water leachate test using the method outlined by Stewart et al. (2013) to measure the concentration of dissolved material in solution for all of the samples used and verify the effectiveness of dosing. Both 1:20 and 1:100 ratios of ash (g) to de-ionised water (ml) were used. The water leachate test findings ([Appendix B](#)) revealed that the soluble components in the samples we dosed (LYT-BAS2, LYT-BAS3, PUN-BAS2, PUN-BAS3, PUP-BAS3) were considerably higher than those that were not dosed and confirms that the samples used provide a suitable means of testing the effects of this characteristic on skid resistance. Additionally, the lowest pH values were generally recorded for the dosed samples.

3.1.2 Test surfaces

Stone Mastic Asphalt (SMA) surfaces are commonly used on modern motorways, such as in parts of the UK and on the Auckland State Highway Network in New Zealand (Boyle 2005). However, concerns have been raised about its use, as initial skid resistance may be low until the thick binder film is worn down: it sometimes takes up to two years for the material to offer an acceptable level of skid resistance (Bastow et al. 2004, BBC 2005, Daily Telegraph 2008). The desire to have good macrotexture led to the development of OGPA (Boyle 2005).

For this study, we focus mainly on tests of skid resistance for SMA surfaces using 300 x 300 x 45 mm slabs, newly constructed by the Road Science Laboratory in Tauranga, New Zealand. We also conducted some comparative tests on Open Graded Porous Asphalt (OGPA) also constructed by the Road Science Laboratory, and on concrete surfaces constructed as 220 x 220 x 40 mm slabs by Firth Concrete. The concrete mix was compiled with the same specifications as used for placement via manual labour and a roller screed on the airfield (i.e. runways, taxiways and hardstand areas) at Auckland Airport, although we note that airfield surfaces vary between countries and airports. However, unless otherwise specified, we refer to SMA surfaces in this paper.

3.1.3 Painted road markings

Under typical conditions, road markings reduce accident rates (NZRF 2005) as they provide continuous visual guidance of features such as road edges and centres. However, when non-mechanical markings such as paint and thermoplastics are applied, the microtexture of the road surface changes and, with thicker non-mechanical markings, the macrotexture also alters as voids in the asphalt become filled. Consequently, localised skid resistance can be substantially reduced. The skid resistance of the markings is generally lower than that for the bare pavement, although the addition of retroreflective glass beads to the surface can increase skid resistance to more acceptable levels (NZRF 2005). As little as 0.1 mm of volcanic ash may obscure road markings (Blake et al. in prep), meaning that drivers may unintentionally travel over marked

road surfaces (e.g. such as crossing centre lines). Further accumulation may inhibit the effectiveness of rumble strips which normally cause vibrations within the vehicle.

Paint is the most common form of road marking material used in many countries, including New Zealand, and is typically applied by spraying in dry film with thicknesses varying from 70 μm to 500 μm (NZRF 2009). In New Zealand, retroreflective glass beads are often applied to longitudinal centre line paint but not to paint on the road margins (Howard Jamison, Roading Supervisor, personal communication, 2014). Road lines are usually re-painted once or twice a year to account for abrasion, with skid resistance decreasing as the paint fills more voids in the asphalt surface. With a typical asphalt lifespan of ~ 10 years, marking paint accumulation can be substantial in places (Howard Jamison, Roading Supervisor, personal communication, 2014). In this study we test skid resistance on SMA slabs, machine painted by Downer Group with a typical road paint (Damar Bead Lock Oil Based Paint containing 63% solids), in four forms:

- 1x application (180-200 μm thick) without retroreflective glass beads
- 1x application (180-200 μm thick) with retroreflective glass beads
- 4x applications (720-800 μm thick) without retroreflective glass beads
- 4x applications (720-800 μm thick) with retroreflective glass beads

The asphalt with one application of paint is used to replicate markings that have been heavily abraded, whereas that with four applications mimics typical marking thickness found on New Zealand roads (Howard Jamison, Roading Supervisor, personal communication, 2014).

3.2 Skid Resistance Testing

The test procedure for the BPT (Figure 4) is standardised in the ASTM E303 (2013) method. It is a dynamic pendulum impact type test, based on the energy loss occurring when a rubber slider edge is propelled across the test surface. The method is intended to correlate with the performance of a vehicle with patterned tyres braking with locked wheels on a wet road at 50 km/h (Impact 2010). Since the BPT is designed to test the skid resistance of extensive surfaces in-situ, care was taken to ensure that the instrument was stable and slabs were aligned before conducting our testing in the laboratory environment. Both 3.00" rubber mounted TRL (55) sliders (used for road testing) and 3.00" CEN sliders (used for airfield testing), purchased from Cooper Technology UK, were used in our study.

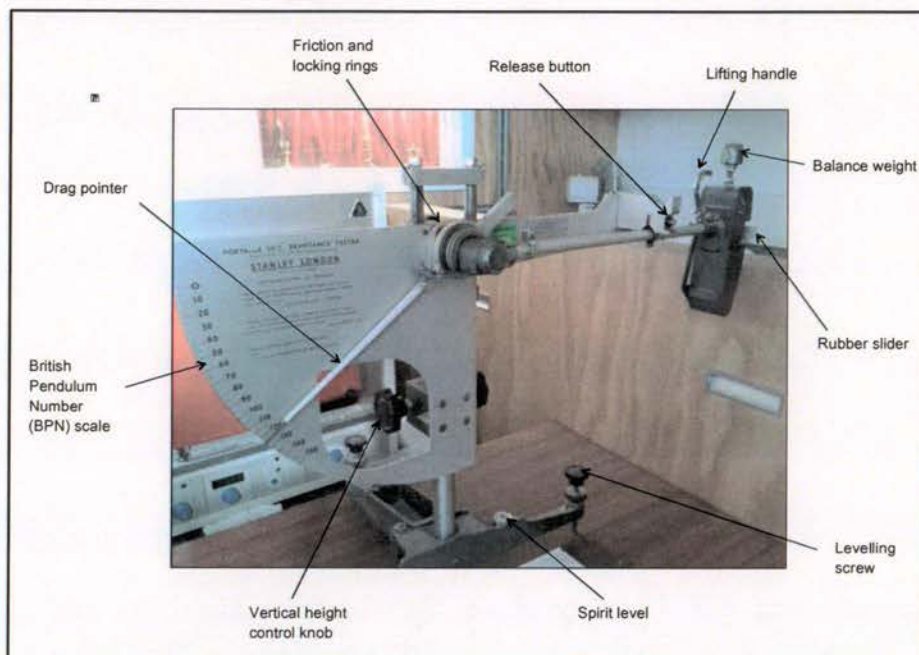


Figure 4. British Pendulum Tester (BPT) used for surface friction testing.

3.2.1 Surfaces not covered by ash

As the ASTM E303 (2013) method states, the direct values are measured as British Pendulum (Tester) Numbers (BPNs). Typically, tests using the BPT are conducted on wet surfaces. However, as we are also investigating the effects of dry volcanic ash on skid resistance, we also ran the experiments under dry conditions. For surfaces not covered in ash, we adopted the same technique as used by the New Zealand Transport Agency (NZTA) (TNZ 2003), whereby for each test surface area, results of a minimum of five successive swings which do not differ by more than 3 BPNs are recorded. The mean of the 5 BPNs is then calculated to give a value representing skid resistance (i.e. the Skid Resistance Value (SRV)). The tests were conducted on every side of each slab to retrieve four SRVs (later averaged) for each condition. CoFs for each mean SRV are calculated using the equation provided by Lester (2014):

$$CoF = (3 \times SRV) / (330 - SRV) \quad (1)$$

3.2.2 Surfaces covered by ash

The ash characteristics analysed during experimentation and production techniques are summarised in [Appendix C](#). For the surfaces covered in ash, we use two test methods to replicate different ash settling conditions in combination with vehicle movement effects:

1. A similar procedure as adopted by the NZTA (TNZ 2003) whereby five successive swings are recorded, which do not differ by more than 3 BPNs and the SRV calculated. Between each swing, ash which has been displaced by the pendulum movement is replenished with new ash of the same type (and re-wetted if applicable) to maintain a consistent depth (and wetness). This test method mimics to some degree the effect of vehicles driving during ash fall, with ash settling on a road surface and filling any voids left by vehicle tyres before the next vehicle passes. A mean SRV is calculated by repeating the test on all four sides of each asphalt slab.
2. Eight successive swings of the pendulum are taken over each ash-covered test surface area but ash is not replenished between each swing. For each swing, the BPN is taken to be the SRV, allowing the change in skid resistance to be observed through analysis of the individual results. If the original surface has been wetted, further water is applied between each swing. To some degree, this method represents vehicle movement over an ash-covered surface in dry or wet conditions, where ashfall onto the road surface has ceased. A mean SRV is calculated for each successive swing by repeating the test on all four sides of each asphalt slab where possible.

In dry field conditions, the impact of remobilised ash might be more substantial than captured in the laboratory tests. However, some remobilisation during experimentation is achieved as a result of the pendulum arm movement and associated ash disturbance.

3.2.3 Cleaning

Following testing, the ash was cleaned from the asphalt concrete slabs by brushing and using compressed air if dry, or a combination of compressed air, water and light scrubbing if wet. Wetted slabs were then left to air-dry for 3-4 days before any further dry tests were conducted.

3.3 Macrotexture

3.3.1 Sand patch method

This volumetric technique is standardised in the ASTM E965 (2006) method and summarised in [Appendix D](#). It involves a procedure for determining the average depth of pavement macrotexture by careful application of a known volume of spherical glass beads on the surface and subsequent measurement of the total area covered. The average pavement macrotexture depth is calculated using the following equation:

$$MTD = 4V / \pi D^2 \quad (2)$$

where MTD = mean texture depth of pavement macrotexture (mm), V = sample volume (mm³) and D = average diameter of the area covered by the material (mm).

We use this approach to determine the macrotexture of new non-contaminated SMA surfaces and SMA surfaces that were contaminated by ash but have undergone testing (10x BPT swings) and cleaning (see [section 3.2.3](#)). The method is not suitable for the airfield concrete slabs due to there being considerably fewer voids at the macrotexture scale and thus a much larger area would be required to conduct the test.

3.3.2 Image analysis

In addition to the ASTM sand patch method, a visual technique involving digital photography and image analysis was adopted to distinguish between ash and asphalt at a macrotextural level on the SMA slabs. This provides a proxy for surface macrotexture and allows the relative success of cleaning techniques in relation to ash removal and skid resistance reduction to be quantitatively assessed through the calculation of remaining ash coverage. The light-coloured rhyolitic volcanic ash (sample ID: HAT-RHY) was used to allow easy visual interpretation between the ash and dark-coloured asphalt concrete.

1. White paint was marked on the edge of the slabs in order to identify the same segment of the slab between each testing round.
2. A Fuji Finepix S100 (FS) digital SLR camera (with settings: Manual, ISO 800, F6.4, 10-second timer) was mounted on a tripod directly above the asphalt slab.
3. Halogen tripod worklights were used to illuminate the surface of the slab and all ambient light was blocked out using black sheeting before images were taken to keep lighting levels consistent between photos.
4. Images were analysed for percentage coverage of ash by means of 'training' and 'segmentation' using 'Ilastik' and 'Photoshop' software.

3.4 Microtexture – Microscopy

A Meiji EMZ-8TRD (0.7-4.5 zoom) stereomicroscope and Lumenera Infinity 1 digital camera were used to capture images of 10 x 10 mm areas on the asphalt slabs and thus enable visual identification of remaining ash particles at a microtextural level. The microscope was mounted directly above the slab and Leica CLS 100 LED fibre-optic lighting was used to illuminate the section of interest, with all ambient light blocked using black sheeting. A portable (300 x 300 mm internal dimension) grid (with 10 mm squares) was constructed to fit securely over the slab and allow easy identification of specific segments between each testing round ([Appendix E](#)).

4. Results and discussion

4.1 Consistent depth

When ash was replenished between each swing, the skid resistance remained relatively constant with time, permitting calculation of a mean SRV for each condition. The mean SRVs and corresponding CoFs for the non-contaminated SMA (new and cleaned) and for the SMA covered by three samples sieved to 1000 µm are shown in [Figure 5](#). Similarly, the SRVs and CoFs for the airfield concrete, both clean and covered by two samples sieved to 1000 µm are shown in [Figure 6](#). The Pupuke volcano sample (PUP-BAS1) was found to have very similar values to the Punatekahi (PUN-BAS1) sample. This was expected as they are both scoriaceous basalt. Due to limitations in available ash and time constraints, full testing was only conducted with one of the scoriaceous samples on the SMA and airfield concrete.

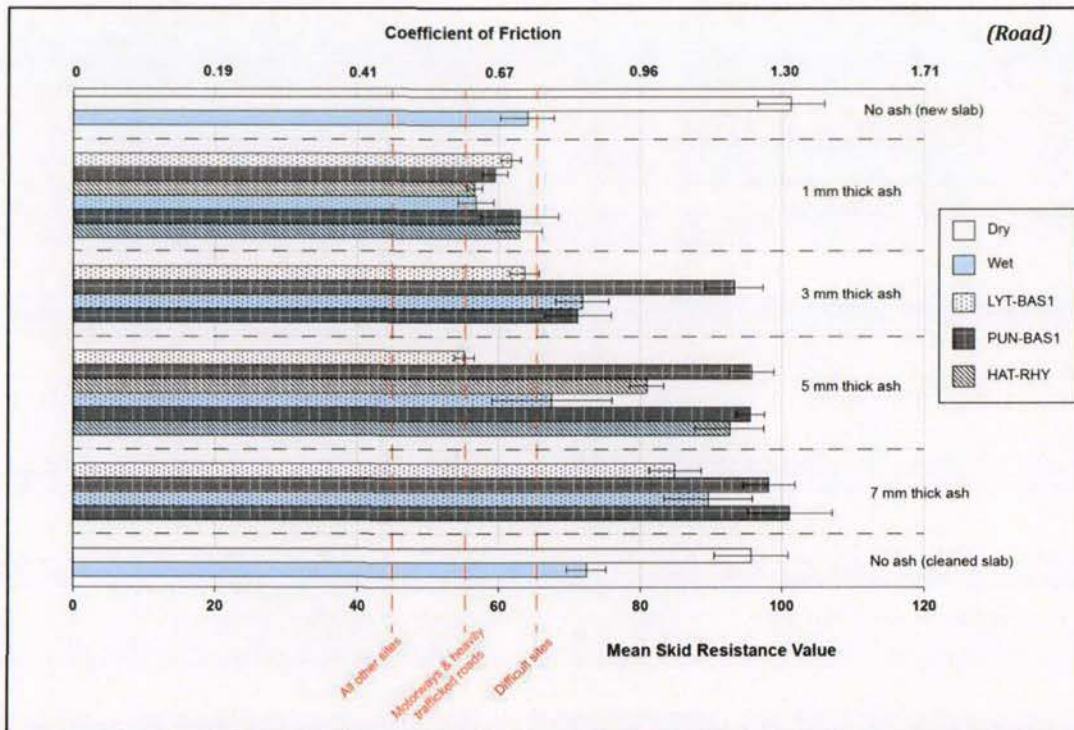


Figure 5. Mean SRVs and CoFs for the non-contaminated SMA and SMA covered in the three ash types sieved to 1000 μm . Wet and dry samples at 1, 3, 5 and 7 mm thicknesses are shown although limitations in the quantity of rhyolite (HAT-RHY) meant that testing was only conducted at 1 and 5 mm thickness for this ash type. The error bars represent the standard deviation for each data set. Also displayed (as red dashed lines) are the minimum recommended SRVs for different road network sites (Table 2).

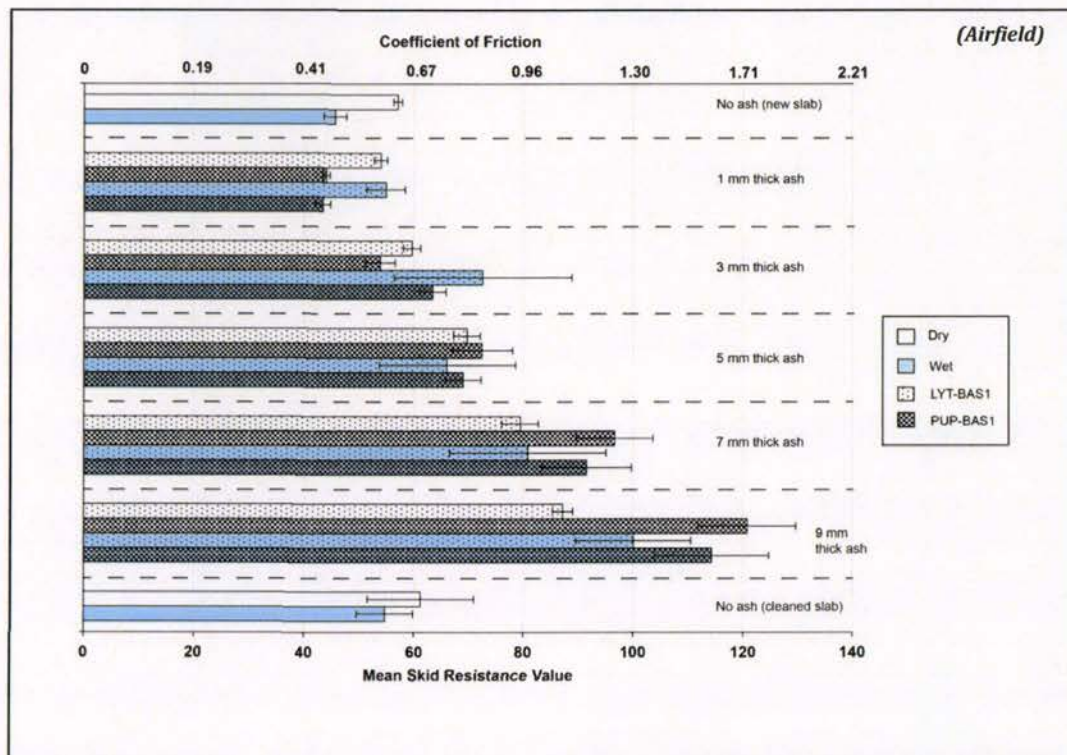


Figure 6. Mean SRVs and CoFs for the non-contaminated airfield concrete and airfield concrete covered in the two ash types sieved to 1000 μm . Wet and dry samples at 1, 3, 5, 7 and 9 mm thicknesses are shown. The error bars represent the standard deviation for each data set.

4.1.1 Ash type and wetness

Anecdotal observations during historical eruptions suggest that skid resistance on roads is reduced following dry unconsolidated ash accumulation. This is consistent with our results, which also reveal that reduced SRVs are particularly pronounced under dry conditions for a 1 mm thick ash layer on asphalt (Figure 5). Mean SRVs for all 1 mm thick ash types fall below the minimum recommended SRV for difficult sites (an SRV of 65). Wet 1 mm ash-covered surfaces are not necessarily more slippery than dry 1 mm ash-covered surfaces and the wet surfaces covered in 1 mm thick ash are only slightly more slippery than the wet asphalt without ash contamination.

For the 3 and 5 mm thick ash-covered asphalt surfaces, we observe different trends. The LYT-BAS1 sample has similar SRVs to the 1 mm thick ash layer and the mean SRV for 5 mm is near the recommended minimum SRV for motorways (SRV 55). Samples PUN-BAS1 and HAT-RHY however, have greater SRVs than those for 1 mm of ash, suggesting that these ash types are perhaps less slippery when thicker, especially sample PUN-BAS1. The wetted PUN-BAS1 and HAT-RHY >1 mm samples have increasing SRVs as thickness increases. SRV values exceed those for bare wet asphalt surfaces and are similar to those for dry bare asphalt surfaces when ash is >5 mm thick. The vesicular nature of these two samples may play a role in increasing SRVs with the individual particles perhaps able to effectively interlock with one another and with the asphalt aggregate beneath. The pumiceous HAT-RHY sample is more friable than the PUN-BAS1 sample, which may explain the slight difference in SRVs between the two. We note that the pendulum arm may be slowed upon initial impact with the thicker deposits, producing higher than true representative SRVs. However, the comparatively low SRVs for the 5 mm thick LYT-BAS1 sample suggest that other ash characteristics are also important.

Compared to asphalt, there is less difference between SRVs for bare airfield concrete surfaces and those covered by 1 mm of ash (Figure 6), perhaps due to the initially smooth surface when bare. However, as with the asphalt, results suggest little difference in slipperiness between wet and dry surfaces with 1 mm of ash deposition. The scoriaceous and vesicular sample PUP-BAS1 exhibits especially large SRVs as thickness is increased, reinforcing our hypothesis that ash of this type is less slippery when thicker. The apparent increase in skid resistance with the addition of ash to SRV values greater than those for bare surfaces may be a function of the pendulum arm slowing upon contact.

4.1.2 Soluble components

There are no clear differences in SRVs observed between non-dosed and dosed LYT-BAS ash at 1 mm thick (Figure 7). However, the highly crystalline properties of this ash type may reduce the impact that dosing has on SRVs. SRVs for the dosed scoriaceous PUN-BAS ash used on road asphalt (Figure 7) and dosed scoriaceous PUP-BAS ash used on airfield concrete (Figure 8) are generally less than those which are not dosed. For all ash thicknesses, the PUN-BAS3 sample (i.e. that dosed in WICL fluid) produce lower SRVs than the PUN-BAS2 sample (i.e. that dosed in RCL fluid), suggesting that the skid resistance of non-crystalline ash-covered road surfaces decreases if the soluble component of the ash increases. This corresponds with Persson et al's (2005) findings from other road contaminants, demonstrating a friction drop at the transition between no rain and rain due to the high-viscosity mix of rain water and road debris. As such, only WICL fluid was used to dose the PUP-BAS sample (used for airfield concrete) to assess results representative of a 'likely worse-case' SRV scenario.

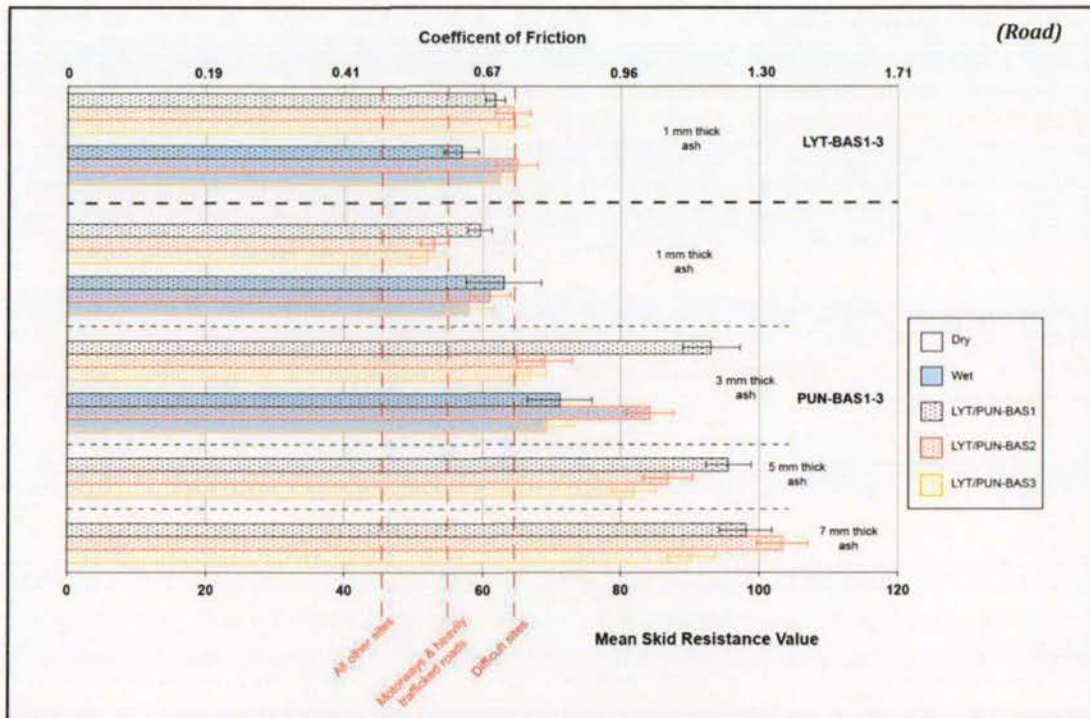


Figure 7. Mean SRVs and CoFs for the road asphalt covered in non-dosed and dosed LYT-BAS and PUN-BAS ash sieved to 1000 μm . Both samples dosed in RCL and WICL fluid under dry and wet conditions are displayed. Due to limitations in dosing fluids and possible interference caused by the crystalline characteristics of the LYT-BAS samples, most testing was undertaken using the PUN-BAS samples. Large quantities of freshly dosed ash samples were required for each thick ash test under wet conditions, hence only dry conditions were analysed for the 5 and 7 mm thick testing rounds. Also displayed (as red dashed lines) are the minimum recommended SRVs for different road network sites (Table 2).

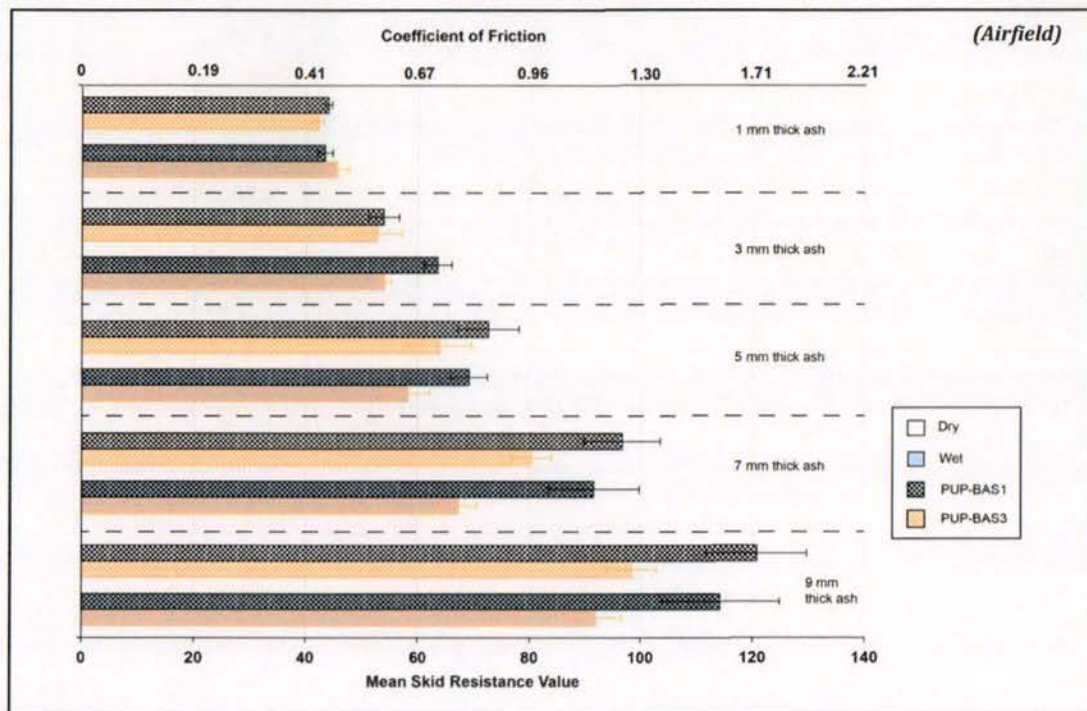


Figure 8. Mean SRVs and CoFs for the airfield concrete covered in non-dosed and dosed PUP-BAS ash sieved to 1000 μm . The samples dosed in WICL fluid under both dry and wet conditions are displayed.

4.1.3 Ash particle size

The mean SRVs for fine-grained basaltic ash (LYT-BAS4) are slightly higher than those for the coarse-grained ash of the same type (LYT-BAS1) when at 1 mm thickness on roads, with mean values for both wet and dry samples above the minimum recommended SRVs for difficult sites (Figure 9). This concurs with field observations made by the Kagoshima City Office staff following frequent volcanic ash deposition on roads from the multiple eruptions of Sakurajima volcano, Japan (since 1955). Reports suggest that the finer ash from the recent eruptions at the Showa crater resulted in less slippery roads than the generally coarser-grained ash produced during past eruptions from the Minami-daki summit area (Kagoshima City Office, personal communication, June 08 2015). We hypothesise that this is due to the finer particles being more easily mobilised and displaced at the tyre-asphalt interface, allowing improved contact between the tyre and asphalt. However, no clear correlations exist between the fine- and coarse-grained ash when at 5 mm thick, perhaps due to both types covering the asphalt surface when the tyre makes contact.

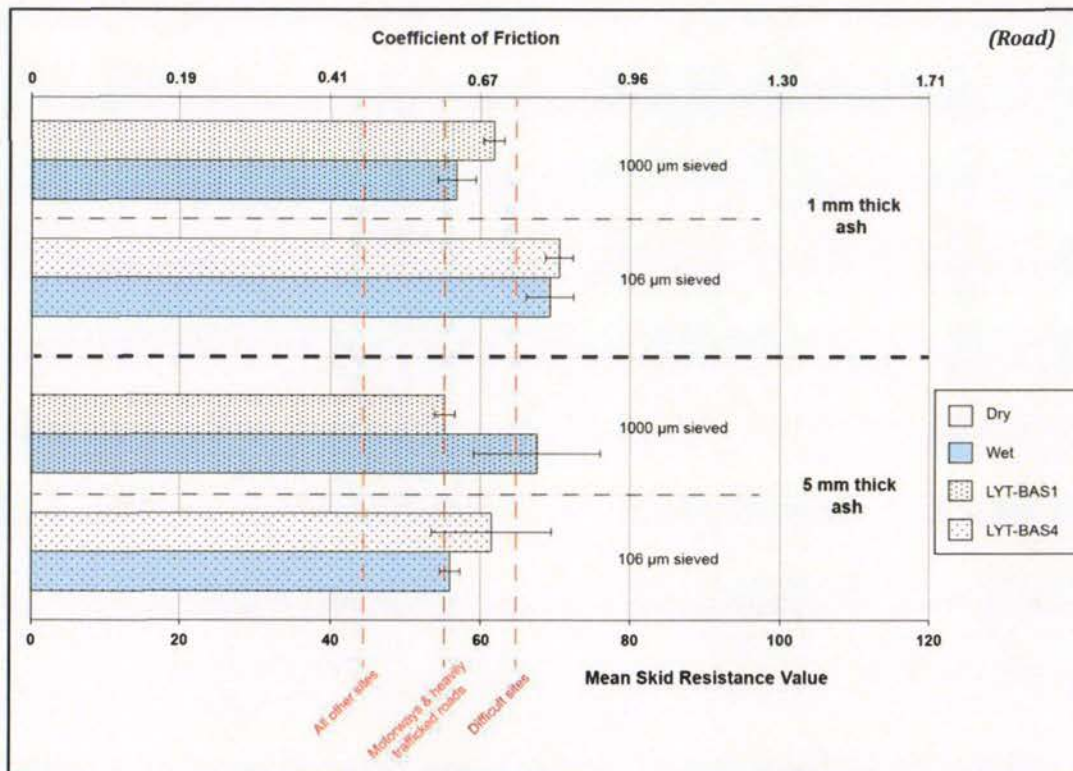


Figure 9. Mean SRVs and CoFs for the asphalt covered in coarse-grained (i.e. LYT-BAS1, 1000 µm sieved) and fine-grained (i.e. LYT-BAS4, 106 µm sieved) samples at 1 mm and 5 mm ash thickness under both dry and wet conditions. Also displayed (as red dashed lines) are the minimum recommended SRVs for different road network sites (Table 2).

4.1.4 Line-painted asphalt surfaces

SRVs can be reduced substantially as a result of road markings, although the addition of retroreflective glass beads can increase values to more acceptable levels (NZRF 2005). This is demonstrated in our findings for wet conditions, in which BPT analysis is typically conducted, with mean SRVs on line-painted asphalt surfaces with no beads and no ash the lowest of all our results. SRVs for these wet surfaces range from 40 to 46, and lie below the minimum recommended skid resistance for 'all other sites' when 4x coats of line paint have been applied (Figure 10). The addition of glass beads does increase SRVs (by around 5), although values are still relatively low. SRVs for 'clean' and dry line-painted asphalt surfaces are very high, but as with non-painted surfaces, the addition of a 1 mm ash layer decreases SRVs substantially. Conversely, the SRVs for wet asphalt concrete increase with a 1 mm ash layer to similar levels as for dry conditions. With the thicker (5 mm) ash layer on top of line-painted surfaces, SRVs increase further by around 20 (Figure 10).

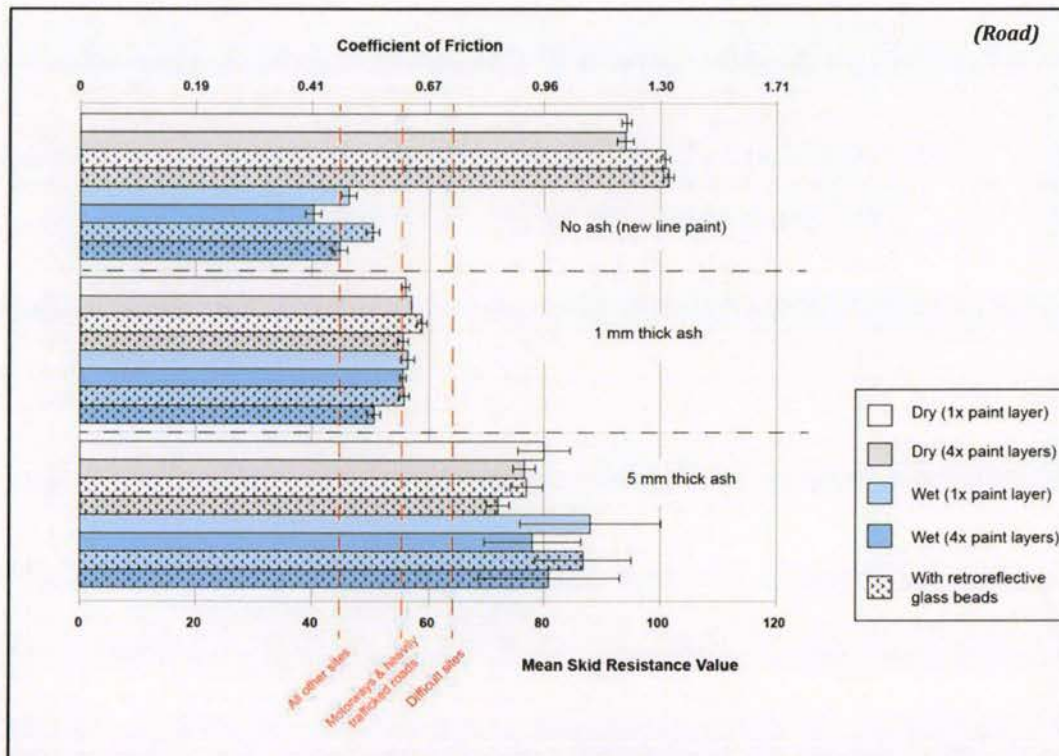


Figure 10. Mean SRVs and CoFs for the road asphalt with line-painted surfaces. Conditions of no ash, 1 mm thick ash, and 5 mm thick ash (using the LYT-BAS1 ash type) were analysed under both wet and dry conditions. Also displayed (as red dashed lines) are the minimum recommended SRVs for different road network sites (Table 2).

4.1.5 Asphalt comparison

Because of increased macrotexture of the surface, higher SRVs (~ 5) were measured on the bare OGPA than the SMA slabs when wet. Similar differences in SRVs existed between the two asphalt types covered by wet volcanic ash (both at 1 mm and 5 mm depths). However, no major differences in SRVs were observed between the two asphalt types when dry, whether surfaces were covered by ash or not.

4.2 Inconsistent Depth

Where ash was not replenished between each swing, SRVs represent those expected for surfaces where ashfall has ceased but where there is some traffic movement.

4.2.1 Ash types and wetness

SRV results obtained for the samples sieved to 1000 μm (at 1mm and 5 mm ash thickness) and deposited on road asphalt are shown in Figure 11. Note that tests of other thicknesses (3, 7 and 9 mm) were also conducted but these have been omitted from the figure for clarity. Despite the large standard deviations, the 5 mm thick PUN-BAS1 and HAT-RHY samples initially produced high SRVs. However, the SRVs recorded for the first 2-3 swings of the pendulum over 5 mm thick ash should be interpreted with caution. This is due to possible interference of the thicker deposit when the pendulum slider first impacts the surface; similar circumstances may occur in the field when initial vehicles are driven into thicker ash deposits. When wet however, the SRVs are higher than the mean recorded on the bare asphalt surface, particularly for the PUN-BAS1 sample, suggesting that thicker layers of vesiculated (and especially harder) volcanic ash are perhaps initially less slippery than thin layers of ash of those ash types. Observations during our experimentation revealed that the wet 5 mm thick vesiculated deposits (PUN-BAS1 and HAT-RHY) consolidated, thus resisting major ash displacement more than for dry ash (Figure 12),

even following several swings of the pendulum arm. The consolidated deposits were very firm to touch and, although further work is required to test this, it is suggested that light vehicles would be able to drive over the surface without sinking substantially.

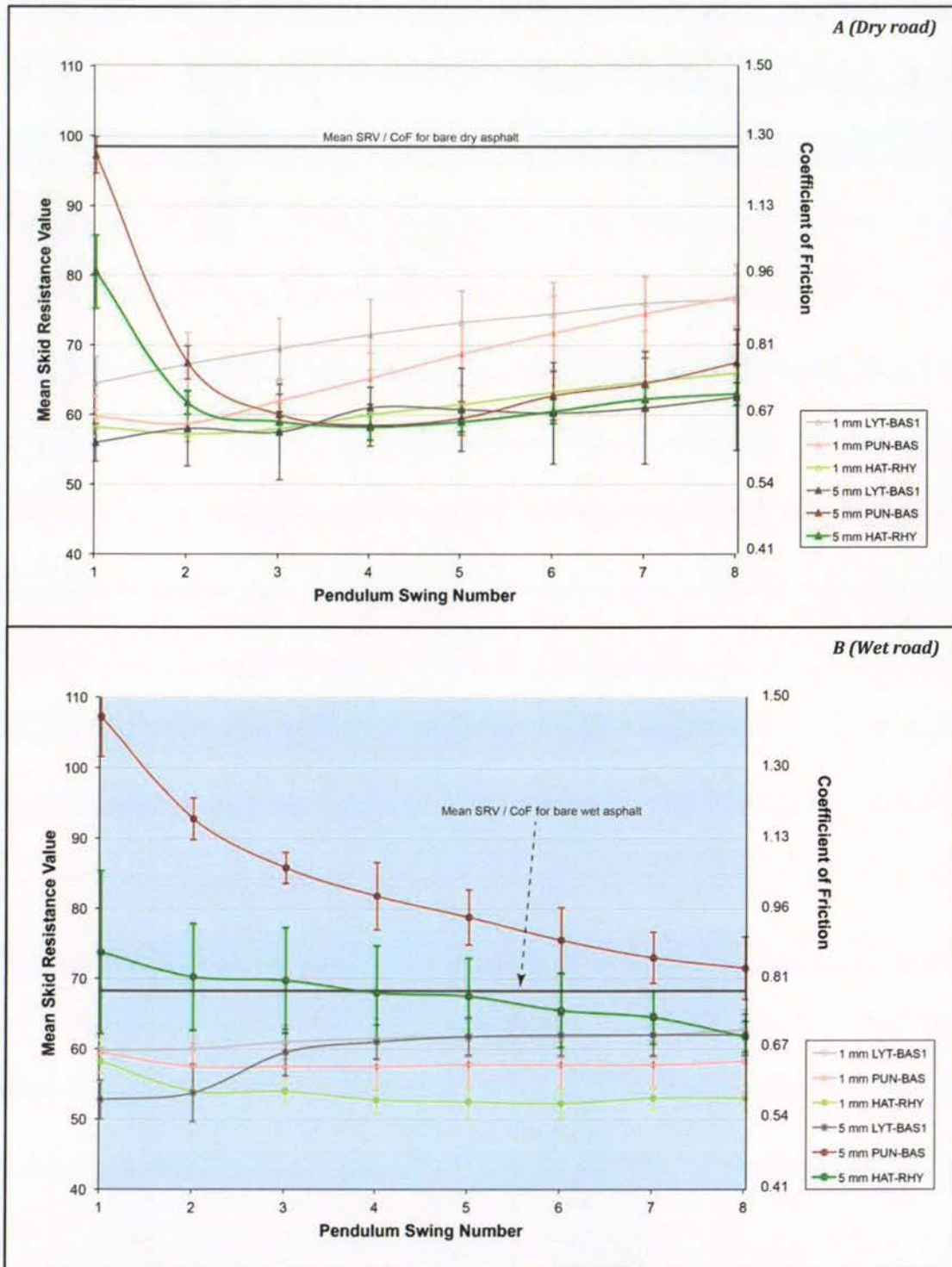


Figure 11. SRVs and corresponding CoFs on asphalt covered by ash sieved to 1000 μm , under (A) dry and (B) wet conditions. Also shown are the mean SRVs for bare asphalt, taken from section 4.1. Error bars display the standard deviations for each pendulum swing number for the different sample types. Note that the first 2-3 swings over 5 mm deposits should be interpreted with caution due to possible impacts on SRVs caused by the initial contact between the pendulum slider and surface.

Very similar patterns in skid resistance were observed for the airfield concrete surfaces where ash was not replenished between swings. The main difference was that the initially high SRVs for the scoriaceous sample (PUP-BAS) decreased more quickly with pendulum swings, most likely due to the ash being more easily displaced from the smoother concrete surface than for asphalt.

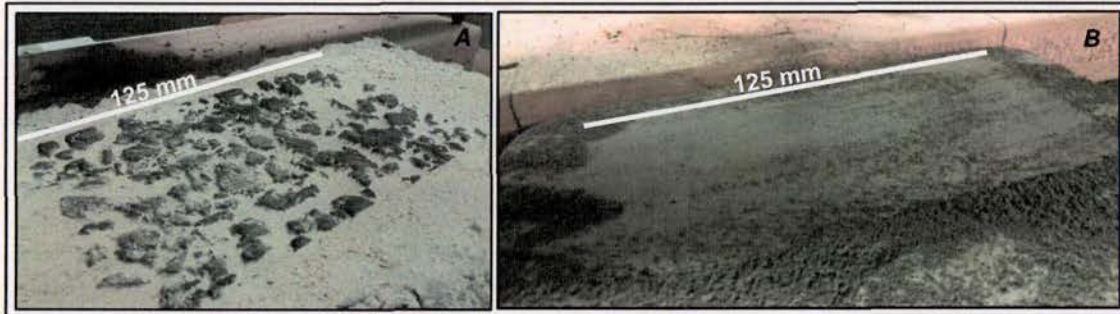


Figure 12. Dry ash displacement from the BPT slider-surface interface after 8x swings of the pendulum arm for (a) SMA, and (b) airfield concrete. Dry ash was displaced from the surface more readily than wet ash.

4.2.2 Ash particle size

No major changes were observed for the fine-grained basaltic ash samples (LYT-BAS4) over the course of the eight pendulum swings on asphalt, other than a gradual increase in SRVs over time, particularly for the dry ash at 1 mm thickness as observed for the coarse-grained samples (Figure 11a). As with the testing where ash was replenished, here SRVs for the fine-grained ash samples were generally slightly higher than those for coarse-grained samples, suggesting that fine-grained ash is a little less slippery than coarser material.

4.2.3 Soluble components

The testing involving non-replenished dosed ash confirmed the key finding already discussed during replenished testing (section 4.1.2): non-crystalline ash containing a higher soluble component content generally produces lower SRVs than undosed ash. However, with an increasing number of swings of the pendulum, this trend becomes less pronounced, particularly under wet conditions where the effect of adding water between each test leaches the samples, thus reducing the soluble component content of the ash.

4.2.4 Line-painted asphalt surfaces

Line-painted asphalt surfaces covered in ash produce relatively low SRVs (Figure 13). Although the first 2-3 swings involving 5 mm thick ash are not considered, it is evident that wet painted surfaces are generally slightly more slippery than painted dry surfaces. The trend of quick SRV recovery (as seen in section 4.2.1) is also evident under dry line-painted conditions, when compared to wet conditions which remain slippery for longer. Under dry conditions, the addition of retroreflective glass in the line-paint appears to aid the recovery of skid resistance over time (as shown by the rising green and orange lines for the latter swings in Figure 13a). However, this trend is not evident for wet conditions.

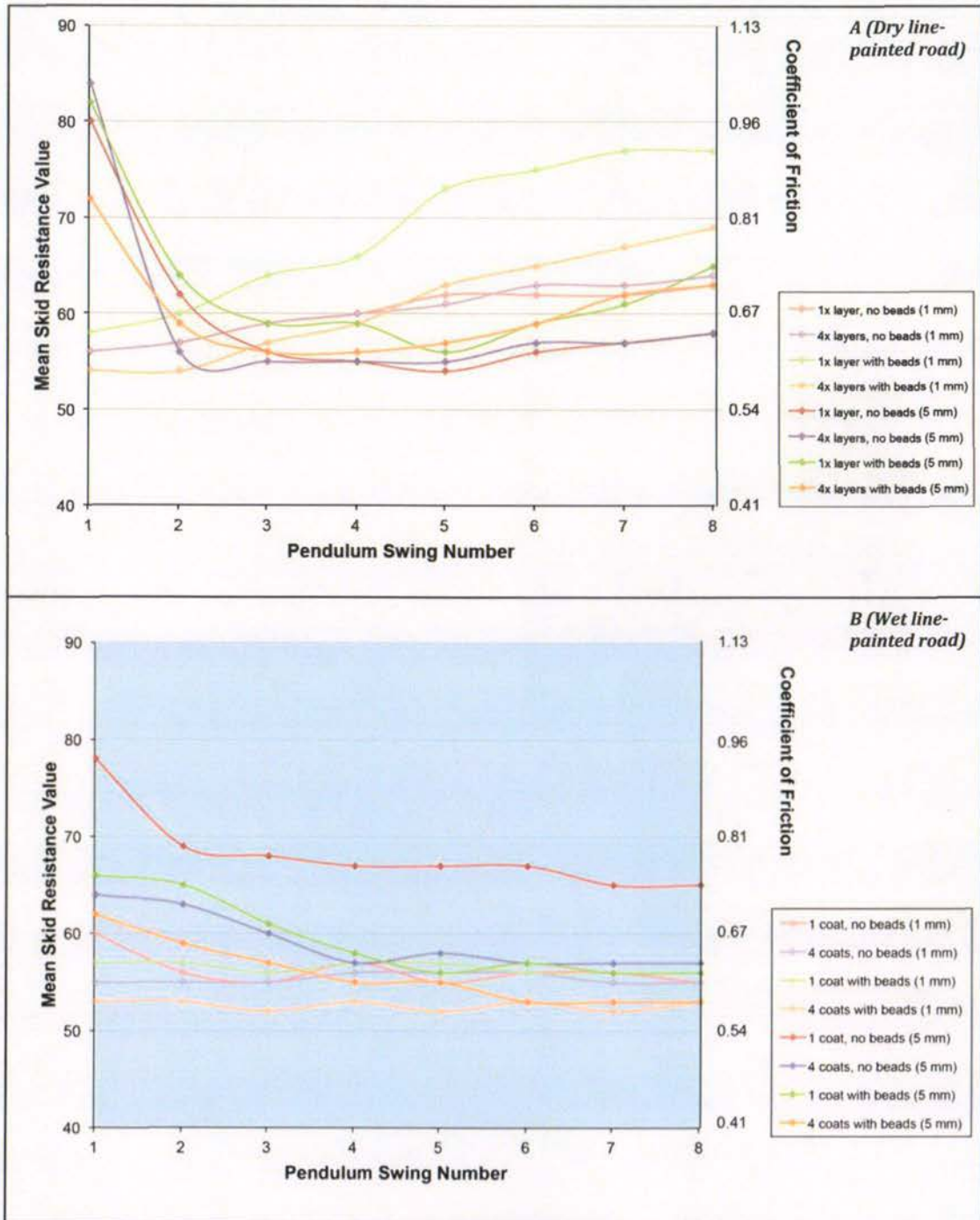


Figure 13. SRVs and corresponding CoFs for line-painted asphalt surfaces covered in 1 mm or 5 mm thick LYT-BAS1, under (A) dry, and (B) wet conditions. Only one test was conducted on each surface type due to the availability of line-painted slabs. Therefore, no standard deviations were calculated and the results should be treated with some caution. Note that the initial 2-3 swings over the 5 mm deposits should be treated with particular caution.

4.3 Surface Macro and Microtexture

4.3.1 Ash displacement and removal

The results for mean macrotexture depth calculated using the sand patch method for the bare, clean, new asphalt surface and the asphalt surface following dry testing and brushing, and cleaning with compressed air after contamination are shown in Table 6.

Table 6. Mean macrotexture depth of asphalt slab before and after testing/cleaning, calculated using the ASTM sand patch method, and percentage ash surface coverage.

Asphalt Concrete Slab Condition	Mean Macrotexture Depth (mm)	Ash surface coverage (%)
Bare, clean and new	1.37	0
Ashed, 10x BPT swings	-	81
Ashed, 10x BPT swings and brushed (10x strokes)	0.99	40
Cleaned with compressed air	1.29	<1

The results for the new slab and pre-contaminated slab after cleaning with compressed air suggest that there is little difference in macrotexture depth after cleaning using this method. However, cleaning using only brush strokes shows a mean macrotexture depth reduction of 0.38 mm, 28% less depth than the original new surface. This suggests that cleaning of dry road surfaces using only brushes may not be entirely effective and that alternative methods should be considered where possible. To confirm this, after brushing and 10x swings of the BPT, some HAT-RHY ash remains - as shown in the digital photography macrotexture image sequence (Figure 14) and semi-quantitative analysis of these images using 'Ilastik' and 'Adobe Photoshop' gives results of surface coverage (Table 6).

Cleaning using high-pressure water spraying and brushing was more effective than brushing alone at removing ash (<1% surface ash coverage afterwards). However, this approach requires large quantities of water and the microscope imagery revealed that some small particles of ash remain on the surface, which would perhaps still reduce skid resistance somewhat. Field observations from Kagoshima, Japan, where high quantities of only low-pressure water are used to clean road surfaces ~~confirm~~ indicates that some ash remains on the road surfaces even immediately after cleaning (Kagoshima City Office, personal communication, June 08 2015). Furthermore, clearing ash from roads using water may cause some drainage systems to become blocked (Barnard 2009), potentially resulting in surface water flooding.

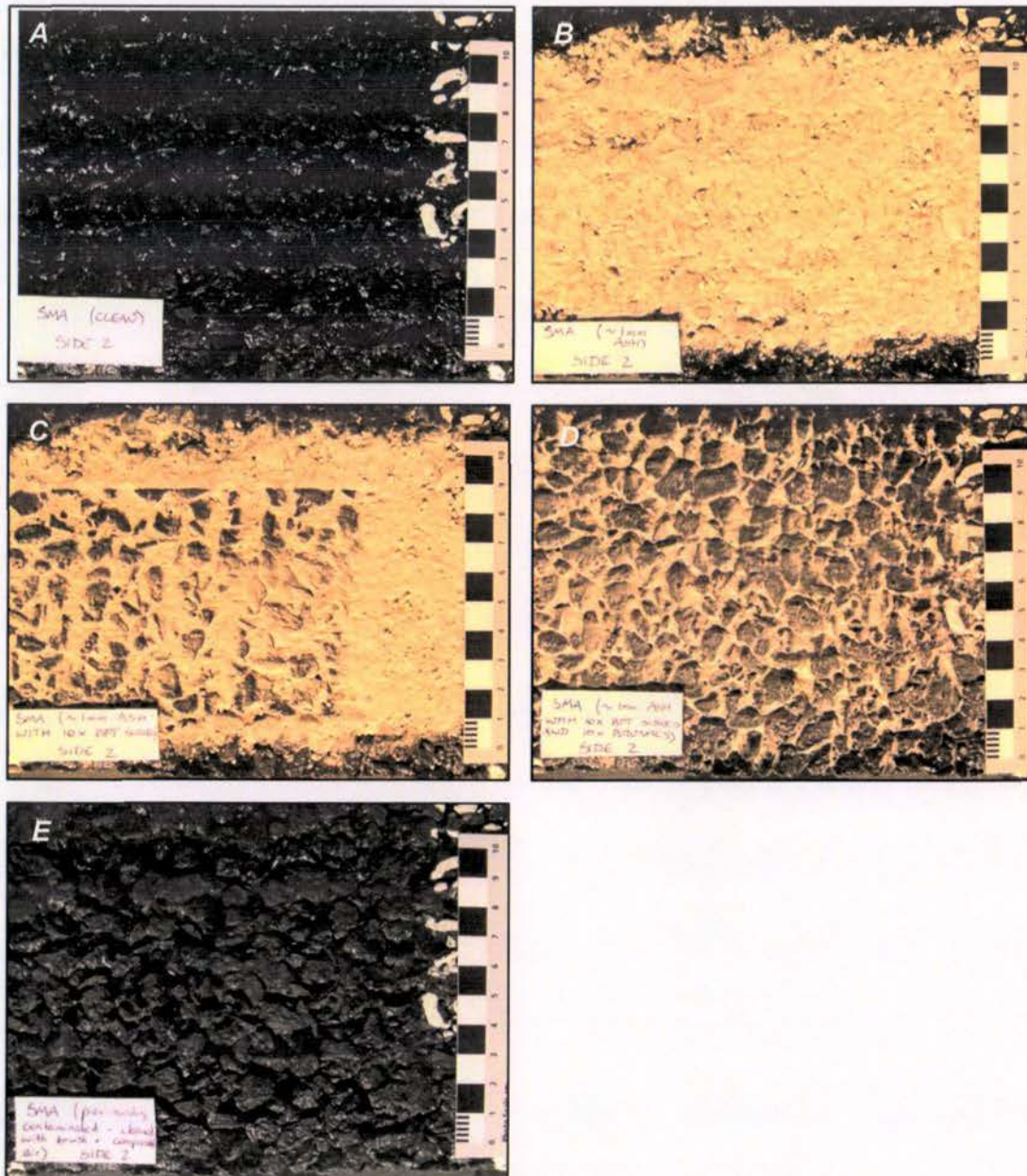


Figure 14. Macrotexture image sequence for asphalt. (A) Clean new slab, (B) covered with 1 mm rhyolitic ash (100% surface coverage), (C) after 10x BPT swings (81% surface ash coverage), (D) after cleaning with 10x brush strokes (40% surface ash coverage), (E) after cleaning with compressed air (<1% surface ash coverage). The macrotexture of the surface is visibly affected in images b-d with much ash remaining between the asphalt's aggregate pore spaces, even after 10x BPT swings and cleaning using a brush.

4.3.2 Temporal change of skid resistance on bare asphalt surfaces

In normal conditions, the skid resistance of bare asphalt surfaces changes over time. Typically, during the first two years following construction it increases as the surface is worn by traffic and rough aggregate surfaces become exposed, and then decreases over time as the aggregates become more polished (Asi 2007). The initial trend of increasing skid resistance was confirmed during our testing of the bare wet asphalt and concrete slabs before and after contamination with ash (but following cleaning), particularly so for the asphalt (Figure 5). We suggest that the abrasive properties of volcanic ash accelerates these processes, especially for our testing as all ash particles were <500 μm in diameter (see section 2.4). Following testing, the SRV of bare wet

asphalt had increased by around 5. The microscopy imagery showed that the lustrous film on the new asphalt slabs had been removed during BPT experimentation (Figure 15).

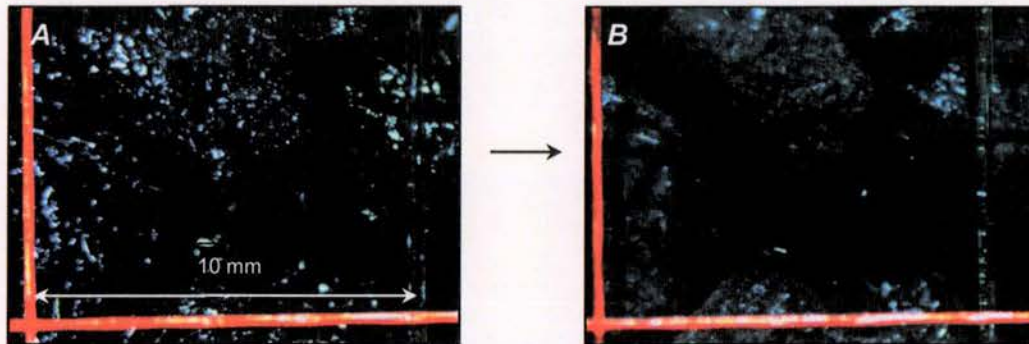


Figure 15. Microscope images on the same segment of asphalt, (A) on the new slab and (B) after contamination with volcanic ash and cleaning with compressed air. Much of the shiny film visible on the surface of the new asphalt has been removed. Note that lighting conditions and microscope settings were consistent for both images.

5. Conclusions

5.1 Key findings

Our experiments suggest that the following lead to particularly reduced skid resistance on asphalt road surfaces and may thus lead to slippery surfaces following volcanic ashfall:

- Thin (~1 mm deep) layers of relatively coarse-grained ash, with ash type having little effect at this depth (average SRVs of 55-65).
- Thicker (~5 mm deep) layers of hard, non-vesiculated ash (average SRVs of 55-60).
- Ash of low crystallinity or containing a high degree of soluble components (average SRVs ~5 lower than for ash that has undergone substantial leaching).
- Line-painted surfaces that are either dry or wet but covered by thin layers of ash, particularly when paint does not incorporate retroreflective glass beads (average SRVs of ~55).

Importantly, the largest change in skid resistance for surfaces that became covered by ash occurs during dry conditions, where SRVs fall to levels just below those for wet non-contaminated surfaces, with similar SRVs as the wet contaminated surfaces. This large reduction in skid resistance may not be expected by motorists who may consequently not adjust driving, potentially resulting in high accident rates. As time goes on, wet ash deposits on roads are most likely to lead to reduced skid resistance, particularly for thicker deposits as these remain slippery for longer (typical SRVs of around 55).

Similarities exist for airfield surfaces and the second and third bullet points above are especially true for the concrete surface type. The following additional key findings are also drawn:

- There is little difference in skid resistance between bare airfield surfaces and those covered by ~1 mm of ash.
- Low crystalline ash containing high soluble components may result in SRVs of up to 20 less than non-dosed samples, particularly if the ash is thicker (~7-9 mm depth).
- Ash is more readily displaced on smoother airfield concrete than road asphalt causing SRVs to recover to 'typical non-contaminated' values at a faster rate with consistent traffic flow.

5.2 Recommendations for road safety

Based on skid resistance analysis, we make the following recommendations to increase road safety in areas with volcanic ashfall exposure of ≤ 5 mm depth:

- During initial ash fall, vehicle speed (or advisory speed) should immediately be reduced to levels below those advised for driving in very wet conditions on that road, whether the surface is wet or dry. Wet ash is not necessarily more slippery than dry ash, at least initially.
- Fresh ash contains more soluble components, which results in lower skid resistance values than for leached ash. Therefore, it is important to advise motorists promptly of any restrictions.
- Particular caution should be taken on dry surfaces that become covered by coarse-grained ash as skid resistance will reduce substantially from what occurs on dry non-contaminated surfaces. The slipperiness of dry surfaces with such contamination may not be expected by motorists (skid resistance values will be similar as for wet fresh ash and slightly less than for wet non-contaminated conditions).
- Road markings may be hidden from view, impacting road safety through lack of visual and audio guidance of road features. Areas of road that are line-painted and covered in thin ash are especially slippery. Motorcyclists and cyclists in particular should take extreme care.

It is unlikely that road closures will be necessary for thin ash accumulations based on loss of skid resistance alone. SRVs rarely fall below the minimum recommended threshold for motorways and heavily trafficked roads (i.e. SRV 55) although many values fall between this and the threshold for minimum recommended skid resistance for difficult sites (i.e. SRV 65). These results are conservative however, because of the typical reduction in skid resistance over the later stages of the pavement life. Based on observations from previous eruptions along with work by Barnard (2009), physical obstruction to road vehicles may occur once ash deposits reach ~ 100 mm and road closures may be necessary at and above this depth. It should be stressed however, that all recommendations given ignore other impacts from volcanic ashfall such as visibility impairment, local road authority decisions, breakdowns and driver behaviour which often introduce further complexities associated with driving in volcanic ashfall. For example, lower thresholds for road closures and lower speed restrictions may be required where visibility is reduced.

5.3 Airport safety

We do not make any specific recommendations for airport safety related to concrete airfield surfaces, although it is highlighted that extensive efforts may be required to clean airfield surfaces as has occurred following historical eruptions (e.g. Chaitén 2008 (Wilson 2009 unpublished field notes), Kelud 2014 (Blake et al. 2015)). It is likely that airports will remain closed until all ash has been cleared from runways due to other potential impacts such as damage to aircraft turbine engines. Our results suggest that residual ash of minimal depths on concrete airfield surfaces is likely to have little effect on skid resistance. However, airport managers should be aware that freshly erupted ash or ash that has not been leached (i.e. containing higher soluble components) will likely be more slippery than that which has persisted in the environment for some time. As with road asphalt, wet ash is not necessarily more slippery than dry ash on airfield concrete and any restrictions implemented should thus be in place for both conditions.

5.4 Recommendations for cleaning

The following advice for road cleaning is given based on our studies of macrotexture and microtexture and from the observations during small-scale cleaning conducted on our slabs between skid resistance tests:

- Brushing alone will not restore surfaces to their original condition in terms of skid resistance. Following simple brushing practices on asphalt roads, the macrotexture depth may be around one third less than the original depth and ~40% ash coverage may occur on the surface.
- If surfaces are dry and contaminated with dry ash, air blasting combined with suction and capture of loosened ash, is an effective way to remove ash from macrotextural pores. Minor quantities of ash may remain at the microtextural level although this is deemed too low to substantially affect skid resistance.
- If surfaces are wet, a combination of water spraying and brushing and/or air blasting (with suction and ash capture) is an effective way to remove most ash and restore surface skid resistance. However, large quantities of water are required and some ash will remain in the asphalt pore spaces, especially if low-pressure water is used. Care should be taken if using water for ash removal due to the potential for blockage of some drainage systems.

Ash remobilisation should be carefully considered prior to cleaning. Extensive (and often expensive) cleaning efforts may be useless if ash continues to fall or is remobilised from elsewhere and deposited onto roads and airfields.

Acknowledgements

We thank the University of Canterbury Mason Trust scheme, New Zealand Earthquake Commission (EQC) and Determining Volcanic Risk in Auckland (DEVORA) project for their support towards the study through the provision of funding. We also express thanks to the organisations and people who helped source equipment that was vital to the project. In particular, we would like to thank Alan Nicholson and John Kooloos of the Civil and Natural Resources Engineering department at the University of Canterbury for the loan of the BPT, and Janet Jackson, Howard Jamison and the wider laboratory and road teams at Downer Group for their support towards coordinating the construction and line-painting of asphalt slabs and for providing Daniel Blake with BPT training. We thank Roy Robertson (Auckland Airport) and Robert McKinnon (Firth Concrete) for their advice on airfield surfaces and for providing the airfield concrete slabs used in this study. Particular thanks also go to the people who provided support with the laboratory set-up at various stages, including technician support from Rob Spiers, Matt Cockcroft, Chris Grimshaw and Sacha Baldwin-Cunningham. We also thank researchers Emily Lambie, Rinze Schuurmans, Alec Wild and Alistair Davies for their assistance with sample preparation and skid resistance testing.

References

- Abdel-Aty, M. Ekram, A-A. Huang, H. Choi, K. (2011) A study on crashes related to visibility obstruction due to fog and smoke. *Accident Analysis and Prevention*, 43:5, pp.1730-1737
- Andrey, J. (1990) Relationships between weather and traffic safety: past, present and future directions. *Climatological Bulletin*, 24, pp.124-136
- Asi, I. (2007) Evaluating skid resistance of different asphalt concrete mixes. *Building and Environment*, 42:1, pp.325-329
- ASTM E303 (2013) Standard test method for measuring surface frictional properties using the British Pendulum Tester. ASTM E303-93 (Reapproved 2013)
- ASTM E965 (2006) Standard test method for measuring pavement macrotexture depth using a volumetric technique. ASTM E965-96 (Reapproved 2006)

- Aström, H. Wallman, C. (2001) Friction measurement methods and the correlation between road friction and traffic safety: a literature review. Swedish National Road and Transport Research Institute (VTI), Linköping, Sweden
- Barnard, S. (2009) The vulnerability of New Zealand lifelines infrastructure to ashfall. PhD Thesis, Hazard and Disaster Management, University of Canterbury, Christchurch, New Zealand
- Bastow, R. Webb, M. Roy, M. Mitchell, J. (2004) An investigation of the skid resistance of stone mastic asphalt laid on a rural English county road network. Transit New Zealand, pp.1-16
<http://www.nzta.govt.nz/resources/surface-friction-conference-2005/7/docs/investigation-skid-resistance-stone-mastic-asphalt-laid-rural-english-county-road-network.pdf> Accessed 16/06/2015
- BBC (2005) 'Hidden menace' on UK's roads. BBC News
http://news.bbc.co.uk/2/hi/programmes/file_on_4/4278419.stm Accessed 12/02/2015
- Benedetto, J. (2002) A decision support system for the safety of airport runways: the case of heavy rainstorms. Transportation Research Part A: Policy and Practice, 8, pp.665-682
- Bennis, T.A. De Wit, L.B. (2003) PIARC State-of-the-art on Friction and IFI. Paper presented at the 1st Annual Australian Runway and Roads Friction Testing Workshop, Sydney, Australia
- Blake, D.M. Wilson, G. Stewart, C. Craig, H.M. Hayes, J.L. Jenkins, S.F. Wilson, T.M. Horwell, C.J. Andrestuti, S. Daniswara, R. Ferdiwijaya, D. Leonard, G.S. Hendrasto, M. Cronin, S. (2015) The 2014 eruption of Kelud volcano, Indonesia: impacts on infrastructure, utilities, agriculture and health. GNS Science Report 2015/15, 139p
- Blake, D.M. Wilson, T.M. Gomez, C. (in prep) Road marking coverage by volcanic ash
- Blastrac (2015) Airport runways: skid resistance and rubber removal. Blastrac, The Netherlands
www.theairportshow.com/Portal/assets/.../BrochureAirport_LR.pdf.aspx Accessed 05/10/2015
- Blong, R.J. (1984) Volcanic hazards: a sourcebook on the effects of eruptions. New South Wales, Australia
- Boyle, T. (2005) Skid resistance management on the Auckland State Highway Network. Transit New Zealand
<http://www.nzta.govt.nz/resources/surface-friction-conference-2005/8/docs/skid-resistance-management-auckland-state-highway-network.pdf> Accessed 16/06/2015
- British Pendulum Manual (2000) Operation manual of the British Pendulum Skid Resistance Tester. Wessex Engineering Ltd., United Kingdom
- Broom, S.J. (2010) Characterisation of "pseudo-ash" for quantitative testing of critical infrastructure components with a focus on roofing fragility. BSc Thesis, University of Canterbury, Christchurch, New Zealand
- Cova, T. Conger, S. (2003) Transportation hazards. In: *Transportation Engineers' Handbook*, Kutz, M. (ed.), Centre for Natural and Technological Hazards, University of Utah
- Daily Telegraph (2008) Get a grip: Motorcycle road safety. Daily Telegraph
<http://www.telegraph.co.uk/motoring/motorbikes/2750422/Motorcycle-road-safety-Get-a-grip.html> Accessed 12/02/2015
- Delmelle, P. Villiérás, F. Pelletier, M. (2005) Surface area, porosity and water adsorption properties of fine volcanic ash particles. *Bulletin of Volcanology*, 67, pp.160-169

Do, M.T. Cerezo, V. Zahouani, H. (2014) Laboratory test to evaluate the effect of contaminants on road skid resistance. Proceedings of the Institution of Mechanical Engineers, Part J: Journal of Engineering Tribology, 228:11, pp.1276-1284

Dookeeram, V. Nataadmadja, A.D. Wilson, D.J. Black, P.M. (2014) The skid resistance performance of different New Zealand aggregate types. IPENZ Transportation Group Conference 23-26 March 2014, Shed 6, Wellington, New Zealand

Dunn, M.G. (2012) Operation of gas turbine engines in an environment contaminated with volcanic ash. Journal of Turbomachinery, 134:5, 18p

EASA (2010) RuFAB – Runway friction characteristics measurement and aircraft braking: volume 3, functional friction. European Aviation Safety Agency, Research Project EASA 2008/4, BMT Fleet Technology Limited, Kanata, Ontario, Canada
<https://easa.europa.eu/system/files/dfu/Report%20Volume%203%20-%20Functional%20friction.pdf> Accessed 05/10/2015

Ergun, M. Iyınam, S. Iyınam, F. (2005) Prediction of road surface friction coefficient using only macro- and microtexture measurements. Journal of Transportation Engineering, 131, pp.311-319

FAA (1997) Measurement, construction and maintenance of skid-resistant airport pavement surfaces. Advisory Circular 150/5320-12C, U.S. Department of Transportation, Federal Aviation Administration http://www.faa.gov/documentLibrary/media/advisory_circular/150-5320-12C/150_5320_12c.PDF Accessed 03/10/2015

Gordon, K.D. Cole, J.W. Rosenberg, M.D. Johnston, D.M. (2005) Effects of volcanic ash on computers and electronic equipment. Natural Hazards, 34, pp.231-262

Guffanti, M. Mayberry, G.C. Casadevall, T.J. Wunderman, R. (2009) Volcanic hazards to airports. Natural Hazards, 51, pp.287-302

Heiken, G. Wohletz, K. (1985) Volcanic ash. University of California Press, Berkeley

Heiken, G. Murphy, M. Hackett, W. Scott, W. (1995) Volcanic hazards to energy infrastructure-ash fallout hazards and their mitigation. World Geothermal Congress, Florence, Italy, pp.2795-2798

Highway Research Board (1972) National Cooperative Highway Research Program Synthesis of Highway Practice 14: skid resistance. Highway Research Board, National Academy of Sciences, Washington D.C.

Hill, D.J. (2014) Filtering out the ash: mitigating volcanic ash ingestion for generator sets. Masters Thesis, Hazard and Disaster Management, University of Canterbury, Christchurch, New Zealand

Horwell, C.J. Baxter, P.J. Hillman, S.E. Damby, D.E. Delmelle, P. Donaldson, K. Dunster, C. Calkins, J.A. Fubini, B. Hoskuldsson, A. Kelly, F.J. Larsen, G. Le Blond, J.S. Livi, K.J.T. Mendis, B. Murphy, F. Sweeney, S. Tetley, T.D. Thordarson, T. Tomatis, M. (2010) Respiratory health hazard assessment of ash from the 2010 eruption of Eyjafjallajökull volcano, Iceland: a summary of initial findings from a multi-centre laboratory study. IVHHN and Durham University, Durham, UK

ICAO (2013) Industry best practices manual for timely and accurate reporting of runway surface conditions by ATS/AIS to flight crew. International Civil Aviation Organisation, Regional Aviation Safety Group (Asian and Pacific Region) <http://www.icao.int/APAC/Documents/edocs/FS-07IBP%20Manual%20on%20Reporting%20of%20Runway%20Surface%20Condition.pdf> Accessed 02/10/2015

Impact (2010) Skid tester: AG190. Impact Test Equipment Ltd http://www.impact-test.co.uk/docs/AG190_HB.pdf Accessed 04/11/2014

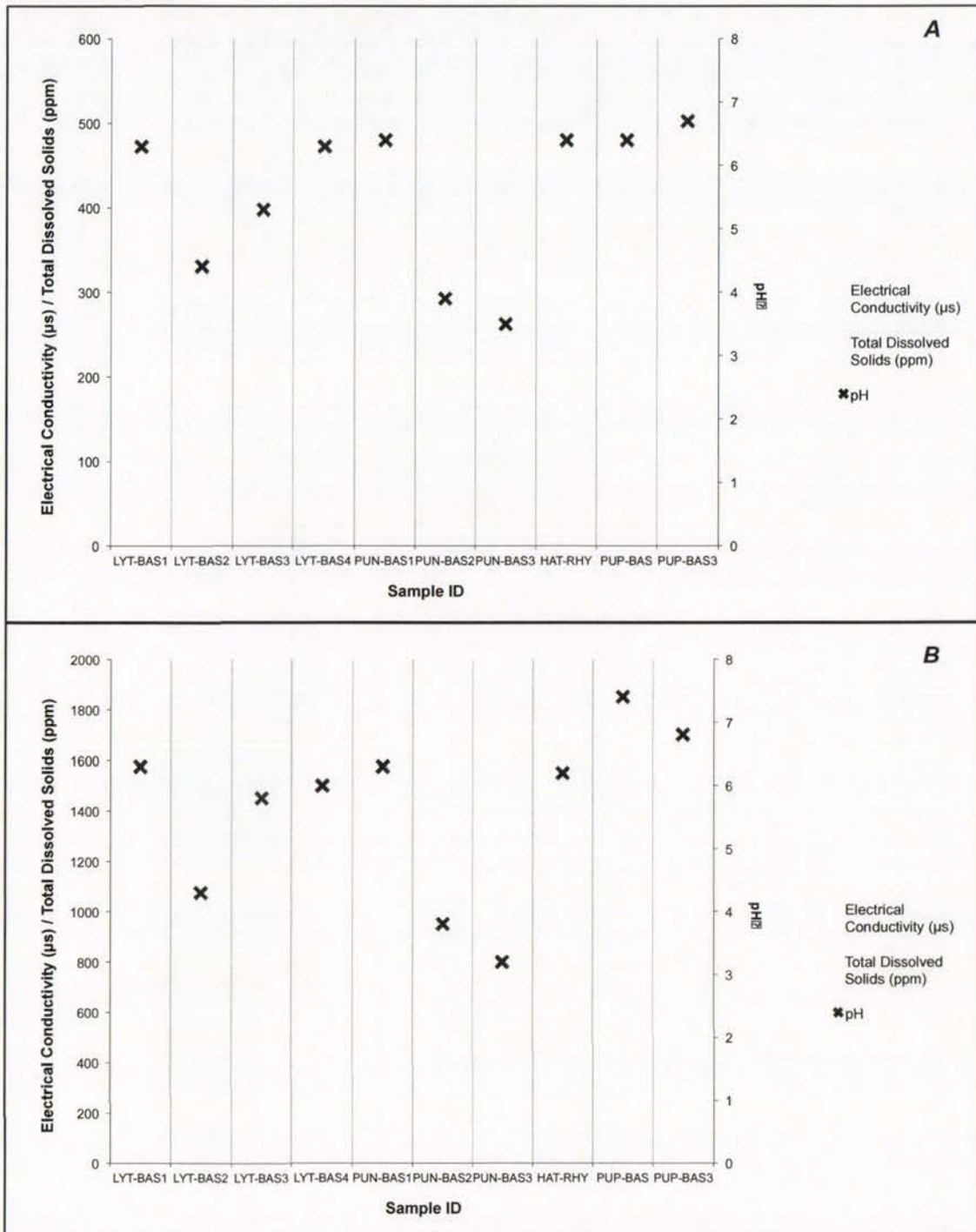
- Jamaludin, D. (2010) BORDA respond to Merapi disaster. Bremen Overseas Research and Development Association, South East Asia <http://www.borda-sea.org/news/borda-sea-news/article/borda-respond-to-merapi-disaster.html> Accessed 20/10/2015
- Johnston, D.M. (1997) Physical and social impacts of past and future volcanic eruptions in New Zealand. PhD Thesis, Earth Science, Massey University, Palmerston North, New Zealand
- Johnston, D.M. Daly, M. (1997) Auckland erupts!! New Zealand Science Monthly, 8:10, pp.6-7
- Khattak, A.J. Knapp, K.K. (2001) Interstate highway crash injuries during winter snow and non-snow events. Transportation Research Board, 1746, pp.30-36
- Labadie, J. R. (1994) Volcanic ash effects and mitigation. Adapted from a report prepared in 1983 for the Air Force Office of Scientific Research and the Defence Advanced Research Projects Agency
- Leonard, G.S. Johnston, D.M. Williams, S. Cole, J.W. Finnis, K. Barnard, S. (2006) Impacts and management of recent volcanic eruptions in Ecuador: lessons for New Zealand. GNS Science Report 2005/20
- Lester, T. (2014) Pedestrian slip resistance testing: AS/NZS 3661.1:1993. Opus International Consultants Ltd. Lower Hut, Wellington, New Zealand
- Matsumoto, H. Okabyashi, T. Mochihara, M. (1988) Influence of eruptions from Mt. Sakurajima on the deterioration of materials. In: Proceedings Kagoshima International Conference on Volcanoes, pp.732-735
- Miller, T.P. Casadevall, T.J. (2000) Volcanic ash hazards to aviation. In: Sigurdsson et al. (eds), Encyclopedia of Volcanoes, Academic Press, San Diego, CA, United States, pp.915-930
- NZRF (2005) Road marking IS road safety, Potters Asia Pacific. New Zealand Road Marking Federation Inc. 2005 Conference
- NZRF (2009) NZRF Roadmarking materials guide. New Zealand Roadmarkers Federation Inc. Auckland, New Zealand
- Oh, S. Chung, K. Ragland, D.R. Chan, C. (2009) Analysis of wet weather related collision concentration locations: empirical assessment of continuous risk profile. In: Proceedings of the 88th Annual Meeting of the Transportation Research Board, Transportation Research Board, Washington D.C, U.S.
- Persson, B.N.J. Tartaglino, U. Albohr, O. (2005) Rubber friction on wet and dry road surfaces: the sealing effect. Physical Review B, 71
- Pyle, D.M. (1989) The thickness, volume and grainsize of tephra fall deposits. Bulletin of Volcanology, 51, pp.1-15
- Qin, X. Noyce, D. Lee, C. Kinar, J.R. (2006) Snowstorm event-based crash analysis. Transportation Research Record, 1948, pp.135-141
- Sarna-Wojcicki, A.M. Shipley, S. Waite, R.B. Dzurisin, D. Wood, S.H. (1981) Areal distribution, thickness, mass, volume, and grain size of air-fall ash from the six major eruptions of 1980. The 1980 Eruptions of Mount Saint Helens, Washington, pp.577-600
- Stewart, C. Horwell, C. Plumlee, G. Cronin, S. Delmelle, P. Baxter, P. Calkins, J. Damby, D. Mormon, S. Oppenheimer, C. (2013) Protocol for analysis of volcanic ash samples for assessment of hazards from leachable elements. IAVCEI, IVHHN, Cities on Volcanoes Commission, USGS, GNS Science

- TNZ (2003) Standard test procedure for measurement of skid resistance using the British Pendulum Tester, Report TNZ T/2:2003. Transit New Zealand, New Zealand
- Tuck, B.H. Huskey, L. Talbot, L. (1992) The economic consequences of the 1989-90 Mt. Redoubt eruptions. Institute of Social and Economic Research, University of Alaska, Anchorage
- USGS (2009) Small explosion produces light ash fall at Soufriere Hills volcano, Montserrat. United States Geological Survey <https://volcanoes.usgs.gov/ash/ashfall.html#eyewitness> Accessed 20/10/2015
- Wardman, J. Sword-Daniels, V. Stewart, C. Wilson, T. (2012a) Impact assessment of the May 2010 eruption of Pacaya volcano, Guatemala. GNS Science Report 2012/09
- Wardman, J.B. Wilson, T.M. Bodger, P.S. Cole, J.W. Johnston, D.M. (2012b) Investigating the electrical conductivity of volcanic ash and its effect on HV power systems. *Physics and Chemistry of the Earth*, 45-46, pp.128-145
- Wilson, D.J. (2006) An analysis of the seasonal and short-term variation of road pavement skid resistance. PhD Thesis, Department of Civil and Environmental Engineering, University of Auckland, Auckland, New Zealand
- Wilson, D.J. Chan, W. (2013) The effects of road roughness (and test speed) on GripTester measurements. NZ Transport Agency Research Report 523, Clearway Consulting Ltd., Auckland, New Zealand
- Wilson, G. Wilson, T. Cole, J. Oze, C. (2012) Vulnerability of laptop computers to volcanic ash and gas. *Natural Hazards*, 63, pp.711-736
- Wilson, G. Wilson, T.M. Deligne, N.I. Cole, J.W. (2014) Volcanic hazard impacts to critical infrastructure: a review. *Journal of Volcanology and Geothermal Research*, 286, pp.148-182
- Wilson, T. Daly, M. Johnston, D. (2009) Review of impacts of volcanic ash on electricity distribution systems, broadcasting and communication networks. Auckland Engineering Lifelines Group, Auckland Regional Council Technical Publication No. 051
- Wilson, T.M. Stewart, C. Cole, J.W. Dewar, D.J. Johnston, D.M. Cronin, S.J. (2011) The 1991 eruption of Volcan Hudson, Chile: impacts on agriculture and rural communities and long-term recovery. GNS Science Report 2009/66, 99p
- Wilson, T.M. Stewart, C. Sword-Daniels, V. Leonard, G.S. Johnston, D.M. Cole, J.W. Wardman, J. Wilson, G. Barnard, S.T. (2012a) Volcanic ash impacts to critical infrastructure. *Physics and Chemistry of the Earth*, 45-46, pp.5-23
- Wilson, T.M. Cole, J. Johnston, D. Cronin, S. Stewart, C. Dantas, A. (2012b) Short- and long-term evacuation of people and livestock during a volcanic crisis: lessons from the 1991 eruption of Volcán Hudson, Chile. *Journal of Applied Volcanology*, 1:1, pp.1-11
- World Road Association-PIARC (1987) "Technical committee report on road surface characteristics", Permanent International Association of Road Congress. Proceedings of the 18th World Congress, Brussels, Belgium

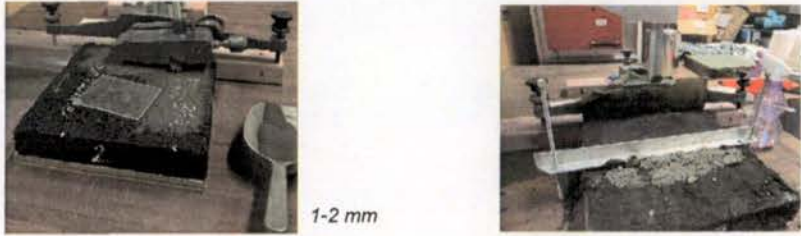
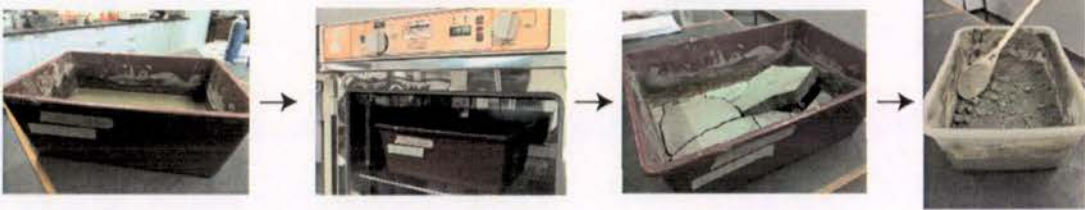
Appendix A. Concentration of elements in the Ruapehu and White Island Crater Lake fluids at the strength used to dose the ash (after Broom 2010, Wilson 2012).

Element	Concentration (mg/L)	
	Ruapehu Crater Lake (100% strength)	White Island Crater Lake (20% strength)
Aluminium (Al)	370	965
Boron (B)	17.2	28.6
Bromine (Br)	10.8	44.2
Calcium (Ca)	909	823
Chlorine (Cl)	5,568	19,452
Fluorine (F)	133	1,518
Iron (Fe)	424	179
Potassium (K)	90	686
Lithium (Li)	0.77	5.60
Magnesium (Mg)	1,067	1,325
Sodium (Na)	660	3,372
Ammonia (NH ₃)	13.0	24.8
Sulfate (SO ₄ ²⁻)	7,988	4,952
pH	1.13	0.07

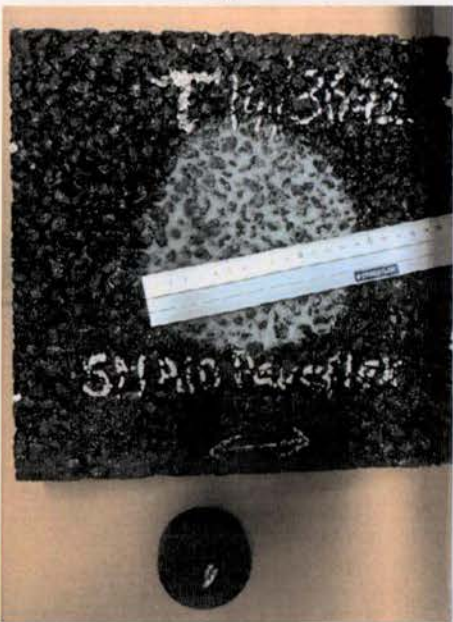
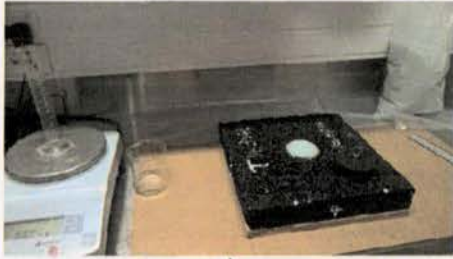
Appendix B. Water leachate results showing relative soluble components (expressed as Electrical Conductivity (EC) and Total Dissolved Solids (TDS)), and pH. A) 1:100 ash to de-ionised water, B) 1:20 ash to de-ionised water.



Appendix C. Ash characteristics analysed during experimentation and illustrations to show production of each characteristic.

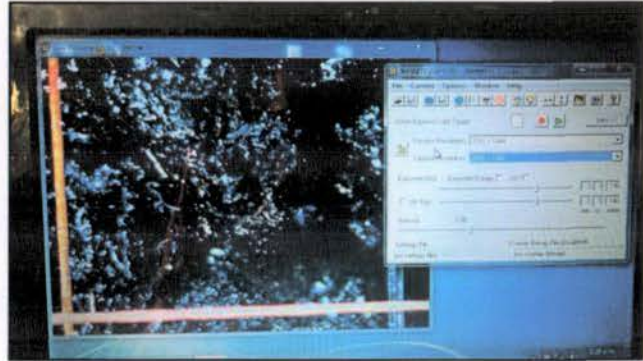
Characteristic	Variables	Method Summary
Ash type	Hard basalt, scoriaceous basalt, pumiceous rhyolite	Different volcano source locations in New Zealand (see figure 3)
Ash grain size	<1000 μm , <106 μm	Rock splitting, crushing and pulverisation (as required), then sieving
 <p><i>Hydraulic press (Hill 2014)</i> <i>Jaw crusher (Hill 2014)</i> <i>Disk pulverisor (Hill 2014)</i> <i>Rock sieves</i></p>		
Ash thickness	1-2 mm, 5 mm	Manual sprinkling (1-2 mm), Metal spacer across ash surface (5 mm)
 <p><i>1-2 mm</i> <i>5 mm</i></p>		
Soluble components	Non-dosed, dosed with Ruapehu Crater Lake fluid, dosed with White Island Crater Lake fluid	Established laboratory dosing technique (see section 2.1.1)
		
Wetness	Wetted to saturation, dry (no added moisture)	Hand-held water sprayer (water at room temperature)
 <p><i>Dry</i> <i>Wet</i></p>		

Appendix D. Summary of sand patch volumetric technique used to calculate the average pavement macrotexture depth (adapted from ASTM E965 2006).



1. Pour glass beads (600-850 μm diameter and minimum 65% true spheres) up to a level on the cylinder which has a known volume.
2. Gently tap base of cylinder several times and add more glass beads to level.
3. Determine mass of material in cylinder (which is used for each measurement).
4. Pour measured volume and weight of material onto asphalt concrete surface.
5. Carefully spread material into circular patch with the rubber disk tool, filling the surface voids flush with the aggregate particle tips.
6. Measure and record the diameter of the circular area covered by the material at four equally spaced locations around the sample circumference.
7. Compute and record the average diameter.
8. Calculate average pavement macrotexture depth using equation (2).

Appendix E. Image capture using stereo-microscope to analyse asphalt at a microtextural scale. Note that the grid squares (left) are spaced at 10 mm intervals.



Evacuations to clean-up: transportation impacts from the 2014 eruption of Kelud volcano

Blake, D.M.^{1*} Hayes, J.¹ Andreastuti, S.² Jenkins, S.³ Wilson, T.M.¹ Stewart, C.⁴ Hendrasto, M.²

¹D.M. Blake, J. Hayes, T.M. Wilson, Department of Geological Sciences, University of Canterbury, Private Bag 4800, Christchurch 8140, New Zealand.

²S. Andreastuti, M. Hendrasto, Centre for Volcanology and Geological Hazard Mitigation (CVGHM), Jl. Diponegoro No. 57, Bandung 40122, West Java, Indonesia

³S.F. Jenkins, School of Earth Sciences, University of Bristol, Wills Memorial Building, Queen's Road, Clifton BS8 1RJ, United Kingdom

⁴C. Stewart, Joint Centre for Disaster Research, Massey University/GNS Science, Massey University Wellington Campus, PO Box 756, Wellington, New Zealand.

* Corresponding author: daniel.blake@pg.canterbury.ac.nz

With over 30 confirmed eruptions in the past 1000 years, nine since the beginning of the twentieth century, the February 2014 eruption and associated hazards from Kelud volcano did not come as a surprise to the majority of residents in proximal areas. Evacuations within all three regencies on the volcano flanks were relatively successful, with over 100,000 people evacuated. Effective monitoring of precursory activity and change in alert levels before the eruption, aided by community preparedness measures and warning systems already in place were critical to the successful evacuations. Some residents however, either evacuated during the eruption itself or sheltered in buildings and left the following day, experiencing tephra hazards on the roads as they travelled. In distal cities such as Yogyakarta, 220 km west of Kelud, the tephra and subsequent transportation impacts were unexpected by most residents and officials, despite experience with hazards from nearby Merapi volcano less than four years earlier.

Transportation in Java was severely affected by the Kelud eruption. Operations at seven airports (four international and three domestic) were disrupted by closures and ~US\$ 20 million of damage was caused to the engines of one aircraft which flew into the volcanic ash cloud. Some air passengers opted for alternative transportation modes such as rail and inter-city buses for long-distance travel due to the cancellation of flights. Many roads in proximal areas (up to 30 km from the vent) were completely destroyed, severely damaged or buried by pyroclastic density currents, lahars, landslides, ballistics and tephra. Tephra caused widespread disruption with government advice to stay off the roads as far away as in Yogyakarta and public bus services cancelled at times. Extensive clean-up operations were necessary following the eruption. However, rapidly implemented, collaborative and proactive approaches to clean-up likely minimised continued impacts associated with the remobilisation of ash.

In this study, we provide an in-depth review of the impacts to transportation during the Kelud 2014 eruption from the time of evacuations until tephra clean-up. Specifically, we:

- Present impact assessments for both proximal areas and the distal city of Yogyakarta and identify thresholds for damage and disruption states associated with transportation infrastructure and for recovery processes such as cleaning and repair.
- Compare these identified thresholds for Kelud with those outlined in existing volcanological literature and observed during other eruptions worldwide, including Mt St Helens, Sakurajima, Pacaya and Puyehue-Cordón Caulle. This allows us to validate our findings and investigate whether the severity of transportation impacts and extent of required clean-up at Kelud could have been better anticipated and prepared for.
- Identify risk management measures implemented prior to the 2014 eruption including warning systems, and physical and community preparedness measures, and analyse their effect on resilience.